Damped response theory

Joanna Kauczor

PhD Thesis

The Lundbeck Foundation Center for Theoretical Chemistry
Department of Chemistry
University of Aarhus

December 2010

Preface

This thesis is submitted to the Faculty of Science at the University of Aarhus to fulfill the requirements for obtaining the PhD degree in chemistry. It contains the results of three years of PhD studies at the Center for Theoretical Chemistry, Department of Chemistry, University of Aarhus, under the supervision of Prof. Poul Jørgensen.

The objective of this thesis is to obtain an efficient solver for so-called response equations that need to be solved to determine molecular properties for the Hartree–Fock and Kohn–Sham Density Functional Theory. The main focus have been put on application of damped response theory in a linear-scaling framework and on determining molecular properties (spectra) for large molecular systems.

List of publications

A. *Quasienergy formulation of damped response theory*
Kasper Kristensen, Joanna Kauczor, Thomas Kjærgaard and Poul Jørgensen
J. Chem. Phys. **131**, 044112 (2009).

B. *On the efficiency of algorithms for solving Hartree–Fock and Kohn–Sham response equations*
Joanna Kauczor, Poul Jørgensen and Patrick Norman
J. Chem. Theory Comput. **7**, 1610 (2011).

C. *Comparison of standard and damped response formulations of Magnetic Circular Dichroism*
Thomas Kjærgaard, Kasper Kristensen, Joanna Kauczor, Poul Jørgensen, Sonia Coriani and Andreas J. Thorvaldsen
J. Chem. Phys. **135**, 024112 (2011).

D. *Damped response theory of two photon absorption*
Kasper Kristensen, Joanna Kauczor, Thomas Kjærgaard, Poul Jørgensen, Andreas J. Thorvaldsen and Antonio Rizzo
J. Chem. Phys. **134**, 214104 (2011).

Miscellaneous

Atomic units are used throughout this thesis unless otherwise stated.

All methods described in this thesis are implemented in a local development version of the quantum chemistry program DALTON [1] and its Linear-Scaling version LSDALTON [2]. All calculations reported in this thesis have been performed in these programs.

Acknowledgments

I would first like to thank my supervisor Prof. Poul Jørgensen for giving me an opportunity to study in his group, and also for his help and supervision during last three years. I would also like to thank Dr. Jeppe Olsen for several enlightening discussions and also help and support he has given me during my PhD studies.

Last three and a half years have been on one (scientific) hand a very short, and on the other (personal) a pretty long time. I learned a lot and (not only my hair color, but also) I changed a lot. There have been good days and bad days, and I cannot imagine I would have made it without a group of people, whom I would now like to thank.

First of all, I would like to thank Dr. Marcin Ziółkowski for his huuuuge help at work and 'in life', and for making everything much easier and better. *Dzięki wielkie, Marcinku!*

I would like to thank my collaborators: Prof. Patrick Norman, whose visit in Aarhus caused a turn in my work and with whom I had several really fruitful scientific discussions; Dr. Thomas Kjærgaard, who, during whole this time, became a good friend of mine and has been my 'go to' person whenever I had any question about the code, I needed a hug or my surname was misspelled in my driving license; and Kasper Kristensen, for all the discussions, help and support he has always given me.

I would like to thank all the current and former members of the quantum chemistry group in Aarhus for all good moments we shared. Especially, I would like to acknowledge my office mate Dr. Peter Seidler, who was like an older brother I have not ever had: I mean he 'stole' chocolate and sweets from me. Since the final straight has been very difficult for me, it was probably even more difficult for people around me. Therefore I would like to acknowledge Dr. Lasse Kragh Sørensen, sharing office with whom has been a pleasure. I would also like to thank Dr. Branislav Jansík, with whom I have had many chats/discussions over the sink, and Ida-Marie Højvik, who showed me the mysterious gym world.

During the years, I met a lot of people at summer/winter schools and conferences and since it is impossible to mention all of them, I will just acknowledge Gosia Olejniczak who

was the best roommate and friend I could imagine. I would also like to thank people at the University of Silesia, in Katowice, Poland, who introduced me to quantum chemistry and without whom none of this would have been possible: Prof. Stanisław Kucharski, and my former supervisor, Szanowny Pan Doktor Tadeusz Pluta, who became a really good friend during last years, and whose emails always made me feel better. I would also like to acknowledge Mrs Iwona Zawadzka, who interested me in chemistry in the first place.

I would like to thank Dr. Marcin Ziółkowski, Dr. Stinne Høst, Dr. Thomas Kjærgaard, Kasper Kristensen and Małgorzata Śpiewak for proofreading this thesis (or its parts) and their precious advise and comments. I would also like to thank Dr. Lara Ferrighi for helping me with figures.

However, since life is not only about work, I wanted to thank all the people who helped me survive in Aarhus, who made my life a better place and had a huge impact on it: Joan Marler and Gülnur Doğan, who have been a great company for girl nights, introduced me to different cultures and have been really good friends over the years; Lara Ferrighi, discussion with whom really broadened my mind (and she also has had an influence on broadening my hips, since she fed me with gorgeous food); Claire Butré, who was my force in learning Danish, and thanks to her organization skills I had a chance to see a lot of beautiful places in Denmark (and Paris, but who would mention it); Maryam Sawa, Rebecca van der Westen, Samir Nezir and Irene Dalsgaard, who were with me when I needed it; Tom Griffiths, who was always a very good friend and tried to improve my English and self-esteem; Herr Doctor (well, now Herr Professor) Mikael Johansson, with whom I have had great talks in Under Masken; Tobias Schwabe, who is a very strong and helpful man, and who knows answers to all these weird questions I always wondered about; Andreas Thorvaldsen, whom I would like to apologize for all my jokes about Tromsø (and I cannot promise I will be better); Thomas Holst, who is an unDanish Dane and made me look differently at many things and Francisco 'Paco' Malagon, who has always made me laugh.

I would like to thank my family. *Bardzo gorąco dziękuję mojej rodzinie za ich wielkie wsparcie i wiarę we mnie. Dziękuję za wyrozumiałość i pomoc w ciągu ostatnich lat. Dziękuję moim rodzicom, babci Eli, cioci Krysi, wujkom Ryśkowi i Jurkowi, i mojemu kuzynostwu: Tomkowi (i Agnieszce), Krzysieńkowi oraz Anecie. Serdecznie dziękuję również mojej Siostrze Agnieszce oraz Szwagrowi Kubie, za ciepły dom, którego drzwi zawsze były dla mnie otwarte, a także za przyjaźń okazaną mi przez całe życie. (Obiecuję być dobrą ciocią dla Bartka.)* I would also like to thank my friends who have had time for me, whenever I visited Poland: Katarzyna Choruży, Agnieszka Pojnar, Agnieszka Urban, Karol Hajzel, Błażej

Falkus, Bartosz Grądecki and many others.

Since I do not think I am getting close to the Nobel prize (neither to an Oscar or an MTV Music Award), I will take my chance now and thank the people who were for me when I needed them the most and had a huge impact on who I am now: Alicja Kołodziejczyk, Dominika Nowakowicz, Weronika Tomaszewska-Collins, Patrycja Sajda-Smoleńska (and her family), Alicja Puchalska, Monika Sołtysiak, Zuzanna Brontke, Jakub Dziewit, Paweł Kapliński and Michał Troc.

And last but not least, I would like to thank the person I am sure I would not make it without. I find myself one of extremely lucky people, who have a good friend who is always there for me, who survived my severe 'break downs', broken heart and all the problems I have had. Who shares with me the good and the bad moments and helps me with my ups and downs. I would like to thank my best friend who has gone with me through this phD, Małgorzata Śpiewak. *Wielkie, wielkie, wielkie dziękuję, Gosia!*

Joanna Kauczor
Aarhus, November 2010

Contents

1 Introduction

The beginning of the 20th century brought significant discoveries in the world of science. These had huge influence on the way nature and matter are perceived nowadays. The foundations of quantum mechanics were established, enabling theoretical investigation of chemical reactions and molecular properties. Since the 1920s, a theoretical treatment of molecular systems using quantum chemistry attracted the attention of many scientific research groups.

An accurate description of the electronic structure and properties of molecular systems may be obtained from the solution to the Schrödinger equation [3]. However, this equation may only be solved analytically for a few model systems. Due to the fact that the analytic solution to the Schrödinger equation is not available for a general system, a number of hierarchical approaches have been formulated for approximate solutions. The traditional way of carrying out electronic structure calculations is using the wavefunction-based methods. The simplest of the methods is the Hartree–Fock (HF) method, where the motion of electrons is described using a mean-field approach [4–6]. In this method, the interaction between the electrons is considered in a field of all electrons, and simultaneous interactions (so-called electron correlation) are neglected. More accurate methods that include the electron-electron interaction are known as the post-HF methods. The simplest is the second-order Møller–Plesset perturbation theory (MP2) [7]. Most successful, nowadays, is the Coupled Cluster (CC) hierarchy [8, 9], which has the advantage that the approximate models keep most important features of the basic theory [10]. An alternative to the wavefunction-based methods is Density Functional Theory (DFT) [11], which is based on the fact that the ground state electronic energy can, in principle, be determined from the electron density. Kohn–Sham DFT (KS-DFT) [12, 13] represents a reasonable compromise between cost and accuracy. However, in its present formulation, it does not provide a systematic error control.

Molecular properties are fundamental quantities underlying the macroscopic behavior of matter, which may be compared to experimental results. Since the seminal work of Pulay [14], great progress has been made in terms of numerical and analytical derivation of molecular properties. Static (time-independent) properties may be obtained from energy derivatives with respect to perturbing field. However, when a molecule interacts with time-dependent electromagnetic field, the energy of the system is not well-defined and therefore its derivatives cannot be used for calculating properties. In this case, properties may be obtained using response theory [15, 16] that determines the response of a molecular system towards weak perturbing fields, such as internal magnetic moments or externally applied electric and magnetic fields. Using quantum-chemical methods, it is nowadays possible to investigate a

large number of molecular properties of increasing complexity, from computationally simple energy differences, such as reaction enthalpies, to more involved higher-order frequency-dependent polarizabilities and multi-photon absorption strengths [17].

The bottleneck for applying quantum-mechanical methods to large systems is the scaling of a computational cost (time) with increasing system size. Formally, HF and KS Self-Consistent Field (SCF) methods scale as $O(N^4)$, where N refers to the system size. Moreover, wavefunction-based correlated methods have a higher scaling, *e.g.* MP2 scales as $O(N^5)$, CC with Singles and Doubles excitations (CCSD) [18] and CC with Singles and Doubles excitations and perturbative Triples (CCDS(T)) [19] scale as $O(N^6)$ and $O(N^7)$, respectively (see Fig. 1.1). With such a scaling, advances in computer hardware alone will never allow calculations on large molecular systems. A significant effort has therefore been directed towards the development of new algorithms with a reduced scaling. The goal is to develop linear-scaling methods, *i.e.* methods where the computational cost scales linearly with the system size, $O(N)$ [20, 21].

During the last two decades, a lot of attention has been focused on developing a linear-scaling framework for carrying out HF and KS-DFT calculations. Two major obstacles have been faced for the optimization of the energy in linear-scaling fashion, namely the construction of the Fock/KS matrix and the generation of a new density matrix. These problem may be circumvented by using a density based formulation of SCF [22]. The linear-scaling development has also been extended to include molecular properties that can be calculated from linear [23], quadratic [24] and higher response functions.

The determination of molecular response properties requires that so-called response equations are solved. In the early days of quantum chemistry, when only small molecular systems

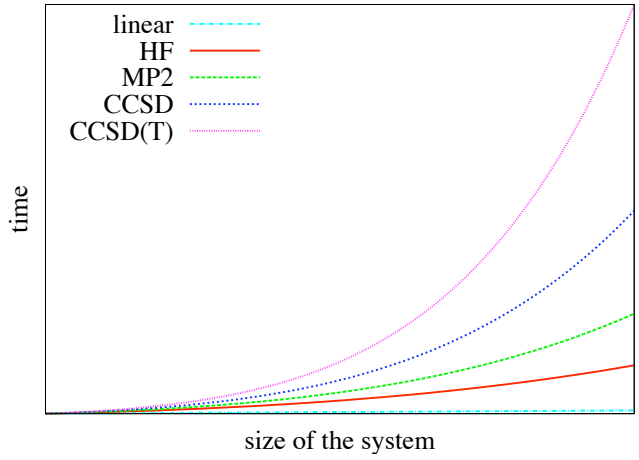

Figure 1.1: Scaling of the SCF method, and hierarchy of correlated methods including MP2, CCSD and CCSD(T).

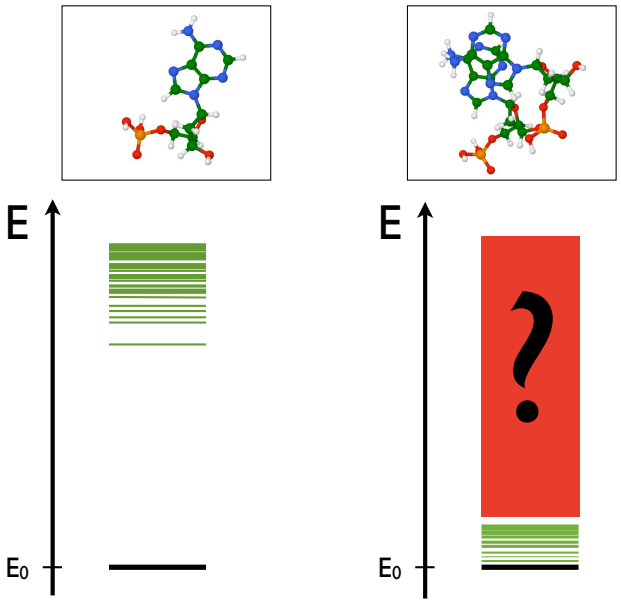

Figure 1.2: The first fifty excitation energies (marked in green) for the DNA fragment consisting of one (left) and two (right) nucleotides. The red rectangle represents the region of the spectrum which is beyond the reach of standard response theory.

were considered, the response equations were set up explicitly and the solutions were obtained by applying standard algorithms of numerical analysis, for example using diagonalization and triangularization methods, *e.g.* Gauss–Jordan elimination or LU-factorization [25–27]. For larger molecular systems, it is impossible to solve response equations explicitly, and using iterative subspace algorithms have therefore become a standard practice.

Molecular properties for ground and excited states, and for transitions between these states, can be determined from molecular response functions and their poles and residues. In standard response theory, absorption spectra are obtained from residues of response functions and are therefore acquired by solving a generalized eigenvalue problem [16]. This iterative procedure starts from the energies of the lowest excited states, and therefore only the lowest excitations are addressed using this approach. For small molecules, in most cases, the lowest excitations are sufficient to obtain the desired absorption spectrum. However, for large systems, where a vast amount of excited states is present, it may be not possible to access all excitation energies of interest using this approach (see Fig. 1.2). The straightforward comparison between standard theory and experiment is therefore impossible in many interesting regions of the spectrum for large molecular systems. This problem can be solved by introducing damped response theory [28, 29].

Damped response theory is based on a phenomenological description, where the excited states are multiplied by a damping factor $[\exp(-2\gamma t)]$, where γ is denoted the inverse effective lifetime or the excited-state lifetime broadening parameter [28–35]. Introducing γ in this manner is equivalent to introducing complex excitation energies, which removes sin-

gularities of the response functions at resonance frequencies. Such a modification leads to real and imaginary components of response functions that may be connected with dispersion and absorption phenomena, respectively. Since the peak spectrum broadening of electronic spectra is by far dominated by collisions, Doppler and vibrational broadening, rather than the natural lifetimes of the excited states [36], an identical damping parameter can be used for all excited states [28,29]. In standard response theory the transitions between the ground and excited states can be presented as a delta-peaked residue spectrum, whereas in an experimental spectrum and in the absorption spectra obtained using damped response theory, the peaks are broadened. The employment of damped response theory gives an opportunity to obtain absorption spectra in any frequency of interest, which may not be possible when the standard response theory is used.

As mentioned before, the determination of molecular response properties requires analysis of frequency-dependent response functions, which translates into solving sets of response equations. The overall structures of the response equations are identical for variational wavefunctions such as the HF and Multi-Configurational SCF (MCSCF) as well as for KS-DFT and therefore the key module in programs devoted to this task is the response equation solver. The large dimensionality imposes the use of iterative algorithms, and criteria against which such solver routines are evaluated are stability and efficiency. Minimal memory usage and disk storage is also required for treating large molecular systems[1] and it should be possible to perform calculations in the entire frequency range. The traditional way of solving large sparse sets of linear equations is based on the iterative subspace approaches, *e.g.* for solving the SCF equations as proposed in Ref. [37]. When equations are solved using the subspace algorithms, vectors from all iterations must be stored on disk, which may become impractical for large molecular systems. It was recognized [38] that the algorithm presented in Ref. [37] leads to an iteration sequence identical to the one obtained using the conjugate gradient (CG) algorithm [39]. The advantage of using a CG formulation (and similarly for the conjugate residual (CR) algorithm [40]) is that only the last three trial vectors are necessary to maintain the information content of all previous trial vectors. The vectors manipulation therefore becomes simplified and the disk storage significantly reduced. In Ref. [41], Olsen *et al.* introduced paired trial vectors in the iterative subspace algorithm which highly improved the performance of the Davidson algorithm [42] used for solving the eigenvalue response equation. Better convergence of the standard response equation was also observed.

The present work focuses on two related topics. The first topic is how to improve the

[1]Naturally, it is also an advantage for calculations on small molecules.

linear response equation solvers within the linear-scaling framework. An attempt of using the CG and CR algorithms for solving standard response equations has also been made. The second topic is how to introduce the damped response theory for HF and KS-DFT in the linear scaling framework and make damped response equation solver easily applicable to higher-order equations. Using damped response theory, the first- and higher-order response equations may be solved in the entire frequency region, which makes it a useful tool for calculating absorption spectra for large molecular systems.

The thesis is organized as follows:

Electronic Structure Theory Short introduction to electronic structure theory, defining terms important in the following chapters for the HF method, KS-DFT and the linear-scaling formulation of both methods.

Standard Response Theory Introduction to response theory for the exact and approximate (HF) state, based on the quasi-energy formulation [43, 44]. The structure of the response matrices is presented in details and the linear-scaling formulation for solving the response equations is discussed.

Damped Response Theory Damped response theory is introduced for the first- and higher-order response equations. The quasi-energy formulation [43, 44] is used in connection with the response parameter elimination rules of Ref. [45] to obtain simple expressions for standard response functions in terms of response parameters. The quasi-energy formulation is also compared to the damped response theory introduced by Norman *et al.* [28], which is based on the Ehrenfest theorem.

Higher-order properties in damped response theory The damped response theory formulation is applied to higher-order properties, such as the magnetic circular dichroism and the two-photon absorption.

Standard iterative algorithms Standard iterative algorithms that may be applied to response equations, such as an iterative subspace algorithm and the CG and CR algorithms are described.

Solving response equations using standard iterative methods General forms of response equations are briefly discussed and the application of standard iterative methods on the response equations is presented. Also problems that may occur if the algorithms are straightforwardly applied to response equations are discussed.

Iterative algorithms with paired trial vectors The iterative subspace algorithms with paired trial vectors [41] for solving standard and eigenvalue response equations are discussed. The damped response equation solver within the linear-scaling framework is introduced and compared to the previously used approach by Norman *et al.* [29].

Iterative algorithms with symmetrized trial vectors Algorithms with symmetrized trial vectors for solving the standard, damped and eigenvalue response equations are introduced.

Illustrative results Numerical examples illustrating the efficiency of the various algorithms are presented and evaluated against such criteria as efficiency, stability and disk storage. Absorption and dispersion spectra determined using the damped response theory are also displayed.

Conclusions Brief conclusions on the performance and efficiency of various algorithms for solving standard, damped and eigenvalue response equations are presented.

2 Electronic Structure Theory

Electronic structure theory describes a system based on the motion of electrons in atoms and molecules. This is done in context of the Born-Oppenheimer approximation [46], which assumes that electronic and nuclear motion in molecules are independent and can be considered separately.

In the electronic structure theory, the electronic Schrödinger equation [3] is solved

$$\hat{H}\Psi = E_0\Psi\,, \tag{2.1}$$

where

- $\hat{H}$ – the time-independent Hamiltonian, often denoted $\hat{H}_0$,
- E_0 – the ground state energy,
- Ψ – the electronic wavefunction that contains all information about the system.

The complexity of the wavefunction Ψ increases with the size of the system, as it depends on $3N_e$ spatial coordinates, where N_e is the number of electrons in the system. The Hamiltonian $\hat{H}$ is given by

$$\hat{H} = \hat{T}_e + \hat{V}_{ne} + \hat{V}_{ee} + h_{nuc}\,, \tag{2.2}$$

where

- $\hat{T}_e$ – the kinetic energy operator,
- $\hat{V}_{ne}$ – the external potential arising from the electron-nuclei attraction,
- $\hat{V}_{ee}$ – the interaction between the electrons,
- h_{nuc} – the constant nuclear-nuclear repulsion,

and may be partitioned in one- and two-electron terms

$$\hat{H} = \sum_{i}^{N_e} \hat{h}_i + \sum_{i\neq j}^{N_e} \hat{g}_{ij} + h_{nuc}\,. \tag{2.3}$$

$\hat{h}_i$ and $\hat{g}_{ij}$ are given as

$$\hat{h}_i = -\frac{1}{2}\nabla_i^2 - \sum_{J}^{N_n} \frac{Z_J}{|\mathbf{R}_J - \mathbf{r}_i|}; \quad \hat{g}_{ij} = \frac{1}{\mathbf{r}_{ij}} = \frac{1}{|\mathbf{r}_j - \mathbf{r}_i|}\,, \tag{2.4}$$

where

- N_n – the number of nuclei,
- Z_J – the charge of the nucleus J,
- $|\mathbf{R}_J - \mathbf{r}_i|$ – the distance between nucleus J and electron i,
- $|\mathbf{r}_j - \mathbf{r}_i|$ – the distance between electrons i and j.

h_{nuc} contains the contribution from internuclear repulsion and is defined as

$$h_{nuc} = \frac{1}{2} \sum_{K \neq L} \frac{Z_K Z_L}{|\mathbf{R}_K - \mathbf{R}_L|} \,. \tag{2.5}$$

h_{nuc} may contain some additional interactions for a specific calculation, for example a calculation of magnetic properties (*e.g.* NMR parameters), where it contains additional purely magnetic interactions, such as the Zeeman interaction between the nuclear magnetic dipole moments and the external magnetic field [47].

In order to solve the Schrödinger equation in Eq. (2.1), the many-electron wavefunction is expanded in terms of N-electron Slater determinants that are built from one-electron functions (spin orbitals) and satisfy the Pauli principle. The Schrödinger equation is solved in the limit of an infinite number of one-electron functions and all possible Slater determinants. However, it is impossible to perform in practice, and therefore some approximations have been introduced. A finite number of one-electron functions (the basis set) has to be chosen. Various methods have been proposed to systematically truncate the N-electron and the one-electron basis. The Schrödinger equation may be solved within a given one-electron basis using all possible Slater determinants, which is called the Full Configuration Interaction Method (FCI) method. However, computational requirements limits its use to very small systems containing only few electrons.

2.1 The Hartree–Fock method

The simplest method in the N-electron basis hierarchy includes only one Slater determinant to describe the N-electron wavefunction and is known as the Hartree–Fock (HF) model [4,5]. The wavefunction has the form

$$\Psi_{HF}(\mathbf{x}_1, \mathbf{x}_2, \ldots, \mathbf{x}_N) = |\psi_1(\mathbf{x}_1)\psi_2(\mathbf{x}_2)\cdots\psi_N(\mathbf{x}_N)| \,, \tag{2.6}$$

where ψ are spin orbitals, containing spatial (ϕ_i) and spin (σ) components

$$\psi_i(\mathbf{x}_i) = \phi_i(\mathbf{r})\sigma(\mathbf{s}) \,. \tag{2.7}$$

The energy is minimized with respect to variations in the molecular orbital (MOs) ϕ_i subject to the constraint that the one-electron functions remain orthonormal. This is equivalent to solving a set of one-electron equations (the canonical HF equations)

$$\hat{F}_i \phi_i = \epsilon_i \phi_i \,, \tag{2.8}$$

where ϵ_i is the orbital energy and $\hat{F}_i$ is the Fock operator given by

$$\hat{F}_i = \hat{h}_i + \sum_j (2\hat{J}_j - \hat{K}_j)\,. \tag{2.9}$$

$\hat{J}$ and $\hat{K}$ are the Coulomb and exchange operators, respectively, and are defined as

$$\hat{J}_i\phi_j(\mathbf{r}_1) = \phi_j \int \phi_i^\star(\mathbf{r}_2)\frac{1}{|\mathbf{r}_1 - \mathbf{r}_2|}\phi_i(\mathbf{r}_2)d\mathbf{r}_2\,, \tag{2.10}$$

$$\hat{K}_i\phi_j(\mathbf{r}_1) = \phi_i \int \phi_i^\star(\mathbf{r}_2)\frac{1}{|\mathbf{r}_1 - \mathbf{r}_2|}\phi_j(\mathbf{r}_2)d\mathbf{r}_2\,. \tag{2.11}$$

The Coulomb contribution describes the interaction between two charge distributions described by $|\phi_i(\mathbf{r}_1)|^2$ and $|\phi_j(\mathbf{r}_2)|^2$. It also contains an unphysical term describing a repulsion between identical electrons (self-interaction). The exchange contribution is a consequence of the antisymmetrization of the wavefunction. It contains a term that exactly cancels out the self-interaction component of the Coulomb contribution.

Since the Fock operator depends on the orbitals, the HF equations in Eq. (2.8) must be solved iteratively in a self-consistent manner. In the HF approximation, each electron is moving in an average field generated by other electrons, *i.e.* a mean-field approximation. When a set of orbitals is determined, the Hartree-Fock energy can be evaluated as

$$E_{HF} = 2\sum_i h_{ii} + \sum_{ij}(2J_{ij} - K_{ij}) + h_{nuc}\,, \tag{2.12}$$

where h_{ii}, J_{ij} and K_{ij} are expectation values of their respective operators. The consequence of replacing the two-electron interaction with the one-electron Fock operator is the negligence of the electron correlation. The correlation energy is defined as the difference between the Hartree–Fock energy and the exact energy.

The molecular orbitals ϕ_i can be expanded in a set of atomic orbitals (AOs) χ_μ

$$\phi_i = \sum_\mu \chi_\mu C_{\mu i}\,. \tag{2.13}$$

For a closed-shell system, inserting this expansion into Eq. (2.8) yields to the Roothaan-Hall equations [48, 49] that can be written as

$$\mathbf{FC} = \mathbf{SC}\boldsymbol{\epsilon}\,, \tag{2.14}$$

where $\mathbf{C}$ contains the MO expansion coefficients of Eq. (2.13), $\boldsymbol{\epsilon}$ is a diagonal matrix containing the orbital energies and $\mathbf{S}$ is the AO overlap matrix given as

$$S_{\mu\nu} = \int \chi_\mu^\star(\mathbf{r})\chi_\nu(\mathbf{r})d\mathbf{r}\,. \tag{2.15}$$

$\mathbf{F}$ is the AO Fock matrix expressed in terms of the one-electron density matrix

$$\mathbf{F}(\mathbf{D}) = \mathbf{h} + \mathbf{G}(\mathbf{D}) \,, \tag{2.16}$$

where the AO density matrix $\mathbf{D}$ is given as

$$\mathbf{D} = \mathbf{C}_{\mathrm{occ}} \mathbf{C}_{\mathrm{occ}}^{\dagger} \,. \tag{2.17}$$

$\mathbf{C}_{\mathrm{occ}}$ denotes the subblock of occupied MO coefficients. $\mathbf{h}$ in Eq. (2.16) is the one-electron Hamiltonian and the elements of $\mathbf{G}(\mathbf{D})$ are given by

$$G_{\mu\nu}(\mathbf{D}) = 2 \sum_{\rho\sigma} g_{\mu\nu\rho\sigma} D_{\rho\sigma} - \sum_{\rho\sigma} g_{\mu\sigma\rho\nu} D_{\rho\sigma} \,. \tag{2.18}$$

In the AO basis, the one- and two-electron integrals are given as

$$h_{\mu\nu} = \int \chi_{\mu}^{\star}(\mathbf{r}_1) \left(-\frac{1}{2} \nabla_1^2 - \sum_{J}^{N_n} \frac{Z_J}{|\mathbf{R}_J - \mathbf{r}_1|} \right) \chi_{\nu}(\mathbf{r}_1) d\mathbf{r}_1 \,, \tag{2.19}$$

$$g_{\mu\nu\rho\sigma} = \int \int \chi_{\mu}^{\star}(\mathbf{r}_1) \chi_{\rho}^{\star}(\mathbf{r}_2) \frac{1}{|\mathbf{r}_1 - \mathbf{r}_2|} \chi_{\nu}(\mathbf{r}_1) \chi_{\sigma}(\mathbf{r}_2) d\mathbf{r}_1 d\mathbf{r}_2 \,. \tag{2.20}$$

Eq. (2.14) represents the HF equations in Eq. (2.8) in the atomic orbital basis.

The Roothaan-Hall equations often converge slowly. Therefore, they are usually combined with a convergence acceleration scheme such as the Direct Inversion in the Iterative Subspace algorithm (DIIS [50, 51]) and the Density Subspace Minimization (DSM [52, 53]). An alternative is the Augmented Roothaan-Hall method (ARH [54]).

The HF method gives a decent description of the system and is used as a starting point for more accurate approximations, which include the effects of electron correlation that are necessary for correct description of *e.g.* dissociation processes or near-degenerate systems. Unfortunately, applying wavefunction-based correlated methods is very expensive (due to their high scaling), and they cannot be used in calculations on large molecular systems.

2.2 Density Functional Theory

As mentioned in the previous section, the cost of a calculation increases with the number of electrons in the system since the wavefunction depends on $3N_e$ spatial coordinates. A different approach was proposed by Hohenberg and Kohn [12], where a molecular system is described by a functional that depends on the electron density $\rho(\mathbf{r})$ given as

$$\rho(\mathbf{r}) = N \int |\Psi(\mathbf{x}_1, \mathbf{x}_2, \cdots, \mathbf{x}_n)|^2 ds_1 d\mathbf{x}_2 \cdots d\mathbf{x}_N \,, \tag{2.21}$$

instead of the wavefunction. The electron density function depends on three coordinates, independently of the size of the system. This approach is known as the Density Functional Theory (DFT).

The Hohenberg–Kohn theorem [12] postulates that the exact ground state electron density may be uniquely associated with an external potential $v_{ext}(\mathbf{r})$ (up to an additive constant). From the Hohenberg–Kohn theorem it follows that the potential $v_{ext}(\mathbf{r})$ is a functional of the electron density $v_{ext}[\rho]$, and that the ground state energy E_0 is a functional of the electron density, in the sense that the density uniquely determines the external potential, which in turn determines the energy $E_0[v_{ext}]$. Hohenberg and Kohn further recast the variational principle in terms of the electron density

$$E_0[v_{ext}] = \min_{\rho}(F[\rho] + \int \rho(\mathbf{r}) v_{ext}[\rho] d\mathbf{r}) \,, \tag{2.22}$$

where the minimum is constrained to densities that are v-representable [55], and $F[\rho]$ is the universal Hohenberg–Kohn functional that is independent of the external potential and given as

$$F[\rho] = E_0[v_{ext}] - \int \rho(\mathbf{r}) v_{ext}[\rho] d\mathbf{r} \,. \tag{2.23}$$

The ground state electron density therefore contains all the information needed to reconstruct the external potential and to obtain the wavefunction and the ground state energy. Unfortunately, the $F[\rho]$ functional is unknown.

A set of equations for finding the density in a self-consistent fashion is known as Kohn–Sham (KS) equations [13]

$$\left(\hat{h}_i + \sum_j 2\hat{J}_j + \frac{\partial E_{xc}}{\partial \rho(\mathbf{r})}\right) \phi_i = \sum_j \epsilon_{ij} \phi_j \,, \tag{2.24}$$

where E_{xc} is the exchange-correlation energy and the density is given by

$$\rho(\mathbf{r}) = \sum_i |\phi_i(\mathbf{r})|^2 \,. \tag{2.25}$$

Eq. (2.24) is similar to the HF equations in Eq. (2.8) and a matrix equation formulation of the KS equations may be obtained

$$\mathbf{F}^{KS}\mathbf{C} = \mathbf{S}\mathbf{C}\boldsymbol{\epsilon} \,, \tag{2.26}$$

where $\mathbf{F}^{KS}$ is the Kohn-Sham matrix given as

$$\mathbf{F}^{KS} = \mathbf{h} + 2\mathbf{J}(\mathbf{D}) + \mathbf{F}^{xc}(\mathbf{D}) \,. \tag{2.27}$$

$\mathbf{F}^{xc}$ is the exchange-correlation matrix in the AO basis

$$F^{xc}_{\mu\nu}(\mathbf{D}) = \int \chi_\mu(\mathbf{r}_1)\chi_\nu(\mathbf{r}_2)v_{xc}(\mathbf{r})d\mathbf{r} = \int \chi_\mu(\mathbf{r}_1)\chi_\nu(\mathbf{r}_2)\frac{\partial E_{xc[\rho]}}{\partial\rho(\mathbf{r})}d\mathbf{r}\,. \tag{2.28}$$

In Eq. (2.28), the exchange-correlation potential $v_{xc}(\mathbf{r})$ has been implicitly defined using

$$\rho(\mathbf{r}) = \sum_{\mu\nu}\chi_\mu(\mathbf{r})\chi_\nu(\mathbf{r})D_{\mu\nu}\,. \tag{2.29}$$

The algorithms for solving the HF and KS-DFT equations are identical. The only difference is in construction of the Fock/KS matrix that in HF has a form of Eq. (2.9) and in KS-DFT of Eq. (2.27).

One of the main tasks of DFT is to construct an approximate exchange-correlation energy. This component arises from the existence of the Coulomb hole (due to the electron-electron repulsion) and the Fermi hole, known also as an exchange hole (due to the Pauli principle resulting in repulsion of electrons of the same spin). There are two types of approximations to the exchange-correlation energy:

- Local Density Approximation (LDA) or Local Spin Density Approximation (LSDA) where the local homogeneity of the density is assumed. The exchange-correlation energy component arising from the local density is a product of volume and density exchange-correlation energy. The LDA approximation is often used for obtaining geometries, vibration frequencies and ionization potentials due to its low cost. The chemical bond energy and intermolecular dispersion interactions calculations are burdened with a large error.

- Non-Local Density Approximation (NLDA) where the density cannot be treated as local and depends on the whole system. The exchange-correlation energy can be approximate *e.g.* from the Gradient Expansion Approximation (GEA) and the Generalized Gradient Approximation (GGA) [56–58], where it is a function of the density ρ and its gradient $\nabla\rho$.

KS-DFT very often gives results that are in excellent agreement with the experiment data, however, it does not provide systematic control of error (in other words, a systematic approach towards the exact solution to the Schrödinger equation). DFT is often use in simulations of large molecules.

2.3 Linear-scaling Hartree–Fock and Density Functional Theory

In Ref. [22], Sałek *et al.* presented a linear-scaling implementation of molecular electronic self-consistent field theory, where the HF and KS-DFT equations are solved iteratively, using the AO basis subspace method. Each iteration consists of the construction of the Fock matrix (time dominating step) and a construction of the new density matrix. In order to obtain linear-scaling, the evaluation procedures in both steps must scale linearly. For the evaluation of Fock/KS matrix to scale linearly, the construction of both the Coulomb and the exchange contributions must scale linearly.

Construction of the two-electron AO integrals scales as $\mathcal{O}(N^4)$ with a size of the system. However, the integrals in Eq. (2.20) vanish if orbitals χ_μ and χ_ν and orbitals χ_ρ and χ_σ do not overlap significantly. Prescreening of integrals can thus reduce the scaling to $\mathcal{O}(N^2)$. The scaling of the Coulomb contribution can be further reduced by using the Fast Multipole Method (FMM) [59], that was originally developed for point charges [60]. The total interaction is split into a near-field short-range interaction (NF), that is calculated exactly and a far-field long-range interaction (FF). The FMM algorithm has been modified to treat continuous charge distributions in the Continuous Fast Multipole Method (CFMM) [61], the Generalized very Fast Multipole Method (GvFMM) [62] and others [63, 64]. Calculation of the Coulomb contribution can be speeded up by using density-fitting techniques [65, 66], where the density is expanded in a set of auxiliary basis functions, thereby reducing the four-center integrals to three- and two-center types. The standard density-fitting method, however, does not scale linearly. To achieve linearly scaled density fitting, two different approaches have been implemented based on the use of a local metric [67–69] and on a spatial partitioning of the electron density [67, 70, 71].

The exchange contribution describes a local quantity, and therefore it should scale linearly. However, as shown in Ref. [72], a straightforward implementation leads to a scaling slightly lower than $\mathcal{O}(N^2)$ due to a slow decay of the off-diagonal elements of the density matrix arising from the basis set superposition errors. To reduce the scaling, a new screening technique was therefore introduced in the order-N exchange (ONX) method [72]. A similar accuracy was accomplished in the near-field exchange (NFX) method [73] based on the FMM technique. The ONX method was then improved by exploiting the locality of the density matrix [74]. The LinK method [75], which is similar to the ONX method was also introduced. LinK, however, also exploits the permutational symmetry of the integrals, which radically speeds up the calculation.

The most popular DFT functionals are of local nature, and it should therefore be possible

to obtain linear scaling. However, the exchange-correlation matrix is evaluated by numerical integration and the complexity depends both on the number of grid points and basis functions. By using the partition functions to decompose the integrals, Pérez–Jordá and Yang [76] presented a linearly scaled scheme that is independent of the number on basis functions. Later, an efficient atomic weight scheme [77] for fast linearly scaled evaluation of the exchange-correlation contribution was developed. There were other attempts to obtain an efficient evaluation of the exchange-correlation contribution that are not presented in this thesis, *e.g.* in Refs. [78, 79].

3 Standard Response Theory

To relate results obtained by theoretical methods to experimental values, it has to be possible to measure calculated quantities experimentally. For that reason, theoretical treatment of molecular properties attracted the attention of many groups. Using quantum chemical methods, it is nowadays possible to investigate a large number of molecular properties of increasing complexity [17].

Static (time-independent) molecular properties, *e.g.* dipole moments and time-independent polarizabilities, may be obtained from the derivatives of the energy with respect to perturbing field. However, a great interest in dynamical (time-dependent) properties led to the development of response theory.

When a molecule is in the presence of a time-dependent external field oscillating with a specified frequency, its observables start to oscillate and therefore become time-dependent. The interaction between the molecular system and the external field may be described using response theory. The response of the observable may be expanded in powers of the field strength: the linear response of the system is determined by the linear response function, the quadratic response of the system by the quadratic response function, etc. [80]. The response functions are used to calculate molecular response properties, *e.g.* a frequency-dependent linear polarizability, may be evaluated from the linear response function. From the poles and residues of the response functions, excitation energies, oscillator strength parameters for multi-photon transitions and excited state properties may be obtained [16].

In this chapter, the interaction between a molecular system and a general time-dependent field will be examined in order to determine the linear and quadratic response functions. Standard response theory for an exact state will be described in Section 3.1, and approximate response theory will be discussed in Section 3.2.

3.1 Exact response theory

In this section response theory for the exact state will be discussed in the quasi-energy formulation. In Section 3.1.1, a framework is introduced. Response functions in the quasi-energy formulation are described in Section 3.1.2 and their physical interpretations are given in Section 3.1.3. In Section 3.1.4, exact response equations are derived and the first- and higher-order equations are described in Sections 3.1.5 and 3.1.6, respectively.

3.1.1 A time evolution of an exact state

The time development of the exact wavefunction of a system in the presence of a general external field is governed by the time-dependent Schrödinger equation, which in atomic units has the form

$$\hat{H}|\bar{0}(t)\rangle = i\frac{\partial}{\partial t}|\bar{0}(t)\rangle\,. \tag{3.1}$$

$\hat{H}$ is the total Hamiltonian operator given as

$$\hat{H} = \hat{H}_0 + \hat{V}^t, \tag{3.2}$$

where $\hat{H}_0$ is the time-independent Hamiltonian of the unperturbed system fulfilling the time-independent Schrödinger equation in Eq. (2.1), and $\hat{V}^t$ is the time-dependent perturbation.

The perturbation operator $\hat{V}^t$ is Hermitian and periodic, and may be written in the frequency (instead of time) domain

$$\hat{V}^t = \sum_{j=-N}^{N} \exp(-i\omega_j t)\hat{V}^{\omega_j}; \qquad \hat{V}^{\omega_j} = \sum_B \varepsilon_B(\omega_j)B\,, \tag{3.3}$$

where $\varepsilon_B(\omega_j)$ is the perturbation strength parameter for the B operator at frequency ω_j that controls the field amplitude. To ensure the Hermiticity of $\hat{V}^t$, the following relations need to be fulfilled

$$\omega_{-j} = -\omega_j\,, \tag{3.4}$$

$$\varepsilon_B(\omega_j) = \varepsilon_B(\omega_{-j})^*\,, \tag{3.5}$$

$$B = B^\dagger\,. \tag{3.6}$$

By combining the frequency (j) and the operator (B) indices into a common index (b), Eq. (3.3) may be written in a compact form

$$\hat{V}^t = \sum_b \exp(-i\omega_b t)\varepsilon_b B\,, \tag{3.7}$$

where $\varepsilon_b = \varepsilon_B(\omega_j) = \varepsilon_B(-\omega_j)^* = \varepsilon^*_{-b}$.

The wave function $|\bar{0}\rangle$ in Eq. (3.1) may be written in a phase-isolated form

$$|\bar{0}\rangle = \exp[-iF(t)]|\tilde{0}\rangle \tag{3.8}$$

where $|\tilde{0}\rangle$ is a time-dependent function that may be expanded in orders of the perturbation strengths

$$|\tilde{0}\rangle = |0\rangle + |\tilde{0}^{(1)}(t)\rangle + |\tilde{0}^{(2)}(t)\rangle + \dots\,, \tag{3.9}$$

and is chosen to be normalized ($\langle\tilde{0}|\tilde{0}\rangle = 1$).

When a time-dependent perturbation is applied, the energy is not an eigenvalue of the total Hamiltonian in Eq. (3.1). Instead, the quasi-energy $Q(t)$ may be introduced as the time derivative of the phase function in Eq. (3.8), $\dot{F}(t)$. Inserting Eq. (3.8) into the time-dependent Schrödinger equation in Eq. (3.1), and using the fact that $\hat{H}$ commutes with the phase factor $\exp[-iF(t)]$, the quasi-energy may be determined as

$$Q(t) = \dot{F}(t) = \langle\tilde{0}|\hat{H} - i\tfrac{\partial}{\partial t}|\tilde{0}\rangle\,. \tag{3.10}$$

Using Eq. (2.1) and the normalization condition, it can be seen that $Q(t) \to E_0$ for the unperturbed system.

3.1.2 Response functions in the quasi-energy formulation

Response theory is based on the fact that the observable of a molecule in the presence of an external field may be expanded in powers of the field strength. In general, the expectation value of an operator A for a time-dependent function $|\bar{0}(t)\rangle$ can be expanded in the series [80]

$$\begin{aligned} A_{\mathrm{Av}}(t) &= \langle\bar{0}(t)|A|\bar{0}(t)\rangle = \langle\tilde{0}(t)|A|\tilde{0}(t)\rangle = \\ &= \langle 0|A|0\rangle + \sum_b \exp(-i\omega_b t)\langle\langle A;B\rangle\rangle_{\omega_b}\varepsilon_b \\ &+ \tfrac{1}{2}\sum_{b,c} \exp[-i(\omega_b+\omega_c)t]\langle\langle A;B,C\rangle\rangle_{\omega_b,\omega_c}\varepsilon_b\varepsilon_c \\ &+ \tfrac{1}{6}\sum_{b,c,d} \exp[-i(\omega_b+\omega_c+\omega_d)t]\langle\langle A;B,C,D\rangle\rangle_{\omega_b,\omega_c,\omega_d}\varepsilon_b\varepsilon_c\varepsilon_d \\ &+ \cdots\,. \end{aligned} \tag{3.11}$$

The function $\langle\langle A;B\rangle\rangle_{\omega_b}$ is denoted the linear response function. The functions $\langle\langle A;B,C\rangle\rangle_{\omega_b,\omega_c}$ and $\langle\langle A;B,C,D\rangle\rangle_{\omega_b,\omega_c,\omega_d}$ are known as the quadratic and cubic response functions, respectively. To obtain a unique definition of the response functions, they are defined to be symmetric with respect to interchange of the integration variables, *i.e.* symmetric under simultaneous permutation of frequency indices and operators (*e.g.* $\langle\langle A;B,C\rangle\rangle_{\omega_b,\omega_c} = \langle\langle A;C,B\rangle\rangle_{\omega_c,\omega_b}$).

Response functions may be identified by applying the quasi-energy formalism [43, 44]. Following Ref. [43], a time-averaged quasi-energy

$$\{Q(t)\}_T = \frac{1}{T}\int_{-T/2}^{T/2} Q(t)dt\,, \tag{3.12}$$

fulfills the variational principle

$$\delta\{Q(t)\}_T = 0\,, \tag{3.13}$$

where T is a common period for all frequencies in V^t in Eq. (3.7). Furthermore, the time-averaged quasi-energy satisfies a generalized Hellmann–Feynman theorem [81, 82]

$$\frac{d\{Q(t)\}_T}{d\varepsilon_a} = \left\{ \langle \tilde{0}|A|\tilde{0}\rangle \exp(-i\omega_a t) \right\}_T . \tag{3.14}$$

By combining Eqs. (3.11) and (3.14) the linear, quadratic, and cubic response functions may be identified as

$$\langle\langle A; B\rangle\rangle_{\omega_b} = \left. \frac{d^2\{Q(t)\}_T}{d\varepsilon_a d\varepsilon_b} \right|_{\varepsilon=0} ; \qquad \omega_a = -\omega_b , \tag{3.15a}$$

$$\langle\langle A; B, C\rangle\rangle_{\omega_b,\omega_c} = \left. \frac{d^3\{Q(t)\}_T}{d\varepsilon_a d\varepsilon_b d\varepsilon_c} \right|_{\varepsilon=0} ; \qquad \omega_a = -\omega_b - \omega_c , \tag{3.15b}$$

$$\langle\langle A; B, C, D\rangle\rangle_{\omega_b,\omega_c,\omega_d} = \left. \frac{d^4\{Q(t)\}_T}{d\varepsilon_a d\varepsilon_b d\varepsilon_c d\varepsilon_d} \right|_{\varepsilon=0} ; \qquad \omega_a = -\omega_b - \omega_c - \omega_d , \tag{3.15c}$$

and similarly for higher-order response functions. ε denotes the entire set of perturbation strengths.

Eqs. (3.15a)–(3.15c) have similar forms in time-independent theory. Dynamic molecular properties may be obtained from quasi-energy derivatives, whereas static properties are constructed as energy derivatives [since the energy is well-defined in the time-independent Schrödinger equation in Eq. (2.1)].

3.1.3 Physical interpretation of response functions

The linear response function has the form [16]

$$\langle\langle A; B\rangle\rangle_\omega = \sum_n \left(\frac{A^{0n} B^{n0}(\omega)}{\omega - \omega_n} - \frac{B^{0n}(\omega) A^{n0}}{\omega + \omega_n} \right) , \tag{3.16}$$

where $A^{nm} = \langle n|A|m\rangle$ is a transition matrix element of the operator A between states $|n\rangle$ and $|m\rangle$. When an external homogeneous electric field oscillating with frequency ω_b is applied on a molecule with a dipole moment μ, the response of the system may be obtained from the expansion in Eq. (3.11), where the operator A refers to the electric dipole operator. The (μ_α, μ_β)th component of the linear response function gives the $\alpha\beta$ component of the frequency-dependent linear polarizability tensor

$$\alpha_{\alpha\beta} = -\langle\langle \mu_\alpha; \mu_\beta \rangle\rangle_{\omega_b} = -\sum_m \left(\frac{\mu_\alpha^{0m} \mu_\beta^{m0}}{\omega_b - \omega_m} - \frac{\mu_\beta^{0m} \mu_\alpha^{m0}}{\omega_b + \omega_m} \right) . \tag{3.17}$$

The frequency-dependent dipole polarizability describes the absorption of one photon of energy ω_b and the emission of one photon of energy ω_b. The residues corresponding to the

poles at $\omega_b = \pm\omega_f$ of Eq. (3.17),

$$\lim_{\omega_b \to \omega_f} (\omega_b - \omega_f) \langle\langle \mu_\alpha; \mu_\beta \rangle\rangle_{\omega_b} = \mu_\alpha^{0f} \mu_\beta^{f0} \,, \tag{3.18a}$$

$$\lim_{\omega_b \to -\omega_f} (\omega_b + \omega_f) \langle\langle \mu_\alpha; \mu_\beta \rangle\rangle_{\omega_b} = -\mu_\alpha^{f0} \mu_\beta^{0f} \,, \tag{3.18b}$$

yield information about the dipole transition matrix element between the reference state $|0\rangle$ and the excited state $|f\rangle$.

The quadratic response function may be written as

$$\begin{aligned} \langle\langle A; B, C \rangle\rangle_{\omega_b, \omega_c} &= \\ &= \frac{1}{2} \Bigg(\frac{A^{0n} B^{nm} C^{m0}}{(\omega_b + \omega_c - \omega_n)(\omega_c - \omega_m)} + \frac{A^{0n} C^{nm} B^{m0}}{(\omega_b + \omega_c - \omega_n)(\omega_b - \omega_m)} + \\ &\quad + \frac{C^{0n} B^{nm} A^{m0}}{(\omega_b + \omega_c + \omega_n)(\omega_c + \omega_m)} + \frac{B^{0n} C^{nm} A^{m0}}{(\omega_b + \omega_c + \omega_n)(\omega_b + \omega_m)} + \\ &\quad + \frac{B^{0n} A^{nm} C^{m0}}{(\omega_b + \omega_n)(\omega_c - \omega_m)} + \frac{C^{0n} A^{nm} B^{m0}}{(\omega_c + \omega_n)(\omega_b - \omega_m)} \Bigg) \,. \end{aligned} \tag{3.19}$$

When a homogeneous electric external fields of frequencies ω_b and ω_c are applied on a molecule with a dipole moment μ, the quadratic response of the system may be obtained from Eq. (3.19), where the operators A, B and C refer to components of the electric dipole operator. The $(\mu_\alpha, \mu_\beta, \mu_\gamma)$-th component of the quadratic response function is identical to the (minus) $(\alpha\beta\gamma)$th component of the electric frequency-dependent dipole hyperpolarizability tensor [83] at frequencies ω_b, ω_c. The frequency-dependent hyperpolarizability describes the absorption of two photons, one of frequency ω_b and one of frequency ω_c, and the emission of one photon of frequency $\omega = \omega_b + \omega_c$.

Various first-, second- and third-order properties and their physical relevance are listed in Table 3.1.

3.1.4 Response equations

The response equations have the same form to all orders in the perturbation. They can be determined by differentiation of Eq. (3.13) with respect to the perturbation strengths. An exponential parameterization of the perturbed wavefunction can be introduced as [16]

$$|\tilde{0}\rangle = \exp[X(t)]|0\rangle \,, \tag{3.20}$$

where $X(t)$ is an anti-Hermitian operator given as

$$X(t) = x_p(t) R_p \,, \tag{3.21}$$

Table 3.1: Definition and physical relevance of the various (frequency-dependent) polarizabilities and hyperpolarizabilities. The table has been taken from Ref. [17].

(hyper)polarizability	physical effect
$\alpha(0;0)$	static polarizability
$\alpha(-\omega;\omega)$	frequency-dependent polarizability
$\beta(0;0,0)$	static first hyperpolarizability
$\beta(-2\omega;\omega,\omega)$	second harmonic generation (SHG)
$\beta(-\omega;\omega,0)$	dc-Pockels effect (dc-P);
	electro-optical Pockels Effect (EOPE)
$\beta(0;-\omega,\omega)$	optical rectification (OR)
$\gamma(0;0,0,0)$	static second hyperpolarizability
$\gamma(-3\omega;\omega,\omega,\omega)$	third harmonic generation (THG)
$\gamma(-2\omega;\omega,\omega,0)$	dc-second harmonic generation (dc-SHG);
	electric field induced SHG (EFISH or ESHG)
$\gamma(-\omega;\omega,-\omega,\omega)$	intensity-dependent refractive index (IDRI);
	degenerate four wave mixing (DFWM)
$\gamma(-\omega_1;\omega_1,-\omega_2,\omega_2)$	ac-Kerr effect (ac-K);
	optical Kerr effect (OKE)
$\gamma(-\omega;\omega,0,0)$	dc-Kerr effect (dc-K);
	electro-optical Kerr effect (EOKE)
$\gamma(0;\omega,-\omega,0)$	dc-optical rectification (dc-OR);
	electric field induced optical rectification (EFIOR)

where the Einstein summation have been used. R_p represents both excitations and deexcitations

$$R_p = \begin{cases} |p\rangle\langle 0| & p{>}0 \\ |0\rangle\langle p| & p{<}0 \end{cases} . \tag{3.22}$$

$|p\rangle$ denotes an excited state state which fulfills the time-independent Schrödinger equation

$$\hat{H}_0|p\rangle = E_p|p\rangle\,, \tag{3.23}$$

and is orthonormal to all other excited states

$$\langle p|n\rangle = \delta_{pn}. \tag{3.24}$$

The time-dependent response parameters $x_p(t)$ in Eq. (3.21) are collected in a vector $\mathbf{x}(t)$ and determine the response of the reference state to the perturbation. $\mathbf{x}(t)$ can be expanded in powers of the perturbation

$$\mathbf{x}(t) = \mathbf{x}^{(1)}(t) + \mathbf{x}^{(2)}(t) + \dots \tag{3.25}$$

where the zeroth-order coefficient vanishes due to the Brillouin theorem [84].

Analogously to the potential expansion in Eq. (3.7), a time-dependent state $|\tilde{0}\rangle$ may be determined using the quasi-energy formulation. The parameters in Eq. (3.25) may be expanded in terms of their frequency components

$$\mathbf{x}^{(1)}(t) = \sum_b \exp(-i\omega_b t)\mathbf{x}^{\omega_b}; \qquad \mathbf{x}^{\omega_b} = \varepsilon_b \mathbf{x}^b\,, \tag{3.26a}$$

$$\mathbf{x}^{(2)}(t) = \sum_{b,c} \exp(-i\omega_{bc} t)\mathbf{x}^{\omega_{bc}}; \qquad \mathbf{x}^{\omega_{bc}} = \frac{1}{2}\varepsilon_b\varepsilon_c \mathbf{x}^{bc}\,, \tag{3.26b}$$

$$\dots$$

$$\mathbf{x}^{(f)}(t) = \sum_{b,\dots,f} \exp(-i\omega_{b\dots f} t)\mathbf{x}^{\omega_{b\dots f}}; \qquad \mathbf{x}^{\omega_{b\dots f}} = \frac{1}{f!}\varepsilon_b \dots \varepsilon_f \mathbf{x}^{b\dots f}\,, \tag{3.26c}$$

where $\omega_{bc} = \omega_b + \omega_c$, $\omega_{b\dots f} = \omega_b + \dots + \omega_f, \dots$. The time derivative of a general response vector $\dot{\mathbf{x}}^{(f)}(t)$ may be written in a simple form

$$\dot{\mathbf{x}}^{(f)}(t) = -i \sum_{b,\dots,f} \omega_{b\dots f} \exp(-i\omega_{b\dots f} t)\mathbf{x}^{\omega_{b\dots f}}\,. \tag{3.27}$$

Using the exponential parameterization in Eq. (3.20), the quasi-energy in Eq. (3.10) takes the form

$$Q(t) = \langle 0| \exp[-X(t)](\hat{H} - i\tfrac{\partial}{\partial t}) \exp[X(t)]|0\rangle\,, \tag{3.28}$$

which leads to the time-averaged quasi-energy

$$\begin{aligned}\{Q(t)\}_T = \big\{ &\langle 0|\hat{H} - i\tfrac{\partial}{\partial t} + [\hat{H}, X(t)] - i\dot{X}(t) + \\ &+\tfrac{1}{2}\big[[\hat{H}, X(t)] - i\dot{X}(t), X(t)\big] + \dots |0\rangle \big\}_T\,,\end{aligned} \tag{3.29}$$

where the Baker-Campbell-Hausdorff (BCH) expansion and the commutator relation

$$[\hat{H} - i\tfrac{\partial}{\partial t}, X(t)] = [\hat{H}, X(t)] - i\dot{X}(t)\,, \tag{3.30}$$

have been used. The time-averaged quasi-energy $\{Q(t)\}_T$ is variational with respect to all response parameters, *e.g.* $x_p^{\omega_{b\dots g}}$. Using Eq. (3.29), Eq. (3.13) may be written as

$$\begin{aligned}0 = \frac{\partial\{Q(t)\}_T}{\partial x_p^{\omega_{b\dots g}}} = \Big\{ &\langle 0|[\hat{H}, R_p] - \omega_{b\dots g} R_p + \tfrac{1}{2}\big[[\hat{H}, R_p] - \omega_{b\dots g} R_p, X(t)\big] + \\ &+ \tfrac{1}{2}[[\hat{H}, X(t)] - i\dot{X}(t), R_p] + \mathcal{O}(X^2)|0\rangle \exp(-i\omega_{b\dots g} t) \Big\}_T\,,\end{aligned} \tag{3.31}$$

where Eq. (3.26c) and (3.27) have been used. $\mathcal{O}(X^2)$ denotes second- and higher-order terms. Response equations to arbitrary order may now be determined by differentiation of Eq. (3.31) with respect to the perturbation strengths.

3.1.5 The first-order equations

The first-order response equation for $\mathbf{x}^b$ is obtained by differentiating Eq. (3.31) with respect to ε_b

$$\begin{aligned} 0 &= \frac{d}{d\varepsilon_b}\left(\frac{\partial\{Q(t)\}_T}{\partial x_p^{\omega_{b\ldots g}}}\right)\Big|_{\varepsilon=0} \\ &= \Big\{\langle 0|[B,R_p] + \tfrac{1}{2}\big[[\hat{H}_0,R_p]-\omega_{b\ldots g}R_p,R_q\big]x_q^b \\ &\quad + \tfrac{1}{2}\big[[\hat{H}_0,R_q]-\omega_b R_q,R_p\big]x_q^b|0\rangle\exp(-i(\omega_b+\omega_{b\ldots g})t)\Big\}_T , \end{aligned} \tag{3.32}$$

where the Einstein summation is used for the repeated index q. Eq. (3.32) may be written as

$$\big(-\tfrac{1}{2}\langle 0|\big[[\hat{H}_0,R_p],R_q\big]+\big[[\hat{H}_0,R_q],R_p\big]|0\rangle - \omega_b\langle 0|[R_p,R_q]|0\rangle\big)x_q^b = \langle 0|[B,R_p]|0\rangle\,, \tag{3.33}$$

or in a more convenient form

$$(\mathbf{E}^{[2]}-\omega_b\mathbf{S}^{[2]})\mathbf{x}^b = \mathbf{g}^b\,, \tag{3.34}$$

where x_q^b have been collected to $\mathbf{x}^b$, and the generalized Hessian $\mathbf{E}^{[2]}$, metric matrix $\mathbf{S}^{[2]}$ and the gradient vector $\mathbf{g}^b$ have been defined as

$$E_{pq}^{[2]} = -\tfrac{1}{2}\langle 0|\big[[\hat{H}_0,R_p],R_q\big]+\big[[\hat{H}_0,R_q],R_p\big]|0\rangle\,, \tag{3.35}$$

$$S_{pq}^{[2]} = \langle 0|[R_p,R_q]|0\rangle\,, \tag{3.36}$$

$$g_p^b = \langle 0|[B,R_p]|0\rangle\,. \tag{3.37}$$

The $\mathbf{E}^{[2]}$ and $\mathbf{S}^{[2]}$ matrices have block structures

$$\mathbf{E}^{[2]} = \begin{pmatrix}\mathbf{A} & \mathbf{B}\\ \mathbf{B}^\star & \mathbf{A}^\star\end{pmatrix}; \quad \mathbf{S}^{[2]} = \begin{pmatrix}\boldsymbol{\Sigma} & \boldsymbol{\Delta}\\ -\boldsymbol{\Delta}^\star & -\boldsymbol{\Sigma}^\star\end{pmatrix}, \tag{3.38}$$

and their detailed composition will be discussed in Section 3.2.2. Inserting the explicit expression for R_p in Eq. (3.22) into Eq. (3.35), $\mathbf{E}^{[2]}$ and $\mathbf{S}^{[2]}$ may be written in diagonal form

$$\mathbf{E}^{[2]} = \begin{pmatrix}\boldsymbol{\omega}_k & \mathbf{0}\\ \mathbf{0} & \boldsymbol{\omega}_k^*\end{pmatrix}; \quad \mathbf{S}^{[2]} = \begin{pmatrix}\mathbf{1} & \mathbf{0}\\ \mathbf{0} & -\mathbf{1}\end{pmatrix}, \tag{3.39}$$

where $\boldsymbol{\omega}_k$ is a diagonal matrix containing the excitation energies.

Using the diagonal structure of the matrices in Eq. (3.39) and assuming that $\omega_k^\star = \omega_k$, the first-order response equation in Eq. (3.34) may be written as

$$\begin{pmatrix} {}^1\mathbf{x}_k^b \\ {}^2\mathbf{x}_{-k}^b \end{pmatrix} = \begin{pmatrix} (\boldsymbol{\omega}_k - \boldsymbol{\omega}_b)^{-1} & \mathbf{0} \\ \mathbf{0} & (\boldsymbol{\omega}_k + \boldsymbol{\omega}_b)^{-1} \end{pmatrix} \begin{pmatrix} {}^1\mathbf{g}_{-k}^b \\ {}^2\mathbf{g}_k^b \end{pmatrix}, \quad (k > 0)\,, \tag{3.40}$$

where $\boldsymbol{\omega}_b$ is a diagonal matrix with the frequency ω_b in all diagonal elements. $\mathbf{x}^b$ and $\mathbf{g}^b$ have been divided into two sub-vectors to emphasize that the upper and lower parts of $\mathbf{x}^b$ decouple due to the diagonal structure of $\mathbf{E}^{[2]}$ and $\mathbf{S}^{[2]}$.

3.1.6 Higher-order equations

The structure of the set of linear equations in Eq. (3.34) can be reproduced for all higher-order response parameters. The f'th order response equation ($f \geq 2$) is obtained by differentiating Eq. (3.31) with respect to the perturbation strength parameters $\{\varepsilon_b, \ldots, \varepsilon_f\}$

$$\begin{aligned} 0 = \frac{d^f}{d\varepsilon_b \ldots d\varepsilon_f} \Big\{ &\langle 0|[\hat{H}, R_p] - \omega_{b\ldots g} R_p + \tfrac{1}{2}\big[[\hat{H}, R_p] - \omega_{b\ldots g} R_p, x(t)\big] + \\ &+ \tfrac{1}{2}[[\hat{H}, x(t)] - i\dot{x}(t), R_p] + \mathcal{O}(x^2)|0\rangle \exp(-i\omega_{b\ldots g} t) \Big\}_T \Big|_{\varepsilon=0} . \end{aligned} \tag{3.41}$$

Eq. (3.41) may be written as

$$\begin{aligned} 0 = \Big\{ \Big(&\langle 0|\tfrac{1}{2}\big[[\hat{H}_0, R_p] - \omega_{b\ldots g} R_p, R_q\big] x_q^{b\ldots f} + \\ &+ \tfrac{1}{2}\big[[\hat{H}_0, R_q] - \omega_{b\ldots f} R_q, R_p\big] x_q^{b\ldots f} |0\rangle + g_p^{b\ldots f} \Big) \exp(-i(\omega_{b\ldots f} + \omega_{b\ldots g})t) \Big\}_T , \end{aligned} \tag{3.42}$$

where the right-hand side vector $\mathbf{g}^{b\ldots f}$ contains only response parameters of orders $(f-1)$ and lower. After rearrangement and insertion of Eqs. (3.35) and (3.36) the f'th order response equation reads

$$(\mathbf{E}^{[2]} - \omega_{b\ldots f}\mathbf{S}^{[2]})\mathbf{x}^{b\ldots f} = \mathbf{g}^{b\ldots f} . \tag{3.43}$$

By comparing Eqs. (3.34) and (3.43), it can be seen that all response equations may be formulated as a system of linear equations of the same form.

The general f'th order response equation in Eq. (3.43) may be written as

$$\begin{pmatrix} {}^1\mathbf{x}_k^{b\ldots f} \\ {}^2\mathbf{x}_{-k}^{b\ldots f} \end{pmatrix} = \begin{pmatrix} (\boldsymbol{\omega}_k - \boldsymbol{\omega}_{b\ldots f})^{-1} & \mathbf{0} \\ \mathbf{0} & (\boldsymbol{\omega}_k + \boldsymbol{\omega}_{b\ldots f})^{-1} \end{pmatrix} \begin{pmatrix} {}^1\mathbf{g}_{-k}^{b\ldots f} \\ {}^2\mathbf{g}_k^{b\ldots f} \end{pmatrix}, \quad (k > 0)\,, \tag{3.44}$$

that is similar to the first-order response equation in Eq. (3.40)

3.2 Approximate Standard Response Theory

In the previous section, the time evolution of an exact wavefunction has been discussed. However, in practice only approximate wavefunctions are available, and response theory therefore has to be considered for such a wavefunction. In this section, the response theory introduced in Section 3.1 will be considered for the HF model discussed in Section 2.1.

In Section 3.2.1, response equations for HF approximate state are derived. Structures of the response matrices are discussed in Section 3.2.2. In Section 3.2.3, the linear-scaling framework for solving response equations is introduced.

3.2.1 Response equations for the Hartree–Fock response theory

In the HF approximation, the wavefunction in the second quantization formulation is given by

$$|0\rangle = a^\dagger_{i\beta}a^\dagger_{i\alpha}a^\dagger_{j\beta}a^\dagger_{j\alpha}\dots a^\dagger_{l\beta}a^\dagger_{l\alpha}|\mathrm{vac}\rangle\,. \tag{3.45}$$

$a^\dagger_{i\beta}a^\dagger_{i\alpha}a^\dagger_{j\beta}a^\dagger_{j\alpha}\dots a^\dagger_{l\beta}a^\dagger_{l\alpha}$ refers to the set of orthonormal spin-orbitals that are occupied in $|0\rangle$, and $a^\dagger_{i\alpha}$ and $a^\dagger_{i\beta}$ refer to spin-orbitals with spin α and β, respectively.

When a time-dependent external field is applied to the system, the wavefunction in Eq. (3.45) changes into another single determinant wavefunction $|\tilde{0}\rangle$. This time-dependence can be introduced (using an exponential parameterization) for the phase-isolated wavefunction for the perturbed system

$$|\tilde{0}\rangle = \exp(i\hat{\kappa})|0\rangle\,, \tag{3.46}$$

where $\hat{\kappa}$ is a Hermitian operator of the form [10]

$$\hat{\kappa} = \sum_{PQ}\kappa_{PQ}(t)(a^\dagger_{P\alpha}a_{Q\alpha} + a^\dagger_{P\beta}a_{Q\beta}) = \sum_p \kappa_p(t)R_p\,, \tag{3.47}$$

for the external field of a singlet symmetry. Indices PQ have been combined to a common index p in R_p, and summation runs over both positive and negative indices.

The parameters $\boldsymbol{\kappa}$ can be expanded in powers of the perturbation [analogously to Eq. (3.25)]

$$\boldsymbol{\kappa} = \boldsymbol{\kappa}^{(1)}(t) + \boldsymbol{\kappa}^{(2)}(t) + \cdots\,, \tag{3.48}$$

where the zeroth-order coefficient vanishes due to the Brillouin theorem [84].

Since the HF wavefunction $|0\rangle$ is variational, a time-dependent HF state $|\tilde{0}\rangle$ may be determined using the quasi-energy formulation in a way analogous to the one described in Section 3.1.4. The parameters in Eq. (3.25) may be expanded in terms of their frequency components as in Eqs. (3.26a)–(3.26c). Using the exponential parameterization in Eq. (3.46),

the time-averaged quasi-energy may be obtained similarly to Eqs. (3.28) and (3.29). Since the time-averaged quasi-energy $\{Q(t)\}_T$ is variational with respect to all response parameters, Eq. (3.13) may be rewritten as

$$0 = \frac{\partial\{Q(t)\}_T}{\partial\kappa_p^{\omega_{b\ldots g}}} = \Big\{\langle 0|[\hat{H}, R_p] - \omega_{b\ldots g}R_p + \tfrac{1}{2}\big[[\hat{H}, R_p] - \omega_{b\ldots g}R_p, \kappa(t)\big] + \\ + \tfrac{1}{2}[[\hat{H}, \kappa(t)] - i\dot{\kappa}(t), R_p] + \mathcal{O}(\kappa^2)|0\rangle \exp(-i\omega_{b\ldots g}t)\Big\}_T , \tag{3.49}$$

which is similar to Eq. (3.31). Response equations may be determined by differentiation of Eq. (3.49) with respect to the perturbation strengths, as shown in Section 3.1. The first-order equations are in the form of Eq. (3.34), where κ_q^b parameters have been collected into $\mathbf{x}^b$, which for the approximate wavefunctions will be denoted as $\boldsymbol{X}$. [2] Both in the exact and the approximate theories the Hessian and metric matrices have the block structure given in Eq. (3.38). Due to the fact that the structures are not identical, as described in details in the next section, the Hessian and metric matrices for an approximate state will be denoted as $\boldsymbol{E}^{[2]}$ and $\boldsymbol{S}^{[2]}$, respectively.

3.2.2 The structure of the response matrices $\boldsymbol{E}^{[2]}$ and $\boldsymbol{S}^{[2]}$

The Hessian and metric matrices, for both exact and approximate wavefunction, are symmetric matrices of the block structure given in Eq. (3.38), where

$$\begin{aligned} A_{pq} &= \langle 0|[[\hat{H}_0, R_{-p}], R_q]|0\rangle, \quad B_{pq} = \langle 0|[[\hat{H}_0, R_{-p}], R_{-q}]|0\rangle, \\ \Sigma_{pq} &= \langle 0|[R_{-p}, R_q]|0\rangle, \qquad \Delta_{pq} = \langle 0|[R_{-p}, R_{-q}]|0\rangle\,. \end{aligned} \tag{3.50}$$

R_p and R_{-p} refer to excitation and deexcitation operators, respectively. $\mathbf{A}$, $\mathbf{B}$ and $\boldsymbol{\Sigma}$ in Eq. (3.38) are symmetric, and $\boldsymbol{\Delta}$ is antisymmetric, in both exact and approximate response theory [16]. For the exact state, R_p in Eq. (3.50) is defined in Eq. (3.22), whereas for the approximate wavefunction it is given as

$$R_p = R_{AI} = \tfrac{1}{\sqrt{2}}(a^\dagger_{A\alpha}a_{I\alpha} + a^\dagger_{A\beta}a_{I\beta})\,. \tag{3.51}$$

I and A refer to occupied and unoccupied molecular orbital (MO) indices, respectively.

For a closed shell system and the HF reference state $|0\rangle$ given in Eq. (3.45), the elements of $\boldsymbol{A}$, $\boldsymbol{B}$, $\boldsymbol{\Sigma}$ and $\boldsymbol{\Delta}$ become [85]

$$A_{pq} = A_{AI,BJ} = \delta_{AB}\delta_{IJ}(\varepsilon_A - \varepsilon_I) + (AI|JB) - (AB|IJ)\,, \tag{3.52a}$$

[2] Italic/Roman notation will be used for response vectors and matrices in the approximate response theory.

$$B_{pq} = B_{AI,BJ} = (AI|BJ) - (AJ|BI)\,, \tag{3.52b}$$

$$\Sigma_{pq} = \delta_{AB}\delta_{IJ}\,, \quad \Delta_{pq} = 0\,, \tag{3.52c}$$

where $(PQ|RS)$ is a two-electron integral in the MO basis. For KS-DFT theory, the two-electron integrals in Eqs. (3.52a) and (3.52b) have to be modified and an exchange-correlation contribution is added [86].

In exact response theory, $\mathbf{E}^{[2]}$ is given in Eq. (3.39). In the approximate response theory, the $\boldsymbol{E}^{[2]}$ matrix can be split into the zeroth and first-order contributions

$$\boldsymbol{E}^{[2]} = \boldsymbol{E}_0^{[2]} + \boldsymbol{E}_1^{[2]}\,. \tag{3.53}$$

$\boldsymbol{E}_0^{[2]}$ is a diagonal matrix containing the molecular orbital energy differences

$$\boldsymbol{E}_0^{[2]} = \begin{pmatrix} \boldsymbol{\varepsilon}_A - \boldsymbol{\varepsilon}_I & \mathbf{0} \\ \mathbf{0} & \boldsymbol{\varepsilon}_A - \boldsymbol{\varepsilon}_I \end{pmatrix}\,, \tag{3.54}$$

and $\boldsymbol{E}_1^{[2]}$ contains the electron-electron repulsion contributions to $\boldsymbol{E}^{[2]}$ as can be seen from Eqs. (3.52a) and (3.52b). For KS-DFT, an exchange-correlation contribution has to be added to $\boldsymbol{E}_1^{[2]}$. The metric matrix $\boldsymbol{S}^{[2]}$ in the MO representation is identical to the $\mathbf{S}^{[2]}$ for the exact state denoted in Eq. (3.39).

The solution vectors in Eq. (3.40) can also for an approximate state be written in the two-component form

$$\boldsymbol{X} = \begin{pmatrix} \boldsymbol{X}_{AI} \\ \boldsymbol{X}_{JB} \end{pmatrix}\,. \tag{3.55}$$

$\boldsymbol{X}_{AI}$ and $\boldsymbol{X}_{JB}$ are the excitation and deexcitation components, respectively.

The eigenvectors of the response eigenvalue equation

$$\boldsymbol{E}^{[2]}\boldsymbol{X}_k = \omega_k \boldsymbol{S}^{[2]}\boldsymbol{X}_k; \qquad \boldsymbol{E}^{[2]}\boldsymbol{X}_{-k} = -\omega_k \boldsymbol{S}^{[2]}\boldsymbol{X}_{-k} \tag{3.56}$$

can be chosen to be orthogonal with respect to the inner product induced by $\boldsymbol{E}^{[2]}$ and to satisfy a generalized normalization condition for $\boldsymbol{S}^{[2]}$

$$\boldsymbol{X}_l^\dagger \boldsymbol{E}^{[2]}\boldsymbol{X}_k = \omega_{k0}\delta_{kl}; \quad \boldsymbol{X}_l^\dagger \boldsymbol{S}^{[2]}\boldsymbol{X}_k = \mathrm{sgn}(k)\delta_{kl}\,, \tag{3.57}$$

respectively [16]. The excitation vectors may be collected as the columns of an eigenvector matrix $\boldsymbol{X}$ with the positive-sign eigenvectors collected first, followed by the negative-sign vectors [24]

$$\boldsymbol{X} = \{\ldots, \boldsymbol{X}_k, \ldots, \boldsymbol{X}_{-k}, \ldots\}\,. \tag{3.58}$$

In matrix form, Eq. (3.57) becomes

$$\boldsymbol{X}^\dagger \boldsymbol{E}^{[2]} \boldsymbol{X} = \begin{pmatrix} \boldsymbol{\omega}_k & \mathbf{0} \\ \mathbf{0} & \boldsymbol{\omega}_k^\star \end{pmatrix}; \quad \boldsymbol{X}^\dagger \boldsymbol{S}^{[2]} \boldsymbol{X} = \begin{pmatrix} \mathbf{1} & \mathbf{0} \\ \mathbf{0} & -\mathbf{1} \end{pmatrix}, \tag{3.59}$$

where $\boldsymbol{\omega}_k$ is a diagonal matrix containing the excitation energies [16], in analogy to exact theory in Eq. (3.39).

For the ground state, $\boldsymbol{E}^{[2]}$ is a positive definite matrix. To see this, $\boldsymbol{E}^{[2]}$ may be transformed to block diagonal form using the unitary matrix $\boldsymbol{U}$

$$\boldsymbol{U} = \frac{1}{\sqrt{2}} \begin{pmatrix} 1 & -1 \\ 1 & 1 \end{pmatrix}, \tag{3.60}$$

giving

$$\boldsymbol{U}^\dagger \boldsymbol{E}^{[2]} \boldsymbol{U} = \begin{pmatrix} \boldsymbol{A}+\boldsymbol{B} & \mathbf{0} \\ \mathbf{0} & \boldsymbol{A}-\boldsymbol{B} \end{pmatrix}. \tag{3.61}$$

$\boldsymbol{A}-\boldsymbol{B}$ represents a stability condition [87] with respect to real variations in the wave function $|0\rangle$, while $\boldsymbol{A}+\boldsymbol{B}$ is the stability condition with respect to an imaginary variation. For $|0\rangle$ being a ground state, both $\boldsymbol{A}-\boldsymbol{B}$ and $\boldsymbol{A}+\boldsymbol{B}$ are positive definite implying that $\boldsymbol{E}^{[2]}$ is positive definite.

It should be noted that $\boldsymbol{E}^{[2]}$ and $\boldsymbol{S}^{[2]}$ in the AO representation have the forms [24]

$$\boldsymbol{E}^{[2]} = \begin{pmatrix} \boldsymbol{A} & \boldsymbol{L} & \boldsymbol{B} \\ \boldsymbol{L}^\dagger & \boldsymbol{N} & \boldsymbol{L}^T \\ \boldsymbol{B}^\star & \boldsymbol{L}^\star & \boldsymbol{A}^\star \end{pmatrix}; \quad \boldsymbol{S}^{[2]} = \begin{pmatrix} \boldsymbol{\Sigma} & \boldsymbol{\theta} & \boldsymbol{\Delta} \\ \boldsymbol{\theta}^\dagger & \boldsymbol{\epsilon} & -\boldsymbol{\theta}^T \\ -\boldsymbol{\Delta}^\star & -\boldsymbol{\theta}^\star & -\boldsymbol{\Sigma}^\star \end{pmatrix} \tag{3.62}$$

where the explicit forms of $\boldsymbol{A}$, $\boldsymbol{B}$, $\boldsymbol{\Sigma}$ and $\boldsymbol{\Delta}$ given in Eq. (3.50)[3] and

$$\begin{aligned} L_{ij} &= \langle 0|[[\hat{H}_0, R_i], D_j]|0\rangle, \quad & N_{ij} &= \langle 0|[[\hat{H}_0, D_i], D_j]|0\rangle, \\ \theta_{ij} &= \langle 0|[R_i, D_j]|0\rangle, & \epsilon_{ij} &= \langle 0|[D_i, D_j]|0\rangle \end{aligned} \tag{3.63}$$

where $R_i^\dagger$, $D_i^\dagger$ and R_i are defined as

$$\begin{aligned} R_i^\dagger &= a_\mu^\dagger a_\nu, \quad \mu > \nu, \\ D_i^\dagger &= a_\mu^\dagger a_\mu, \\ R_i &= a_\nu^\dagger a_\mu, \quad \mu > \nu. \end{aligned} \tag{3.64}$$

μ, ν refer to atomic orbital indices and the $\boldsymbol{\epsilon}$ matrix vanishes for real orbitals.

[3]Matrices have the same form [given in Eq. (3.50)] in both MO and AO representations. The difference is that R_p in Eq. (3.50), is given by Eq. (3.51) in MO representation and by Eq. (3.64) in AO representation.

3.2.3 Linear-scaling framework

The major challenge in the computation of the linear and quadratic response functions is to obtain the solution to the set of response equations of the form in Eq. (3.43). In Ref. [23], Coriani *et al.* presented a linear-scaling implementation of HF and KS-DFT response equations for calculations of frequency-dependent molecular properties and excitation energies. The response equations are solved iteratively, using an AO basis subspace method. In order to obtain linear scaling the evaluation of all terms entering the response functions must scale linearly.

Since the linear equations are solved iteratively, the explicit forms of the generalized Hessian matrix $\boldsymbol{E}^{[2]}$ and the metric matrix $\boldsymbol{S}^{[2]}$ are not required. Linear transformations on vector $\mathbf{b}$, are defined as [23, 88]

$$\boldsymbol{\sigma} = \boldsymbol{E}^{[2]}(\boldsymbol{b}) = \mathbf{F}[\mathbf{b},\mathbf{D}]_{\mathbf{S}}\mathbf{S} - \mathbf{S}[\mathbf{b},\mathbf{D}]_{\mathbf{S}}\mathbf{F} + \mathbf{G}([\mathbf{b},\mathbf{D}]_{\mathbf{S}})\mathbf{DS} - \mathbf{SDG}([\mathbf{b},\mathbf{D}])_{\mathbf{S}}\,, \tag{3.65}$$

$$\boldsymbol{\rho} = \boldsymbol{S}^{[2]}(\boldsymbol{b}) = \mathbf{S}[\mathbf{b},\mathbf{D}]_{\mathbf{S}}\mathbf{S}\,, \tag{3.66}$$

where $\mathbf{F}$ is the Fock/KS matrix defined in Eq. (2.16), $\mathbf{D}$ is the AO density matrix given in Eq. (2.17) and $\mathbf{S}$ is the AO overlap matrix in Eq. (2.15). $\mathbf{G}(\mathbf{D})$ denotes the Coulomb and exchange contributions and for the perturbation field of singlet symmetry is given in Eq. (2.18). In KS-DFT, there is an additional contribution to $\mathbf{G}(\mathbf{D})$ from the exact-correlation potential.

The response theory formulation is based on atomic orbitals to exploit locality. Since the transformations in Eqs. (3.65) and (3.66) are based on matrix-matrix multiplications, significant savings can be obtained using sparse algebra, and linear-scaling can be achieved for this method.

4 Damped Response Theory

As mentioned in the previous chapter, to obtain frequency-dependent molecular properties, response equations need to be solved. Standard response functions have singularities when one or more of the optical frequencies equals an excitation energy [16], which leads to divergence when solving the response equations and an unphysical behavior for molecular properties. To obtain the correct physical behavior at resonance frequencies, the excited states damping factor (γ), also called an inverse effective lifetime or an excited-state lifetime broadening parameter [28–34], has been introduced.

In Ref. [28], Norman *et al.* extended the standard response theory formulation,[4] to include a phenomenological damping term that effectively introduces finite lifetimes of the excited states [34]. The approach by Norman *et al.* has been successfully applied to calculate a wide range of linear molecular properties including one-photon absorption (OPA) spectra and dispersion coefficients [29, 33, 89–94], optical rotation and electronic circular dichroism spectra [95–99], X-ray absorption and natural circular dichroism spectra [100–105], the dynamic dipole magnetizability [106] and relativistic linear response functions [107]. Nonlinear properties such as Raman scattering [108–118], the electro-optical Kerr effect, magnetic circular dichroism spectra [119–121] and the two-photon resonant enhanced second-harmonic generation response [28] corresponding to residues of the quadratic response function have also been addressed.

In Ref. [33] (Paper A), the quasi-energy formulation of the damped response theory has been presented. The use of the quasi-energy formulation allows to obtain directly the computationally simplest expressions for damped response functions by applying a set of response parameter elimination rules [45], which minimize the total number of damped response equations to be solved. In addition, in this formulation, perturbation-dependent basis sets by Thorvaldsen *et al.* [122] may easily be used to obtain gauge-origin independent results.

In Section 4.1, phenomenological damping of excited states is introduced. Exact damped response theory is described in Section 4.2. In Section 4.3 damped response equations are analyzed and the structure of damped response vectors at different frequencies is discussed in Section 4.4. In Section 4.5 and 4.6 damped linear and quadratic response theories are described, respectively. Damped response theory for an approximate state is given in Section 4.7 and in Section 4.8, comparison to the approach by Norman *et al.* [28] is presented.

[4] The formulation of the standard response theory based on the Ehrenfest theorem [15].

4.1 Phenomenological damping of excited states

A molecular system described by the Hamiltonian $\hat{H}_0$ and characterized by Eqs. (3.23) and (3.24) is considered. The time-dependent excited state $|n(t)\rangle$ obtained by multiplying $|n\rangle$ by an exponential phase factor

$$|n(t)\rangle = e^{-iE_n t}|n\rangle\,, \tag{4.1}$$

trivially satisfies the time-dependent Schrödinger equation

$$i\frac{\partial|n(t)\rangle}{\partial t} = H_0|n(t)\rangle = E_n|n(t)\rangle\,. \tag{4.2}$$

The norm of $|n(t)\rangle$ is constant in time, $\langle n(t)|n(t)\rangle = \langle n|n\rangle = 1$, and no decay occurs from the excited state to the ground state (or other excited states), suggesting that the lifetime of the excited state $|n(t)\rangle$ is infinite. In reality, an excited state has a finite lifetime which is not readily described by the Hamiltonian $\hat{H}_0$. However, a phenomenological description of the lifetime may be introduced by multiplying Eq. (4.1) with an exponential damping factor $e^{-\frac{1}{2}\Gamma_n t}$ to obtain the damped excited state $|\bar{n}(t)\rangle$ [30–32]

$$|\bar{n}(t)\rangle = e^{-\frac{1}{2}\Gamma_n t}|n(t)\rangle = e^{-i(E_n - \frac{i}{2}\Gamma_n)t}|n\rangle\,. \tag{4.3}$$

The norm of the damped excited state $|\bar{n}(t)\rangle$ decays exponentially in time

$$\langle\bar{n}(t)|\bar{n}(t)\rangle = e^{-\Gamma_n t}\,, \tag{4.4}$$

and Γ_n^{-1} may therefore be interpreted as the lifetime of the excited state $|\bar{n}(t)\rangle$, *i.e.* the time it takes before the population of the excited state has decreased by a factor of e^{-1}.

The non-damped state $|n(t)\rangle$ in Eq. (4.2) has a real energy E_n. By contrast, the damped excited state $|\bar{n}(t)\rangle$ does not possess a well-defined real energy due to its finite lifetime

$$i\frac{\partial|\bar{n}(t)\rangle}{\partial t} = (E_n - \tfrac{i}{2}\Gamma_n)|\bar{n}(t)\rangle\,. \tag{4.5}$$

The damping of the excited states is effectively obtained by introducing complex excitation energies $\bar{E}_n$

$$E_n \to \bar{E}_n = E_n - i\gamma_n; \qquad \gamma_n = \tfrac{1}{2}\Gamma_n\,, \tag{4.6}$$

for all excited states $|n(t)\rangle$, as may be seen comparing Eqs. (4.1) and (4.3).

In standard response theory (described in Chapter 3), transitions between the ground state and excited states are described in terms of oscillator strengths that are obtained from residues of response functions. This gives rise to a delta-peaked residue spectrum (absorption spectrum). In an experimental absorption spectrum, the peaks are broadened and the

oscillator strength is obtained by integration over the absorption band representing the electronic transition. The broadening of the electronic absorption bands may be associated with contributions arising from different physical phenomena:

- The isolated, non-moving molecule possesses a finite lifetime due to spontaneous emission which gives rise to an energy uncertainty manifested in a broadening of the absorption bands.
- The vibrational substructure of electronic absorption spectra leads to a broadening of the absorption bands.
- In an experiment, the molecules are moving relative to the detector which leads to Doppler broadening.
- Collisions among molecules perturb the electron densities and therefore the excited state energies leading to a broadening of the absorption bands.

The broadening of the absorption bands has been performed theoretically using a phenomenological description where an effective lifetime is introduced to account for the above physical phenomena [28–35]. In practice the broadening related to all the above phenomena is treated collectively and therefore the same lifetime $\Gamma^{-1} = (2\gamma)^{-1}$ is used for all excited states [28, 29, 33], where γ is an empirical parameter. In that case Eq. (4.6) simplifies to

$$E_n \to \bar{E}_n = E_n - i\gamma\,. \tag{4.7}$$

In response theory, the excited state energy E_n always enters in combination with the ground state energy E_0 as the excitation energy $\omega_n = E_n - E_0$, and Eq. (4.7) then corresponds to the replacement

$$\omega_n \to \bar{\omega}_n = \omega_n - i\gamma, \tag{4.8}$$

since the lifetime of the ground state is infinite and consequently $\Gamma_0 = 0$.

Response function theory where the replacement in Eq. (4.8) is carried out, is called damped response theory. When the damped response theory is used, singularities of the response functions at resonance frequencies are removed. For real perturbations operators, the real and the imaginary component of the damped response functions describes dispersion and absorption processes, respectively.

Molecular absorption properties in damped response theory will have an imposed Lorentzian line-shape function, which is identical to the one obtained from the solution to the

Schrödinger equation for a two-state system, where the coefficient of the upper level is required to decay exponentially in time [123]. The line-shape function associated with pure Doppler broadening is Gaussian, whereas the line-shape function describing pure collision broadening is Lorentzian (see *e.g.* Ref. [124]). The experimental line-shape function is more complicated, as it encompasses all the phenomena discussed above, but the structure of an absorption spectrum obtained using damped response theory will be qualitatively correct.

In standard response theory the absorption spectra are obtained by superimposing Lorentzian line-shape functions onto the stick spectra obtained by solving a generalized eigenvalue problem. This approach is feasible for small systems, which have a relatively low density of low lying excited states. In case of large molecular systems with a high density of low lying states, it may be difficult to determine the absorption spectra using standard response theory. The damped response theory can be used to determine the absorption spectra in the whole frequency range. The spectra obtained with standard and damped response theory are similar.[5]

Throughout this chapter, a bar denotes a quantity in damped response theory, whereas the bar is omitted for the corresponding quantity in standard (non-damped) response theory.

4.2 Introduction to the exact damped response theory

The response parameters are obtained by solving response equations that contain redefined excitation energies [Eqs. (4.8)]. In damped response theory, the replacement in Eq. (4.8) is carried out in $\mathbf{E}^{[2]}$ in Eq. (3.39) to obtain the damped generalized Hessian $\bar{\mathbf{E}}^{[2]}$

$$\begin{aligned}\mathbf{E}^{[2]} \rightarrow \bar{\mathbf{E}}^{[2]} = \begin{pmatrix} \bar{\boldsymbol{\omega}}_k & \mathbf{0} \\ \mathbf{0} & \bar{\boldsymbol{\omega}}_k^{\star} \end{pmatrix} &= \begin{pmatrix} \boldsymbol{\omega}_k - i\boldsymbol{\gamma} & \mathbf{0} \\ \mathbf{0} & (\boldsymbol{\omega}_k - i\boldsymbol{\gamma})^{\star} \end{pmatrix} \\ &= \begin{pmatrix} \boldsymbol{\omega}_k - i\boldsymbol{\gamma} & \mathbf{0} \\ \mathbf{0} & \boldsymbol{\omega}_k + i\boldsymbol{\gamma} \end{pmatrix} = \mathbf{E}^{[2]} - i\gamma\mathbf{S}^{[2]}\,, \end{aligned} \tag{4.9}$$

where $\boldsymbol{\gamma}$ is a diagonal matrix containing the damping parameter γ.

Excitation energies also occur in higher-order $\mathbf{E}^{[g]}$ matrices ($g \geq 3$) defined from the g'th order term of the BCH expansion of the quasi-energy in Eq. (3.29)

$$E^{[g]}_{p_1 p_2 p_3 \ldots p_g} = \tfrac{1}{g!}\langle 0|\big[\ldots\big[[\hat{H}_0, R_{p_1}], R_{p_2}\big], \ldots, R_{p_g}\big]|0\rangle; \qquad (g \geq 3)\,. \tag{4.10}$$

[5] The one-photon absorption (OPA) spectra are identical for the standard and damped response theory. Higher-order properties are not identical but similar, as will be discussed in Chapter 5.

Excitation energies enter Eq. (4.10) due to the presence of $\hat{H}_0$. The substitution in Eq. (4.8) for a general $\mathbf{E}^{[g]}$ matrix may be carried out in the same manner as for $\mathbf{E}^{[2]}$ in Eq. (4.9)

$$\mathbf{E}^{[g]} \rightarrow \mathbf{E}^{[g]} - i\gamma\mathbf{S}^{[g]}\,, \tag{4.11}$$

where $\mathbf{S}^{[g]}$ ($g\geq 3$) is given by

$$S^{[g]}_{p_1p_2p_3\ldots p_g} = \tfrac{1}{g!}\langle 0|\big[\ldots[R_{p_1},R_{p_2}],\ldots,R_{p_g}\big]|0\rangle; \qquad (g\geq 3). \tag{4.12}$$

Response functions and response equations are obtained as derivatives of Eq. (3.29) and Eq. (3.31) with respect to the perturbation strengths. It may be seen that $\mathbf{E}^{[g]}$ always occurs in combination with $-\omega\mathbf{S}^{[g]}$ for a frequency ω and damped response theory may therefore be obtained by making the replacement

$$\mathbf{E}^{[g]} - \omega\mathbf{S}^{[g]} \rightarrow \mathbf{E}^{[g]} - (\omega + i\gamma)\mathbf{S}^{[g]}\,, \tag{4.13}$$

whenever $(\mathbf{E}^{[g]} - \omega\mathbf{S}^{[g]})$ occurs in either the response equations or in the expressions for response functions. For odd values of g, $\mathbf{E}^{[g]}$ and $\mathbf{S}^{[g]}$ are zero in exact theory. In approximate theories $\mathbf{S}^{[g]}$ is also zero for odd values of g and therefore the replacement in Eq. (4.13) is only important for even values of g in both exact and approximate theories.

Excitation energies occur in response function theory only in connection with the $\mathbf{E}^{[g]}$ matrix, and therefore damped response function theory may be obtained from the standard response function theory, simply by making the replacement in Eq. (4.13).

4.3 Analysis of the damped response equations

From Eqs. (3.34) and (4.9), the damped first-order response equation may be written as

$$\big[\mathbf{E}^{[2]} - (\omega_b + i\gamma)\mathbf{S}^{[2]}\big]\bar{\mathbf{x}}^b = \mathbf{g}^b\,. \tag{4.14}$$

$\bar{\mathbf{x}}^b$ is the complex damped response vector ($\bar{\mathbf{x}}^b = \bar{\mathbf{x}}^b_R + i\bar{\mathbf{x}}^b_I$), whereas in standard theory it is either purely real (*e.g.* when the perturbing operator B is an electric dipole operator) or purely imaginary (*e.g.* when B is a magnetic dipole operator). The first-order right-hand side vector $\mathbf{g}^b$ is identical to the right-hand side vector in standard theory in Eq. (3.37) as it does not depend on the excitation energies. Eq. (4.14) can be written out explicitly

$$\begin{pmatrix} {}^1\bar{\mathbf{x}}^b_k \\ {}^2\bar{\mathbf{x}}^b_{-k} \end{pmatrix} = \begin{pmatrix} (\boldsymbol{\omega}_k - \boldsymbol{\omega}_b - i\boldsymbol{\gamma})^{-1} & \mathbf{0} \\ \mathbf{0} & (\boldsymbol{\omega}_k + \boldsymbol{\omega}_b + i\boldsymbol{\gamma})^{-1} \end{pmatrix} \begin{pmatrix} {}^1\mathbf{g}^b_{-k} \\ {}^2\mathbf{g}^b_k \end{pmatrix}, \quad (k>0)\,. \tag{4.15}$$

Expressing the elements of the $[\mathbf{E}^{[2]} - (\omega_b + i\gamma)\mathbf{S}^{[2]}]^{-1}$ matrix and the right-hand side vector $\mathbf{g}^b$ in terms of their real and imaginary components allows to separate Eq. (4.15) into two equations for the real and the imaginary component of $\bar{\mathbf{x}}^b$, respectively

$$\begin{pmatrix} {}^1\bar{\mathbf{x}}_R^b \\ {}^2\bar{\mathbf{x}}_R^b \end{pmatrix} = \begin{pmatrix} \boldsymbol{\mathcal{D}}(\omega_b) & \mathbf{0} \\ \mathbf{0} & \boldsymbol{\mathcal{D}}(-\omega_b) \end{pmatrix} \begin{pmatrix} {}^1\mathbf{g}_R^b \\ {}^2\mathbf{g}_R^b \end{pmatrix} - \begin{pmatrix} \boldsymbol{\mathcal{A}}(\omega_b) & \mathbf{0} \\ \mathbf{0} & -\boldsymbol{\mathcal{A}}(-\omega_b) \end{pmatrix} \begin{pmatrix} {}^1\mathbf{g}_I^b \\ {}^2\mathbf{g}_I^b \end{pmatrix} , \quad (4.16a)$$

$$\begin{pmatrix} {}^1\bar{\mathbf{x}}_I^b \\ {}^2\bar{\mathbf{x}}_I^b \end{pmatrix} = \begin{pmatrix} \boldsymbol{\mathcal{A}}(\omega_b) & \mathbf{0} \\ \mathbf{0} & -\boldsymbol{\mathcal{A}}(-\omega_b) \end{pmatrix} \begin{pmatrix} {}^1\mathbf{g}_R^b \\ {}^2\mathbf{g}_R^b \end{pmatrix} + \begin{pmatrix} \boldsymbol{\mathcal{D}}(\omega_b) & \mathbf{0} \\ \mathbf{0} & \boldsymbol{\mathcal{D}}(-\omega_b) \end{pmatrix} \begin{pmatrix} {}^1\mathbf{g}_I^b \\ {}^2\mathbf{g}_I^b \end{pmatrix} . \quad (4.16b)$$

$\boldsymbol{\mathcal{D}}$ and $\boldsymbol{\mathcal{A}}$ are diagonal matrices containing the dispersion and the absorption line-shape functions, respectively

$$\mathcal{D}_k(\omega) = \frac{\omega_k - \omega}{(\omega_k - \omega)^2 + \gamma^2}; \qquad \mathcal{D}_k(-\omega) = \frac{\omega_k + \omega}{(\omega_k + \omega)^2 + \gamma^2} , \quad (4.17a)$$

$$\mathcal{A}_k(\omega) = \frac{\gamma}{(\omega_k - \omega)^2 + \gamma^2}; \qquad \mathcal{A}_k(-\omega) = \frac{\gamma}{(\omega_k + \omega)^2 + \gamma^2} . \quad (4.17b)$$

The index convention for excitation energies $\omega_k = \omega_{-k}$ has been used and thus $\mathcal{D}_k = \mathcal{D}_{-k}$ and $\mathcal{A}_k = \mathcal{A}_{-k}$. $\mathcal{D}_k(\omega)$ and $\mathcal{D}_k(-\omega)$ are antisymmetric and zero at $\omega = \omega_k$ and $\omega = -\omega_k$, respectively, whereas the Lorentzian functions $\mathcal{A}_k(\omega)$ and $\mathcal{A}_k(-\omega)$ are symmetric and reach

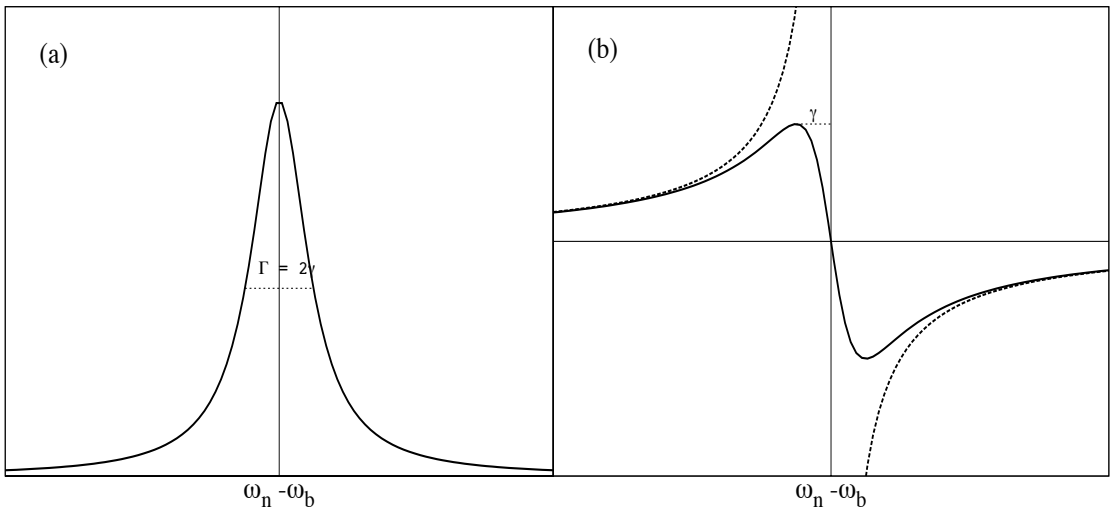

Figure 4.1: (a) Absorption line-shape function $\mathcal{A}_n(\omega) = \frac{\gamma}{(\omega_n-\omega)^2+\gamma^2}$ as a function of ω. The full width at half maximum equals the inverse lifetime $\Gamma = 2\gamma$; (b) **Solid line**: Dispersion line-shape function $D_n(\omega) = \frac{\omega_n-\omega}{(\omega_n-\omega)^2+\gamma^2}$ as function of ω. **Dashed line**: Dispersion line-shape function for $\gamma = 0$ where a pole is obtained at $\omega = \omega_n$. Note that the two functions approach each other when ω is off-resonance.

their maximum values at $\omega = \omega_k$ and $\omega = -\omega_k$, respectively. Line-shapes of dispersion $\mathcal{D}_n(\omega)$ and absorption $\mathcal{A}_n(\omega)$ functions are plotted in Fig. 4.1.

4.4 The structure of the damped response vector

In this section, the structures of the damped response vectors at different frequencies are discussed. In Sections 4.4.1 and 4.4.2, response vectors of the first- and higher-order damped response equations are analyzed, respectively.

For real wavefunctions, the right-hand side vector is either purely real or purely imaginary. To simplify the discussion, it can be assumed that $\mathbf{g}_I^b = \mathbf{0}$.

4.4.1 The first-order damped response equation

Using the assumption that the right-hand side vector is purely real, the first-order equations in Eqs. (4.16a) and (4.16b) become

$$\begin{pmatrix} {}^1\bar{\mathbf{x}}_R^b \\ {}^2\bar{\mathbf{x}}_R^b \end{pmatrix} = \begin{pmatrix} \boldsymbol{\mathcal{D}}(\omega_b) & \mathbf{0} \\ \mathbf{0} & \boldsymbol{\mathcal{D}}(-\omega_b) \end{pmatrix} \begin{pmatrix} {}^1\mathbf{g}_R^b \\ {}^2\mathbf{g}_R^b \end{pmatrix}, \tag{4.18a}$$

$$\begin{pmatrix} {}^1\bar{\mathbf{x}}_I^b \\ {}^2\bar{\mathbf{x}}_I^b \end{pmatrix} = \begin{pmatrix} \boldsymbol{\mathcal{A}}(\omega_b) & \mathbf{0} \\ \mathbf{0} & -\boldsymbol{\mathcal{A}}(-\omega_b) \end{pmatrix} \begin{pmatrix} {}^1\mathbf{g}_R^b \\ {}^2\mathbf{g}_R^b \end{pmatrix}. \tag{4.18b}$$

The structure of the damped response vectors differs depending on whether the optical frequency is close to an excitation energy or in a far-off-resonance region.

The p'th element of the real part of the response vector may be identified from Eq. (4.18a) as

$$(\bar{x}_R^b)_p = \mathcal{D}_p(\pm\omega_b)(g_R^b)_{-p}\,, \tag{4.19}$$

where the plus sign corresponds to an element in the upper part of $\bar{\mathbf{x}}_R^b$ and the minus sign refers to an element in the lower part of $\bar{\mathbf{x}}_R^b$. Since the inverted effective lifetime of the excited states is much smaller than the optical frequencies, and assuming that the excited states are all non-degenerate, in the resonance region the n'th element $(\bar{x}_R^b)_n$ in Eq. (4.19) is much larger than the remaining elements $(\bar{x}_R^b)_p$ $(p \neq n)$ at $\omega_b \approx \omega_n$. This is due to the fact that $\mathcal{D}_p(\pm\omega_b)$ goes to zero when ω_b is far from $\pm\omega_p$, and the following approximation may be applied

$$(\bar{x}_R^b)_p \approx \mathcal{D}_p(\omega_b)(g_R^b)_{-p}\delta_{pn} \qquad (\omega_b \approx \omega_n)\,. \tag{4.20}$$

As may be seen from the plot of $\mathcal{D}_n(\omega_b)$ in Fig. 4.1b, close to resonance, $(\bar{x}_R^b)_n$ is the dominant element in the $\bar{\mathbf{x}}_R^b$ response vector.

From Eq. (4.18b), the p'th component of $\bar{\mathbf{x}}_I^b$ is given by

$$(\bar{x}_I^b)_p = \pm\mathcal{A}_p(\pm\omega_b)(g_R^b)_{-p}\,. \tag{4.21}$$

The dominating element of $\bar{\mathbf{x}}_I^b$ at $\omega_b \approx \omega_n$ is $(\bar{\mathbf{x}}_I^b)_n$, since the line-shape function $\mathcal{A}_p(\pm\omega_b)$ goes to zero when ω_b is far from the excitation energy, and therefore the imaginary component of the damped response parameter is proportional to the residue of the standard response parameter at $\omega_b = \omega_n$.

In the off-resonance region, γ^2 may be omitted in the denominator of the dispersion line-shape function in Eq. (4.17a) [since $\gamma \ll (\omega_b \pm \omega_k)$] and Eq. (4.18a) may be written as

$$\begin{pmatrix} {}^1\bar{\mathbf{x}}_R^b \\ {}^2\bar{\mathbf{x}}_R^b \end{pmatrix} \approx \begin{pmatrix} (\boldsymbol{\omega}_k - \boldsymbol{\omega}_b)^{-1} & \mathbf{0} \\ \mathbf{0} & (\boldsymbol{\omega}_k + \boldsymbol{\omega}_b)^{-1} \end{pmatrix} \begin{pmatrix} {}^1\mathbf{g}_R^b \\ {}^2\mathbf{g}_R^b \end{pmatrix} \qquad \text{(off-resonance)}\,. \tag{4.22}$$

By comparing Eq. (4.22) to the standard first-order response equation Eq. (3.40) it can be seen that the real part of the damped response vector $\bar{\mathbf{x}}_R^b$ and the standard response vector $\mathbf{x}^b$ are approximately equal at off-resonance frequencies. It can be also seen in Fig. 4.1b that the dispersion line-shape function $\mathcal{D}_n(\omega)$ approaches the standard line-shape function ($\gamma = 0$) at off-resonance frequencies.

At off-resonance frequencies, the imaginary part of the solution vector $\bar{\mathbf{x}}_I^b$ in Eq. (4.18b) is very small, since the absorption line-shape function in Eq. (4.17b) goes to zero (see Fig. 4.1a).

4.4.2 The f'th order damped response equation

The results obtained for the damped first-order response parameters may easily be generalized to the f'th order response equation ($f \geq 2$). The general f'th order response equation

$$\left[\mathbf{E}^{[2]} - (\omega_{b\ldots f} + i\gamma)\mathbf{S}^{[2]}\right]\bar{\mathbf{x}}^{b\ldots f} = \bar{\mathbf{g}}^{b\ldots f}\,, \tag{4.23}$$

may be written in the same way as the first-order equation in Eq. (4.15)

$$\begin{pmatrix} {}^1\bar{\mathbf{x}}_k^{b\ldots f} \\ {}^2\bar{\mathbf{x}}_{-k}^{b\ldots f} \end{pmatrix} = \begin{pmatrix} (\boldsymbol{\omega}_k - \boldsymbol{\omega}_{b\ldots f} - i\boldsymbol{\gamma})^{-1} & \mathbf{0} \\ \mathbf{0} & (\boldsymbol{\omega}_k + \boldsymbol{\omega}_{b\ldots f} + i\boldsymbol{\gamma})^{-1} \end{pmatrix} \begin{pmatrix} {}^1\bar{\mathbf{g}}_{-k}^{b\ldots f} \\ {}^2\bar{\mathbf{g}}_k^{b\ldots f} \end{pmatrix}\,, \tag{4.24}$$

and the real and imaginary components of $\bar{\mathbf{x}}^{b\ldots f} = \bar{\mathbf{x}}_R^{b\ldots f} + i\bar{\mathbf{x}}_I^{b\ldots f}$ may therefore be written as

$$\begin{aligned} \begin{pmatrix} {}^1\bar{\mathbf{x}}_R^{b\ldots f} \\ {}^2\bar{\mathbf{x}}_R^{b\ldots f} \end{pmatrix} &= \begin{pmatrix} \boldsymbol{\mathcal{D}}(\omega_{b\ldots f}) & \mathbf{0} \\ \mathbf{0} & \boldsymbol{\mathcal{D}}(-\omega_{b\ldots f}) \end{pmatrix} \begin{pmatrix} {}^1\bar{\mathbf{g}}_R^{b\ldots f} \\ {}^2\bar{\mathbf{g}}_R^{b\ldots f} \end{pmatrix} \\ &\quad - \begin{pmatrix} \boldsymbol{\mathcal{A}}(\omega_{b\ldots f}) & \mathbf{0} \\ \mathbf{0} & -\boldsymbol{\mathcal{A}}(-\omega_{b\ldots f}) \end{pmatrix} \begin{pmatrix} {}^1\bar{\mathbf{g}}_I^{b\ldots f} \\ {}^2\bar{\mathbf{g}}_I^{b\ldots f} \end{pmatrix}\,, \end{aligned} \tag{4.25a}$$

and

$$\begin{pmatrix} {}^1\bar{\mathbf{x}}_I^{b\ldots f} \\ {}^2\bar{\mathbf{x}}_I^{b\ldots f} \end{pmatrix} = \begin{pmatrix} \boldsymbol{\mathcal{A}}(\omega_{b\ldots f}) & \mathbf{0} \\ \mathbf{0} & -\boldsymbol{\mathcal{A}}(-\omega_{b\ldots f}) \end{pmatrix} \begin{pmatrix} {}^1\bar{\mathbf{g}}_R^{b\ldots f} \\ {}^2\bar{\mathbf{g}}_R^{b\ldots f} \end{pmatrix} + \begin{pmatrix} \boldsymbol{\mathcal{D}}(\omega_{b\ldots f}) & \mathbf{0} \\ \mathbf{0} & \boldsymbol{\mathcal{D}}(-\omega_{b\ldots f}) \end{pmatrix} \begin{pmatrix} {}^1\bar{\mathbf{g}}_I^{b\ldots f} \\ {}^2\bar{\mathbf{g}}_I^{b\ldots f} \end{pmatrix} , \tag{4.25b}$$

respectively, which is equivalent to Eqs. (4.16a) and (4.16b).

4.5 Damped linear response theory

In standard response theory the linear response function is given by Eq. (3.16). The response parameters x_p^b in Eq. (3.40) are the only quantities that depend on the excitation energies, and therefore the damped linear response function may be obtained from Eq. (3.16) by replacing the standard response parameters x_p^b by the damped response parameters $\bar{x}_p^b$

$$\langle\langle \overline{A;B} \rangle\rangle_{\omega_b} = \langle\langle \overline{A;B} \rangle\rangle_{\omega_b}^R + i\langle\langle \overline{A;B} \rangle\rangle_{\omega_b}^I , \tag{4.26}$$

where

$$\langle\langle \overline{A;B} \rangle\rangle_{\omega_b}^R = (g_R^a)_p(\bar{x}_R^b)_p , \tag{4.27a}$$

$$\langle\langle \overline{A;B} \rangle\rangle_{\omega_b}^I = (g_R^a)_p(\bar{x}_I^b)_p . \tag{4.27b}$$

Using the assumption in Eq. (4.20), in the resonance region ($\omega_b \approx \omega_n$), the n'th element of the response vector in Eq. (4.27a) qualitatively determines the overall structure of $\langle\langle \overline{A;B} \rangle\rangle_{\omega_b}^R$

$$\langle\langle \overline{A;B} \rangle\rangle_{\omega_b}^R \approx \mathcal{D}_n(\omega_b)(g_R^a)_n(g_R^b)_{-n} \qquad (\omega_b \approx \omega_n) . \tag{4.28}$$

If $\gamma = 0$ in Eq. (4.28), $\langle\langle \overline{A;B} \rangle\rangle_{\omega_b}^R$ reduced to the standard response function $\langle\langle A;B \rangle\rangle_{\omega_b}$, which has a pole at $\omega_b = \omega_n$. The standard response equation thus diverges at $\omega_b = \omega_n$ as illustrated by the dotted curve in Fig. 4.1b. In the damped response theory the divergence at $\omega_b = \omega_n$ is avoided and a physically correct behavior over the entire frequency range is obtained.

$\langle\langle \overline{A;B} \rangle\rangle_{\omega_b}^I$ is proportional to the residue of the linear response function $\langle\langle A;B \rangle\rangle_{\omega_b \to \omega_n}$. The plot of $\mathcal{A}_n(\omega_b)$ in Fig. 4.1b shows the behavior of $\langle\langle \overline{A;B} \rangle\rangle_{\omega_b}^I$ at $\omega_b \approx \omega_n$. It is clear that $\langle\langle \overline{A;B} \rangle\rangle_{\omega_b}^I$ represents a residue spectrum with a peak broadening of $\Gamma = 2\gamma$ at full width half maximum. In general, a residue spectrum describes an absorption process, *e.g.* if A and B are components of the electric dipole operator [see Eq. (3.18a)], then $A^{0n}B^{n0}$ describes a component of the transition strength matrix for the $|0\rangle \rightarrow |n\rangle$ transition.

In the off-resonance region the real part of the damped response function approximately equals the standard response function

$$\langle\langle \overline{A;B} \rangle\rangle^{R}_{\omega_b} \approx \langle\langle A;B \rangle\rangle_{\omega_b} \qquad \text{(off-resonance)}\,, \tag{4.29}$$

whereas the imaginary part of the damped linear response function in Eq. (4.27b) is approximately zero

$$\langle\langle \overline{A;B} \rangle\rangle^{I}_{\omega_b} \approx 0 \qquad \text{(off-resonance)}\,. \tag{4.30}$$

4.6 Damped quadratic response theory

The standard quadratic response function may be written as

$$\langle\langle A;B,C \rangle\rangle_{\omega_b,\omega_c} = A^{[2]}_{pq} x^b_p x^c_q + B^{[2]}_{pq} x^a_p x^c_q + C^{[2]}_{pq} x^a_p x^b_q\,. \tag{4.31}$$

Since the excitation energies only enter in Eq. (4.31) via the first-order response vectors, $\langle\langle \overline{A;B,C} \rangle\rangle_{\omega_b,\omega_c}$ is obtained by replacing the standard response vectors (x^a, x^b, and x^c) by the corresponding damped response vectors ($\bar{x}^a$, $\bar{x}^b$, and $\bar{x}^c$)

$$\langle\langle \overline{A;B,C} \rangle\rangle_{\omega_b,\omega_c} = A^{[2]}_{pq} \bar{x}^b_p \bar{x}^c_q + B^{[2]}_{pq} \bar{x}^a_p \bar{x}^c_q + C^{[2]}_{pq} \bar{x}^a_p \bar{x}^b_q\,, \tag{4.32}$$

where the damped response vectors $\bar{x}^a$, $\bar{x}^b$, and $\bar{x}^c$ are determined from Eq. (4.14). The $A^{[2]}$ matrix is defined as

$$A^{[2]}_{pq} = \begin{cases} -\tilde{A}^{pq} & \text{for } p<0; \quad q>0 \\ -\tilde{A}^{qp} & \text{for } p>0; \quad q<0 \\ 0 & \text{otherwise} \end{cases}\,, \tag{4.33}$$

where

$$\tilde{A}^{pq} = A^{pq} - A^{00}\delta_{pq}\,, \tag{4.34}$$

and the notation introduced in Section 3.1.3 has been used.

The form of the damped response equations depend on the chosen elimination rule, due to the fact that the Hellmann-Feynman theorem is not satisfied when an empirical damping parameter is introduced. In Eq. (4.32), the damped quadratic response function is defined in accordance with Wigner's $2n{+}1$ rule [45, 125] and according to the $n{+}1$ rule [45] it is given as

$$\overline{\langle\langle A;B,C \rangle\rangle}_{\omega_b,\omega_c} \;=\; \sum_p g^a_p \bar{x}^{bc}_p + \sum_{pq} A^{[2]}_{pq} \bar{x}^b_p \bar{x}^c_q\,, \tag{4.35}$$

where the summations run over both positive and negative indices. g_p^a is defined as

$$g_{-p}^a = -A^{p0}; \qquad g_p^a = A^{0p}\,. \tag{4.36}$$

The second-order response vectors in Eq. (4.35) may be obtained from Eq. (4.24) where ($\omega_{bc} = \omega_b + \omega_c = -\omega_a$) and the second-order right-hand side vector is given as

$${}^1\bar{g}_{-k}^{bc} = \sum_{p>0}\left(\frac{B^{0p}\tilde{C}^{pk}}{\omega_p - \omega_b - i\gamma} + \frac{C^{0p}\tilde{B}^{pk}}{\omega_p - \omega_c - i\gamma}\right), \tag{4.37a}$$

$${}^2\bar{g}_{k}^{bc} = -\sum_{p>0}\left(\frac{B^{0p}\tilde{C}^{pk}}{\omega_p + \omega_b + i\gamma} + \frac{C^{0p}\tilde{B}^{pk}}{\omega_p + \omega_c + i\gamma}\right). \tag{4.37b}$$

As demonstrated in Paper C, using Eq. (4.32) for the damped quadratic response function in derivation of higher-order properties, may lead to a cancellation of terms, resulting in unphysical response functions, and therefore Eq. (4.35) should, instead, be used.[6] However, Eq. (4.35) is equivalent to Eq. (4.32), if $\bar{x}^b$ and $\bar{x}^c$ have the form of Eq. (4.15), whereas $\bar{x}^a$ is given as

$$\begin{pmatrix} {}^1\bar{\mathbf{x}}_k^a \\ {}^2\bar{\mathbf{x}}_{-k}^a \end{pmatrix} = \begin{pmatrix} (\omega_k - \omega_a + i\gamma)^{-1} & 0 \\ 0 & (\omega_k + \omega_a - i\gamma)^{-1} \end{pmatrix} \begin{pmatrix} {}^1\mathbf{g}_{-k}^a \\ {}^2\mathbf{g}_k^a \end{pmatrix}, \tag{4.38}$$

and this form will be used in Chapter 5.

In approximate theory, $\mathbf{E}^{[3]}$ is nonzero and in principle the replacement in Eq. (4.13) for $g = 3$ should also be carried out

$$\mathbf{E}^{[3]} - \omega\mathbf{S}^{[3]} \rightarrow \mathbf{E}^{[3]} - (\omega + i\gamma)\mathbf{S}^{[3]}\,. \tag{4.39}$$

However, since $\mathbf{S}^{[3]}$ is zero in variational approximate theories, this replacement is of no significance in neither exact nor approximate theory.

Damped quadratic response functions are used in *e.g.* calculation of Magnetic Circular Dichroism (MCD) as will be shown in Section 5.1. Damped cubic response theory in the context of Two-Photon Absorption (TPA) will be considered in Section 5.2.

4.7 Damped response theory for a variational approximate state

The treatment of damped response theory for an exact state presented above may be generalized to approximate variational methods (such as HF, KS-DFT and CI), where the $\mathbf{E}^{[g]}$

[6] It has been concluded that the n+1 rule should be used in the damped response theory for higher-order equations.

and $\mathbf{S}^{[g]}$ matrices enter in the same way as in exact theory. Therefore the procedure for obtaining damped response functions in Section 4.2 may also be applied in these theories. The only modification is that the excitation/deexcitation operator R_p in Eq. (3.22) must be replaced by the corresponding operator in the approximate theory of interest.

To illustrate the equivalence between exact theory and a variational approximate theory, it is convenient to express $(\mathbf{E}^{[2]} - \omega\mathbf{S}^{[2]})^{-1}$ in the form,

$$\begin{aligned}(\mathbf{E}^{[2]} - \omega\mathbf{S}^{[2]})^{-1} &= \begin{pmatrix} (\boldsymbol{\omega}_k - \boldsymbol{\omega})^{-1} & \mathbf{0} \\ \mathbf{0} & (\boldsymbol{\omega}_k^* + \boldsymbol{\omega})^{-1} \end{pmatrix} \\ &= \sum_{k>0} \left[(\omega_k - \omega)^{-1} \mathbf{x}_k \mathbf{x}_k^\dagger + (\omega_k^* + \omega)^{-1} \mathbf{x}_{-k} \mathbf{x}_{-k}^\dagger \right] \\ &\to \sum_{k>0} \left[(\omega_k - \omega - i\gamma)^{-1} \mathbf{x}_k \mathbf{x}_k^\dagger + (\omega_k + \omega + i\gamma)^{-1} \mathbf{x}_{-k} \mathbf{x}_{-k}^\dagger \right], \end{aligned} \tag{4.40}$$

where Eq. (3.39) have been used. Complex excitation energies have been introduced according to Eq. (4.8) and the excitation vectors $\mathbf{x}_k$ are given by

$$(x_k)_p = \delta_{pk}\,, \tag{4.41}$$

and satisfy the generalized eigenvalue equation

$$\mathbf{E}^{[2]}\mathbf{x}_k = \omega_k \mathbf{S}^{[2]}\mathbf{x}_k; \qquad \mathbf{E}^{[2]}\mathbf{x}_{-k} = -\omega_k \mathbf{S}^{[2]}\mathbf{x}_{-k}\,, \tag{4.42}$$

which follows straightforwardly from Eqs. (3.39) and (4.41).

In HF, KS-DFT, and CI, the spectral representation of $(\boldsymbol{E}^{[2]} - \omega\boldsymbol{S}^{[2]})^{-1}$ [24] may be introduced and complex excitation energies are obtained in analogy with Eq. (4.40)

$$\begin{aligned}(\boldsymbol{E}^{[2]} - \omega\boldsymbol{S}^{[2]})^{-1} &= \sum_{k>0} \left[(\omega_k - \omega)^{-1} \boldsymbol{X}_k \boldsymbol{X}_k^\dagger + (\omega_k^* + \omega)^{-1} \boldsymbol{X}_{-k} \boldsymbol{X}_{-k}^\dagger \right] \\ &\to \sum_{k>0} \left[(\omega_k - \omega - i\gamma)^{-1} \boldsymbol{X}_k \boldsymbol{X}_k^\dagger + (\omega_k + \omega + i\gamma)^{-1} \boldsymbol{X}_{-k} \boldsymbol{X}_{-k}^\dagger \right], \end{aligned} \tag{4.43}$$

where ω_k is an excitation energy in approximate theory, and $\boldsymbol{X}_k$ is an eigenvector obtained from the generalized eigenvalue problem in Eq. (3.56).

The equations in approximate theories are completely equivalent to the corresponding equations in exact theory and therefore all damped response equations in approximate theory have the form of Eq. (4.23) with approximate Hessian and metric matrices $\boldsymbol{E}^{[2]}$ and $\boldsymbol{S}^{[2]}$. This structure of the damped response equations for a variational approximate state was also obtained by Norman *et al.* [28, 29].

4.8 Comparison to the approach by Norman *et al.*

The foundation for the formulation of damped response theory described above is the introduction of complex excitation energies into standard response functions as discussed by Barron in Ref. [32] in combination with the quasi-energy formulation of response theory [43, 44] and the elimination rules of Ref. [45]. In the formulation presented by Norman *et al.* in Ref. [28], the foundation for the treatment of finite lifetime effects in exact theory is the damped Ehrenfest equation

$$\frac{\partial}{\partial t}\langle\tilde{0}|R_p|\tilde{0}\rangle = -i\langle\tilde{0}|[R_p,\hat{H}]|\tilde{0}\rangle - \gamma\langle\tilde{0}|R_p|\tilde{0}\rangle\,, \tag{4.44}$$

where the second term on the right-hand side is added to the standard Ehrenfest equation to obtain a phenomenological description of all damping effects [34]. The first-order damped response equation is obtained by the substitution

$$\omega\mathbf{S}^{[2]} \rightarrow (\omega + i\gamma)\mathbf{S}^{[2]}\,, \tag{4.45}$$

and similarly for higher-order $\mathbf{S}^{[g]}$ terms, equivalent to the replacement in Eq. (4.13). The term $-\gamma\mathbf{S}^{[2]}$ is introduced from the last term on the right-hand side in Eq. (4.44).

In HF theory the starting point in the work by Norman *et al.* [28] is the HF counterpart to the damped exact Ehrenfest equation in Eq. (4.44) which is given by

$$\frac{\partial}{\partial t}\langle\tilde{0}|\hat{t}_p^\dagger|\tilde{0}\rangle - \langle\tilde{0}|\frac{\partial}{\partial t}\hat{t}_p^\dagger|\tilde{0}\rangle = -i\langle\tilde{0}|[\hat{t}_p^\dagger,H]|\tilde{0}\rangle - \gamma\langle\tilde{0}|\hat{q}_p^\dagger|\tilde{0}\rangle\,, \tag{4.46}$$

where $\hat{q}_p^\dagger$ are orbital rotation operators, and $\hat{t}_p^\dagger = \exp[X(t)]\hat{q}_p^\dagger\exp[-X(t)]$ are time-transformed operators. The terms in Eq. (4.46) containing $\hat{t}_p^\dagger$ constitute the standard Ehrenfest equation in HF theory [16], whereas the second term on the right-hand side has been added by Norman *et al.* to describe all damping effects. The addition of $-\gamma\langle\tilde{0}|\hat{q}_p^\dagger|\tilde{0}\rangle$ ensures that the transition from standard to damped response theory in Eq. (4.45) is reproduced also in HF theory.

The explicit form of a damped response function depends on the particular rule applied for eliminating response parameters. Damped response theory based on solving the Ehrenfest equation in Eq. (4.44) and identifying response functions from the average value of an A operator gives response functions that are identical to the ones obtained within the quasi-energy formalism by differentiating the generalized Hellmann-Feynman equation in Eq. (3.14) (corresponding to the n+1 elimination rule where all response parameters referencing the perturbation a are eliminated whereas all response parameters referencing $bc\ldots$ are kept). The formulation presented by Norman *et al.* does not allow for a direct identification of

response functions complying with one of the more general elimination rules described in Ref. [45].

5 Higher-order properties in damped response theory

In the previous chapter, damped response theory was introduced. It was shown that the damped response equations may be solved in the whole frequency range, in contrast to the standard response equations which have singularities in the resonance regions. Damped response theory is important for large molecular systems, since it is impossible to determine entire absorption spectrum using standard response theory, due to a high density of low lying excited states, which is characteristic for large systems.

In this chapter, application of the damped response theory to higher-order properties, such as Magnetic Circular Dichroism (MCD) in Section 5.1 and Two-Photon Absorption (TPA) in Section 5.2 is presented.

5.1 Damped Magnetic Circular Dichroism

As discussed in Chapter 3, a system in the presence of a time-dependent external field interacts with the field, and observables depend on the frequency of the field. When an external magnetic field is applied to a molecule, it becomes optically active. This phenomenon is known as Magneto-Optical Activity (MOA), and originates due to the fact that the molecule interacts differently with the right and left circularly polarized components of plane-polarized light. Two effects are observed:

- Magneto-Optical Rotation (MOR) – the rotation of the plane of polarization of the emerging light in the transparent regions of the sample. MOR is conventionally rationalized in terms of the so-called Verdet constant [126], which is connected to the dipole-dipole magnetic dipole hyperpolarizability [32, 127, 128].

- Magnetic Circular Dichroism (MCD) – an induced ellipticity of the incident linearly polarized light, due to the differential absorption of left and right light components [32, 127–131].

MCD is traditionally rationalized in terms of three magnetic rotatory strengths, known as the Faraday $\mathcal{A}$, $\mathcal{B}$ and $\mathcal{C}$ terms [128, 131–136]:

- The $\mathcal{A}$ term arises due to Zeeman splitting of spectral lines into left and right circularly polarized components. The $\mathcal{A}$ term only contributes, if either the ground or the excited state is degenerate. The small Zeeman splitting makes the oppositely signed transitions from right and left circularly polarized light almost cancel out, that leads

to the derivative shape of the band. The $\mathcal{A}$ term may be associated with the double residue of an appropriate quadratic response function [16].

- The $\mathcal{B}$ term arises due to the field-induced mixing of energy levels. The $\mathcal{B}$ term describes the MCD spectrum of an electronic transition in a molecule without degeneracies of electronic states. It contributes to the spectrum with an absorption band shape. The $\mathcal{B}$ term may be identified from a single residue of an appropriate quadratic response function [16].

- The $\mathcal{C}$ term only appears, if the ground state is degenerate and will not be discussed here.

The MCD spectrum may be obtained from the sum of $\mathcal{A}$, $\mathcal{B}$ and $\mathcal{C}$ terms calculated for the electronic transitions. However, this procedure is numerically unstable for near-degenerate states. This instability may be avoided by using damped response theory (described in Chapter 4) for higher-order equations [33, 119–121]. However, when this approach is used, the individual Faraday $\mathcal{A}$ and $\mathcal{B}$ terms cannot be obtained directly. They can be extracted from the spectral profile, however this approach may be problematic for spectra containing overlapping bands, and valuable information may be lost. A solution to this problem can be obtained using the combined standard and damped response theory, as proposed by Kjærgaard *et al.* in Paper C.

In Section 5.1.1, it is shown how the ellipticity (and therefore the total MCD spectrum) may be determined from a damped quadratic response function. In Section 5.1.2, performance of the standard and damped response theory is compared for chosen systems with nearly-degenerate states when the MCD spectrum is calculated.

5.1.1 Calculating the ellipticity using damped response theory

For plane-polarized light propagating in the Z direction of a space-fixed frame, the ellipticity θ of a sample of randomly moving molecules in the presence of a magnetic field directed along the Z axis, is given by [32] (see Appendix A in Paper C for details)

$$\theta = \frac{1}{12}\omega\mu_0 clN\varepsilon_{\alpha\beta\gamma}\mathrm{Re}\left(\overline{\langle\langle \mu_\alpha;\mu_\beta,m_\gamma\rangle\rangle}_{\omega,0}\right)B_Z\,. \tag{5.1}$$

m_α and μ_α are the Cartesian components of the magnetic and electric dipole operator in the molecular-fixed frame, ω is the optical frequency, N is the number density of molecules, μ_0 is the permeability of vacuum, l is the length of the sample, and c is the speed of light in

vacuum. The Einstein summation in connection with the Levi-Civita tensor $\varepsilon_{\alpha\beta\gamma}$ has been used. Using the fact that

$$\varepsilon_{\alpha\beta\gamma}\langle\langle\mu_\alpha;\mu_\beta,m_\gamma\rangle\rangle_{\omega,0} = \varepsilon_{\alpha\beta\gamma}\langle\langle\mu_\gamma;m_\beta,\mu_\alpha\rangle\rangle_{0,\omega}\,, \tag{5.2}$$

and denoting μ_γ, m_β and μ_α as A, B and C, respectively, Eq. (5.1) may be expressed as

$$\theta \;=\; \frac{1}{2}KB_Z\omega\mathrm{Re}\left(\varepsilon_{\alpha\beta\gamma}\overline{\langle\langle\mu_\gamma;m_\beta,\mu_\alpha\rangle\rangle}_{0,\omega}\right) = \frac{1}{2}KB_Z\omega\mathrm{Re}\left(\varepsilon_{cba}\overline{\langle\langle A;B,C\rangle\rangle}_{0,\omega}\right)\,, \tag{5.3}$$

where $K = \frac{1}{6}\mu_0 clN$ and the indices of the Levi-Civita tensor have been changed accordingly ($\varepsilon_{\alpha\beta\gamma} \rightarrow \varepsilon_{cba}$). Note that $\omega = -\omega_a = \omega_c$, where ω_a and ω_c denote frequencies associated with operator A and C, respectively.

The form of the damped quadratic response function $\overline{\langle\langle A;B,C\rangle\rangle}_{\omega_b,\omega_c}$ is described in Section 4.6. The form of the damped response functions depends on the chosen elimination rule [45], as discussed in Section 4.8. It was concluded in Paper C[7] that the n+1 rule should be used in the damped response theory for higher-order functions. Therefore, in the following derivations, the form of the damped quadratic response function in Eq. (4.32) will be used, where response vectors $\bar{x}^b$ and $\bar{x}^c$ are expressed in Eq. (4.15), while $\bar{x}^a$ is given in Eq. (4.38). This is equivalent to the form of the damped quadratic response function obtained using the n+1 rule, given in Eq. (4.35).

The only components of the full damped quadratic response function in Eq. (4.32) that give a significant contributions in the absorptive frequency region (ω_c close to an excitation energy ω_j) are the terms that would be singular in standard response theory. Remaining terms are therefore omitted for analysis purposes. A simplified damped response function may thus be written as

$$\begin{aligned}
\overline{\langle\langle A;B,C\rangle\rangle}_{0,\omega_c} \;\approx\; & \sum_{p\neq 0}\sum_{q\neq 0}\frac{B^{0p}\tilde{A}^{pq}C^{q0}}{(\omega_p+i\gamma)(\omega_q-\omega_c-i\gamma)} \\
+\; & \sum_{p\neq 0}\sum_{q\neq 0}\frac{A^{0p}\tilde{B}^{pq}C^{q0}}{(\omega_p+\omega_a-i\gamma)(\omega_q-\omega_c-i\gamma)} \\
+\; & \sum_{p\neq 0}\sum_{q\neq 0}\frac{A^{0p}\tilde{C}^{pq}B^{q0}}{(\omega_p+\omega_a-i\gamma)(\omega_q-i\gamma)}, \quad (\omega_c\approx\omega_j)\,.
\end{aligned} \tag{5.4}$$

Note that the summations run over only positive indices, which refer to excited states. Assuming that s denotes a component of the possibly degenerate state j and ($\omega_c \approx \omega_j$), only $q = j_s$ contributes significantly in the first term of Eq. (5.4), $p = j_s$ in the third term, and

[7] After Paper A had been published.

in the second term, both $q = j_s$ and $p = j_s$ give significant contributions. Eq. (5.4) may therefore be written as

$$\begin{aligned}
\overline{\langle\langle A;B,C\rangle\rangle}_{0,\omega_c} &\approx \sum_{p\neq 0}\sum_{s}\frac{B^{0p}\tilde{A}^{pj_s}C^{j_s0}}{(\omega_p+i\gamma)(\omega_j-\omega_c-i\gamma)} \\
&+ \sum_{p\neq 0}\sum_{s}\frac{A^{0p}\tilde{B}^{pj_s}C^{j_s0}}{(\omega_p+\omega_a-i\gamma)(\omega_j-\omega_c-i\gamma)} \\
&+ \sum_{q\neq 0}\sum_{s}\frac{A^{0j_s}\tilde{B}^{j_sq}C^{q0}}{(\omega_j+\omega_a-i\gamma)(\omega_q-\omega_c-i\gamma)} \\
&+ \sum_{q\neq 0}\sum_{s}\frac{A^{0j_s}\tilde{C}^{j_sq}B^{q0}}{(\omega_j+\omega_a-i\gamma)(\omega_q-i\gamma)}, \quad (\omega_c\approx\omega_j)\,. \qquad (5.5)
\end{aligned}$$

Introducing the dispersion $\mathcal{D}_j(\omega)$ and absorption $\mathcal{A}_j(\omega)$ line-shape functions given in Eqs. (4.17a) and (4.17b), respectively, and due to the fact that in the resonance region $\mathcal{D}_j(\omega_c) = \mathcal{D}_j(-\omega_a) \approx 0$, Eq. (5.5) may be approximated as

$$\begin{aligned}
\overline{\langle\langle A;B,C\rangle\rangle}_{0,\omega_c} &\approx \sum_{p\neq 0}\sum_{s}\Big(B^{0p}\tilde{A}^{pj_s}C^{j_s0}\Big)\Big(\mathcal{D}_p(0)-i\mathcal{A}_p(0)\Big)i\mathcal{A}_j(\omega_c) \qquad (5.6)\\
&+ \sum_{p\neq 0}\sum_{s}\Big(A^{0p}\tilde{B}^{pj_s}C^{j_s0}\Big)\Big(\mathcal{D}_p(-\omega_a)+i\mathcal{A}_p(-\omega_a)\Big)i\mathcal{A}_j(\omega_c) \\
&+ \sum_{q\neq 0}\sum_{s}\Big(A^{0j_s}\tilde{B}^{j_sq}C^{q0}\Big)(-\omega_a)\Big(\mathcal{D}_q(\omega_c)+i\mathcal{A}_q(\omega_c)\Big)i\mathcal{A}_j \\
&+ \sum_{q\neq 0}\sum_{s}\Big(A^{0j_s}\tilde{C}^{j_sq}B^{q0}\Big)(-\omega_a)\Big(\mathcal{D}_q(0)+i\mathcal{A}_q(0)\Big)i\mathcal{A}_j, \quad (\omega_c\approx\omega_j)\,.
\end{aligned}$$

The MCD spectrum is described by the real component of the damped response function [as can be seen from Eq. (5.3)], and therefore only the real part of Eq. (5.6) is considered. Using the fact that A and C are real, whereas B is a purely imaginary operator, and combining terms of the real component in Eq. (5.6) by applying the Levi-Civita tensor, yields

$$\begin{aligned}
\mathrm{Re}\Big(\varepsilon_{cba}\overline{\langle\langle A;B,C\rangle\rangle}_{0,\omega_c}\Big) &\approx -2\sum_{p\neq 0}\sum_{s}\varepsilon_{cba}\mathrm{Im}\Big(B^{0p}\tilde{A}^{pj_s}C^{j_s0}\Big)\mathcal{D}_p(0)\mathcal{A}_j(\omega_c) \qquad (5.7)\\
&\quad -2\sum_{p\neq 0}\sum_{s}\varepsilon_{cba}\mathrm{Im}\Big(\tilde{B}^{pj_s}C^{j_s0}A^{0p}\Big)\mathcal{D}_p(\omega_c)\mathcal{A}_j(\omega_c), \quad (\omega_c\approx\omega_j)\,,
\end{aligned}$$

since $\omega_a = -\omega_c$. Writing out the explicit term for $p = j_t$ in the second summation gives

$$\begin{aligned}\mathrm{Re}(\varepsilon_{cba}\overline{\langle\langle A;B,C\rangle\rangle}_{0,\omega_c}) \;\approx\; & -2\sum_{p\neq 0}\sum_{s}\varepsilon_{cba}\mathrm{Im}\Big(B^{0p}\tilde{A}^{pj_s}C^{j_s0}\Big)\mathcal{D}_p(0)\mathcal{A}_j(\omega_c) \\ & -2\sum_{p\neq 0,p\neq j}\sum_{s}\varepsilon_{cba}\mathrm{Im}\Big(\tilde{B}^{pj_s}C^{j_s0}A^{0p}\Big)\mathcal{D}_p(\omega_c)\mathcal{A}_j(\omega_c) \\ & -2\sum_{s,t}\varepsilon_{cba}\mathrm{Im}\Big(\tilde{B}^{j_tj_s}C^{j_s0}A^{0j_t}\Big)\mathcal{D}_j(\omega_c)\mathcal{A}_j(\omega_c), \quad (\omega_c \approx \omega_j)\,.\end{aligned} \tag{5.8}$$

Note that for a non-degenerate (real) exited state j, the last term vanishes due to an anti-symmetric character of $\tilde{B}^{j_tj_s}$.

Assuming that the excited states are well-separated, the approximation

$$\mathcal{D}_p(\omega_c) \approx \frac{1}{\omega_p - \omega_c}; \qquad \omega_c \approx \omega_j, \quad p \neq j\,, \tag{5.9}$$

may be used to write Eq. (5.8) as

$$\begin{aligned}\mathrm{Re}(\varepsilon_{cba}\overline{\langle\langle A;B,C\rangle\rangle}_{0,\omega_c}) \;\approx\; & -2\sum_{s}\Bigg(\sum_{p\neq 0}\frac{\mathrm{Im}(B^{0p}A^{pj_s}C^{j_s0})}{\omega_p} + 2\sum_{p\neq\{j\}}\frac{\mathrm{Im}(B^{pj_s}C^{j_s0}A^{0p})}{\omega_p-\omega_c}\Bigg)\mathcal{A}_j(\omega_c) \\ & -2\sum_{st}\mathrm{Im}\Big(B^{j_tj_s}C^{j_s0}A^{0j_t}\Big)\mathcal{D}_j(\omega_c)\mathcal{A}_j(\omega_c)\,, \qquad (\omega_c \approx \omega_j)\,,\end{aligned} \tag{5.10}$$

where $\{j\}$ denotes a set of (possibly degenerate) excited states with energy ω_j. In Eq. (5.10), the condition $p \neq 0$ has been removed from the summation in the third term by expanding $\tilde{A}^{pj_s}$ according to Eq. (4.33). $\tilde{B}^{pq}$ equals B^{pq}, due to the fact that a real ground non-degenerate state $|0\rangle$ is considered.

The Faraday $\mathcal{A}$ and $\mathcal{B}$ terms may be introduced (in accordance with Ref. [32]) as[8]

$$\mathcal{A}(0\to j) \;=\; \frac{1}{2}\sum_{st}\varepsilon_{cba}\mathrm{Im}\Big(B^{j_tj_s}C^{j_s0}A^{0j_t}\Big) = \frac{1}{2}\varepsilon_{cba}\sum_{s}B^{\bar{j}_s\bar{j}_s}\mathrm{Im}\Big(A^{0\bar{j}_s}C^{\bar{j}_s0}\Big)\,, \tag{5.11}$$

$$\mathcal{B}(0\to j) \;=\; \sum_{s}\varepsilon_{cba}\Bigg(\sum_{p\neq 0}\frac{\mathrm{Im}(B^{0p}A^{pj_s}C^{j_s0})}{\omega_p} + \sum_{p\neq\{j\}}\frac{\mathrm{Im}(B^{pj_s}C^{j_s0}A^{0p})}{\omega_p-\omega}\Bigg)\,. \tag{5.12}$$

For the $\mathcal{A}$ term, the real degenerate states j_s have been expanded in complex states $\bar{j}_s$, that diagonalize the imaginary B operator.

Using Eqs. (5.11) and (5.12), Eq. (5.10) may be written as

$$\varepsilon_{cba}\mathrm{Re}(\overline{\langle\langle A;B,C\rangle\rangle}_{0,\omega_c} = -2\mathcal{A}_j(\omega_c)\mathcal{B}(0\to j) - 4\mathcal{A}_j(\omega_c)\mathcal{D}_j(\omega_c)\mathcal{A}(0\to j) \qquad (\omega_c \approx \omega_j)\,. \tag{5.13}$$

[8]Where the notation $A = \mu_\gamma$, $B = m_\beta$ and $C = \mu_\alpha$ has been used.

Using that $\omega_c = \omega$ and inserting Eq. (5.13) into Eq. (5.3), the following expression for the ellipticity is obtained

$$\theta = -\frac{1}{12}\omega\mu_0 clNB_Z\Big(2\mathcal{A}_j(\omega)\mathcal{B}(0\to j) + 4\mathcal{A}_j(\omega)\mathcal{D}_j(\omega)\mathcal{A}(0\to j)\Big) \qquad (\omega \approx \omega_j)\,. \tag{5.14}$$

Noting that

$$\frac{\partial \mathcal{A}_j(\omega)}{\partial \omega} = 2\mathcal{D}_j(\omega)\mathcal{A}_j(\omega)\,, \tag{5.15}$$

it may be seen that the Faraday $\mathcal{B}$ terms are associated with an absorption line-shape function, whereas the $\mathcal{A}$ terms are associated with a derivative line-shape function. Eq. (5.14) may be written as

$$\theta = -\tfrac{1}{6}\omega\mu_0 clNB_z\Big(\mathcal{A}_j(\omega)\mathcal{B}(0\to j) + \tfrac{\partial \mathcal{A}_j(\omega)}{\partial \omega}\mathcal{A}(0\to j)\Big) \qquad (\omega \approx \omega_j)\,. \tag{5.16}$$

Eq. (5.3) gives therefore an MCD spectrum with contributions from both the Faraday $\mathcal{A}$ and $\mathcal{B}$ terms. The $\mathcal{A}$ and $\mathcal{B}$ contributions cannot be separated, however the spectral profile can be used to extract information about the individual $\mathcal{A}$ and $\mathcal{B}$ terms, according to the method-of-moments [131, 137][9]

$$\mathcal{A}(0\to j) = \frac{1}{33.53}\int_j (\tilde{\nu} - \tilde{\nu}_j)\frac{[\theta]_M}{\tilde{\nu}}d\tilde{\nu}\,, \tag{5.17}$$

$$\mathcal{B}(0\to j) = -\frac{1}{33.53}\int_j \frac{[\theta]_M}{\tilde{\nu}}d\tilde{\nu}\,, \tag{5.18}$$

where $\tilde{\nu}$ is a wavenumber. The molecular ellipticity $[\theta]_M$ is related to ellipticity θ in Eq. (5.1) by

$$[\theta]_M = \frac{M\theta}{cl}\,, \tag{5.19}$$

where M is the molecular mass, c the concentration (in g/100 cm^3) and l the path length (dm).

The individual $\mathcal{A}$ and $\mathcal{B}$ terms can be calculated directly using standard response theory from the double and single residue of the standard quadratic response function, respectively

$$\mathcal{A}(0\to j) = -\frac{1}{2}\varepsilon_{cba}\mathrm{Im}\Bigg\{\lim_{\omega_a\to-\omega_j}(\omega_a+\omega_j)\Bigg(\lim_{\omega_c\to\omega_j}(\omega_c-\omega_j)\langle\langle A;B,C\rangle\rangle_{\omega_b,\omega_c}\Bigg)\Bigg\}\,, \tag{5.20}$$

$$\mathcal{B}(0\to j) = -\varepsilon_{cba}\mathrm{Im}\Bigg\{\lim_{\omega_c\to\omega_j}(\omega_c-\omega_j)\langle\langle A;B,C\rangle\rangle_{0,\omega_c}\Bigg\}\,. \tag{5.21}$$

It should be noted that the expression in Eq. (5.21) is only valid for a non-degenerate excited state j, see Paper C for details.

[9] The method-of-moments expressions rely on different line-shape functions than Eqs. (4.17a) and (4.17b), but the general principle is applicable.

5.1.2 Numerical instabilities for non-degenerate states

Qualitatively correct spectra in the entire frequency range may be obtained using damped response theory, due to the fact the line-shape functions are build into the theory. In standard response theory MCD spectra are obtained from the residues of the quadratic response functions, and singularities may occur for near-degenerate states (see Paper C for details).

In Fig. 5.1, an MCD spectrum is displayed for a model H_3 molecule, in a D_{3h} and C_{2v} molecular configurations. Calculations have been performed at the HF level of theory using the minimal Hückel basis, with only one $1s$ orbital on each Hydrogen atom. This basis have been chosen, due to the fact that the MCD spectrum for this system consists of only the $\mathcal{A}$ term[10] in configuration D_{3h}, whereas in configuration C_{2v}, it contains a positive and a negative $\mathcal{B}$ term, see Figs. 5.1a and 5.1b, respectively. The molecular ellipticity $[\theta]_M$ (given in units: deg $\cdot$ dl^{-}1$\cdot$dm$^{-1}\cdot$mol$^{-1}\cdot$G^{-1}) is plotted against wavenumber ν.

The $\mathcal{A}$ term arises in the MCD spectrum, only if either the ground or the excited state

[10]Usually an $\mathcal{A}$ term occur in the MCD spectrum in combination with a $\mathcal{B}$ term.

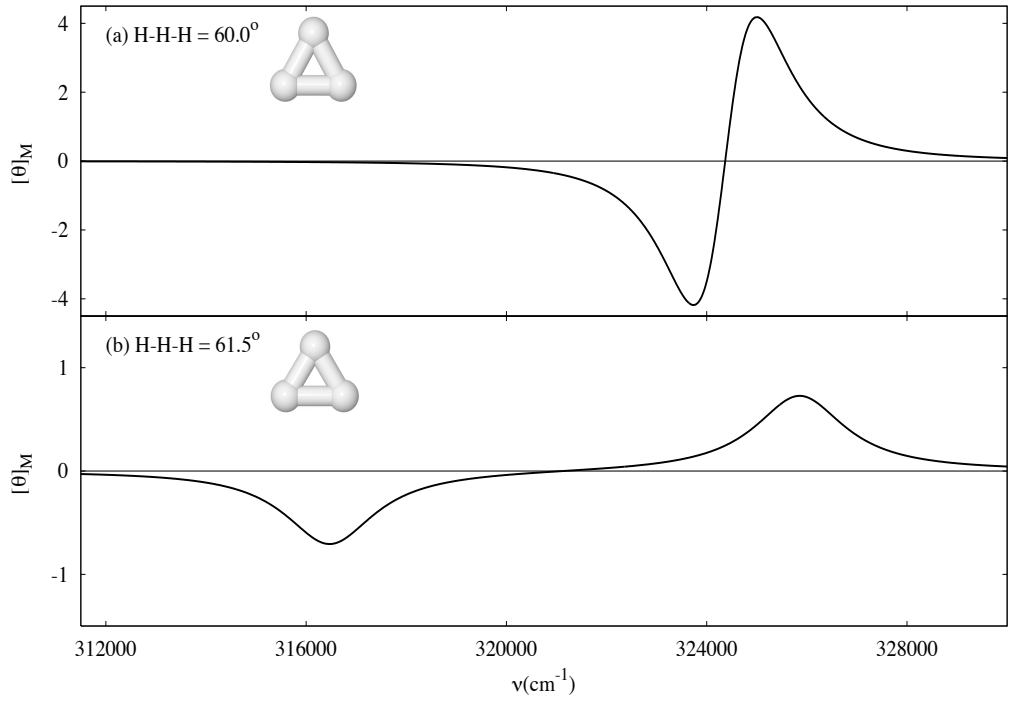

Figure 5.1: The MCD spectra for an H_3 model molecule in **(a)** a D_{3h} configuration, **(b)** a C_{2v} configuration with a $\widehat{\mathrm{HHH}}$ angle of 61.5°, HF/Hückel basis, $\gamma = 0.005$ a.u..

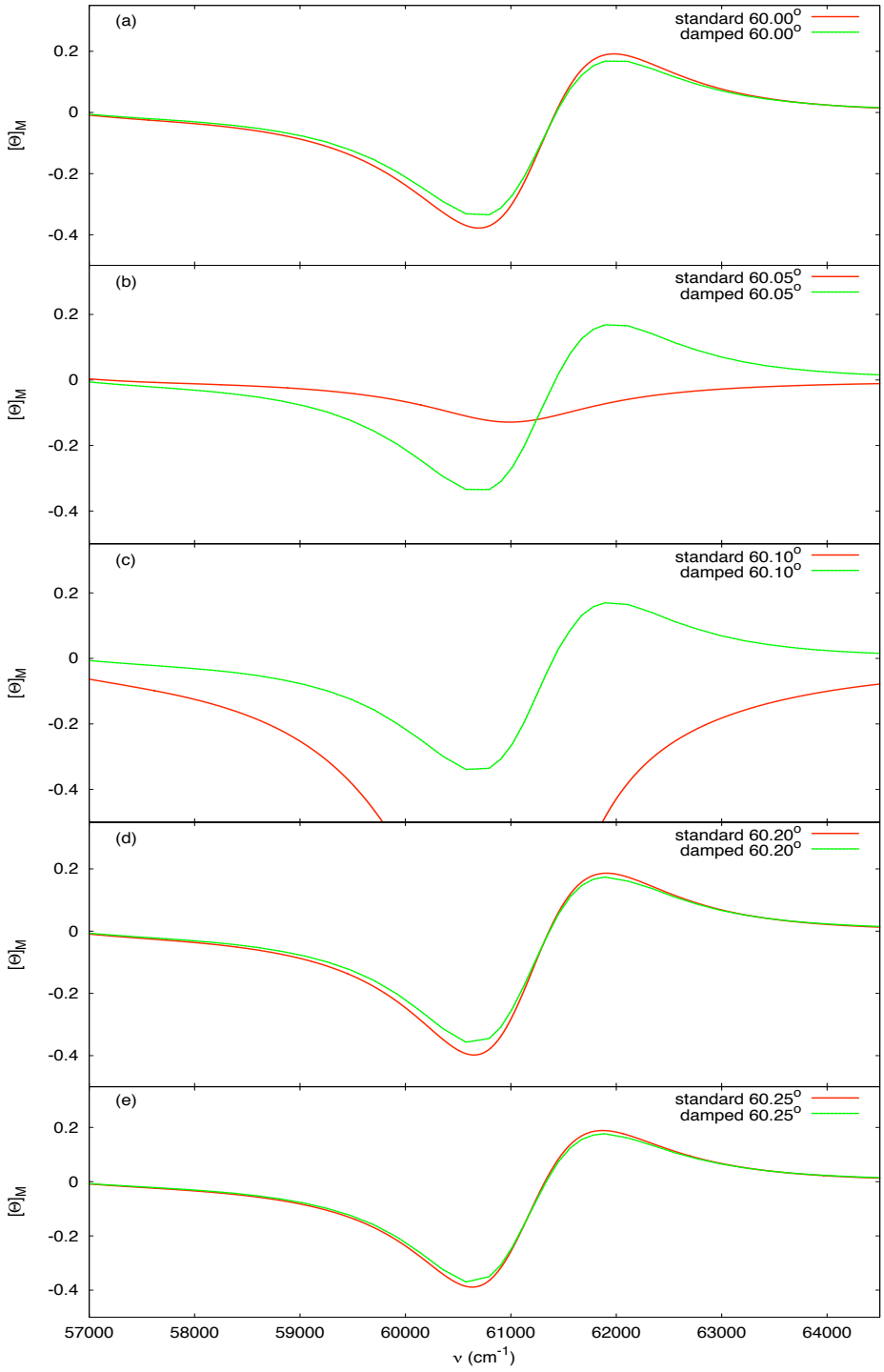

Figure 5.2: The MCD spectra for cyclopropane obtained using the damped (red) and standard (green) response theories. Standard spectra have been simulated by calculation of individual $\mathcal{A}$ and $\mathcal{B}$ terms. **(a)** a D_{3h} configuration, **(b)**–**(e)** C_{2v} configurations with a $\widehat{\mathrm{CCC}}$ angle of 60.05°, 60.10°, 60.20° and 60.25°, respectively; B3LYP/cc-pVDZ, $\gamma = 0.005$ a.u..

is degenerate. Therefore, as the structure of the system in configuration C_{2v} approaches the geometry with symmetry D_{3h}, the two $\mathcal{B}$ terms for non-degenerate states (Fig. 5.1b) become an $\mathcal{A}$ term for the degenerate state (Fig. 5.1a). It can be seen from Fig. 5.1 that the $\mathcal{A}$ term is associated with the derivative line-shape function, whereas the $\mathcal{B}$ term contributes to the spectrum with an absorption line-shape function band, as discussed in Section 5.1.1.

In Fig. 5.2, a more chemically relevant example is given. An MCD spectrum for cyclopropane is displayed, determined using standard and damped response theories at the B3LYP/aug-cc-pVDZ [138,139] level of theory. In Fig. 5.2a, the cyclopropane molecule with molecular symmetry D_{3h}, presented in Fig. 5.3b, is considered. This system has a doubly-degenerate state g with two components g_f and g_j. Changing one of the $\widehat{\mathrm{CCC}}$ angles of cyclopropane, lowers the molecular symmetry to C_{2v} (Fig. 5.3a), and the degenerate g state splits into two non-degenerate states f and j. The MCD spectrum of the cyclopropane in molecular symmetry C_{2v} is depicted in Figs. 5.2b–5.2e.

As mentioned above, the $\mathcal{A}$ term arises only in case of degenerate ground or excited state. Therefore, similarly as for H_3, when the structure of the system in Fig. 5.3a approaches the geometry in Fig. 5.3b, the two $\mathcal{B}$ terms for f and j states, transform into a $\mathcal{B}$ term and an

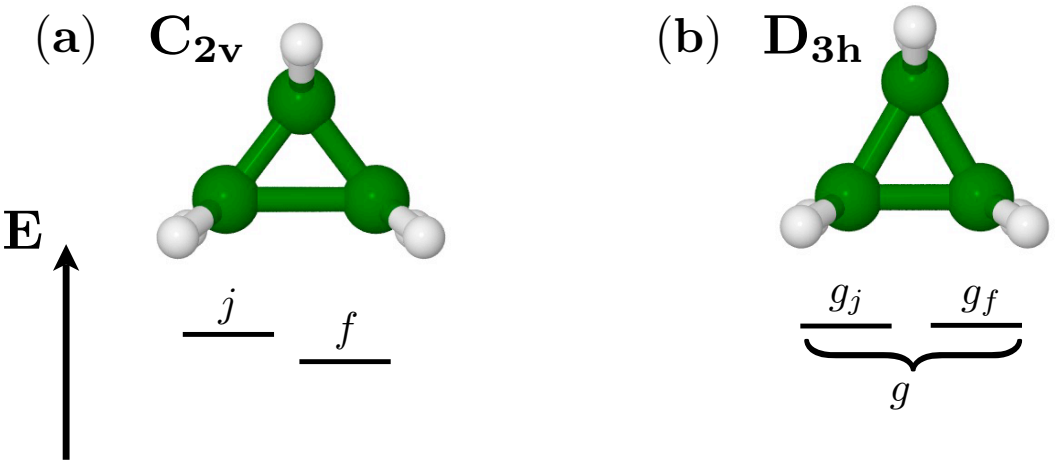

$$\theta^{fj} = -K\omega\Big\{\mathcal{A}_j(\omega)\mathcal{B}(0\to j) + \mathcal{A}_f(\omega)\mathcal{B}(0\to f)\Big\}$$

$$\theta^{g_f g_j} = -K\omega\Big\{\mathcal{A}_g(\omega)\mathcal{B}(0\to g) + \frac{\partial\mathcal{A}_g(\omega)}{\partial\omega}\mathcal{A}(0\to g)\Big\}$$

Figure 5.3: Cyclopropane in **(a)** a C_{2v} and **(b)** a D_{3h} configuration. The C_{2v} configuration is obtained by increasing one of the $\widehat{\mathrm{CCC}}$ angles. Contributions to the ellipticity in particular configurations are given below the figures.

$\mathcal{A}$ term for the degenerate g state. The $\mathcal{A}$ term enters when state f approaches state j, due to the fact that a factor in the line-shape function cancels a term in the original $\mathcal{B}$ terms for the states f and j, as derived in detail in Paper C. In Figs. 5.2b and 5.2c, the numerical instabilities for the non-degenerate states, due to the incorrect treating of this cancellation, are displayed. As can be seen in Fig. 5.2, numerical instabilities are observed when line-shape functions are superimposed onto the $\mathcal{B}$ terms calculated using standard response theory to simulate an experimental spectrum (red curve). In contrast, in the damped response theory formulation for MCD, the line-shape functions are built into the theory and no such instabilities occur, as can be seen from Figs. 5.2b and 5.2c (green curve).

From Figure 5.2, it may be concluded that the individual $\mathcal{A}$ and $\mathcal{B}$ terms, obtained using the standard response theory for molecules with near-degenerate states, may not be reliable due to numerical instabilities. However, no such problems occur when the damped response theory is used. Therefore, it is advantageous to verify the results obtained with standard response theory for molecules with near-degenerate states, using damped response theory.

5.2 Damped Two-Photon Absorption

Another example of a higher-order property is the Two-Photon Absorption (TPA). TPA describes a simultaneous absorption of two photons of frequencies ω_a and ω_b in order to excite a molecule from one state (usually the ground state $|0\rangle$) to a higher energy state $|n\rangle$. The energy difference between the lower and upper states of the molecule is equal to the sum of the energies of the two photons ($\omega_n = \omega_a + \omega_b$).

The (a, b)th component of the two-photon transition amplitude tensor $T^{ab}_{0n}(\omega_a, \omega_b)$ may be written as [140, 141]

$$T^{ab}_{0n}(\omega_a, \omega_b) = \sum_{p>0} \left(\frac{A^{0p}\tilde{B}^{pn}}{\omega_p - \omega_a} + \frac{B^{0p}\tilde{A}^{pn}}{\omega_p - \omega_b} \right), \tag{5.22}$$

where the notation introduced in Section 3.1.3 and in Eq. (4.34) has been used. The summation runs over all excited states and A and B are components of the electric dipole operator.

Assuming that the two photons have the same energy, (*i.e.* $\omega_a = \omega_b = \omega$), $T^{ab}_{0n}(\omega, \omega)$ becomes a symmetric tensor. Together with the assumption that all excited states are real, the symmetry relations hold

$$T^{ab}_{0n}(\omega, \omega) = T^{ab}_{0n}(\omega, \omega)^* = T^{ba}_{0n}(\omega, \omega) = T^{ba}_{0n}(\omega, \omega)^* . \tag{5.23}$$

The isotropically averaged expression for the TPA strength $\langle \delta \rangle$ in a sample of randomly

tumbling molecules is given by [141]

$$\begin{aligned}\langle\delta(\omega)\rangle &= \langle T^{ab}_{0n}(\omega,\omega)T^{cd}_{0n}(\omega,\omega)\rangle_{av} \\ &= \frac{1}{30}\sum_{a,b}\left\{F T^{aa}_{0n}(\omega,\omega)T^{bb}_{0n}(\omega,\omega) + (G+H)T^{ab}_{0n}(\omega,\omega)T^{ab}_{0n}(\omega,\omega)\right\},\end{aligned} \tag{5.24}$$

where the sums run over the x, y, z components of the molecular axes, and the numbers F, G, and H depend on the polarization of the incident photons, *e.g.* if both photons are linearly polarized with parallel propagation, $F = G = H = 2$ [141].

In standard response theory, the TPA amplitude may formally be determined from a residue analysis of the quadratic response function [16]. However, the physical observable, *i.e.* the TPA strength tensor $T^{ab}_{0n}(\omega,\omega)T^{cd}_{0n}(\omega,\omega)$ in Eq. (5.24) is determined from a residue of the cubic response function at $\omega_{cd} = \omega_n$

$$T^{ab}_{0n}(-\omega_a,-\omega_b)T^{cd}_{0n}(\omega_c,\omega_d) = \lim_{\omega_{cd}\to\omega_n}(\omega_{cd}-\omega_n)\langle\langle\mu^a;\mu^b,\mu^c,\mu^d\rangle\rangle_{\omega_b,\omega_c,\omega_d}\,. \tag{5.25}$$

When identifying the residue of the cubic response function at $\omega_{cd} = \omega_n$ only terms containing x^{cd}_n will contribute

$$\lim_{\omega_{cd}\to\omega_n}(\omega_{cd}-\omega_n)\langle\langle\mu^a;\mu^b,\mu^c,\mu^d\rangle\rangle_{\omega_b,\omega_c,\omega_d} = \lim_{\omega_{cd}\to\omega_n}(\omega_{cd}-\omega_n)\langle\langle\mu^a;\mu^b,\mu^c,\mu^d\rangle\rangle_{\omega_b,\omega_c,\omega_d}(x^{cd})\,, \tag{5.26}$$

and therefore it is sufficient to consider $\langle\langle\mu^a;\mu^b,\mu^c,\mu^d\rangle\rangle_{\omega_b,\omega_c,\omega_d}(x^{cd})$ expressed as

$$\begin{aligned}\langle\langle\mu^a;\mu^b,\mu^c,\mu^d\rangle\rangle_{\omega_b,\omega_c,\omega_d}(x^{cd}) = -\sum_{q>0}\Bigg\{&\frac{T^{ab}_{0q}(-\omega_a,-\omega_b)T^{cd}_{0q}(\omega_c,\omega_d)}{\omega_q-\omega_{cd}} \\ &+\frac{T^{ab}_{0q}(\omega_a,\omega_b)T^{cd}_{0q}(-\omega_c,-\omega_d)}{\omega_q+\omega_{cd}}\Bigg\},\end{aligned} \tag{5.27}$$

as a modified standard TPA response function.

When the optical frequency equals a lower lying excitation energy ($\omega = \omega_m = \omega_n/2$), the standard expression for $T^{ab}_{0n}(\omega,\omega)$ diverges. This problem does not occur when the damped cubic response theory is used to describe TPA [33], as will be discussed in the following sections.

5.2.1 Two-photon absorption in damped response theory

Damped response theory may be applied to the modified standard TPA response function in Eq. (5.27), since only terms containing x^{cd}_n contribute to the residue of the cubic response

function at $\omega_{cd} = \omega_n$. The damped TPA response function $\langle\langle\overline{A;B,C,D}\rangle\rangle_{\omega_b,\omega_c,\omega_d}(\bar{x}^{cd})$ may therefore be written as (see Papers A and D for details)

$$\begin{aligned}\langle\langle\overline{A;B,C,D}\rangle\rangle_{\omega_b,\omega_c,\omega_d}(\bar{x}^{cd}) &= -\sum_{q>0}\Bigg\{\frac{T^{ab}_{0q}(-\omega_a - i\gamma, -\omega_b - i\gamma)T^{cd}_{0q}(\omega_c + i\gamma, \omega_d + i\gamma)}{\omega_q - \omega_{cd} - i\gamma} \\ &\qquad + \frac{T^{ab}_{0q}(\omega_a + i\gamma, \omega_b + i\gamma)T^{cd}_{0q}(-\omega_c - i\gamma, -\omega_d - i\gamma)}{\omega_q + \omega_{cd} + i\gamma}\Bigg\} \\ &= -\sum_{q>0}\Bigg\{\frac{T^{ab}_{0q}(\omega - i\gamma, \omega - i\gamma)T^{cd}_{0q}(\omega + i\gamma, \omega + i\gamma)}{\omega_q - 2\omega - i\gamma} \\ &\qquad + \frac{T^{ab}_{0q}(-\omega + i\gamma, -\omega + i\gamma)T^{cd}_{0q}(-\omega - i\gamma, -\omega - i\gamma)}{\omega_q + 2\omega + i\gamma}\Bigg\},\end{aligned} \tag{5.28}$$

where the following frequency relations have been used to obtain the last equality

$$\omega_a = \omega_b = -\omega; \qquad \omega_c = \omega_d = \omega; \qquad \omega_{cd} = \omega_c + \omega_d = 2\omega\,. \tag{5.29}$$

The (a,b)th component of the two-photon transition amplitude tensor for a complex frequency in Eq. (5.28) is given as

$$T^{ab}_{0n}(-\omega_a - i\gamma, -\omega_b - i\gamma) = \sum_{p>0}\left(\frac{A^{0p}\tilde{B}^{pn}}{\omega_p + \omega_a + i\gamma} + \frac{B^{0p}\tilde{A}^{pn}}{\omega_p + \omega_b + i\gamma}\right). \tag{5.30}$$

The norm of the denominator in the first term of Eq. (5.28) is smaller than in the second term, since $\omega > 0$. Furthermore, the norm of the damped TPA amplitudes is much larger in the first term than in the second

$$|T^{ab}_{0q}(\omega - i\gamma, \omega - i\gamma)| \;\gg\; |T^{ab}_{0q}(-\omega + i\gamma, -\omega + i\gamma)|\,, \tag{5.31a}$$

$$|T^{cd}_{0q}(\omega + i\gamma, \omega + i\gamma)| \;\gg\; |T^{cd}_{0q}(-\omega - i\gamma, -\omega - i\gamma)|\,, \tag{5.31b}$$

as follows from Eq. (5.22). The first term in Eq. (5.28) is therefore significantly larger than the second term, and for analysis purposes only the first term will be considered

$$\langle\langle\overline{A;B,C,D}\rangle\rangle_{\omega_b,\omega_c,\omega_d}(\bar{x}^{cd}) \approx -\sum_{q>0}\frac{T^{ab}_{0q}(\omega - i\gamma, \omega - i\gamma)T^{cd}_{0q}(\omega + i\gamma, \omega + i\gamma)}{\omega_q - 2\omega - i\gamma}\,. \tag{5.32}$$

The isotropic average of the imaginary components of the numerator in Eq. (5.32) vanishes, as discussed in Paper D, and only the real parts of the damped TPA strength components contribute to the physical observable TPA. The (a,b,c,d)th component of the damped

TPA strength tensor component in Eq. (5.32) may thus be written as

$$\begin{aligned} T_{0q}^{ab}(\omega - i\gamma, \omega - i\gamma) T_{0q}^{cd}(\omega + i\gamma, \omega + i\gamma) = \\ &= P_{ab}\Big[\sum_{p>0} \frac{A^{0p}\tilde{B}^{pq}}{\omega_p - \omega + i\gamma}\Big] P_{cd}\Big[\sum_{r>0} \frac{C^{0r}\tilde{D}^{rq}}{\omega_r - \omega - i\gamma}\Big] \\ &= P_{ab}P_{cd} \sum_{p>0,r>0} \Big\{ A^{0p}\tilde{B}^{pq}C^{0r}\tilde{D}^{rq}\big[\mathcal{D}_p(\omega)\mathcal{D}_r(\omega) + \mathcal{A}_p(\omega)\mathcal{A}_r(\omega)\big] \Big\} \\ &= \Phi_q^{abcd}(\omega) + \Lambda_q^{abcd}(\omega)\,, \end{aligned} \tag{5.33}$$

where the P_{ab} operator creates a sum of the two possible permutations for the A and B operators, and the dispersion $\mathcal{D}(\omega)$ and absorption $\mathcal{A}(\omega)$ functions are given in Eqs. (4.17a) and (4.17b), respectively. In Eq. (5.33), the damped TPA strength functions $\Phi_q^{abcd}(\omega)$ and $\Lambda_q^{abcd}(\omega)$ have been introduced as

$$\Phi_q^{abcd}(\omega) = P_{ab}P_{cd} \sum_{p>0,r>0} A^{0p}\tilde{B}^{pq}C^{0r}\tilde{D}^{rq}\mathcal{D}_p(\omega)\mathcal{D}_r(\omega)\,, \tag{5.34a}$$

$$\Lambda_q^{abcd}(\omega) = P_{ab}P_{cd} \sum_{p>0,r>0} A^{0p}\tilde{B}^{pq}C^{0r}\tilde{D}^{rq}\mathcal{A}_p(\omega)\mathcal{A}_r(\omega)\,. \tag{5.34b}$$

Note that both $\Phi_q^{abcd}(\omega)$ and $\Lambda_q^{abcd}(\omega)$ are purely real.

Inserting Eq. (5.33) into Eq. (5.32) gives

$$\begin{aligned} \langle\langle \overline{A; B, C, D} \rangle\rangle_{\omega_b,\omega_c,\omega_d}(\bar{x}^{cd}) &\approx -\sum_{q>0} \frac{\Phi_q^{abcd}(\omega) + \Lambda_q^{abcd}(\omega)}{\omega_q - 2\omega - i\gamma} \\ &= -\sum_{q>0} \big[\Phi_q^{abcd}(\omega) + \Lambda_q^{abcd}(\omega)\big]\big[\mathcal{D}_q(2\omega) + i\mathcal{A}_q(2\omega)\big]\,. \end{aligned} \tag{5.35}$$

The imaginary part of Eq. (5.35) represents a spectrum of the (a, b, c, d)th component of the damped TPA tensor $[\Phi_q^{abcd}(\omega) + \Lambda_q^{abcd}(\omega)]$. It is thus convenient to introduce a function $W^{abcd}(\omega)$, which is the negative imaginary component of Eq. (5.35)

$$W^{abcd}(\omega) = -\mathrm{Im}\big[\langle\langle \overline{A; B, C, D} \rangle\rangle_{\omega_b,\omega_c,\omega_d}(\bar{x}^{cd})\big] \approx W_\Phi^{abcd}(\omega) + W_\Lambda^{abcd}(\omega)\,, \tag{5.36}$$

where

$$W_\Phi^{abcd}(\omega) = \sum_{q>0} \Phi_q^{abcd}(\omega)\mathcal{A}_q(2\omega)\,, \tag{5.37a}$$

$$W_\Lambda^{abcd}(\omega) = \sum_{q>0} \Lambda_q^{abcd}(\omega)\mathcal{A}_q(2\omega)\,. \tag{5.37b}$$

$W^{abcd}(\omega)$ generally differs from a standard TPA stick spectrum with superimposed Lorentzian line-shape functions (for details, see Paper D). If ω is in a far-off-resonance region,

the standard TPA spectrum with superimposed line-shape functions and the damped TPA spectrum are similar, as will be discussed in Section 5.2.2. However, if ω is close to resonance the spectrum determined using the standard response theory diverges, whereas the damped TPA spectrum is still well-defined, as demonstrated in Section 5.2.3. In Section 5.2.4, the relative magnitudes of the damped TPA strengths for these two cases will be compared.

5.2.2 The single-resonance case

In general, the broadening factor γ is much smaller than the optical frequencies. Therefore, if the optical frequency in Eqs. (4.17a) and (4.17b) is far from ω_k, the γ^2 factor in the denominator of $\mathcal{D}_k(\omega)$ may be omitted, and $\mathcal{A}_k(\omega)$ is close to zero. $\Lambda_q^{abcd}(\omega)$ in Eq. (5.34b) is therefore close to zero

$$\Lambda_q^{abcd}(\omega) \approx 0\,, \qquad (\omega \text{ far-off-resonance})\,, \tag{5.38}$$

whereas $\Phi_q^{abcd}(\omega)$ approximately equals the standard TPA strength in Eq. (5.22) evaluated at the optical frequency ω

$$\Phi_q^{abcd}(\omega) \approx T_{0q}^{ab}(\omega,\omega)T_{0q}^{cd}(\omega,\omega)\,, \qquad (\omega \text{ far-off-resonance})\,. \tag{5.39}$$

Inserting Eq. (5.39) into Eq. (5.37a) gives

$$W^{abcd}(\omega) \approx W_\Phi^{abcd}(\omega) \approx \sum_{q>0} T_{0q}^{ab}(\omega,\omega)T_{0q}^{cd}(\omega,\omega)\mathcal{A}_q(2\omega)\,, \qquad (\omega \text{ far-off-resonance})\,. \tag{5.40}$$

Thus, when ω is far-off-resonance, $W^{abcd}(\omega)$ represents a γ-broadened standard TPA spectrum, where the standard TPA strength $T_{0q}^{ab}(\omega,\omega)T_{0q}^{cd}(\omega,\omega)$ for the $|0\rangle\!\rightarrow\!|q\rangle$ transition is weighted by the absorption line-shape function $\mathcal{A}_q(2\omega)$ centered at ω_q.

5.2.3 The double-resonance case

In the double-resonance case, both ω and 2ω are close to resonance ($\omega \approx \omega_m$ and $2\omega \approx \omega_n$, see Fig. 5.4). In this case the standard expression for the TPA amplitude in Eq. (5.22) becomes artificially large, and it diverges in the limit where $\omega = \omega_m = \omega_n/2$, whereas when damped response theory is used, no such problems occur.

When ω is close to ω_m, the mth term will dominate in the sum-over-states expression for the TPA amplitude in Eq. (5.22), and the expression for the standard TPA strength approximately becomes

$$\begin{aligned} &T_{0n}^{ab}(\omega_n/2,\omega_n/2)T_{0n}^{cd}(\omega_n/2,\omega_n/2) \approx \\ &\qquad \approx P_{ab}P_{cd}\big(A^{0m}B^{mn}C^{0m}D^{mn}\big)\frac{1}{(\omega_m-\omega_n/2)^2}, \quad (\omega \approx \omega_m \approx \omega_n/2)\,, \end{aligned} \tag{5.41}$$

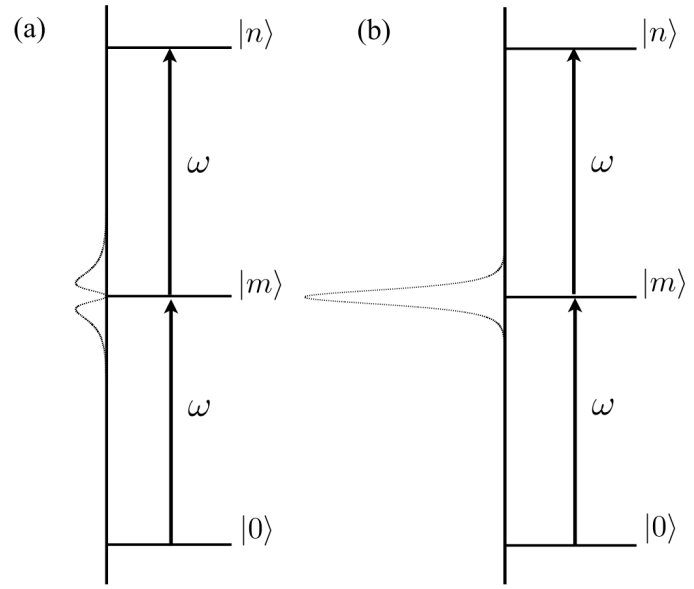

Figure 5.4: Illustration of the TPA $|0\rangle \rightarrow |n\rangle$ transition in the case of exact double-resonance $\omega = \omega_m = \omega_n/2$. To the left of the figures: **(a)** $\mathcal{D}_m(\omega)^2\mathcal{A}_n(2\omega)$, which determines the overall structure of $W_\Phi^{abcd}(\omega)$; **(b)** $\mathcal{A}_m(\omega)^2\mathcal{A}_n(2\omega)$, which determines the overall structure of $W_\Lambda^{abcd}(\omega)$.

which diverges when $\omega_m = \omega_n/2$. Using Eq. (5.41), the standard stick spectrum with a superimposed line-shape function is given by

$$\begin{aligned}&\mathrm{TPA}_{|0\rangle\rightarrow|n\rangle}(\text{standard}) \approx \\ &\qquad \approx P_{ab}P_{cd}\big(A^{0m}B^{mn}C^{0m}D^{mn}\big)\frac{1}{(\omega_m-\omega_n/2)^2}\mathcal{A}_n(2\omega), \quad (\omega\approx\omega_m\approx\omega_n/2). \quad (5.42)\end{aligned}$$

In analogy with the standard case, at $\omega \approx \omega_m$ the mth term will dominate the overall shapes of $\Phi_n^{abcd}(\omega)$ and $\Lambda_n^{abcd}(\omega)$ in Eqs. (5.34a) and (5.34b)

$$\Phi_n^{abcd}(\omega) \approx P_{ab}P_{cd}\big(A^{0m}B^{mn}C^{0m}D^{mn}\big)\mathcal{D}_m(\omega)^2\,, \qquad (\omega\approx\omega_m\approx\omega_n/2)\,, \quad (5.43a)$$

$$\Lambda_n^{abcd}(\omega) \approx P_{ab}P_{cd}\big(A^{0m}B^{mn}C^{0m}D^{mn}\big)\mathcal{A}_m(\omega)^2\,, \qquad (\omega\approx\omega_m\approx\omega_n/2)\,. \quad (5.43b)$$

In the double-resonance case the damped TPA expressions may be approximated by the nth term in the sum-over-states expression in Eq. (5.37)

$$W_\Phi^{abcd}(\omega) \approx P_{ab}P_{cd}\big(A^{0m}B^{mn}C^{0m}D^{mn}\big)\mathcal{D}_m(\omega)^2\mathcal{A}_n(2\omega), \quad (\omega\approx\omega_m\approx\omega_n/2)\,, \quad (5.44a)$$

$$W_\Lambda^{abcd}(\omega) \approx P_{ab}P_{cd}\big(A^{0m}B^{mn}C^{0m}D^{mn}\big)\mathcal{A}_m(\omega)^2\mathcal{A}_n(2\omega), \quad (\omega\approx\omega_m\approx\omega_n/2)\,. \quad (5.44b)$$

In Fig. 5.4, the TPA transition $|0\rangle \rightarrow |n\rangle$ transition is illustrated, in the case of exact double-resonance. In Fig. 5.4a, $\mathcal{D}_m(\omega)^2\mathcal{A}_n(2\omega)$ is plotted which determines the overall structure of $W_\Phi^{abcd}(\omega)$ function. The overall structure of $W_\Lambda^{abcd}(\omega)$ is govern by $\mathcal{A}_m(\omega)^2\mathcal{A}_n(2\omega)$ which is displayed in Fig. 5.4b. From the shape of $\mathcal{D}_m(\omega)$ [in Eq. (4.17a)], it may be seen that

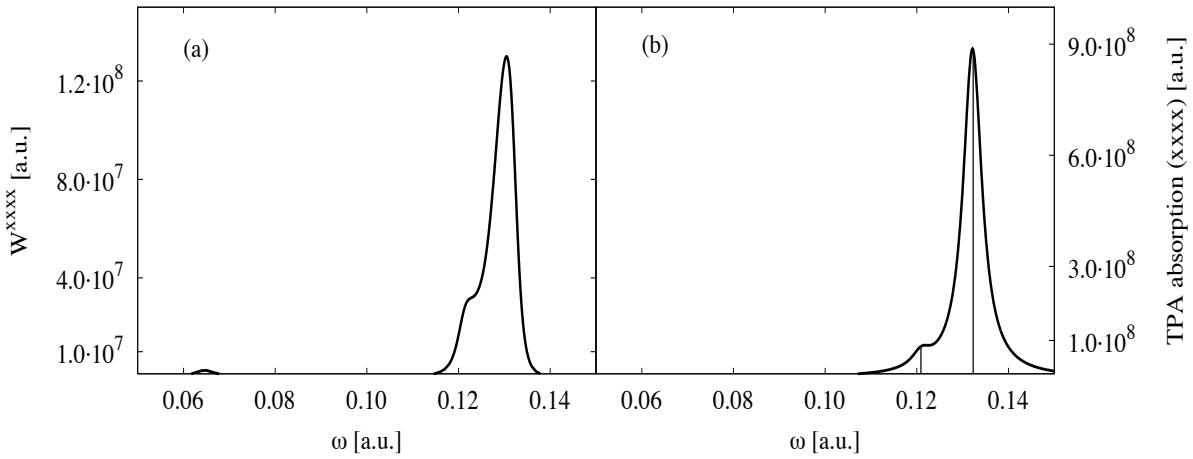

Figure 5.5: TPA spectra for LiH (aligned along the x-axis) at the CAM-B3LYP/cc-pVDZ level of theory using the experimental equilibrium geometry 1.5957 Å. The broadening parameter $\gamma = 0.005$ a.u. **(a)** Damped TPA spectrum. **(b)** Standard TPA spectrum with superimposed line-shape functions, where the positions of $\omega_4/2$ and $\omega_7/2$ are indicated by vertical bars.

$W_\Phi^{abcd}(\omega)$ approaches zero when $\omega \to \omega_m$, whereas $W_\Lambda^{abcd}(\omega)$ has the shape of an absorption line-shape function with a maximum at $\omega = \omega_m$. In the double-resonance case, $W_\Lambda^{abcd}(\omega)$ therefore dominates the overall structure of $W^{abcd}(\omega)$ in contrast to the single-resonance case in Eq. (5.40), where $W_\Phi^{abcd}(\omega)$ is the dominant contribution.

5.2.4 Comparing the single-resonance and approximate double-resonance cases

In this section, the single-resonance case will be compared to the approximate double-resonance case (ω_m is close to $\omega_n/2$). In the approximate double-resonance case, the mth term in the standard TPA amplitude in Eq. (5.22) becomes artificially large, and the perturbation analysis [leading to Eq. (5.22)] is not strictly valid.

In Fig. 5.5, the TPA spectrum for LiH is shown, using (a) damped response theory and (b) standard response theory (stick spectrum with superimposed absorption line-shape functions), at the CAM-B3LYP/cc-pVDZ [142] level of theory. For this molecule, the fourth ($\omega_4 = 0.242$ a.u.) and the seventh ($\omega_7 = 0.264$ a.u.) excited states have the largest TPA strengths, and half their excitation energies approximately equal the first excitation energy ($\omega_1 = 0.129$ a.u.). Transitions $|0\rangle \to |n\rangle$ ($n = 4, 7$) can therefore be considered as approximate double-resonance transitions.

As can be seen in Fig. (5.5), the spectrum of LiH is completely dominated by the presence

of two large peaks, corresponding to the $|0\rangle \rightarrow |4\rangle$ and $|0\rangle \rightarrow |7\rangle$ transitions, respectively. The appearances of the same transitions are quite different in Figs. 5.5a and 5.5b. This is due to the fact that the damped and standard TPA expressions differ significantly in the approximate double-resonance case (see Paper D for details). Note in particular that the positions of the two peak maxima in the damped spectrum in Fig. 5.5a are closer than in the stick spectrum, and that the TPA values in the standard spectrum are nearly an order of magnitude larger than those in the damped spectrum in this case.

In standard (Fig. 5.5b) as well as damped (Fig. 5.5a) response theory, the approximate double-resonance TPA strengths are much larger than the single-resonance TPA strengths, as may be seen by considering the single resonance at frequency $\omega \approx 0.065$ a.u..

5.3 Summary of the damped MCD and TPA analysis

Damped response theory yields qualitatively correct MCD and TPA spectra at all optical frequencies, in contrast to standard response theory, where divergence or numerical instabilities may occur. However, the actual values and peak broadenings in a damped spectrum depend entirely on the empirical broadening parameter γ, and therefore the spectra obtained using damped response theory can be expected to be only qualitatively correct.

For large molecules, the density of the excited states is generally very large, but only a very limited number of the excited states are associated with large absorption strengths. Using standard response theory techniques [16], each excited state must be addressed individually, regardless of its associated absorption strength, making the determination of absorption spectra highly intractable for large molecules. In damped response theory, the focus on the excitations with significant absorption strengths is built into the theory, making damped response theory a very powerful tool for calculating absorption spectra for large molecules [33].

6 Standard iterative algorithms

The solution of linear equations is a central task in obtaining molecular properties. In the early days of quantum chemistry, only small molecular systems were treated and linear equations were solved explicitly by applying standard algorithms of numerical analysis, *e.g.* diagonalization and triangularization methods [25–27]. For larger molecular systems, solving equations explicitly became impossible and iterative subspace algorithms were introduced in quantum chemistry. For example, Pople *et al.* [37] solved the coupled HF equations and Purvis and Bartlett [143] the CCSD amplitude equations using iterative subspace algorithms. When equations are solved using the subspace algorithms, vectors from all iterations must be stored on disk, which becomes impractical for large molecular systems.

The solution of linear equations with a symmetric and positive definite matrix may be formulated as the minimization of a quadratic function. The standard method for this minimization is the conjugate gradient (CG) algorithm [39, 144–146], where in each iteration a new direction, conjugate to all previous directions, is added. The CG algorithm is designed such that the solution vector obtained from the last three trial vectors is identical to the one determined from a subspace algorithm containing all n vectors. In the conventional formulation of the CG algorithm, each iteration can be expressed in terms of a unidirectional search, where the search direction may be determined from information from the last iteration. The handling and storage of trial vectors therefore becomes simplified compared to an iterative subspace formulation. In Ref. [38], Wormer *et al.* recognized that both the subspace iterative algorithms used in Refs. [37] and [143] and the CG algorithm lead to an identical iteration sequence. However, the CG algorithm may only be used for solving linear equations with a positive definite matrix. The conjugate residual (CR) algorithm [40] may be applied to a set of linear equations with a non-positive definite matrix and shares the very attractive feature with the CG algorithm that each iteration can be expressed in terms of a unidirectional search where the search direction may be determined from information from the last iteration. Also, when the CR algorithm is used, the storage and manipulation of a large number of directions may be avoided.

In this chapter, selected iterative algorithms for solving a set of linear equations of the form

$$\mathbf{A}\mathbf{x} = \mathbf{b}\,, \tag{6.1}$$

will be described, where $\mathbf{A}$ is a non-singular matrix of dimension d. The residual $\mathbf{r}$ of Eq. (6.1) for a general vector $\mathbf{x}$ is given as

$$\mathbf{r} = \mathbf{b} - \mathbf{A}\mathbf{x}\,. \tag{6.2}$$

A general iterative subspace algorithm will be described in Section 6.1, while the CG and CR algorithms are described in Sections 6.2 and 6.3, respectively.

6.1 Iterative subspace algorithm

An iterative subspace algorithm is a standard approach for solving a set of linear equations of the form in Eq. (6.1). This approach is very general and can be used in cases where $\mathbf{A}$ is complex, non-Hermitian and/or non-positive definite. A flowchart of the subspace iterative algorithm for solving linear equations is given in Fig. 6.1.

After iteration n of a subspace iterative algorithm, n trial vectors

$$\mathbf{x}^n = \{\mathbf{x}_1, \mathbf{x}_2, ..., \mathbf{x}_n\}\,, \tag{6.3}$$

have been obtained. A subspace of n linearly transformed vectors

$$(\mathbf{Ax})^n = \{\mathbf{Ax}_1, \mathbf{Ax}_2, ..., \mathbf{Ax}_n\}\,, \tag{6.4}$$

is also known. Eq. (6.1) is solved in a reduced subspace of $\mathbf{x}^n$, giving a reduced subspace equation of the form

$$\begin{pmatrix} \mathbf{x}_1^\dagger\mathbf{Ax}_1 & \mathbf{x}_1^\dagger\mathbf{Ax}_2 & \dots & \dots & \mathbf{x}_1^\dagger\mathbf{Ax}_{n-1} & \mathbf{x}_1^\dagger\mathbf{Ax}_n \\ \mathbf{x}_2^\dagger\mathbf{Ax}_1 & \mathbf{x}_2^\dagger\mathbf{Ax}_2 & \dots & \dots & \mathbf{x}_2^\dagger\mathbf{Ax}_{n-1} & \mathbf{x}_2^\dagger\mathbf{Ax}_n \\ \dots & \dots & \dots & \dots & \dots & \dots \\ \dots & \dots & \dots & \dots & \dots & \dots \\ \mathbf{x}_{n-1}^\dagger\mathbf{Ax}_1 & \mathbf{x}_{n-1}^\dagger\mathbf{Ax}_2 & \dots & \dots & \mathbf{x}_{n-1}^\dagger\mathbf{Ax}_{n-1} & \mathbf{x}_{n-1}^\dagger\mathbf{Ax}_n \\ \mathbf{x}_n^\dagger\mathbf{Ax}_2 & \mathbf{x}_n^\dagger\mathbf{Ax}_2 & \dots & \dots & \mathbf{x}_n^\dagger\mathbf{Ax}_{n-1} & \mathbf{x}_n^\dagger\mathbf{Ax}_n \end{pmatrix} \begin{pmatrix} \alpha_1^{(n)} \\ \alpha_2^{(n)} \\ \vdots \\ \vdots \\ \alpha_{n-1}^{(n)} \\ \alpha_n^{(n)} \end{pmatrix} = \begin{pmatrix} \mathbf{x}_1^\dagger\mathbf{b} \\ \mathbf{x}_2^\dagger\mathbf{b} \\ \vdots \\ \vdots \\ \mathbf{x}_{n-1}^\dagger\mathbf{b} \\ \mathbf{x}_n^\dagger\mathbf{b} \end{pmatrix}, \tag{6.5}$$

which determines the optimal solution vector $\tilde{\mathbf{x}}_{n+1}$ in the subspace $\mathbf{x}^n$

$$\tilde{\mathbf{x}}_{n+1} = \sum_{i=1}^{n} \alpha_i^{(n)} \mathbf{x}_i\,. \tag{6.6}$$

The residual vector $\mathbf{r}_{n+1}$ in Eq. (6.2) for an optimal vector in Eq. (6.6) is given as

$$\mathbf{r}_{n+1} = \mathbf{b} - \mathbf{A}\tilde{\mathbf{x}}_{n+1} = \mathbf{b} - \sum_{i=1}^{n} \alpha_i^{(n)} \mathbf{Ax}_i\,. \tag{6.7}$$

The residual vector is calculated to check for convergence of the iterative scheme and to obtain a new trial vector. The iterative procedure is converged when the residual norm $||\mathbf{r}_{n+1}||$ is smaller than a preset threshold. The new trial vector $\mathbf{x}_{n+1}$, equal to the residual

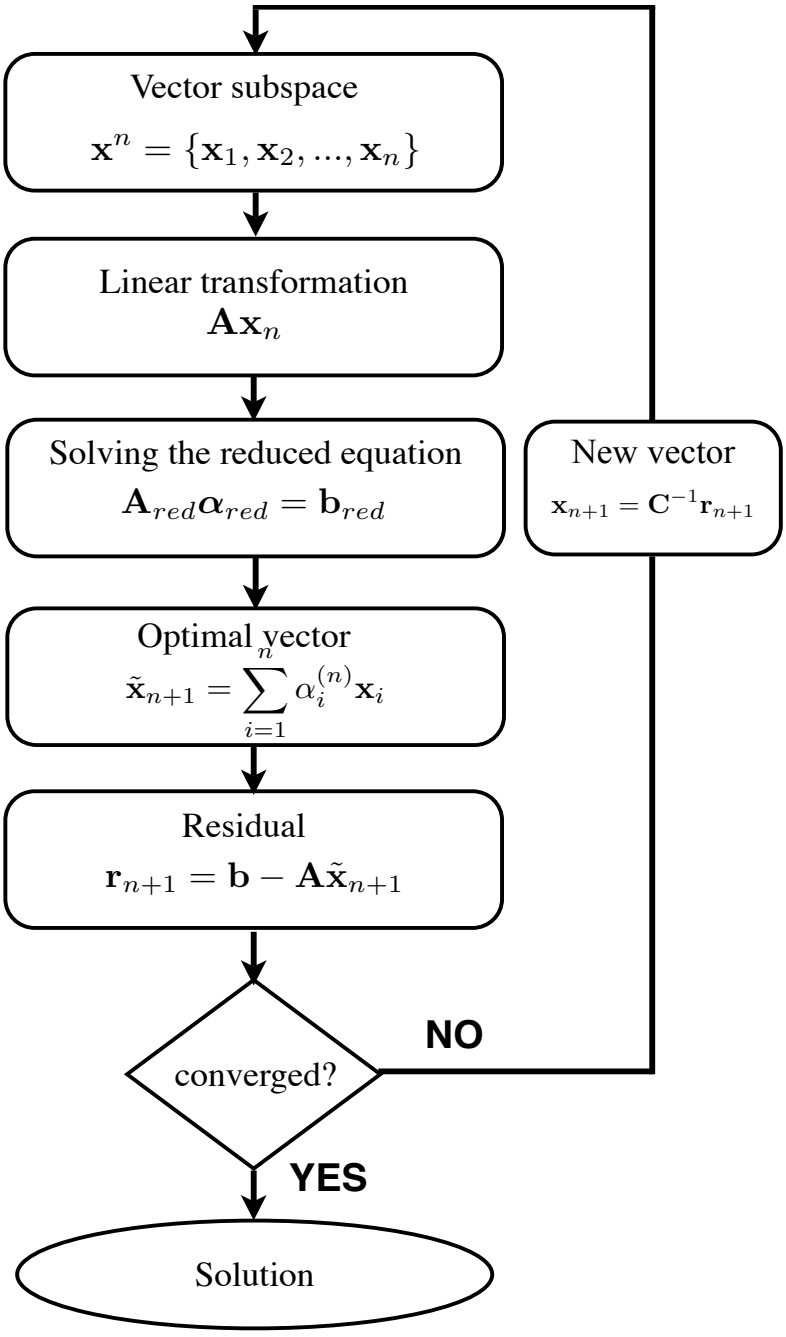

Figure 6.1: Flowchart of the subspace iterative algorithm for solving linear equations.

$\mathbf{r}_{n+1}$, is added to the subspace in Eq. (6.3) and the iteration procedure is continued until convergence is obtained.

The convergence of the algorithm depends on the condition number of $\mathbf{A}$. The condition number may be decreased, and therefore the convergence of the algorithm may be improved, by introducing preconditioning [147] in Eq. (6.1). The new trial vector is then obtained from the preconditioned residual as

$$\mathbf{x}_{n+1} = \mathbf{C}^{-1}\mathbf{r}_{n+1}\,, \tag{6.8}$$

where preconditioner $\mathbf{C}$ is an easily invertible approximation to $\mathbf{A}$ in Eq. (6.1).

The iterative subspace algorithm is commonly used in quantum chemistry for solving sets of linear equations. It has the advantage that it may be applied for all types of linear equations (with a non-singular matrix $\mathbf{A}$). However, whole sets of vectors $\mathbf{x}^n$ and $(\mathbf{Ax})^n$ in Eqs. (6.3) and (6.4), respectively, have to be stored on disk. For calculations on large molecular systems, disk storage requirements may therefore be high.

6.2 The conjugate gradient algorithm

The CG algorithm is an iterative method for solving a set of linear equations of the form in Eq. (6.1), where $\mathbf{A}$ is a real symmetric and positive definite matrix. The solution to Eq. (6.1) may be obtained by minimization of the quadratic function

$$f(\mathbf{x}) = \frac{1}{2}\mathbf{x}^T\mathbf{Ax} - \mathbf{x}^T\mathbf{b}\,, \tag{6.9}$$

as will be now described.

After n iterations, n optimal solution vectors $\mathbf{x}^n$ as in Eq. (6.3), n residuals $\mathbf{r}^n$

$$\mathbf{r}^n = \{\mathbf{r}_1, \mathbf{r}_2, ..., \mathbf{r}_n\}\,, \tag{6.10}$$

and $n-1$ directions $\mathbf{p}^{n-1}$

$$\mathbf{p}^{n-1} = \{\mathbf{p}_1, \mathbf{p}_2, ..., \mathbf{p}_{n-1}\}\,, \tag{6.11}$$

are known. The residual $\mathbf{r}$ is given in Eq. (6.2).

It may be shown that the previous directions and residuals fulfill the relations

$$\mathbf{r}_i^T\mathbf{p}_j = 0, \quad \mathbf{r}_i^T\mathbf{r}_j = 0, \qquad i,j = 1,2,\ldots,n, \quad i > j, \tag{6.12a}$$

$$\mathbf{r}_i^T\mathbf{Ap}_j = 0, \qquad i,j = 1,2,\ldots,n, \quad i > j+1, \tag{6.12b}$$

$$\mathbf{p}_i^T\mathbf{Ap}_j = \mathbf{p}_i^T\mathbf{Ap}_j\delta_{ij}, \qquad i,j = 1,2\ldots,n-1\,. \tag{6.12c}$$

The new trial vector may be written as a general vector in the space spanned by the previous search directions $\mathbf{p}^{n-1}$ in Eq. (6.11) and the current residual $\mathbf{r}_n$

$$\mathbf{x}_{n+1} = \mathbf{x}_n + \sum_{i=1}^{n-1} \alpha_i^{(n)} \mathbf{p}_i + \alpha_n^{(n)} \mathbf{r}_n \,. \tag{6.13}$$

Minimizing $f(\mathbf{x}_{n+1})$ in Eq. (6.9) with respect to n free parameters leads to a subspace equation

$$\begin{pmatrix} \mathbf{p}_1^T\mathbf{A}\mathbf{p}_1 & \mathbf{p}_1^T\mathbf{A}\mathbf{p}_2 & \dots & \dots & \mathbf{p}_1^T\mathbf{A}\mathbf{p}_{n-1} & \mathbf{p}_1^T\mathbf{A}\mathbf{r}_n \\ \mathbf{p}_2^T\mathbf{A}\mathbf{p}_1 & \mathbf{p}_2^T\mathbf{A}\mathbf{p}_2 & \dots & \dots & \mathbf{p}_2^T\mathbf{A}\mathbf{p}_{n-1} & \mathbf{p}_2^T\mathbf{A}\mathbf{r}_n \\ \dots & \dots & \dots & \dots & \dots & \dots \\ \dots & \dots & \dots & \dots & \dots & \dots \\ \mathbf{p}_{n-1}^T\mathbf{A}\mathbf{p}_1 & \mathbf{p}_{n-1}^T\mathbf{A}\mathbf{p}_2 & \dots & \dots & \mathbf{p}_{n-1}^T\mathbf{A}\mathbf{p}_{n-1} & \mathbf{p}_{n-1}^T\mathbf{A}\mathbf{r}_n \\ \mathbf{r}_n^T\mathbf{A}\mathbf{p}_0 & \mathbf{r}_n^T\mathbf{A}\mathbf{p}_1 & \dots & \dots & \mathbf{r}_n^T\mathbf{A}\mathbf{p}_{n-1} & \mathbf{r}_n^T\mathbf{A}\mathbf{r}_n \end{pmatrix} \begin{pmatrix} \alpha_1^{(n)} \\ \alpha_2^{(n)} \\ \vdots \\ \vdots \\ \alpha_{n-1}^{(n)} \\ \alpha_n^{(n)} \end{pmatrix} = \begin{pmatrix} \mathbf{p}_1^T\mathbf{r}_n \\ \mathbf{p}_2^T\mathbf{r}_n \\ \vdots \\ \vdots \\ \mathbf{p}_{n-1}^T\mathbf{r}_n \\ \mathbf{r}_n^T\mathbf{r}_n \end{pmatrix}, \tag{6.14}$$

that is equivalent to

$$\begin{pmatrix} \mathbf{p}_1^T\mathbf{A}\mathbf{p}_1 & 0 & \dots & 0 & 0 & 0 \\ 0 & \mathbf{p}_2^T\mathbf{A}\mathbf{p}_2 & \dots & 0 & 0 & 0 \\ \dots & \dots & \dots & \dots & \dots & \dots \\ \dots & \dots & \dots & \dots & \dots & \dots \\ 0 & 0 & \dots & \mathbf{p}_{n-2}^T\mathbf{A}\mathbf{p}_{n-2} & 0 & 0 \\ 0 & 0 & \dots & 0 & \mathbf{p}_{n-1}^T\mathbf{A}\mathbf{p}_{n-1} & \mathbf{p}_{n-1}^T\mathbf{A}\mathbf{r}_n \\ 0 & 0 & \dots & 0 & \mathbf{r}_n^T\mathbf{A}\mathbf{p}_{n-1} & \mathbf{r}_n^T\mathbf{A}\mathbf{r}_n \end{pmatrix} \begin{pmatrix} \alpha_1^{(n)} \\ \alpha_2^{(n)} \\ \vdots \\ \vdots \\ \alpha_{n-2}^{(n)} \\ \alpha_{n-1}^{(n)} \\ \alpha_n^{(n)} \end{pmatrix} = \begin{pmatrix} 0 \\ 0 \\ \vdots \\ \vdots \\ 0 \\ 0 \\ \mathbf{r}_n^T\mathbf{r}_n \end{pmatrix}, \tag{6.15}$$

where the relations in Eqs. (6.12a)–(6.12c) have been used. It may be seen from Eq. (6.15) that only three last trial vectors are necessary to obtain the optimal solution vector in iteration $n+1$.

It can be seen from Eq. (6.16) that solving the reduced space equation in Eq. (6.15) can be avoided, due to the fact that only last three trial vectors contain all the information necessary to obtain the optimal solution vector. The solution vector $\mathbf{x}_{n+1}$ is obtained directly as a product of matrix-matrix addition and multiplication. Furthermore, the optimal solution vector $\mathbf{x}_{n+1}$ may be expressed in terms of a single search direction $\mathbf{p}_n$ and of the optimal step-length $\alpha_n^{(n)}$ as

$$\mathbf{x}_{n+1} = \mathbf{x}_n + \alpha_n^{(n)} \mathbf{p}_n \,, \tag{6.16}$$

where

$$\mathbf{p}_n = \mathbf{r}_n - \frac{\mathbf{p}_{n-1}^T \mathbf{A}\mathbf{r}_n}{\mathbf{p}_{n-1}^T \mathbf{A}\mathbf{p}_{n-1}} \mathbf{p}_{n-1}\,, \tag{6.17}$$

$$\alpha_n^{(n)} = \frac{\mathbf{p}_n^T \mathbf{r}_n}{\mathbf{p}_n^T \mathbf{A}\mathbf{p}_n}\,. \tag{6.18}$$

The residual of $\mathbf{x}_{n+1}$ in then obtained as

$$\mathbf{r}_{n+1} = \mathbf{r}_n - \alpha_n^{(n)} \mathbf{A}\mathbf{p}_n\,. \tag{6.19}$$

Eqs. (6.12a)–(6.12c) are valid for n increased by one and the iteration procedure of the CG is established.

The iterations are continued until convergence is obtained. Preconditioning may be introduced in the CG algorithm to improve convergence, as will be discussed in context of the CR algorithm in Section 6.3.2.

The advantage of the CG algorithm is that in iteration n only three vectors: $\mathbf{x}_n$, $\mathbf{r}_n$ and $\mathbf{p}_{n-1}$, have to be stored on disk. However, the CG algorithm (in this formulation) may only be applied to a set of linear equations with a positive definite matrix $\mathbf{A}$.

6.3 The conjugate residual algorithm

In this section, the CR algorithm is described (discussed in details in Ref. [148]). The CR algorithm is analogous to the CG algorithm and has similar advantages enabling storage reduction, but may be applied to linear (and also non-linear) equations with non-positive matrices $\mathbf{A}$. The CR algorithm shares some equations with the CG algorithm, however they will be repeated for convenience. The CR algorithm in its standard form is described in Section 6.3.1 and the preconditioned CR algorithm is discussed in Section 6.3.2.

6.3.1 The Conjugate residual in its standard form

In this section, the CR algorithm in its standard form is discussed. The CR algorithm is an iterative method for solving a set of linear equations of the form in Eq. (6.1), where $\mathbf{A}$ is a symmetric but not necessarily positive definite matrix. The solution to Eq. (6.1) is obtained by minimization of the squared residual norm

$$g(\mathbf{x}) = \mathbf{r}^T \mathbf{r}\,, \tag{6.20}$$

as

$$\frac{\partial g(\mathbf{x})}{\partial \mathbf{x}} = 2\mathbf{A}(\mathbf{A}\mathbf{x} - \mathbf{b}) = 0\,. \tag{6.21}$$

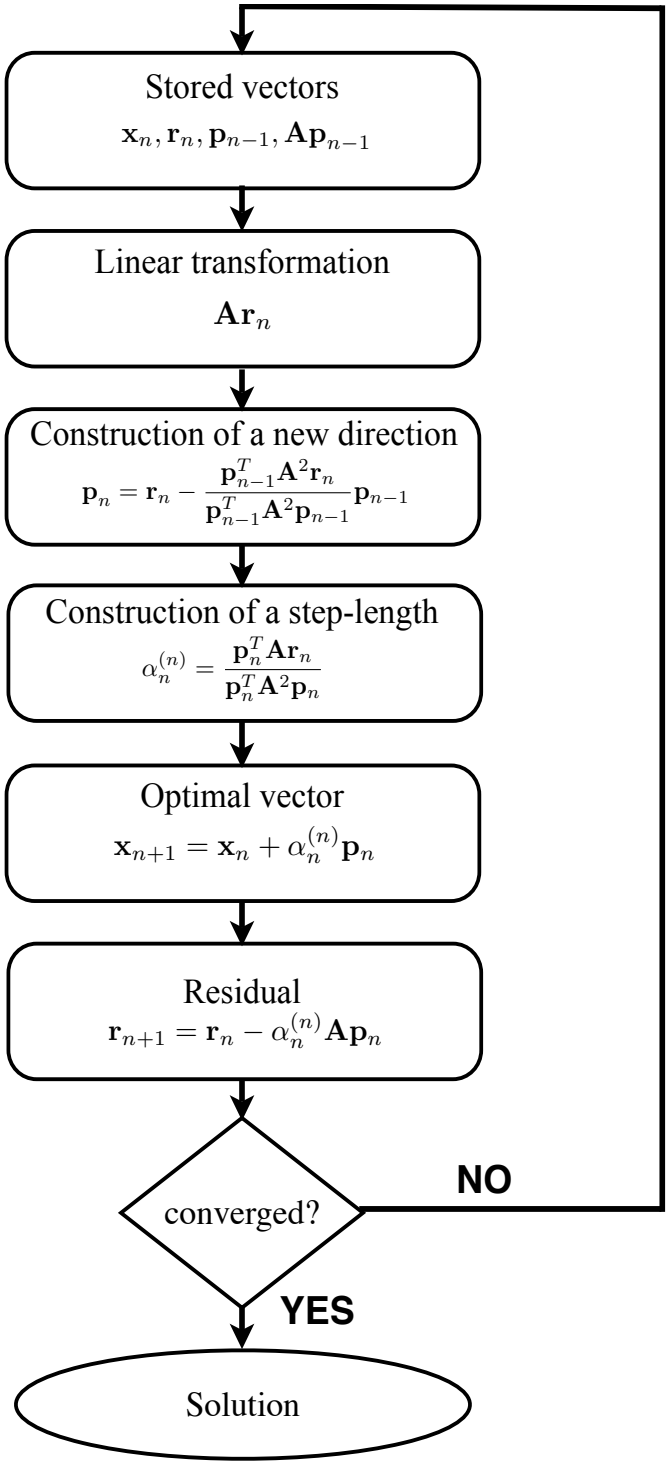

Figure 6.2: Flowchart of the conjugate residual algorithm.

After n iterations, n optimal solution vectors $\mathbf{x}^n$ in Eq. (6.3), n residuals $\mathbf{r}^n$ in Eq. (6.10) and $n-1$ directions $\mathbf{p}^{n-1}$ in Eq. (6.11) are known. It may be shown that the previous directions and residuals fulfill the relations

$$\mathbf{r}_i^T\mathbf{A}\mathbf{p}_j = 0, \quad \mathbf{r}_i^T\mathbf{A}\mathbf{r}_j = 0, \qquad i,j = 1,2,\ldots,n, \quad i > j, \tag{6.22a}$$

$$\mathbf{r}_i^T\mathbf{A}^2\mathbf{p}_j = 0, \qquad i,j = 1,2,\ldots,n, \quad i > j+1, \tag{6.22b}$$

$$\mathbf{p}_i^T\mathbf{A}^2\mathbf{p}_j = \mathbf{p}_i^T\mathbf{A}^2\mathbf{p}_j\delta_{ij}, \qquad i,j = 1,2,\ldots,n-1\,, \tag{6.22c}$$

analogously to Eqs. (6.12a)–(6.12c) in the CG algorithm.

The new trial vector may be written as a general vector in the space spanned by the previous search directions $\mathbf{p}^{n-1}$ in Eq. (6.11) and the current residual $\mathbf{r}_n$

$$\mathbf{x}_{n+1} = \mathbf{x}_n + \sum_{i=1}^{n-1}\alpha_i^{(n)}\mathbf{p}_i + \alpha_n^{(n)}\mathbf{r}_n\,, \tag{6.23}$$

which is identical to Eq. (6.13).

Minimizing $g(\mathbf{x}_{n+1})$ in Eq. (6.20) with respect to n free parameters leads to a subspace equation

$$\begin{pmatrix} \mathbf{p}_0^T\mathbf{A}^2\mathbf{p}_0 & 0 & \ldots & 0 & 0 & 0 \\ 0 & \mathbf{p}_1^T\mathbf{A}^2\mathbf{p}_1 & \ldots & 0 & 0 & 0 \\ \ldots & \ldots & \ldots & \ldots & \ldots & \ldots \\ \ldots & \ldots & \ldots & \ldots & \ldots & \ldots \\ 0 & 0 & \ldots & \mathbf{p}_1^T\mathbf{A}^2\mathbf{p}_1 & 0 & 0 \\ 0 & 0 & \ldots & 0 & \mathbf{p}_{n-1}^T\mathbf{A}^2\mathbf{p}_{n-1} & \mathbf{p}_{n-1}^T\mathbf{A}^2\mathbf{r}_n \\ 0 & 0 & \ldots & 0 & \mathbf{r}_n^T\mathbf{A}^2\mathbf{p}_{n-1} & \mathbf{r}_n^T\mathbf{A}^2\mathbf{r}_n \end{pmatrix} \begin{pmatrix} \alpha_0^{(n)} \\ \alpha_1^{(n)} \\ \vdots \\ \vdots \\ \alpha_{n-2}^{(n)} \\ \alpha_{n-1}^{(n)} \\ \alpha_n^{(n)} \end{pmatrix} = \begin{pmatrix} 0 \\ 0 \\ \vdots \\ \vdots \\ 0 \\ 0 \\ \mathbf{r}_n^T\mathbf{A}\mathbf{r}_n \end{pmatrix}, \tag{6.24}$$

where relations in Eqs. (6.22a)-(6.22c) have been used. From Eq. (6.24) it may be seen that also in the CR algorithm only last three trial vectors are necessary to obtain the optimal solution vector in iteration $n+1$.

Analogously to the CG algorithm, in the CR algorithm the optimal solution vector $\mathbf{x}_{n+1}$ may be expressed in terms of a single search direction $\mathbf{p}_n$ and of the optimal step-length $\alpha_n^{(n)}$ as

$$\mathbf{x}_{n+1} = \mathbf{x}_n + \alpha_n^{(n)}\mathbf{p}_n\,, \tag{6.25}$$

which is identical to Eq. (6.16). Direction $\mathbf{p}_n$ and step-length $\alpha_n^{(n)}$ are now given as

$$\mathbf{p}_n = \mathbf{r}_n - \frac{\mathbf{p}_{n-1}^T\mathbf{A}^2\mathbf{r}_n}{\mathbf{p}_{n-1}^T\mathbf{A}^2\mathbf{p}_{n-1}}\mathbf{p}_{n-1}\,, \tag{6.26}$$

$$\alpha_n^{(n)} = \frac{\mathbf{p}_n^T \mathbf{A}\mathbf{r}_n}{\mathbf{p}_n^T \mathbf{A}^2 \mathbf{p}_n}\,, \tag{6.27}$$

respectively. The residual of $\mathbf{x}_{n+1}$ is identical to Eq. (6.19)

$$\mathbf{r}_{n+1} = \mathbf{r}_n - \alpha_n^{(n)} \mathbf{A}\mathbf{p}_n\,. \tag{6.28}$$

Eqs. (6.22a)–(6.22c) are valid for n increased by one and the iteration procedure of the CR algorithm is established. The iterations are continued until convergence is obtained. A flowchart of the conjugate residual algorithm is presented in Fig. 6.2.

In the CR algorithm, all but the last direction may thus be discarded. In iteration n only four vectors: $\mathbf{x}_n$, $\mathbf{p}_{n-1}$, $\mathbf{A}\mathbf{p}_{n-1}$ and $\mathbf{r}_n$ need to be stored in memory. The main difference between the CG and the CR algorithm is that the step-length in the CG algorithm is determined from a minimization of $f(\mathbf{x}_{n+1})$ in Eq. (6.9), whereas in the CR algorithm, the step-length is determined from a minimization of $g(\mathbf{x}_{n+1})$ in Eq. (6.20). The CR algorithm may therefore be used also when the matrix $\mathbf{A}$ in Eq. (6.1) is not positive definite, which does not hold for the CG algorithm. Furthermore, the CR algorithm may be generalized to non-linear equations as the residual norm that is minimized in CR may straightforwardly be obtained also for a set of non-linear equations.

6.3.2 The preconditioned conjugate residual algorithm

To improve the convergence of the CR algorithm, the set of linear equations in Eq. (6.1) may be solved in a preconditioned form. A coordinate transformation may be introduced that produces a new set of equations with a matrix that has a lower condition number compared to $\mathbf{A}$. This may be done by multiplying Eq. (6.1) with the transpose of a non-singular matrix $\mathcal{P}$, yielding

$$\mathbf{A}^{\mathcal{P}}\mathbf{Y} = \mathbf{b}^{\mathcal{P}}\,, \tag{6.29}$$

where

$$\mathbf{A}^{\mathcal{P}} = \mathcal{P}^T \mathbf{A}\mathcal{P}; \quad \mathbf{Y} = \mathcal{P}^{-1}\mathbf{x}; \quad \mathbf{b}^{\mathcal{P}} = \mathcal{P}^T\mathbf{b}\,. \tag{6.30}$$

Eq. (6.29) may be solved using the CR algorithm and the solution may then be transformed to the original coordinates. Alternatively, Eq. (6.29) may be solved in the original basis using modified CR equations, as will be now described. The residual in the $\mathbf{Y}$ basis is given as

$$\mathbf{r}^{\mathcal{P}} = \mathbf{b}^{\mathcal{P}} - \mathbf{A}^{\mathcal{P}}\mathbf{Y} = \mathcal{P}^T\mathbf{r}\,. \tag{6.31}$$

Optimal directions are obtained by minimizing $g(\mathbf{x}_{n+1})$ in analogy to Eq. (6.20)

$$g^{\mathcal{P}}(\mathbf{x}) = (\mathbf{r}^{\mathcal{P}})^T\mathbf{r}^{\mathcal{P}} = \mathbf{r}^T\mathcal{P}\mathcal{P}^T\mathbf{r} = \mathbf{r}^T\mathbf{C}^{-1}\mathbf{r}\,, \tag{6.32}$$

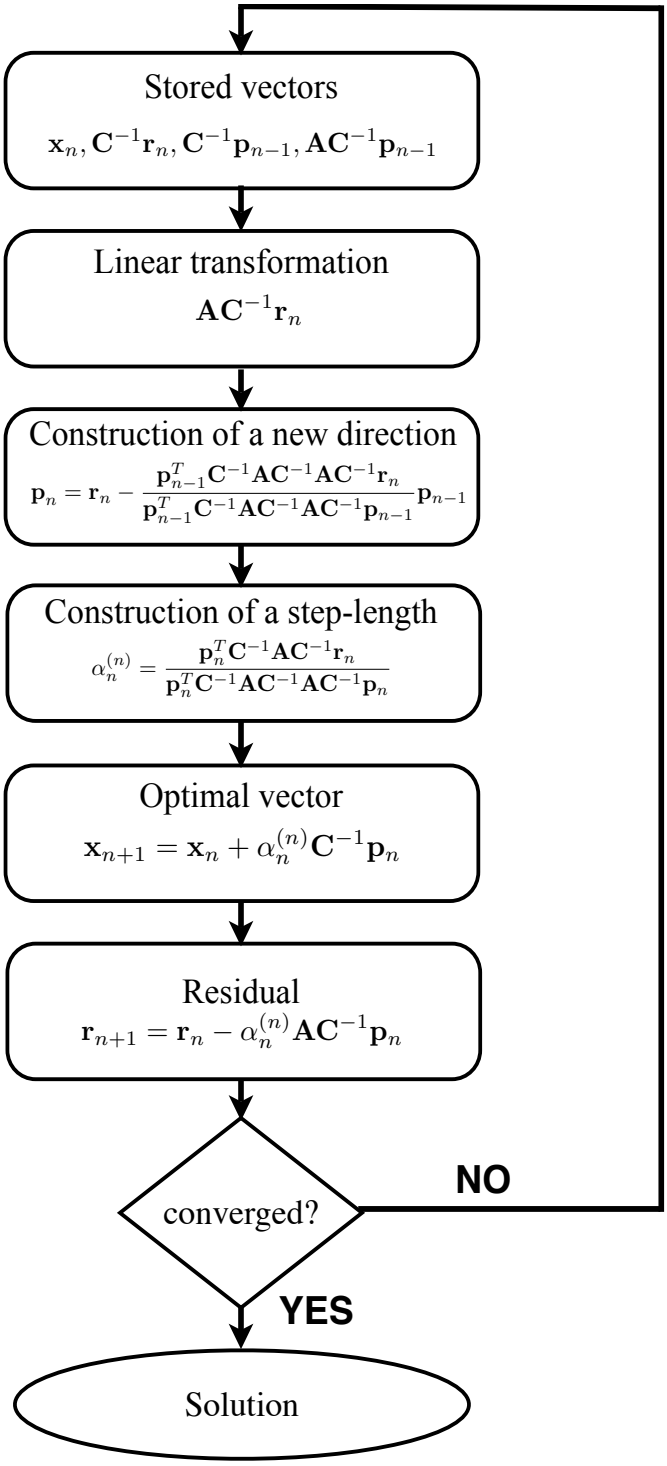

Figure 6.3: Flowchart of the preconditioned conjugate residual algorithm.

where

$$\mathbf{C}^{-1} = \mathcal{P}\mathcal{P}^T \,. \tag{6.33}$$

The preconditioned analogue to Eqs. (6.25)–(6.28) may be written as [148]

$$\mathbf{x}_{n+1} = \mathbf{x}_n + \alpha_n^{(n)} \mathbf{C}^{-1}\mathbf{p}_n \,, \tag{6.34}$$

where

$$\mathbf{p}_n = \mathbf{r}_n - \frac{\mathbf{p}_{n-1}^T \mathbf{C}^{-1}\mathbf{A}\mathbf{C}^{-1}\mathbf{A}\mathbf{C}^{-1}\mathbf{r}_n}{\mathbf{p}_{n-1}^T \mathbf{C}^{-1}\mathbf{A}\mathbf{C}^{-1}\mathbf{A}\mathbf{C}^{-1}\mathbf{p}_{n-1}}\mathbf{p}_{n-1} \,, \tag{6.35}$$

$$\alpha_n^{(n)} = \frac{\mathbf{p}_n^T \mathbf{C}^{-1}\mathbf{A}\mathbf{C}^{-1}\mathbf{r}_n}{\mathbf{p}_n^T \mathbf{C}^{-1}\mathbf{A}\mathbf{C}^{-1}\mathbf{A}\mathbf{C}^{-1}\mathbf{p}_n} \,, \tag{6.36}$$

and

$$\mathbf{r}_{n+1} = \mathbf{r}_n - \alpha_n^{(n)} \mathbf{A}\mathbf{C}^{-1}\mathbf{p}_n \,. \tag{6.37}$$

Choosing $\mathcal{P}^T$ such that $\mathbf{C}$ is a good approximation to $\mathbf{A}$ ensures that the linear equations are solved in a basis where the matrix has a lower condition number. A flowchart of the preconditioned conjugate residual algorithm is given in Fig. 6.3.

The literature [148] gives the impression that the preconditioned CR algorithm may be applied whenever $\mathbf{C}$ is a good approximation to $\mathbf{A}$. However, note that the step-length in the preconditioned CR algorithm is determined from a minimization of $g^{\mathcal{P}}(\mathbf{x}_{n+1})$ in Eq. (6.32), not a minimization of $g(\mathbf{x}_{n+1})$ in Eq. (6.20). The minimization of $g^{\mathcal{P}}(\mathbf{x}_{n+1})$ is well-defined only when $\mathbf{C}^{-1}$ may be decomposed as in Eq. (6.33). This requires that $\mathbf{C}^{-1}$ is positive definite. It thus may be concluded that the preconditioned CR algorithm may be applied only for a positive definite preconditioner $\mathbf{C}^{-1}$,[11] although in several numerical examples, the performance of the preconditioned CR algorithm for a non-positive definite matrix and preconditioner, is benign.

[11] Unfortunately, this observation has been made long after it should had been made and therefore results obtained using the CR algorithm are reported in this thesis.

7 Solving response equations using iterative methods

Molecular properties are fundamental quantities underlying the macroscopic behavior of matter and their determination constitutes one of the most fruitful areas of interplay between experiment and theory [149]. Frequency-dependent molecular properties, as discussed in previous chapters, may be determine by solving response equations.

Assuming that the unperturbed wavefunction $|0\rangle$ is real, the response equations can be written in a general form

$$(\boldsymbol{E}^{[2]} - z\boldsymbol{S}^{[2]})\boldsymbol{X} = \boldsymbol{g}^b\,, \tag{7.1}$$

where $\boldsymbol{E}^{[2]}$ and $\boldsymbol{S}^{[2]}$ are the generalized Hessian and metric matrices, respectively, given in Eq. (3.38). z denotes a general frequency parameter, $\boldsymbol{g}^b$ is a property gradient and $\boldsymbol{X}(z)$ is the solution vector also known as the linear response vector. For the real wavefunction, response matrices $\boldsymbol{E}^{[2]}$ and $\boldsymbol{S}^{[2]}$ are real, while $\boldsymbol{X}$, $\boldsymbol{g}^b$ and z may be complex depending on which type of response equation is considered.

In this thesis, solving three different types of response equations is discussed:

- The Standard response equation
  The standard response equation has the form given in Eq. (3.34)

  $$(\boldsymbol{E}^{[2]} - \omega\boldsymbol{S}^{[2]})\boldsymbol{X} = \boldsymbol{G}\,, \tag{7.2}$$

  where ω is a real frequency parameter and $\boldsymbol{G}$ is a real generalized gradient type vector. Eq. (7.2) represents a set of linear equations for a symmetric matrix.

- The Damped response equation
  The damped response equation has a form

  $$(\boldsymbol{E}^{[2]} - (\omega + i\gamma)\boldsymbol{S}^{[2]})(\boldsymbol{X}^R + i\boldsymbol{X}^I) = \boldsymbol{G}^R + i\boldsymbol{G}^I\,. \tag{7.3}$$

  The frequency parameter z in Eq. (7.1) is complex, where ω is a real frequency and γ is a damping parameter also known as an inverse effective lifetime parameter or an excited-state lifetime broadening parameter [28–34], as discussed in Section 4.1. The gradient and the solution vector are complex. The real and the imaginary component of the solution vector describes dispersion and absorption processes, respectively. The damping parameter γ has been introduced in the response equation to correct an unphysical behavior of molecular properties in resonance regions, when one or more of the optical frequencies equals an excitation energy. Due to the introduction of a

complex optical frequency, $(\boldsymbol{E}^{[2]} - (\omega + i\gamma)\boldsymbol{S}^{[2]})$ becomes non-Hermitian. Eq. (7.3), however, remains linear.

- The Response eigenvalue equation
  Excitation energies occur at the poles of the linear response function. The excitation energies may be determined by solving the generalized eigenvalue equation where the right-hand side vector $\boldsymbol{g}^b$ in Eq. (7.1) is a zero vector

$$(\boldsymbol{E}^{[2]} - \omega_{p0}\boldsymbol{S}^{[2]})\boldsymbol{X}_p = \boldsymbol{0}\,. \tag{7.4}$$

  ω_{p0} is the excitation energy from state $|0\rangle$ to state $|p\rangle$ and $\boldsymbol{X}_p$ is the corresponding eigensolution. Since $\boldsymbol{S}^{[2]}$ is not a positive definite matrix Eq. (7.4) becomes a non-Hermitian eigenvalue equation.

In this chapter, applying subspace iterative algorithms presented in Chapter 6 to response equations is discussed. In Section 7.1, the general subspace approach is introduced, and is discussed in context of the eigenvalue, standard and damped response equations in Sections 7.2, 7.3 and 7.4, respectively. In Chapter 8, an algorithm with paired trial vectors is described. An algorithm with symmetrized trial vectors is introduced in Chapter 9.

7.1 The general subspace iterative algorithm

In electronic structure theory, response equations [Eq. (7.1)] are solved using subspace iterative algorithms based on the one presented in Section 6.1. In the subspace iterative algorithms, equations are solved in the reduced space build based on the fact that the linear transformations of the generalized Hessian $\boldsymbol{E}^{[2]}$ and metric $\boldsymbol{S}^{[2]}$ matrices on a trial vector $\boldsymbol{b}$, given in Eqs. (3.65) and (3.66), can be carried out

$$\boldsymbol{\sigma} = \boldsymbol{E}^{[2]}\boldsymbol{b}\,, \quad \boldsymbol{\rho} = \boldsymbol{S}^{[2]}\boldsymbol{b}\,. \tag{7.5}$$

A flowchart of the general subspace iterative algorithm for solving linear response equations is presented in Fig. 7.1.

After iteration n of a subspace iterative algorithm, n trial vectors

$$\boldsymbol{b}^n = \{\boldsymbol{b}_1, \boldsymbol{b}_2, ..., \boldsymbol{b}_n\}\,, \tag{7.6}$$

and the linearly transformed vectors

$$\boldsymbol{\sigma}^n = \{\boldsymbol{\sigma}_1, \boldsymbol{\sigma}_2, ..., \boldsymbol{\sigma}_n\}\,, \quad \boldsymbol{\rho}^n = \{\boldsymbol{\rho}_1, \boldsymbol{\rho}_2, ..., \boldsymbol{\rho}_n\}\,, \tag{7.7}$$

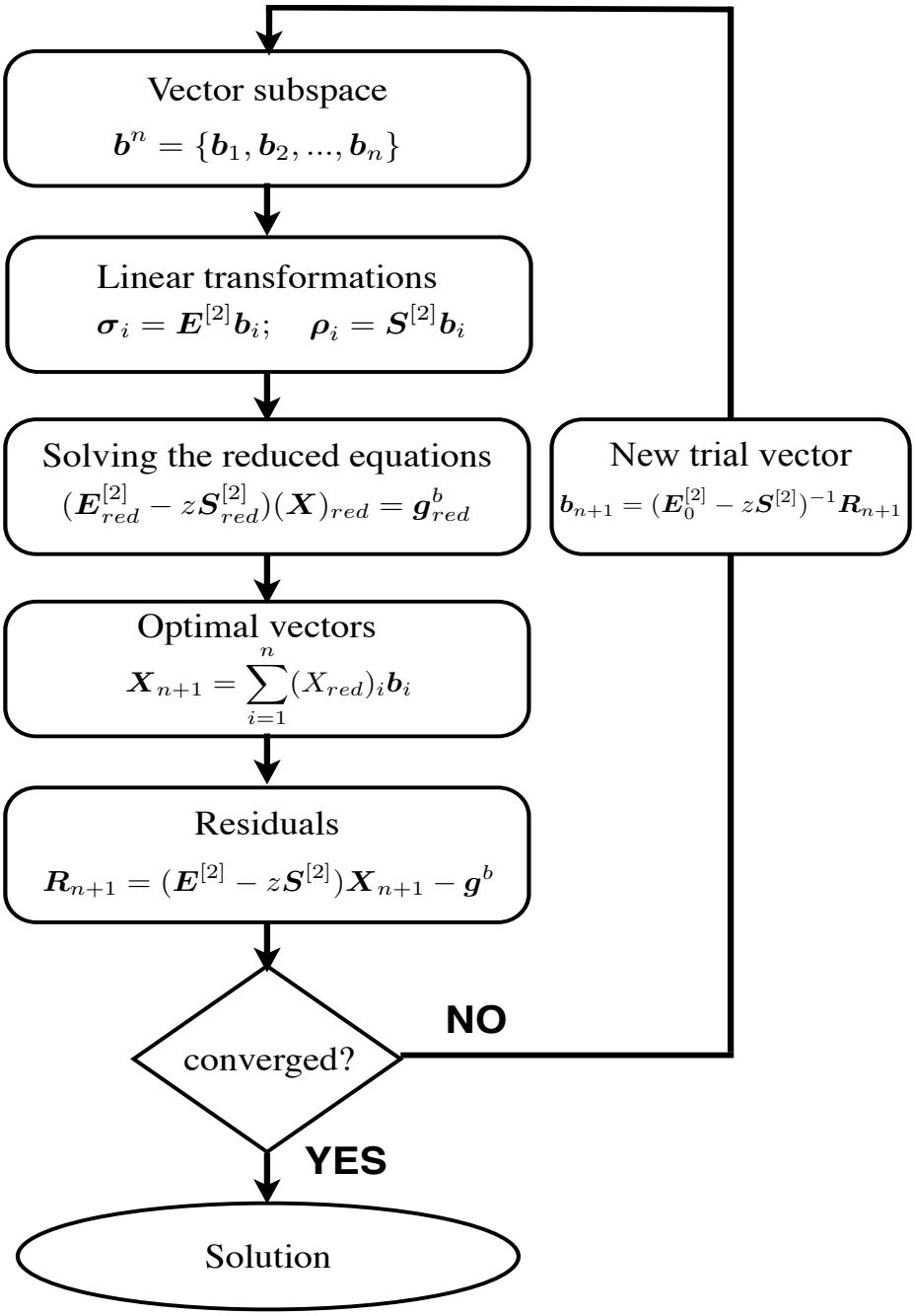

Figure 7.1: Flowchart of the general subspace iterative algorithm for solving linear response equations.

have been obtained. Reduced response equations are set up in the subspace $\boldsymbol{b}^n$ in analogy to Eq. (6.5), giving

$$(\boldsymbol{E}^{[2]}_{red} - z\boldsymbol{S}^{[2]}_{red})(\boldsymbol{X})_{red} = \boldsymbol{g}^b_{red}\,, \tag{7.8}$$

where

$$(\boldsymbol{E}^{[2]}_{red})_{ij} = \boldsymbol{b}^\dagger_i\boldsymbol{\sigma}_j\,, \quad (\boldsymbol{S}^{[2]}_{red})_{ij} = \boldsymbol{b}^\dagger_i\boldsymbol{\rho}_j\,, \tag{7.9}$$

$\boldsymbol{g}^b_{red}$ is equal to zero when the eigenvalue equation is solved and for the standard and damped response equation it has the form

$$(\boldsymbol{g}^b_{red})_i = \boldsymbol{b}^\dagger_i\boldsymbol{g}^b\,. \tag{7.10}$$

Eq. (7.8) determines the optimal solution vector $\boldsymbol{X}_{n+1}$ in the subspace $\boldsymbol{b}^n$

$$\boldsymbol{X}_{n+1} = \sum_{i=1}^{n}(X_{red})_i\boldsymbol{b}_i\,, \tag{7.11}$$

in analogy to Eq. (6.6). The residual vector for the response equations is given as

$$\boldsymbol{R}_{n+1} = (\boldsymbol{E}^{[2]} - z\boldsymbol{S}^{[2]})\boldsymbol{X}_{n+1} - \boldsymbol{g}^b = \sum_{i=1}^{n}(X_{red})_i(\boldsymbol{\sigma}_i - z\boldsymbol{\rho}_i) - \boldsymbol{g}^b\,. \tag{7.12}$$

The residual vector is calculated to check for convergence of the iterative scheme and to obtain a new trial vector. The iterative procedure is converged when the residual norm $||\boldsymbol{R}_{n+1}||$ is smaller than a preset threshold. The new trial vector $\boldsymbol{b}_{n+1}$ is added to the subspace in Eq. (7.6) and the iteration procedure is continued until convergence is obtained.

The convergence of the algorithm is determined by the condition number of the response matrix $(\boldsymbol{E}^{[2]} - z\boldsymbol{S}^{[2]})$, *i.e.* the ratio between the smallest and largest eigenvalue of the response matrix $(z^{\max}_{p0}/z^{\min}_{p0})$. The $\boldsymbol{B}$ matrix in Eq. (3.38) represents a matrix element between the reference state $|0\rangle$ and a doubly excited state and is small compared to $\boldsymbol{A}$ in Eq. (3.38), which is the singly excited configuration interaction (CI) matrix for the HF reference state. The convergence of the standard response equations is therefore determined by the condition number of the $\boldsymbol{A}$ matrix.

To improve the convergence of the response equations, preconditioning may be introduced, as mentioned in Section 6.1. The new trial vector is then obtained from the preconditioned residual as

$$\boldsymbol{b}_{n+1} = \boldsymbol{L}^{-1}\boldsymbol{R}_{n+1}\,, \tag{7.13}$$

where preconditioner $\boldsymbol{L}$ is an easily constructed approximation to $(\boldsymbol{E}^{[2]} - z\boldsymbol{S}^{[2]})$. In the MO representation, $\boldsymbol{S}^{[2]}$ is diagonal [see Eq. (3.39b)] and $\boldsymbol{E}^{[2]}$ is a diagonally dominant matrix

[see Eq. (3.53)], and therefore $(\boldsymbol{E}_0^{[2]} - z\boldsymbol{S}^{[2]})^{-1}$ is easy to construct and may be used as a preconditioner.

For the preconditioned equation, a convergence rate of an algorithm is determined by the condition number of the matrix

$$\begin{aligned}(\boldsymbol{E}_0^{[2]} - z\boldsymbol{S}^{[2]})^{-1}(\boldsymbol{E}^{[2]} - z\boldsymbol{S}^{[2]}) &= (\boldsymbol{E}_0^{[2]} - z\boldsymbol{S}^{[2]})^{-1}[(\boldsymbol{E}_0^{[2]} - z\boldsymbol{S}^{[2]}) + \boldsymbol{E}_1^{[2]}] \\ &= \mathbf{1} + (\boldsymbol{E}_0^{[2]} - z\boldsymbol{S}^{[2]})^{-1}\boldsymbol{E}_1^{[2]}\,. \end{aligned} \tag{7.14}$$

The condition number of the preconditioned equation is therefore determined by the eigenvalues of $[(\boldsymbol{E}_0^{[2]} - z\boldsymbol{S}^{[2]})^{-1}\boldsymbol{E}_1^{[2]}]$. For small values of parameter z the condition number is determined by $(\boldsymbol{E}_0^{[2]})^{-1}\boldsymbol{E}_1^{[2]}$ and is significantly reduced compared to the condition number of the non-preconditioned equation, as the dominant contribution to the large eigenvalues is removed. However, when the real contribution to z (frequency ω) approaches the orbital energy difference for the lowest excitation energies, the preconditioner becomes nearly singular and slower convergence is observed. In principle, the remedy to this problem can be using a high value of imaginary component of z (damping parameter γ). However, the excited state lifetime parameter γ must be chosen small to obtain results that have a physical meaning.

In Sections 7.2, 7.3 and 7.4 procedures for solving the eigenvalue response equation, standard response equation and damped response equation, respectively, are given in details. Encountered problems are also discussed.

7.2 The response eigenvalue equation

When the eigenvalue equation in Eq. (7.4) is solved, the algorithm that is used determines the way of obtaining new trial vectors. In this thesis two algorithms for obtaining new trial vectors when using the iterative subspace approach are discussed, the Davidson algorithm [42], in Section 7.2.1, and the Olsen algorithm [150], in Section 7.2.2. However, both the Davidson and the Olsen algorithms were designed for solving a Hermitian eigenvalue equation, and when they are applied for the non-Hermitian eigenvalue problem some difficulties may occur, as will be discussed in Section 7.2.3.

7.2.1 The Davidson algorithm

Solving the response eigenvalue equation using the Davidson algorithm is similar to solving the standard response equation as described in Section 7.1. A new trial vector is obtained in the Davidson algorithm according to Eq. (7.13), where the matrix $\boldsymbol{L}$ is a diagonal approximation to $(\boldsymbol{E}^{[2]} - \omega_{p0}^R\boldsymbol{S}^{[2]})$ as discussed in the previous section.

For the linear equations, improved convergence is obtained when $\boldsymbol{E}_0$ becomes an improved approximation to $\boldsymbol{E}^{[2]}$ matrix. When $\boldsymbol{E}_0^{[2]}$ is replaced by $\boldsymbol{E}^{[2]}$ the converged solution is obtained for a set of linear equations in one iteration. When the eigenvalue equation is solved using the Davidson algorithm a problem arises in the limit where $\boldsymbol{E}_0^{[2]}$ is approaching $\boldsymbol{E}^{[2]}$, as no new direction is generated. This problem is avoided using the Olsen algorithm, which is described in the next section.

7.2.2 The Olsen algorithm

In the Olsen algorithm, a new trial vector is obtained in a perturbation method scheme. The Olsen algorithm will be introduced in context of solving the response eigenvalue equation.

It is assumed that an approximate solution $\boldsymbol{X}^0$ to the response eigenvalue equation is known. This may be the optimal solution vector $(\boldsymbol{X}_p)_{n+1}$ in Eq. (7.11). The approximate solution $\boldsymbol{X}^0$ satisfies the normalization condition in Eq. (3.57). In the Olsen algorithm, the zeroth-order eigenvalue ω_{p0}^0 is obtained from projecting the eigenvalue equation in Eq. (7.4) with $(\boldsymbol{X}^0)^T$

$$(\boldsymbol{X}^0)^T(\boldsymbol{E}^{[2]} - \omega_{p0}^0\boldsymbol{S}^{[2]})\boldsymbol{X}^0 = 0\,, \tag{7.15}$$

however, ω_{p0}^0 in Eq. (7.15) is identical to z obtained in Eq. (7.8).[12]

To construct an improved solution vector in the Olsen algorithm, Eq. (7.4) is expressed in terms of a zeroth-order and correction components

$$\omega_{p0} = \omega_{p0}^0 + \omega_{p0}^1\,, \tag{7.16}$$

$$\boldsymbol{X}_p = \boldsymbol{X}^0 + \boldsymbol{X}^1\,, \tag{7.17}$$

where ω_{p0}^1 and $\boldsymbol{X}^1$ are correction terms to the eigenvalue ω_{p0}^0 and the eigenvector $\boldsymbol{X}^0$, respectively. The $\boldsymbol{E}^{[2]}$ matrix is also written in terms of a zeroth-order and a correction component, as in Eq. (3.53).

Inserting Eqs. (3.53), (7.16) and (7.17) into Eq. (7.4) gives

$$\left((\boldsymbol{E}_0^{[2]} + \boldsymbol{E}_1^{[2]}) - (\omega_{p0}^0 + \omega_{p0}^1)\boldsymbol{S}^{[2]}\right)(\boldsymbol{X}^0 + \boldsymbol{X}^1) = \boldsymbol{0}\,. \tag{7.18}$$

$\boldsymbol{X}^1$ can be determined from Eq. (7.18) by neglecting the terms that are quadratic in the corrections

$$\boldsymbol{X}^1 \;=\; -\left(\boldsymbol{E}_0^{[2]} - \omega_{p0}^0\boldsymbol{S}^{[2]}\right)^{-1}\left[\left(\boldsymbol{E}^{[2]} - \omega_{p0}^0\boldsymbol{S}^{[2]}\right)\boldsymbol{X}^0 - \omega_{p0}^1\boldsymbol{S}^{[2]}\boldsymbol{X}^0\right]\,. \tag{7.19}$$

[12] Assuming that z is real.

ω_{p0}^1 may be determined by requiring that the eigenvectors correction $\boldsymbol{X}^1$ is orthogonal to $\boldsymbol{X}^0$ in the generalized matrix $\boldsymbol{S}^{[2]}$

$$(\boldsymbol{X}^1)^T \boldsymbol{S}^{[2]} \boldsymbol{X}^0 = 0\,, \tag{7.20}$$

giving

$$\omega_{p0}^1 = \frac{(\boldsymbol{X}^0)^T \boldsymbol{S}^{[2]} \left(\boldsymbol{E}_0^{[2]} - \omega_{p0}^0 \boldsymbol{S}^{[2]}\right)^{-1} \left(\boldsymbol{E}^{[2]} - \omega_{p0}^0 \boldsymbol{S}^{[2]}\right) \boldsymbol{X}^0}{(\boldsymbol{X}^0)^T \boldsymbol{S}^{[2]} \left(\boldsymbol{E}_0^{[2]} - \omega_{p0}^0 \boldsymbol{S}^{[2]}\right)^{-1} \boldsymbol{S}^{[2]} \boldsymbol{X}^0}\,. \tag{7.21}$$

The inverse matrix $(\boldsymbol{E}_0^{[2]} - \omega_p^0 \boldsymbol{S}^{[2]})^{-1}$ is easily constructed as described in Section 7.1. Using $\boldsymbol{E}^{[2]}\boldsymbol{X}^0$ and $\boldsymbol{S}^{[2]}\boldsymbol{X}^0$ [that have been calculated when the residual vector in Eq. (7.12) has been constructed] and ω_{p0}^1 from Eq. (7.21), the correction vector $\boldsymbol{X}_p^1$ may be obtained from Eq. (7.19). $\boldsymbol{X}^1$ is added to the trial vector subspaces in Eq. (7.6) and the iteration procedure is continued until convergence.

Note that neglecting the second term in Eq. (7.19) leads to the Davidson algorithm. The second term in Eq. (7.19) ensures that a new improved trial vector is obtained also when $\boldsymbol{E}_0^{[2]}$ is approaching $\boldsymbol{E}^{[2]}$. In fact, when $\boldsymbol{E}_0^{[2]}$ in the Olsen algorithm is replaced by $\boldsymbol{E}^{[2]}$, the inverse-iteration method with the Rayleigh quotient [10, 144, 151] is established and cubic convergence is obtained [10].

7.2.3 Problems when solving the response eigenvalue equation

The response eigenvalue equation of the form in Eq. (7.4) represents a non-Hermitian eigenvalue equation. In addition, in early iterative subspace algorithms the response eigenvalue equation was expressed as

$$\boldsymbol{S}^{[2]} \boldsymbol{E}^{[2]} \boldsymbol{X} = \omega \boldsymbol{X}\,, \tag{7.22}$$

due to the fact that in the canonical MO representation, $\boldsymbol{S}^{[2]}$ is an easily invertible matrix [$(\boldsymbol{S}^{[2]})^{-1} = \boldsymbol{S}^{[2]}$]. However, Eq. (7.22) represents also a non-Hermitian eigenvalue equation. Both the Davidson and the Olsen algorithms were designed for solving a Hermitian eigenvalue problem, and therefore it was problematic to solve response eigenvalue equation using an iterative subspace algorithm.

When a Hermitian eigenvalue equation is solved, the subspace eigenvalue equation always has real eigenvalues, and monotonic convergence to the lowest eigenvalues is obtained due to MacDonald's theorem [152]. When a non-Hermitian eigenvalue equation is solved there is no guarantee that the eigenvalues will be real, and therefore the eigenvalues of the reduced generalized eigenvalue equation may be complex. In both the Olsen and Davidson algorithms it is assumed that ω_{p0}^R is real, therefore some difficulties may occur when the non-Hermitian

eigenvalue equation is solved and new trial vectors cannot be obtained due to the complex eigenvalues. This problem was encountered by Bouman *et al.* [153] when applied the Davidson algorithm on the response eigenvalue equation in Eq. (7.22) [154]. Also, the monotonic convergence to the lowest eigenvalues is lost when the non-Hermitian eigenvalue is solved. Neither the Davidson algorithm nor the Olsen algorithm may therefore be used directly for solving the response eigenvalue equation in Eq. (7.4).

In Chapters 8 and 9, it is discussed how the non-Hermitian eigenvalue equation may be transformed to a Hermitian eigenvalue equation and solved using a generalization of the Davidson or Olsen iterative subspace algorithm.

7.3 The standard response equation

The standard response equation in Eq. (7.2) represents a set of linear equations with a symmetric matrix. The algorithm commonly used for solving linear equations with a symmetric matrix is the CG algorithm, described in Section 6.2. By using a CG implementation, the set of vectors stored on disk may be significantly reduced to only the last three vectors, and the storing and manipulation of large amount of directions (trial vectors) can be avoided.

The CG algorithm may be applied only to equations with positive definite matrix. For angular frequencies ω that are larger than the first transition frequency in the system, the response matrix $(\boldsymbol{E}^{[2]} - \omega\boldsymbol{S}^{[2]})$ is not positive definite, and the CG algorithm cannot be used. The standard response equation may, in principle, be solved using the CR algorithm, presented in Section 6.3. The CR algorithm has the same attractive features as the CG algorithm and is applicable for equations with non-positive definite matrix, as discussed in Section 6.3.1. However, the preconditioned CR algorithm may be applied safely only if the preconditioner in Eq. (7.13) is positive definite, as described in Section 6.3.2.

7.4 The damped response equation

The damped response equation of the form Eq. (7.3) represents a set of linear equations for a non-Hermitian matrix. Eq. (7.3) may be solved using real arithmetic when expressed in terms of the two equations

$$(\boldsymbol{E}^{[2]} - \omega\boldsymbol{S}^{[2]})\boldsymbol{X}^R = \boldsymbol{G}^R - \gamma\boldsymbol{S}^{[2]}\boldsymbol{X}^I\,, \tag{7.23a}$$

$$(\boldsymbol{E}^{[2]} - \omega\boldsymbol{S}^{[2]})\boldsymbol{X}^I = \boldsymbol{G}^I + \gamma\boldsymbol{S}^{[2]}\boldsymbol{X}^R\,, \tag{7.23b}$$

where $\boldsymbol{G}^R$ and $\boldsymbol{G}^I$ is the real and the imaginary component of $\boldsymbol{G}$, respectively. Eqs. (7.23a) and (7.23b) are obtained by separating Eq. (7.3) into a real and an imaginary component.

Eqs. (7.23a) and (7.23b) couple the real and imaginary components of the solution vector via the right-hand sides. When Eqs. (7.23a) and (7.23b) are solved separately, it leads to divergence in the resonance region, where the solution vector has a large eigenvector component in both $\boldsymbol{X}^R$ and $\boldsymbol{X}^I$. In the resonance region, the coupling between $\boldsymbol{X}^R$ and $\boldsymbol{X}^I$ needs to be considered explicitly to get a robust and fast convergence. This may be done by combining Eqs. (7.23a) and (7.23b)

$$\begin{pmatrix} \boldsymbol{E}^{[2]} - \omega \boldsymbol{S}^{[2]} & \gamma \boldsymbol{S}^{[2]} \\ \gamma \boldsymbol{S}^{[2]} & -(\boldsymbol{E}^{[2]} - \omega \boldsymbol{S}^{[2]}) \end{pmatrix} \begin{pmatrix} \boldsymbol{X}^R \\ \boldsymbol{X}^I \end{pmatrix} = \begin{pmatrix} \boldsymbol{G}^R \\ -\boldsymbol{G}^I \end{pmatrix} . \tag{7.24}$$

Eq. (7.24) is a standard set of linear equations for a symmetric, but not positive definite, real matrix where the coupling between $\boldsymbol{X}^R$ and $\boldsymbol{X}^I$ is taken into account explicitly. Since the CG algorithm may be applied only on equations with positive definite matrix, it cannot be used for solving Eq. (7.24). However, Eq. (7.24) may, in principle, be solved using the CR algorithm with a less efficient, but positive definite preconditioner.

It should be noted that the algorithm presented in this section has not been used in practice and is introduced here for simplifying discussion following in next chapters.

8 Iterative algorithms with paired trial vectors

In the previous chapter standard iterative algorithms for solving response equations in the general form have been introduced. As discussed in Section 3.2.2, the response matrices $\boldsymbol{E}^{[2]}$ and $\boldsymbol{S}^{[2]}$, and therefore the response equations, have block structures given in Eq. (3.38. Imposing this structure on the reduced subspace eigenvalue equation [41], was a remedy for problems discussed in Section 7.2.3. Introducing paired structure in the reduced subspace standard response equation, led to improvement in convergence [41]. The block structure of reduced response equation may be obtained by adding trial vectors in the iterative subspace algorithm in pairs, as will be described in this chapter.

The algorithm with paired trial vectors is described in context of solving the eigenvalue and standard response equations in Sections 8.1 and 8.2, respectively. In Section 8.3, general implementation is discussed in context of solving response equations in the linear-scaling framework [23]. In Section 8.4, the algorithms with paired trial vectors for solving damped response equations are introduced and compared with the previously used algorithm [29].

8.1 The eigenvalue equation

From the block diagonal form of $\boldsymbol{E}^{[2]}$ in Eq. (3.61), it can be seen that for a ground state wavefunction $|0\rangle$, Eq. (7.4) may be viewed as a symmetric eigenvalue equation. A ground state must be stable both with respect to real and imaginary variations [87] and both $\boldsymbol{A}+\boldsymbol{B}$ and $\boldsymbol{A}-\boldsymbol{B}$ must therefore be positive definite. When $\boldsymbol{A}+\boldsymbol{B}$ and $\boldsymbol{A}-\boldsymbol{B}$ are positive definite, $\boldsymbol{E}^{[2]}$ is also positive definite and Eq. (7.4) expressed as

$$(\tfrac{1}{\omega_{p0}}\boldsymbol{E}^{[2]} - \boldsymbol{S}^{[2]})\boldsymbol{X}_p = \boldsymbol{0}\,, \tag{8.1}$$

becomes a symmetric eigenvalue equation with eigenvalues $\frac{1}{\omega_{p0}}$.

Eq. (8.1) has a block structure, and it is advantageous to keep this structure in the reduced subspace equations. For that reason Olsen *et al.* introduced pairing in the iterative subspace algorithm in Ref. [41], as will be described in this section.

In algorithm by Olsen *et al.*, trial vectors are added to the subspace in pairs. Together with a trial vector $\boldsymbol{b}$

$$\boldsymbol{b} = \begin{pmatrix} b_{AI} \\ b_{JB} \end{pmatrix}\,, \tag{8.2}$$

its paired counterpart $\boldsymbol{b}^P$

$$\boldsymbol{b}^P = \begin{pmatrix} b_{JB} \\ b_{AI} \end{pmatrix}\,, \tag{8.3}$$

is added.

From the linear transformations of $\boldsymbol{E}^{[2]}$ and $\boldsymbol{S}^{[2]}$ on a trial vector $\boldsymbol{b}$ in Eq. (7.5), the linear transformations on the paired vector $\boldsymbol{b}^P$ are obtained at no extra cost as [23]

$$\boldsymbol{\sigma}_i^P = \boldsymbol{E}^{[2]}\boldsymbol{b}_i^P\,, \quad -\boldsymbol{\rho}_i^P = \boldsymbol{S}^{[2]}\boldsymbol{b}_i^P\,. \tag{8.4}$$

Eq. (8.4) is straightforwardly obtained from the two component expressions in Eqs. (3.38), (8.2) and (8.3).

In an iterative subspace algorithm where trial vectors are added in pairs, after n iterations a reduced space $\boldsymbol{b}^{2n}$ consists of $2n$ trial vector

$$\boldsymbol{b}^{2n} = \{\boldsymbol{b}_1, \boldsymbol{b}_2, ..., \boldsymbol{b}_n, \boldsymbol{b}_1^P, \boldsymbol{b}_2^P, ..., \boldsymbol{b}_n^P\}\,. \tag{8.5}$$

The spaces of linear transformed vectors $\boldsymbol{\sigma}^{2n}$ and $\boldsymbol{\rho}^{2n}$ are also known. Due to no cost in obtaining the paired counterparts, paired vectors are not stored on disk, and therefore the storage does not increase compared to the algorithm presented in Section 7.1.

The reduced matrix equations of the form in Eq. (7.8) are constructed with the matrix elements of the reduced generalized Hessian and metric matrices as

$$(\boldsymbol{E}_{red}^{[2]})_{ij} = (\boldsymbol{b}_i^{2n})^T\boldsymbol{\sigma}_j^{2n}\,, \quad (\boldsymbol{S}_{red}^{[2]})_{ij} = (\boldsymbol{b}_i^{2n})^T\boldsymbol{\rho}_j^{2n}\,, \tag{8.6}$$

respectively. In the two-component form $\boldsymbol{E}_{red}^{[2]}$ and $\boldsymbol{S}_{red}^{[2]}$ may be expressed as

$$\boldsymbol{E}_{red}^{[2]} = \begin{pmatrix} \boldsymbol{A}_{red} & \boldsymbol{B}_{red} \\ \boldsymbol{B}_{red} & \boldsymbol{A}_{red} \end{pmatrix}, \quad \boldsymbol{S}_{red}^{[2]} = \begin{pmatrix} \boldsymbol{\Sigma}_{red} & \boldsymbol{\Delta}_{red} \\ -\boldsymbol{\Delta}_{red} & -\boldsymbol{\Sigma}_{red} \end{pmatrix}, \tag{8.7}$$

where $\mathbf{A}_{red}$, $\mathbf{B}_{red}$ and $\boldsymbol{\Sigma}_{red}$ are symmetric and $\boldsymbol{\Delta}_{red}$ is an antisymmetric matrix of the dimension n. The reduced subspace matrices thus have the same structure as their full matrix counterparts in Eq. (3.38).

Solving the reduced eigenvalue problem Eq. (7.8) yields the excitation energy ω_{p0}^R and an eigenvector $(\boldsymbol{X}_p)_{n+1}$ in the subspace Eq. (8.5)

$$(\boldsymbol{X}_p)_{n+1} = \sum_{i=1}^{2n}(X_{red})_i\boldsymbol{b}_i\,. \tag{8.8}$$

The residual for $(\boldsymbol{X}_p)_{n+1}$ becomes

$$\boldsymbol{R}_{n+1} = (\boldsymbol{E}^{[2]} - \omega_{p0}^R\boldsymbol{S}^{[2]})(\boldsymbol{X}_p)_{n+1} = \sum_{i=1}^{2n}[(X_p)_{red}]_i(\boldsymbol{\sigma}_i^{2n} - \omega_{p0}^R\boldsymbol{\rho}_i^{2n})\,. \tag{8.9}$$

The residual norm is calculated as a convergence test. A new trial vector $\boldsymbol{b}_{n+1}$ can be obtained according to Eq. (7.13), and the new trial vector together with its paired counterpart $\boldsymbol{b}_{n+1}^{P}$ are added to the reduced subspace in Eq. (8.5). Monotonic convergence is obtained for the eigenvalues of the reduced space, see Appendix C in Paper B for details.

Due to the fact that all the response equations have the block structure, imposing the block structure in the reduced subspace equation (by adding trial vectors in pairs) may be used to improve the convergence when solving the standard linear response equations in Eq. (7.2) and the damped response equation in Eq. (7.3). In Section 8.2, the algorithm with paired trial vectors for solving the standard response equation will be described. In Section 8.4, an extension of the paired algorithm for solving damped response equation will be introduced.

8.2 The standard response equations

When pairing is used to solve a standard response equation in Eq. (7.2), the algorithm is very similar to the one presented for the eigenvalue equation in Section 8.1. The reduced equation in Eq. (7.8) is solved in the reduced space spanned by the subspace in Eq. (8.5), where the matrix elements of the reduced generalized Hessian and metric matrices are given in Eq. (8.6), and the reduced right-hand side is given by

$$(\boldsymbol{g}_{red}^{b})_i = (\boldsymbol{b}_i^{2n})^T \boldsymbol{G}\,. \tag{8.10}$$

The residual becomes

$$\boldsymbol{R}_{n+1} = (\boldsymbol{E}^{[2]} - \omega \boldsymbol{S}^{[2]})\boldsymbol{X}_{n+1} - \boldsymbol{G} = \sum_{i=1}^{2n} (X_{red})_i (\boldsymbol{\sigma}_i^{2n} - \omega \boldsymbol{\rho}_i^{2n}) - \boldsymbol{G}\,. \tag{8.11}$$

The residual norm is calculated to check for convergence and residuals are used to obtain a new trial vector$\boldsymbol{b}_{n+1}$, which together with its paired counterpart $\boldsymbol{b}_{n+1}^{P}$ is added to the reduced subspace and the iterations are continued until convergence.

As described in Section 7.3, it would be advantageous to solve the standard response equation Eq. (7.2) using the CG algorithm, where the last three trial vectors are sufficient to keep the information of all previous trial vectors. However, when together with the trial vector its paired counterpart is added to the reduced space, no similar reduction in the number of subspace vectors can be obtained, as shown in Appendix A, and all vectors have to be stored.

8.3 Implementation details

In Ref. [23], Coriani *et al.* described in detail a linear-scaling implementation of an algorithm with paired trial vectors for the standard response equation and the eigenvalue equation. In this implementation, expressions for the response functions are derived using a non-redundant exponential parameterization of the density matrix in the AO basis [155].

Linear-scaling is obtained when all the key computational steps in solving the response equation scale linearly. Coriani *et al.* proposed an AO preconditioning that fulfilled this condition. In the AO basis, the overlap matrix $\mathbf{S}$ may be factorized

$$\mathbf{S} = \mathbf{V}^T\mathbf{V}\,, \tag{8.12}$$

where $\mathbf{V}$ is either an upper triangular matrix $\mathbf{U}$ in the Cholesky basis, or the principal square-root matrix $\mathbf{S}^{-1/2}$ in the Löwdin basis. The Hessian formulated in the orthogonalized AO (OAO) basis is diagonally dominant. There is a slight preference for the Löwdin basis, since it resembles most closely the original AO basis, ensuring the locality of orbitals is preserved to the greatest possible extend [156]. In addition, the condition number of the OAO matrices is reduced significantly, and the convergence of Eq. (7.4) is significantly improved.

For solving the damped response equations, the MO preconditioner is used.[13] The preconditioner contains redundant unoccupied-occupied components. The projectors $\mathcal{P}$ and $\mathcal{P}^T$ are introduced to circumvent this problem. The projections $\mathcal{P}$ and $\mathcal{P}^T$ have the forms [23, 155]

$$\mathcal{P}(\mathbf{X}) = \mathbf{P}_{\mathrm{o}}\mathbf{X}\mathbf{P}_{\mathrm{v}}^T + \mathbf{P}_{\mathrm{v}}\mathbf{X}\mathbf{P}_{\mathrm{o}}^T\,, \quad \mathcal{P}^T(\mathbf{X}) = \mathbf{P}_{\mathrm{o}}^T\mathbf{X}\mathbf{P}_{\mathrm{v}} + \mathbf{P}_{\mathrm{v}}^T\mathbf{X}\mathbf{P}_{\mathrm{o}}\,. \tag{8.13}$$

$\mathbf{P}_{\mathrm{o}}$ and $\mathbf{P}_{\mathrm{v}}$ are projectors onto the occupied and virtual orbital spaces, respectively,

$$\mathbf{P}_{\mathrm{o}} = \mathbf{D}\mathbf{S}\,, \quad \mathbf{P}_{\mathrm{v}} = \mathbf{1} - \mathbf{D}\mathbf{S}\,. \tag{8.14}$$

In addition, to ensure that new trial vectors are linearly independent of the previous ones, the trial vectors are orthonormalized

$$(\boldsymbol{b}_i)^T\boldsymbol{b}_j = (\boldsymbol{b}_i^P)^T\boldsymbol{b}_j^P = \delta_{ij}, \quad (\boldsymbol{b}_i^P)^T\boldsymbol{b}_j = (\boldsymbol{b}_i)^T\boldsymbol{b}_j^P = 0. \tag{8.15}$$

The implementation schemes used to obtain the linear-scaling algorithm for solving the standard response equations are used also in the case of the damped response equation, as will be described in the next section.

[13] Introducing preconditioning in AO (or another local basis) is planed.

8.4 The damped response equation

In an iterative subspace algorithm for solving the damped response equation [in Eqs. (4.23) and (7.3)] where the trial vectors are added in pairs, the trial vectors are split into the real $\boldsymbol{X}^R$ and imaginary $\boldsymbol{X}^I$ components. This means that the reduced subspace will contain improved trial vectors for both the real and imaginary components of the solution vector together with their paired counterparts, and four vectors will be added in each iteration.

As mentioned is Section 7.4, Eq. (7.3) may be separated into a real and an imaginary part as in Eqs. (7.23a) and (7.23b). The difficulties involved in solving Eq. (7.3) [or equivalently Eqs. (7.23a) and (7.23b)] depend on whether the frequency ω is in a resonance or a far-off-resonance region. If the frequency is in a far-off-resonance region, the coupling between the real and imaginary components of the solution vector is small. In this region, the solution to Eq. (7.3) may be obtained by solving Eqs. (7.23a) and (7.23b) using a common subspace for the two equations. New trial vectors may thus be added using a strategy similar to the one used when solving a standard response equation described in Section 8.2. This algorithm is described in Section 8.4.1 and is denoted the one-subspace approach.

In the resonance region, the solution vector has a large eigenvector component in both $\boldsymbol{X}^R$ and $\boldsymbol{X}^I$ leading to a large coupling between $\boldsymbol{X}^R$ and $\boldsymbol{X}^I$ when solving Eqs. (7.23a) and (7.23b), which may cause divergence. In this case, Eq. (7.3) should be solved using a single subspace, where the coupling in the solution vector is taken into account explicitly. This approach will be described in Section 8.4.2 and is denoted the two-level-subspace approach, due to the fact that two different subspaces are used, one for solving Eq. (7.3) (macro-subspace) and one for generating new trial vectors (micro-subspace). Since convergence of the algorithm may be improved by introducing preconditioning, the preconditioned two-level-subspace approach will be presented in Section 8.4.3. A comparison to previously used algorithm by Norman *et al.* [29] is given in Section 8.4.4.

8.4.1 One-subspace approach

A good performance of the one-subspace approach is observed when the frequency ω is far from an excitation energy, leading to a small coupling between the real and the imaginary components of the solution vector. In practice it can be used to determine the general structure of the spectrum. If convergence is not obtained after a few iterations with the one-subspace approach, it suggests that the frequency of interest is in the resonance region, and to obtain the correct result the robust two-level-subspace approach must be applied.

In the one-subspace approach, the coupled equations in Eqs. (7.23a) and (7.23b) are

solved simultaneously. After the n'th iteration, a subspace consisting of pairs of trial vectors has been generated

$$\boldsymbol{b}^{4n} = \{\boldsymbol{b}_1^R, \boldsymbol{b}_1^{R,P}, \boldsymbol{b}_1^I, \boldsymbol{b}_1^{I,P}, \boldsymbol{b}_2^R, \boldsymbol{b}_2^{R,P}, \boldsymbol{b}_2^I, \boldsymbol{b}_2^{I,P}, ..., \boldsymbol{b}_n^R, \boldsymbol{b}_n^{R,P}, \boldsymbol{b}_n^I, \boldsymbol{b}_n^{I,P}\}\,, \tag{8.16}$$

and the linearly transformed vectors $\boldsymbol{\sigma}^{4n}$ and $\boldsymbol{\rho}^{4n}$ are also known. The response equations in Eqs. (7.23a) and (7.23b) may be solved in the reduced space of Eq. (8.16)

$$(\boldsymbol{E}_{red}^{[2]} - \omega \boldsymbol{S}_{red}^{[2]})\boldsymbol{X}_{red}^R = \boldsymbol{\mathcal{G}}_{red}^R\,, \tag{8.17a}$$

$$(\boldsymbol{E}_{red}^{[2]} - \omega \boldsymbol{S}_{red}^{[2]})\boldsymbol{X}_{red}^I = \boldsymbol{\mathcal{G}}_{red}^I\,, \tag{8.17b}$$

where the matrix elements of the reduced generalized Hessian and metric matrices are given as

$$(\boldsymbol{E}_{red}^{[2]})_{ij} = (\boldsymbol{b}_i^{4n})^T \boldsymbol{\sigma}_j^{4n}, \quad (\boldsymbol{S}_{red}^{[2]})_{ij} = (\boldsymbol{b}_i^{4n})^T \boldsymbol{\rho}_j^{4n}, \tag{8.18}$$

and the reduced right-hand sides are given by

$$(\boldsymbol{\mathcal{G}}_{red}^R)_i = (\boldsymbol{b}_i^{4n})^T \boldsymbol{\mathcal{G}}^R = (\boldsymbol{b}_i^{4n})^T (\boldsymbol{G}^R - \gamma \boldsymbol{S}^{[2]} \boldsymbol{X}_n^I)\,, \tag{8.19a}$$

$$(\boldsymbol{\mathcal{G}}_{red}^I)_i = (\boldsymbol{b}_i^{4n})^T \boldsymbol{\mathcal{G}}_n^I = (\boldsymbol{b}_i^{4n})^T (\boldsymbol{G}^I + \gamma \boldsymbol{S}^{[2]} \boldsymbol{X}_n^R)\,, \tag{8.19b}$$

where $\boldsymbol{X}_n^R$ and $\boldsymbol{X}_n^I$ are the optimal solution vectors in iteration n. The $\boldsymbol{\mathcal{G}}_{red}$ matrix is constructed in each iteration [due to the fact that the right-hand sides in Eqs. (7.23a) and (7.23b) contain $\gamma \boldsymbol{S}^{[2]} \boldsymbol{X}_n^I$ and $\gamma \boldsymbol{S}^{[2]} \boldsymbol{X}_n^R$ components, respectively, and therefore change in each iteration] in contrast to $\boldsymbol{E}_{red}^{[2]}$ and $\boldsymbol{S}_{red}^{[2]}$, which may be simply extended.

From the solution to the reduced problem Eqs. (8.17a) and (8.17b), the optimal solution vectors of the (n+1)'th iteration $\boldsymbol{X}_{n+1}^R$ and $\boldsymbol{X}_{n+1}^I$ may be determined as

$$\boldsymbol{X}_{n+1}^R = \sum_i (X_{red}^R)_i \boldsymbol{b}_i^{4n}; \quad \boldsymbol{X}_{n+1}^I = \sum_i (X_{red}^I)_i \boldsymbol{b}_i^{4n}. \tag{8.20}$$

The residuals for the optimal solutions $\boldsymbol{X}_{n+1}^R$ and $\boldsymbol{X}_{n+1}^I$ are constructed as

$$\begin{aligned} \boldsymbol{R}_{n+1}^R &= (\boldsymbol{E}^{[2]} - \omega \boldsymbol{S}^{[2]})\boldsymbol{X}_{n+1}^R - \boldsymbol{G}^R + \gamma \boldsymbol{S}^{[2]} \boldsymbol{X}_{n+1}^I \\ &= \sum_{i=1}^{4n} [(X_{red}^R)_i (\boldsymbol{\sigma}_i^{4n} - \omega \boldsymbol{\rho}_i^{4n}) + (\boldsymbol{X}_{red}^I)_i \gamma \boldsymbol{\rho}_i^{4n}] - \boldsymbol{G}^R\,, \end{aligned} \tag{8.21a}$$

and

$$\begin{aligned} \boldsymbol{R}_{n+1}^I &= (\boldsymbol{E}^{[2]} - \omega \boldsymbol{S}^{[2]})(\boldsymbol{X}_D^I)_{n+1} - \boldsymbol{G}^I - \gamma \boldsymbol{S}^{[2]} (\boldsymbol{X}_D^R)_{n+1} \\ &= \sum_{i=1}^{4n} [(X_{red}^I)_i (\boldsymbol{\sigma}_i^{4n} - \omega \boldsymbol{\rho}_i^{4n}) - (\boldsymbol{X}_{red}^R)_i \gamma \boldsymbol{\rho}_i^{4n}] - \boldsymbol{G}^I\,, \end{aligned} \tag{8.21b}$$

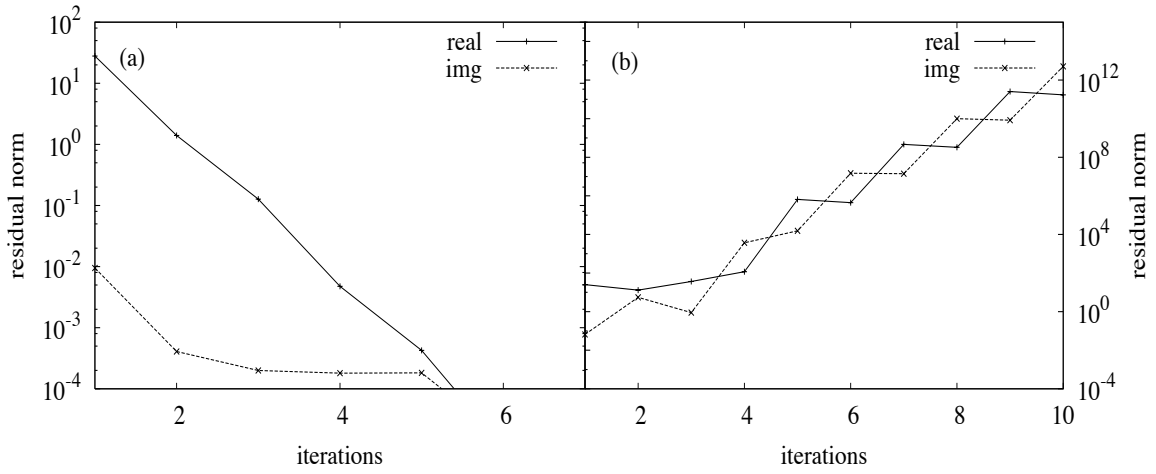

Figure 8.1: Convergence of the xx component of the linear polarizability for a DNA fragment consist of one nucleotide, obtained using the one-subspace approach **(a)** far from an excitation energy, $\omega = 0.1$ a.u., **(b)** close to an excitation energy, $\omega = 0.55$ a.u..

respectively. Convergence is obtained when the sum of the norms of $\boldsymbol{R}^R_{n+1}$ and $\boldsymbol{R}^I_{n+1}$ is smaller than a preset threshold. New trial vectors are generated from the preconditioned residuals $\boldsymbol{R}^R_{n+1}$ and $\boldsymbol{R}^I_{n+1}$ and added to the subspace in Eq. (8.16).

Figure 8.1 illustrates the convergence obtained in a calculation of the xx component of the linear polarizability for a DNA fragment consisting of one nucleotide using the one-subspace approach. In Fig. 8.1a, the convergence in the far-off-resonance region is displayed. Solving Eqs. (7.23a) and (7.23b) simultaneously leads to a rapid convergence due to a small coupling between the real and the imaginary component of the solution vector. Figure 8.1b illustrates the case where the frequency of interest is in the resonance region. Using the one-subspace approach then leads to divergence, due to a large coupling between the real and imaginary components of the solution vector. In this case it is necessary to use the much more robust two-level-subspace approach.

8.4.2 Two-level-subspace approach

In the two-level-subspace approach after n iterations, Eq. (7.3) has been solved in a subspace containing $4n$ trial vectors [see Eq. (8.16)]. The subspace analogue of Eq. (7.3) reads

$$(\boldsymbol{E}^{[2]}_{red} - (\omega + i\gamma)\boldsymbol{S}^{[2]}_{red})(\boldsymbol{X}^R + i\boldsymbol{X}^I)_{red} = (\boldsymbol{G}^R + i\boldsymbol{G}^I)_{red}\,, \tag{8.22}$$

where the matrix elements of the reduced generalized Hessian and metric matrices are given in Eq. (8.18) and the reduced right-hand side is given as

$$[(\boldsymbol{G}^R + i\boldsymbol{G}^I)_{red}]_i = (\boldsymbol{b}_i^{4n})^T(\boldsymbol{G}^R + i\boldsymbol{G}^I)\,. \tag{8.23}$$

In this case, $\boldsymbol{E}^{[2]}_{red}$, $\boldsymbol{S}^{[2]}_{red}$, and $\boldsymbol{G}_{red}$ are all constructed by extending the subspaces from the previous iterations.

From the solution to the reduced equation Eq. (8.22), the optimal solution vectors of the (n+1)'th iteration, $\boldsymbol{X}^R_{n+1}$ and $\boldsymbol{X}^I_{n+1}$, are obtained using Eq. (8.20) and the residuals $\boldsymbol{R}^R_{n+1}$ and $\boldsymbol{R}^I_{n+1}$ may be constructed from Eqs. (8.21a) and (8.21b). The residuals $\boldsymbol{R}^R_{n+1}$ and $\boldsymbol{R}^I_{n+1}$ are used to test for convergence.

In the two-level-subspace approach, new trial vectors are generated by solving the standard response equations separately

$$(\boldsymbol{E}^{[2]} - \omega\boldsymbol{S}^{[2]})\boldsymbol{b}^R_{n+1} = \boldsymbol{G}^R - \gamma\boldsymbol{S}^{[2]}(\boldsymbol{X}^I_{n+1} + \boldsymbol{R}^I_{n+1}) = \boldsymbol{\mathcal{G}}^R\,, \tag{8.24a}$$

$$(\boldsymbol{E}^{[2]} - \omega\boldsymbol{S}^{[2]})\boldsymbol{b}^I_{n+1} = \boldsymbol{G}^I + \gamma\boldsymbol{S}^{[2]}(\boldsymbol{X}^R_{n+1} + \boldsymbol{R}^R_{n+1}) = \boldsymbol{\mathcal{G}}^I\,, \tag{8.24b}$$

using the standard subspace algorithm for response equations described in Section 8.2. ($\boldsymbol{X}^R_{n+1}$+$\boldsymbol{R}^R_{n+1}$) and ($\boldsymbol{X}^I_{n+1}$+$\boldsymbol{R}^I_{n+1}$) are used to construct right-hand sides, as the residuals represent improvements to the solution vector from the orthogonal complement to the subspace $\boldsymbol{b}^{4n}$ in Eq. (8.16).

As initial guesses for $\boldsymbol{b}^R_1$ and $\boldsymbol{b}^I_1$, the solutions of the standard response equation may be used where the right-hand side $\boldsymbol{\mathcal{G}}^R$ is equal to the real component of $\boldsymbol{g}^b$, and $\boldsymbol{\mathcal{G}}^I$ is given by

$$\boldsymbol{\mathcal{G}}^I = \boldsymbol{G}^I + \gamma\boldsymbol{S}^{[2]}\boldsymbol{b}^R_1\,, \tag{8.25}$$

where $\boldsymbol{b}^R_1$ is the solution to the real response equation. Trial vectors used in obtaining $\boldsymbol{b}^R_1$ and $\boldsymbol{b}^I_1$ may be stored and used as start guesses for constructing new trial vectors in the macro-subspace.

Figure 8.2 illustrates the convergence in the micro-subspaces for macro-iteration 1, 2 and 3 in the two-level-subspace algorithm. In the upper panel of Fig. 8.2, the previous trial vectors are used as initial guesses in the micro-iterations while in the lower panels the solutions to the micro-iterations are constructed from scratch in each macro-iteration. The computational cost of the first macro-iteration is the same, while starting from the second macro-iteration an improvement in convergence is seen in the approach shown in the upper panel. Convergence is obtained after about 15 micro-iterations, where in contrast about 70 micro-iterations are needed when the vectors are not stored.

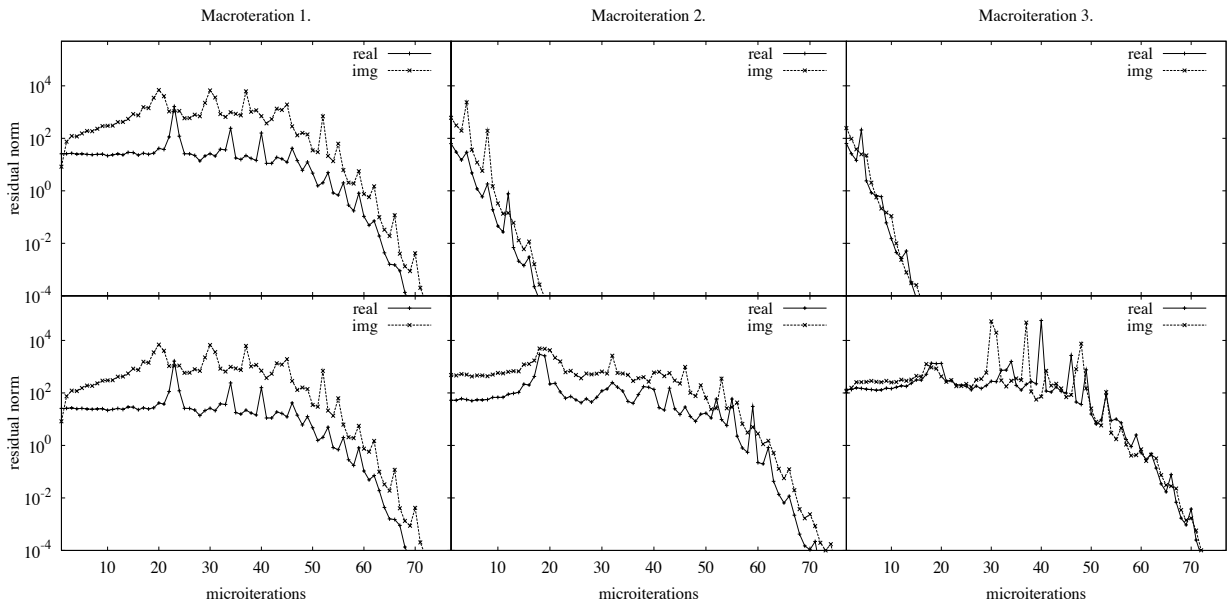

Figure 8.2: Convergence of the first three macro-iterations of the xx component of the linear polarizability for a DNA fragment consisting of two nucleotides, obtained using the two-level-subspace approach, $\omega = 0.25$ a.u., $\gamma = 0.005$ a.u.; **Upper panel:** trial vectors used to obtain an optimal vector in the first macro-iteration are stored and used as a start guesses in the next macro-iterations, **Lower panel**: trial vectors not stored.

8.4.3 Preconditioned two-level-subspace approach

Convergence in the global subspace may be sped up by preconditioning equation in Eq. (7.3) with a preconditioner $\boldsymbol{E}_0^{[2]}$.[14] Using this preconditioner, instead of solving Eq. (7.3) an equation of the form

$$\mathcal{P}(\boldsymbol{E}_0^{[2]})^{-1}\mathcal{P}^T(\boldsymbol{E}^{[2]} - (\omega + i\gamma)\boldsymbol{S}^{[2]})\mathcal{P}(\boldsymbol{X}^R + i\boldsymbol{X}^I) = \mathcal{P}(\boldsymbol{E}_0^{[2]})^{-1}\mathcal{P}^T(\boldsymbol{G}^R + i\boldsymbol{G}^I)\,, \tag{8.26}$$

is solved, where the projections $\mathcal{P}$ and $\mathcal{P}^T$ have been defined in Eq. (8.13).

In the n'th iteration, Eq. (8.26) has been solved in a subspace $\boldsymbol{b}^{4n}$ consisting of the paired trial vectors introduced in Eq. (8.16). $\tilde{\boldsymbol{\sigma}}^{4n}$ and $\tilde{\boldsymbol{\rho}}^{4n}$ (defined below) are also known. The complex reduced space equation

$$[\tilde{\boldsymbol{E}}_{red}^{[2]} - (\omega + i\gamma)\tilde{\boldsymbol{S}}_{red}^{[2]}](\boldsymbol{X}_{n+1}^R + \boldsymbol{X}_{n+1}^I)_{red} = (\tilde{\boldsymbol{G}}^R + i\tilde{\boldsymbol{G}}^I)_{red}\,, \tag{8.27}$$

is solved, where the matrix elements of the reduced generalized Hessian and metric matrices

[14] It is assumed here that the $\omega\boldsymbol{S}^{[2]}$ and $\gamma\boldsymbol{S}^{[2]}$ terms in the preconditioner can be neglected due to the fact that ω and γ are small. A more efficient preconditioner will be presented in the next chapter.

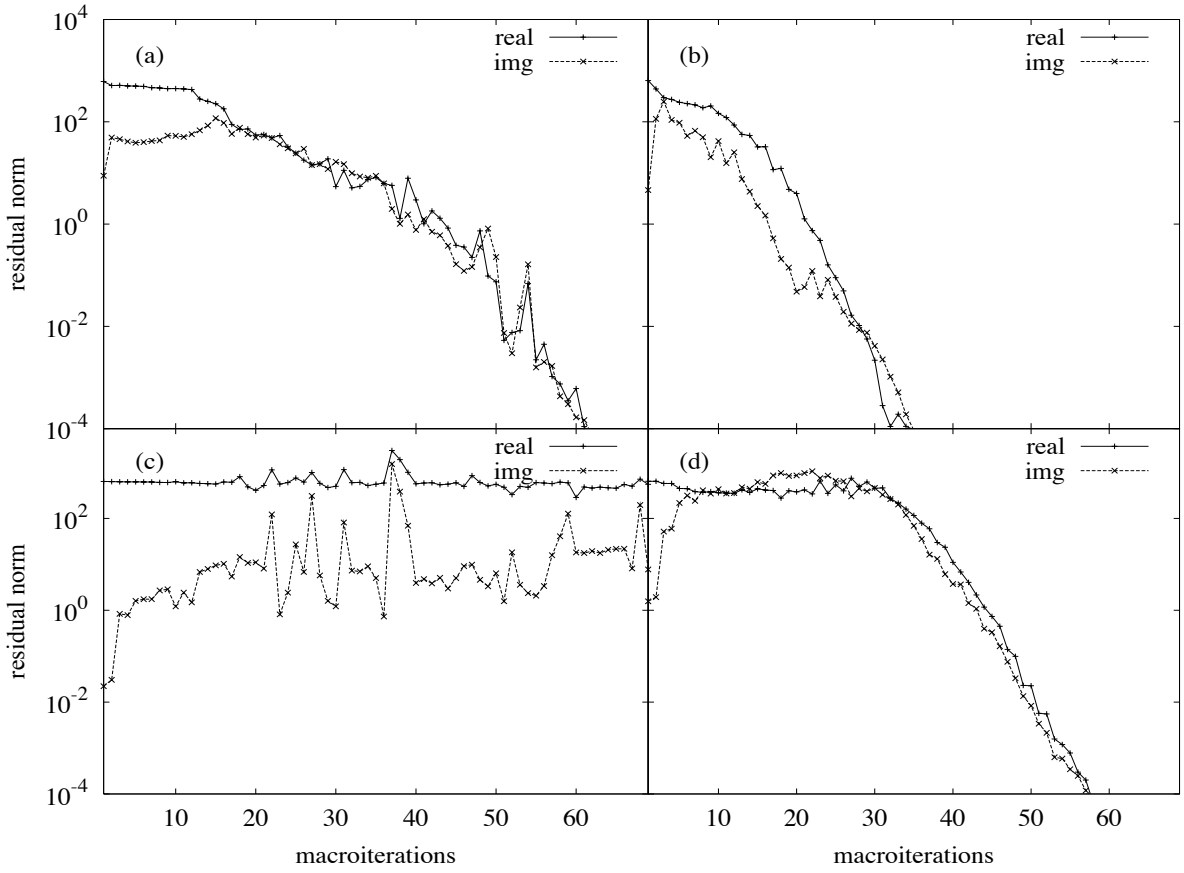

Figure 8.3: Global convergence of the xx component of the linear polarizability for a DNA fragment consisting of two nucleotides, obtained using the two-level-subspace approach **(a)** and **(c)** without preconditioning; **(b)** and **(d)** with preconditioning; **(a)** and **(b)** $\omega = 0.25$ a.u.; **(c)** and **(d)** $\omega = 0.45$ a.u.; $\gamma = 0.005$ a.u..

and the gradient vector are given as

$$(\tilde{\boldsymbol{E}}^{[2]}_{red})_{ij} = (\boldsymbol{b}^{4n}_i)^T \tilde{\boldsymbol{\sigma}}^{4n}_j = (\boldsymbol{b}^{4n}_i)^T \mathcal{P}(\boldsymbol{E}^{[2]}_0)^{-1} \mathcal{P}^T (\boldsymbol{\sigma}^{4n}_j), \tag{8.28a}$$

$$(\tilde{\boldsymbol{S}}^{[2]}_{red})_{ij} = (\boldsymbol{b}^{4n}_i)^T \tilde{\boldsymbol{\rho}}^{4n}_j = (\boldsymbol{b}^{4n}_i)^T \mathcal{P}(\boldsymbol{E}^{[2]}_0)^{-1} \mathcal{P}^T (\boldsymbol{\rho}^{4n}_j), \tag{8.28b}$$

and

$$[(\tilde{\boldsymbol{G}}^R + i\tilde{\boldsymbol{G}}^I)_{red}]_i = (\boldsymbol{b}^{4n}_i)^T \mathcal{P}(\boldsymbol{E}^{[2]}_0)^{-1} \mathcal{P}^T (\boldsymbol{G}^R + i\boldsymbol{G}^I)\,, \tag{8.28c}$$

respectively. From the solution to the reduced equation Eq. (8.27), the optimal solution vectors of the $(n+1)$'th iteration, $\boldsymbol{X}^R_{n+1}$ and $\boldsymbol{X}^I_{n+1}$, are obtained using Eq. (8.20), and the residuals $\boldsymbol{R}^R_{n+1}$ and $\boldsymbol{R}^I_{n+1}$ are constructed from Eqs. (8.21a) and (8.21b).

New trial vectors are generated by solving the following equations separately

$$\mathcal{P}(\boldsymbol{E}_0^{[2]})^{-1}\mathcal{P}^T(\boldsymbol{E}^{[2]} - \omega\boldsymbol{S}^{[2]})\boldsymbol{b}_{n+1}^R = \\ \mathcal{P}(\boldsymbol{E}_0^{[2]})^{-1}\mathcal{P}^T\{\boldsymbol{G}^R - \gamma\boldsymbol{S}^{[2]}[\boldsymbol{X}_{n+1}^I + \mathcal{P}(\boldsymbol{E}_0^{[2]})^{-1}\mathcal{P}^T(\boldsymbol{R}_{n+1}^I)]\}\,, \tag{8.29a}$$

and

$$\mathcal{P}(\boldsymbol{E}_0^{[2]})^{-1}\mathcal{P}^T(\boldsymbol{E}^{[2]} - \omega\boldsymbol{S}^{[2]})\boldsymbol{b}_{n+1}^I = \\ \mathcal{P}(\boldsymbol{E}_0^{[2]})^{-1}\mathcal{P}^T\{\boldsymbol{G}^I + \gamma\boldsymbol{S}^{[2]}[\boldsymbol{X}_{n+1}^R + \mathcal{P}(\boldsymbol{E}_0^{[2]})^{-1}\mathcal{P}^T(\boldsymbol{R}_{n+1}^R)]\}\,. \tag{8.29b}$$

The solutions to Eqs. (8.29a) and (8.29b) are equivalent to the ones obtained by solving separately the standard response equations

$$(\boldsymbol{E}^{[2]} - \omega\boldsymbol{S}^{[2]})\boldsymbol{b}_{n+1}^R = \boldsymbol{G}^R - \gamma\boldsymbol{S}^{[2]}(\boldsymbol{X}_{n+1}^R + \mathcal{P}(\boldsymbol{E}_0^{[2]})^{-1}\mathcal{P}^T(\boldsymbol{R}_{n+1}^I))\,, \tag{8.30a}$$

$$(\boldsymbol{E}^{[2]} - \omega\boldsymbol{S}^{[2]})\boldsymbol{b}_{n+1}^I = \boldsymbol{G}^I + \gamma\boldsymbol{S}^{[2]}(\boldsymbol{X}_{n+1}^R + \mathcal{P}(\boldsymbol{E}_0^{[2]})^{-1}\mathcal{P}^T(\boldsymbol{R}_{n+1}^R))\,, \tag{8.30b}$$

using the standard subspace algorithm for response equations described in Section 8.2.

Figure 8.3 displays the convergence obtained using the two-level-subspace approach for two chosen frequencies. Results shown in Figs. 8.3a and 8.3c have been obtained using the algorithm presented in Section 8.4.2, and Figs. 8.3b and 8.3d show results obtained using the preconditioned algorithm (described above). The results reported in Fig. 8.3b have been obtained in half the number of iterations compared to the results showed in Fig. 8.3a. For higher frequency, convergence has not been obtained in 60 iterations using the non-preconditioned algorithm, as can be seen from Fig. 8.3c, whereas when the preconditioned algorithm has been used, (relatively) fast convergence can be observed (see Fig. 8.3d). Figure 8.3 displays the same behavior in the convergence of the real and imaginary components of the solution of Eq. (7.3), due to the fact that they depend on each other, as may be seen from Eqs. (7.23a) and (7.23b).

8.4.4 Comparison to the approach by Norman *et al.*

In the approach for solving the complex response equation in Eq. (7.3), presented by Norman *et al.* [29], the complex response equation is solved using an algorithm reminiscent of the two-level-subspace approach described in Section 8.4.2. However, their approach does not involve the simpler algorithm described in Section 8.4.1, which is used mainly to scan the spectrum and determine the region where the more robust solver needs to be applied. That makes the computational cost for calculations with frequencies far from any excitation

energies much higher compared to the two-level-subspace approach. The implementation presented in Ref. [29] is computationally more demanding than the two-level-subspace approach, since it relies on solving a generalized eigenvalue problem to generate start vectors. The first eigenvectors are a very good approximation for the solution of Eq. (7.3) close to the excitation energy, but not necessarily for large systems having many small excitation energies in the low frequency region (see *e.g.* Fig 1.2). For the DNA fragment consisting of two nucleotides, the first 50 excitations are very low lying states with small intensities, and are not a good approximation for states with higher excited states. In the approach presented above the solutions to the standard response equations are used where the right-hand sides are equal to the real component of $\boldsymbol{g}^b$ and Eq. (8.25). They give reasonably good starting guesses for all frequencies. Another difference is the generation of the new trial vectors in macro-subspace. In the approach presented in Ref. [29], new trial vectors are in each macro-iteration generated from scratch by solving the standard response equations with an improved right-hand side. In the approach described in Section 8.4.2, the vectors used to construct the first trial vectors in the global space are stored and give a very good starting guesses for trial vectors in next macro-iterations, which improves convergence radically (see Fig. 8.2). However, it should be noted that the improvement in convergence is on the expense of disk storage, and using the two-level-subspace may therefore be impractical (or even impossible) for very large systems.

9 Iterative algorithms with symmetrized trial vectors

In the previous section, the algorithms with paired trial vectors have been introduced for solving response equations in Eqs. (7.2)–(7.4). An improvement in convergence has been observed when these algorithms have been used [41], however, an attempt to apply CG/CR algorithms on the standard and damped response equation turned out unsuccessfully, see Appendix A.

Saue and co-workers [157–159] introduced a symmetry division of trial vectors for solving the standard response and eigenvalue equations in the four-component HF and DFT approximations. In their approach, trial vectors are split according to their Hermiticity and time-reversal symmetry, which are the two fundamental operator symmetries in a relativistic framework. The trial vectors are complex due to the complex nature of the four-component wavefunction, however, the reduced subspace equations remain real, due to the symmetry properties of $\boldsymbol{E}^{[2]}$ and $\boldsymbol{S}^{[2]}$. Recently, Villaume *et al.* [160] have generalized this approach to solve the damped response equation, including a presentation of a highly efficient preconditioner. In spirit of this work, an algorithm with symmetrized trial vectors is introduced in this section, which combines the improvement in convergence (due to spanning larger space than in the general subspace approach presented in Section 7.1) with a very efficient preconditioner used to obtain new trial vectors. In case of the damped response equation the disk storage can be significantly reduced compared to when the two-level-subspace and preconditioned two-level-subspace approaches have been applied.

In Section 9.1, an introduction to the algorithm with symmetrized trial vectors is given. In Sections 9.2, 9.3, and 9.4, the algorithm with symmetrized trial vectors will be introduced for solving the response eigenvalue equation, the standard response equation and the damped response equation, respectively. In Sections 9.4.1 and 9.5, the algorithm is compared to the one proposed by Villaume *et al.* in Ref. [160] and to the algorithm with paired trial vectors described in Section 8, respectively.

9.1 Introduction

A vector may be written as a sum of a symmetric and an antisymmetric component. Due to the features of linear transformations $\boldsymbol{\sigma}$ and $\boldsymbol{\rho}$ described below, it might be advantageous to split the trial vectors in this fashion during the iterative procedure. Using this scheme, the paired structure of the Hessian and metric matrices in the reduced space is imposed during the whole iterative procedure.

The symmetric (g) and antisymmetric (u) trial vectors are defined as

$$\boldsymbol{b}_g = \begin{pmatrix} b_{IA} \\ b_{IA} \end{pmatrix}, \tag{9.1}$$

and

$$\boldsymbol{b}_u = \begin{pmatrix} b_{JB} \\ -b_{JB} \end{pmatrix}, \tag{9.2}$$

respectively. The symmetry of a trial vector is conserved for the $\boldsymbol{E}^{[2]}$ linear transformation

$$\boldsymbol{\sigma}_g = \boldsymbol{E}^{[2]}\boldsymbol{b}_g; \quad \boldsymbol{\sigma}_u = \boldsymbol{E}^{[2]}\boldsymbol{b}_u\,, \tag{9.3}$$

and reversed for the $\boldsymbol{S}^{[2]}$ linear transformation

$$\boldsymbol{\rho}_g = \boldsymbol{S}^{[2]}\boldsymbol{b}_u; \quad \boldsymbol{\rho}_u = \boldsymbol{S}^{[2]}\boldsymbol{b}_g\,. \tag{9.4}$$

It should be noted that each of the linear transformations $\boldsymbol{\sigma}_g$ and $\boldsymbol{\sigma}_u$ ($\boldsymbol{\rho}_g$ and $\boldsymbol{\rho}_u$) can be carried out with an operation cost equal to half of the cost of linear transformation $\boldsymbol{\sigma}$ ($\boldsymbol{\rho}$) on a general trial vector given in Eq. (7.5).

The symmetry of the $\boldsymbol{E}^{[2]}$ and $\boldsymbol{S}^{[2]}$ matrices in Eqs. (9.3) and (9.4) makes it advantageous to split the solution to the response equations Eqs. (7.2) and (7.4) into symmetric and antisymmetric components

$$\boldsymbol{X} = \boldsymbol{X}_g + \boldsymbol{X}_u\,, \tag{9.5}$$

and the solution to the damped response equation Eq. (7.3) in terms of the Hermitian and anti-Hermitian components

$$\boldsymbol{X} = \boldsymbol{X}^H + \boldsymbol{X}^A\,, \tag{9.6}$$

where

$$\boldsymbol{X}^H = \boldsymbol{X}_g^R + i\boldsymbol{X}_u^I, \quad \boldsymbol{X}^A = \boldsymbol{X}_u^R + i\boldsymbol{X}_g^I\,, \tag{9.7}$$

and $\boldsymbol{X}_g^R$, $\boldsymbol{X}_g^I$, $\boldsymbol{X}_u^R$ and $\boldsymbol{X}_u^I$ are real.

9.2 The response eigenvalue equation

Using the symmetry of the $\boldsymbol{E}^{[2]}$ and $\boldsymbol{S}^{[2]}$ matrices and expressing the solution vector as in Eq. (9.5), the response eigenvalue equation in Eq. (7.4) may be written in the two-component form

$$\begin{pmatrix} \boldsymbol{E}^{[2]} & -\omega_{p0}\boldsymbol{S}^{[2]} \\ -\omega_{p0}\boldsymbol{S}^{[2]} & \boldsymbol{E}^{[2]} \end{pmatrix} \begin{pmatrix} \boldsymbol{X}_{g,p} \\ \boldsymbol{X}_{u,p} \end{pmatrix} = \begin{pmatrix} \boldsymbol{0} \\ \boldsymbol{0} \end{pmatrix}, \tag{9.8}$$

where the coupling that occurs between the two components $\boldsymbol{X}_{g,p}$ and $\boldsymbol{X}_{u,p}$ is introduced explicitly. Eq. (9.8) may be written as a standard eigenvalue equation

$$\begin{pmatrix} \boldsymbol{E}^{[2]} & \boldsymbol{0} \\ \boldsymbol{0} & \boldsymbol{E}^{[2]} \end{pmatrix} \begin{pmatrix} \boldsymbol{X}_{g,p} \\ \boldsymbol{X}_{u,p} \end{pmatrix} = \omega_p \begin{pmatrix} \boldsymbol{0} & \boldsymbol{S}^{[2]} \\ \boldsymbol{S}^{[2]} & \boldsymbol{0} \end{pmatrix} \begin{pmatrix} \boldsymbol{X}_{g,p} \\ \boldsymbol{X}_{u,p} \end{pmatrix}, \tag{9.9}$$

where $\begin{pmatrix} \boldsymbol{0} & \boldsymbol{S}^{[2]} \\ \boldsymbol{S}^{[2]} & \boldsymbol{0} \end{pmatrix}$ is a generalized metric which is not positive definite. However, if $\begin{pmatrix} \boldsymbol{E}^{[2]} & \boldsymbol{0} \\ \boldsymbol{0} & \boldsymbol{E}^{[2]} \end{pmatrix}$ is viewed as a metric, Eq. (9.9) is a standard eigenvalue equation for a Hermitian matrix $\begin{pmatrix} \boldsymbol{0} & \boldsymbol{S}^{[2]} \\ \boldsymbol{S}^{[2]} & \boldsymbol{0} \end{pmatrix}$.

Eq. (9.8) may be solved using an iterative subspace algorithm where in each iteration, a symmetric and an antisymmetric trial vector is added. After iteration n, two sets of trial vectors have been constructed

$$\boldsymbol{b}_g^m = \{\boldsymbol{b}_{1g}, \boldsymbol{b}_{2g}, ..., \boldsymbol{b}_{mg}\}, \tag{9.10a}$$

$$\boldsymbol{b}_u^k = \{\boldsymbol{b}_{1u}, \boldsymbol{b}_{2u}, ..., \boldsymbol{b}_{ku}\}, \tag{9.10b}$$

(where $m, k \leq n$) and the linearly transformed vectors $\boldsymbol{\sigma}_g^m$, $\boldsymbol{\sigma}_u^k$, $\boldsymbol{\rho}_u^m$ and $\boldsymbol{\rho}_g^k$ are known. Eq. (9.8) is solved in the subspace given by Eqs. (9.10a) and (9.10b)

$$\begin{pmatrix} \boldsymbol{E}^{[2]}_{red,gg} & -\omega^R_{p0}\boldsymbol{S}^{[2]}_{red,gu} \\ -\omega^R_{p0}\boldsymbol{S}^{[2]}_{red,ug} & \boldsymbol{E}^{[2]}_{red,uu} \end{pmatrix} \begin{pmatrix} (\boldsymbol{X}_{g,p})_{red} \\ (\boldsymbol{X}_{u,p})_{red} \end{pmatrix} = \begin{pmatrix} \boldsymbol{0} \\ \boldsymbol{0} \end{pmatrix}, \tag{9.11}$$

where

$$\begin{aligned} \boldsymbol{E}^{[2]}_{red,gg} &= \boldsymbol{b}_g^T \boldsymbol{E}^{[2]} \boldsymbol{b}_g, \quad \boldsymbol{E}^{[2]}_{red,uu} = \boldsymbol{b}_u^T \boldsymbol{E}^{[2]} \boldsymbol{b}_u, \\ \boldsymbol{S}^{[2]}_{red,gu} &= \boldsymbol{b}_g^T \boldsymbol{S}^{[2]} \boldsymbol{b}_u, \quad \boldsymbol{S}^{[2]}_{red,ug} = \boldsymbol{b}_u^T \boldsymbol{S}^{[2]} \boldsymbol{b}_g . \end{aligned} \tag{9.12}$$

The optimal vectors in the subspace in Eqs. (9.10a) and (9.10b) read

$$\boldsymbol{X}_{n+1,g,p} = \sum_{i=1}^{m} [(X_{g,p})_{red}]_i \boldsymbol{b}_{ig}, \tag{9.13a}$$

$$\boldsymbol{X}_{n+1,u,p} = \sum_{i=1}^{k} [(X_{u,p})_{red}]_i \boldsymbol{b}_{iu} . \tag{9.13b}$$

From the solution vectors the residuals may be obtained as

$$\begin{aligned} \boldsymbol{R}_{n+1,g} &= \boldsymbol{E}^{[2]} \boldsymbol{X}_{n+1,g,p} - \omega^R_{p0} \boldsymbol{S}^{[2]} \boldsymbol{X}_{n+1,u,p} \\ &= \sum_{i=1}^{m} ((X_{g,p})_{red})_i \boldsymbol{\sigma}_{ig} - \omega^R_{p0} \sum_{i=1}^{k} ((X_{u,p})_{red})_i \boldsymbol{\rho}_{ig} , \end{aligned} \tag{9.14a}$$

$$\begin{aligned} \boldsymbol{R}_{n+1,u} &= \boldsymbol{E}^{[2]}\boldsymbol{X}_{n+1,u,p} - \omega^R_{p0}\boldsymbol{S}^{[2]}\boldsymbol{X}_{n+1,g,p} \\ &= \sum_{i=1}^{k}((X_{u,p})_{red})_i\boldsymbol{\sigma}_{iu} - \omega^R_{p0}\sum_{i=1}^{m}((X_{g,p})_{red})_i\boldsymbol{\rho}_{iu}\,, \end{aligned} \tag{9.14b}$$

and are used to check for convergence.

New trial vectors $\boldsymbol{b}_{n+1,g}$ and $\boldsymbol{b}_{n+1,u}$ may be obtained from the optimal solution vectors $\boldsymbol{X}_{n+1,g}$ and $\boldsymbol{X}_{n+1,u}$ using the Davidson and the Olsen algorithms, as will be described in Sections 9.2.1 or 9.2.2, respectively. The new trial vectors are added to the reduced subspaces in Eqs. (9.10a) and (9.10b) and the iterative procedure is repeated until convergence.

9.2.1 New trial vectors using the Davidson algorithm

In the Davidson algorithm (see Section 7.2.1), a new trial vector is obtained using Eq. (7.13). Using the residuals and trial vectors expressed in terms of a symmetric and antisymmetric component, Eq. (7.13) may be expressed as

$$(\boldsymbol{b}_{n+1,g} + \boldsymbol{b}_{n+1,g}) = (\boldsymbol{E}^{[2]}_0 - \omega^R_{p0}\boldsymbol{S}^{[2]})^{-1}(\boldsymbol{R}_{n+1,g} + \boldsymbol{R}_{n+1,u})\,. \tag{9.15}$$

Eq. (9.15) may be expressed in the two-component form

$$\begin{pmatrix} \boldsymbol{b}_{n+1,g} \\ \boldsymbol{b}_{m+1,u} \end{pmatrix} = [(\boldsymbol{E}^{[2]}_0)^2 - (\omega^R_p)^2(\boldsymbol{S}^{[2]})^2]^{-1} \begin{pmatrix} \boldsymbol{E}^{[2]}_0 & \omega^R_{p0}\boldsymbol{S}^{[2]} \\ \omega^R_{p0}\boldsymbol{S}^{[2]} & \boldsymbol{E}^{[2]}_0 \end{pmatrix} \begin{pmatrix} \boldsymbol{R}_{n+1,g} \\ \boldsymbol{R}_{n+1,u} \end{pmatrix}, \tag{9.16}$$

giving directly a new symmetric and an antisymmetric trial vector.

9.2.2 New trial vectors using the Olsen algorithm

After iteration n in the subspace algorithm presented in Section 9.2, the optimal solution vectors $\boldsymbol{X}_{n+1,g,p}$ and $\boldsymbol{X}_{n+1,u,p}$ in Eqs. (9.13a) and (9.13b), the residuals vectors given in Eqs. (9.14a) and (9.14b) and the eigenvalue ω^R_{p0} have been determined. It can be assumed that the optimal vectors $\boldsymbol{X}_{n+1,g,p}$ and $\boldsymbol{X}_{n+1,u,p}$ constitute the zeroth-order solution to the eigenvalue equation in the Olsen algorithm (see Section 7.2.2) and for simplicity they may be written as

$$\boldsymbol{X}^0 = \begin{pmatrix} \boldsymbol{X}^0_g \\ \boldsymbol{X}^0_u \end{pmatrix} = \begin{pmatrix} \boldsymbol{X}_{n+1,g,p} \\ \boldsymbol{X}_{n+1,u,p} \end{pmatrix}. \tag{9.17}$$

The optimal vector $\boldsymbol{X}^0$ satisfies a normalization condition analogous to Eq. (3.57)

$$(\boldsymbol{X}^0)^T \begin{pmatrix} \boldsymbol{0} & \boldsymbol{S}^{[2]} \\ \boldsymbol{S}^{[2]} & \boldsymbol{0} \end{pmatrix} \boldsymbol{X}^0 = (\boldsymbol{X}^0_g)^T\boldsymbol{S}^{[2]}\boldsymbol{X}^0_u + (\boldsymbol{X}^0_u)^T\boldsymbol{S}^{[2]}\boldsymbol{X}^0_g = 1\,. \tag{9.18}$$

ω_{p0}^R is the zeroth-order eigenvalue ω_{p0}^0. The Olsen algorithm may now be used as described in Section 7.2.2.

Expressing Eq. (9.8) in terms of the zeroth-order and correction components, given in Eqs. (3.53), (7.16) and (7.17), yields

$$\begin{pmatrix} \boldsymbol{E}_0^{[2]} + \boldsymbol{E}_1^{[2]} & -(\omega_{p0}^0 + \omega_{p0}^1)\boldsymbol{S}^{[2]} \\ -(\omega_{p0}^0 + \omega_{p0}^1)\boldsymbol{S}^{[2]} & \boldsymbol{E}_0^{[2]} + \boldsymbol{E}_1^{[2]} \end{pmatrix} (\boldsymbol{X}^0 + \boldsymbol{X}^1) = \boldsymbol{0}\,. \tag{9.19}$$

By neglecting terms that are quadratic in the correction, $\boldsymbol{X}^1$ may be obtained as

$$\begin{aligned} \boldsymbol{X}^1 &= -\begin{pmatrix} \boldsymbol{E}_0^{[2]} & -\omega_{p0}^0\boldsymbol{S}^{[2]} \\ -\omega_{p0}^0\boldsymbol{S}^{[2]} & \boldsymbol{E}_0^{[2]} \end{pmatrix}^{-1} \left[\begin{pmatrix} \boldsymbol{E}^{[2]} & -\omega_{p0}^0\boldsymbol{S}^{[2]} \\ -\omega_{p0}^0\boldsymbol{S}^{[2]} & \boldsymbol{E}^{[2]} \end{pmatrix} \boldsymbol{X}^0 - \omega_{p0}^1 \begin{pmatrix} \boldsymbol{0} & \boldsymbol{S}^{[2]} \\ \boldsymbol{S}^{[2]} & \boldsymbol{0} \end{pmatrix} \boldsymbol{X}^0 \right] \\ &= -\boldsymbol{L}^{-1} \left[\boldsymbol{R}_{n+1} - \omega_{p0}^1 \begin{pmatrix} \boldsymbol{0} & \boldsymbol{S}^{[2]} \\ \boldsymbol{S}^{[2]} & \boldsymbol{0} \end{pmatrix} \boldsymbol{X}^0 \right], \end{aligned} \tag{9.20}$$

where $\boldsymbol{L}^{-1}$ is an easily constructed preconditioner matrix showed in Section 9.2.1, and $\boldsymbol{R}_{n+1}$ is given as

$$\boldsymbol{R}_{n+1} = \begin{pmatrix} \boldsymbol{R}_{n+1,g} \\ \boldsymbol{R}_{n+1,u} \end{pmatrix} = \begin{pmatrix} \boldsymbol{E}^{[2]} & -\omega_p^0\boldsymbol{S}^{[2]} \\ -\omega_p^0\boldsymbol{S}^{[2]} & \boldsymbol{E}^{[2]} \end{pmatrix} \boldsymbol{X}^0\,, \tag{9.21}$$

where $\boldsymbol{R}_{n+1,g}$ and $\boldsymbol{R}_{n+1,u}$ are the residual vectors given in Eqs. (9.14a) and (9.14b). Requiring that the eigenvector correction $\boldsymbol{X}^1$ is orthogonal to $\boldsymbol{X}^0$ in the generalized $\boldsymbol{S}^{[2]}$ [as given in Eq. (7.20)], ω_{p0}^1 may be determined in analogy with Eq. (7.21)

$$\begin{aligned} \omega_{p0}^1 &= \frac{(\boldsymbol{X}^0)^T \begin{pmatrix} \boldsymbol{0} & \boldsymbol{S}^{[2]} \\ \boldsymbol{S}^{[2]} & \boldsymbol{0} \end{pmatrix} \begin{pmatrix} \boldsymbol{E}_0^{[2]} & -\omega_{p0}^0\boldsymbol{S}^{[2]} \\ -\omega_{p0}^0\boldsymbol{S}^{[2]} & \boldsymbol{E}_0^{[2]} \end{pmatrix}^{-1} \begin{pmatrix} \boldsymbol{E}^{[2]} & -\omega_{p0}^0\boldsymbol{S}^{[2]} \\ -\omega_{p0}^0\boldsymbol{S}^{[2]} & \boldsymbol{E}^{[2]} \end{pmatrix} \boldsymbol{X}^0}{(\boldsymbol{X}^0)^T \begin{pmatrix} \boldsymbol{0} & \boldsymbol{S}^{[2]} \\ \boldsymbol{S}^{[2]} & \boldsymbol{0} \end{pmatrix} \begin{pmatrix} \boldsymbol{E}_0^{[2]} & -\omega_{p0}^0\boldsymbol{S}^{[2]} \\ -\omega_{p0}^0\boldsymbol{S}^{[2]} & \boldsymbol{E}_0^{[2]} \end{pmatrix}^{-1} \begin{pmatrix} \boldsymbol{0} & \boldsymbol{S}^{[2]} \\ \boldsymbol{S}^{[2]} & \boldsymbol{0} \end{pmatrix} \boldsymbol{X}^0} \\ &= \frac{(\boldsymbol{X}^0)^T \begin{pmatrix} \boldsymbol{0} & \boldsymbol{S}^{[2]} \\ \boldsymbol{S}^{[2]} & \boldsymbol{0} \end{pmatrix} \boldsymbol{L}^{-1}\boldsymbol{R}_{n+1}}{(\boldsymbol{X}^0)^T \begin{pmatrix} \boldsymbol{0} & \boldsymbol{S}^{[2]} \\ \boldsymbol{S}^{[2]} & \boldsymbol{0} \end{pmatrix} \boldsymbol{L}^{-1} \begin{pmatrix} \boldsymbol{0} & \boldsymbol{S}^{[2]} \\ \boldsymbol{S}^{[2]} & \boldsymbol{0} \end{pmatrix} \boldsymbol{X}^0}\,. \end{aligned} \tag{9.22}$$

Using the Olsen algorithm, new trial vectors are obtained without additional linear transformations compared to the Davidson algorithm, as can be seen from Eq. (9.20). The term $\begin{pmatrix} \boldsymbol{0} & \boldsymbol{S}^{[2]} \\ \boldsymbol{S}^{[2]} & \boldsymbol{0} \end{pmatrix} \boldsymbol{X}^0$ is determined when the residual vectors are calculated.

9.3 The standard response equation

Inserting Eq. (9.5) into Eq. (7.2) and writing Eq. (7.2) in the two-component form gives

$$\begin{pmatrix} \boldsymbol{E}^{[2]} & -\omega\boldsymbol{S}^{[2]} \\ -\omega\boldsymbol{S}^{[2]} & \boldsymbol{E}^{[2]} \end{pmatrix} \begin{pmatrix} \boldsymbol{X}_g \\ \boldsymbol{X}_u \end{pmatrix} = \begin{pmatrix} \boldsymbol{G}_g \\ \boldsymbol{G}_u \end{pmatrix} , \tag{9.23}$$

where $\boldsymbol{G}_g$ and $\boldsymbol{G}_u$ are the symmetric and antisymmetric components of the gradient vector $\boldsymbol{G}$, respectively. Eq. (9.23) may be solved using a subspace algorithm as for the response eigenvalue equation. Assuming that after iteration n subspaces of the form Eqs. (9.10a) and (9.10b) have been constructed, the reduced standard response equation

$$\begin{pmatrix} \boldsymbol{E}^{[2]}_{red,gg} & -\omega\boldsymbol{S}^{[2]}_{red,gu} \\ -\omega\boldsymbol{S}^{[2]}_{red,ug} & \boldsymbol{E}^{[2]}_{red,uu} \end{pmatrix} \begin{pmatrix} (\boldsymbol{X}_g)_{red} \\ (\boldsymbol{X}_u)_{red} \end{pmatrix} = \begin{pmatrix} \boldsymbol{G}_{red,g} \\ \boldsymbol{G}_{red,u} \end{pmatrix} , \tag{9.24}$$

are solved, where the reduced Hessian and metric matrices are given in Eq. (9.12) and the reduced right-hand side vector reads

$$\boldsymbol{G}_{red,g} = \boldsymbol{b}_g^T \boldsymbol{G}_g, \quad \boldsymbol{G}_{red,u} = \boldsymbol{b}_u^T \boldsymbol{G}_u. \tag{9.25}$$

Solving Eq. (9.24) leads to the optimal solution vectors given in Eqs. (9.13a) and (9.13b). The residuals $\boldsymbol{R}_{n+1,g}$ and $\boldsymbol{R}_{n+1,u}$ may then be obtained as

$$\begin{aligned} \boldsymbol{R}_{n+1,g} &= \boldsymbol{E}^{[2]}\boldsymbol{X}_{n+1,g} - \omega\boldsymbol{S}^{[2]}\boldsymbol{X}_{n+1,u} - \boldsymbol{G}_g \\ &= \sum_{i=1}^{n}((X_g)_{red})_i\boldsymbol{\sigma}_{ig} - \omega\sum_{i=1}^{n}((X_u)_{red})_i\boldsymbol{\rho}_{ig} - \boldsymbol{G}_g \, , \end{aligned} \tag{9.26a}$$

$$\begin{aligned} \boldsymbol{R}_{n+1,u} &= \boldsymbol{E}^{[2]}\boldsymbol{X}_{n+1,u} - \omega\boldsymbol{S}^{[2]}\boldsymbol{X}_{n+1,g} - \boldsymbol{G}_u \\ &= \sum_{i=1}^{n}((X_u)_{red})_i\boldsymbol{\sigma}_{iu} - \omega\sum_{i=1}^{n}((X_g)_{red})_i\boldsymbol{\rho}_{iu} - \boldsymbol{G}_u \, . \end{aligned} \tag{9.26b}$$

From the residuals, new trial vectors may be constructed by preconditioning according to Eq. (9.16) where ω_{p0}^R is replaced by ω. The iterative sequence is continued until convergence.

Eq. (9.23) constitutes a set of linear equations for a symmetric matrix. This means that for small frequency parameter ω Eq. (9.23) may be solved using the CG algorithm. For higher frequencies, the matrix in Eq. (9.23) is not positive definite, therefor, in principle, the CR algorithm may be applied in this case, however not with the efficient preconditioner, see Section 6.3.2.

9.4 The damped response equation

The damped response equation may be solved in an analogous way using the algorithm with symmetrized trial vectors.

Inserting Eq. (9.6) into the damped response equation in Eq. (7.3) gives a set of linear equations for each of the four components $\boldsymbol{X}_g^R$, $\boldsymbol{X}_u^R$, $\boldsymbol{X}_g^I$ and $\boldsymbol{X}_u^I$

$$\begin{aligned}
\boldsymbol{E}^{[2]}\boldsymbol{X}_g^R - \omega\boldsymbol{S}^{[2]}\boldsymbol{X}_u^R + \gamma\boldsymbol{S}^{[2]}\boldsymbol{X}_u^I &= \boldsymbol{G}_g^R\,,\\
\boldsymbol{E}^{[2]}\boldsymbol{X}_u^R - \omega\boldsymbol{S}^{[2]}\boldsymbol{X}_g^R + \gamma\boldsymbol{S}^{[2]}\boldsymbol{X}_g^I &= \boldsymbol{G}_u^R\,,\\
\boldsymbol{E}^{[2]}\boldsymbol{X}_u^I - \omega\boldsymbol{S}^{[2]}\boldsymbol{X}_g^I - \gamma\boldsymbol{S}^{[2]}\boldsymbol{X}_g^R &= \boldsymbol{G}_u^I\,,\\
\boldsymbol{E}^{[2]}\boldsymbol{X}_g^I - \omega\boldsymbol{S}^{[2]}\boldsymbol{X}_u^I - \gamma\boldsymbol{S}^{[2]}\boldsymbol{X}_u^R &= \boldsymbol{G}_g^I\,,
\end{aligned} \tag{9.27}$$

where $\boldsymbol{G}_g^R$ and $\boldsymbol{G}_u^R$ ($\boldsymbol{G}_g^I$ and $\boldsymbol{G}_u^I$) are the symmetric and antisymmetric components of the real (imaginary) part of the gradient vector $\boldsymbol{G}$. Eq. (9.6) may be expressed in terms of a coupled set of linear equations for a real symmetric matrix

$$\begin{pmatrix}
\boldsymbol{E}^{[2]} & -\omega\boldsymbol{S}^{[2]} & \gamma\boldsymbol{S}^{[2]} & 0\\
-\omega\boldsymbol{S}^{[2]} & \boldsymbol{E}^{[2]} & 0 & \gamma\boldsymbol{S}^{[2]}\\
\gamma\boldsymbol{S}^{[2]} & 0 & -\boldsymbol{E}^{[2]} & \omega\boldsymbol{S}^{[2]}\\
0 & \gamma\boldsymbol{S}^{[2]} & \omega\boldsymbol{S}^{[2]} & -\boldsymbol{E}^{[2]}
\end{pmatrix}
\begin{pmatrix}
\boldsymbol{X}_g^R\\ \boldsymbol{X}_u^R\\ \boldsymbol{X}_u^I\\ \boldsymbol{X}_g^I
\end{pmatrix}
=
\begin{pmatrix}
\boldsymbol{G}_g^R\\ \boldsymbol{G}_u^R\\ -\boldsymbol{G}_u^I\\ -\boldsymbol{G}_g^I
\end{pmatrix}. \tag{9.28}$$

where the coupling between the different components is considered explicitly. Eq. (9.28) may be solved in the reduced subspace spanned by real vectors

$$\boldsymbol{b}_g^{R,p} = \{\boldsymbol{b}_{1g}^R, \boldsymbol{b}_{2g}^R, ..., \boldsymbol{b}_{pg}^R\}, \tag{9.29a}$$
$$\boldsymbol{b}_u^{R,q} = \{\boldsymbol{b}_{1u}^R, \boldsymbol{b}_{2u}^R, ..., \boldsymbol{b}_{qu}^R\}, \tag{9.29b}$$
$$\boldsymbol{b}_g^{I,r} = \{\boldsymbol{b}_{1g}^I, \boldsymbol{b}_{2g}^I, ..., \boldsymbol{b}_{rg}^I\}, \tag{9.29c}$$
$$\boldsymbol{b}_u^{I,s} = \{\boldsymbol{b}_{1u}^I, \boldsymbol{b}_{2u}^I, ..., \boldsymbol{b}_{su}^I\}\,, \tag{9.29d}$$

(where $p, q, r, s \leq n$), analogously to the standard response equation. The residuals are given as

$$\begin{aligned}
\boldsymbol{R}_g^R &= \boldsymbol{E}^{[2]}\boldsymbol{X}_g^R - \omega\boldsymbol{S}^{[2]}\boldsymbol{X}_u^R + \gamma\boldsymbol{S}^{[2]}\boldsymbol{X}_u^I - \boldsymbol{G}_g^R\,,\\
\boldsymbol{R}_u^R &= \boldsymbol{E}^{[2]}\boldsymbol{X}_u^R - \omega\boldsymbol{S}^{[2]}\boldsymbol{X}_g^R + \gamma\boldsymbol{S}^{[2]}\boldsymbol{X}_g^I - \boldsymbol{G}_u^R\,,\\
\boldsymbol{R}_u^I &= -\boldsymbol{E}^{[2]}\boldsymbol{X}_u^I + \omega\boldsymbol{S}^{[2]}\boldsymbol{X}_g^I + \gamma\boldsymbol{S}^{[2]}\boldsymbol{X}_g^R + \boldsymbol{G}_u^I\,,\\
\boldsymbol{R}_g^I &= -\boldsymbol{E}^{[2]}\boldsymbol{X}_g^I + \omega\boldsymbol{S}^{[2]}\boldsymbol{X}_u^I + \gamma\boldsymbol{S}^{[2]}\boldsymbol{X}_u^R + \boldsymbol{G}_g^I\,,
\end{aligned} \tag{9.30}$$

and are used to check for convergence. In the subspace iterative approach, new trial vectors

are obtained by preconditioning residuals in accordance to Eq. (7.13)

$$\begin{pmatrix} \boldsymbol{b}^R_{n+1,g} \\ \boldsymbol{b}^R_{n+1,u} \\ -\boldsymbol{b}^I_{n+1,u} \\ -\boldsymbol{b}^I_{n+1,g} \end{pmatrix} = \mathcal{P} \otimes \begin{pmatrix} \mathcal{A} & \mathcal{B} & \mathcal{C} & \mathcal{D} \\ \mathcal{B} & \mathcal{A} & \mathcal{D} & \mathcal{C} \\ \mathcal{C} & \mathcal{D} & -\mathcal{A} & -\mathcal{B} \\ \mathcal{D} & \mathcal{C} & -\mathcal{B} & -\mathcal{A} \end{pmatrix} \begin{pmatrix} R^R_g \\ R^R_u \\ R^I_u \\ R^I_g \end{pmatrix} , \tag{9.31}$$

where $\mathcal{P}$, $\mathcal{A}$, $\mathcal{B}$, $\mathcal{C}$ and $\mathcal{D}$ are given by

$$\begin{aligned} \mathcal{P} &= [(\boldsymbol{E}_0^2 - (\omega^2 - \gamma^2)\mathbf{1})^2 + 4\omega^2\gamma^2\mathbf{1}]^{-1} , \\ \mathcal{A} &= \boldsymbol{E}_0^{[2]}[(\boldsymbol{E}_0^{[2]})^2 - (\omega^2 - \gamma^2)\mathbf{1}] , \\ \mathcal{B} &= \omega\boldsymbol{S}^{[2]}[(\boldsymbol{E}_0^{[2]})^2 - (\omega^2 + \gamma^2)\mathbf{1}] , \\ \mathcal{C} &= -\gamma\boldsymbol{S}^{[2]}[(\boldsymbol{E}_0^{[2]})^2 + (\omega^2 + \gamma^2)\mathbf{1}] , \\ \mathcal{D} &= -2\omega\gamma\boldsymbol{E}_0^{[2]}\mathbf{1} . \end{aligned} \tag{9.32}$$

The condition number of Eq. (9.28) is significantly reduced by the preconditioning in Eq. (9.31) and the convergence is radically improved.

9.4.1 Damped response equations using the algorithm of Villaume *et al.*

In Ref. [160], Villaume *et al.* described how the response equations within relativistic theory may be efficiently solved using the algorithm where the solution vectors are split according to their Hermiticity and the time-reversal symmetry

$$\boldsymbol{X} = \boldsymbol{X}^{++} + \boldsymbol{X}^{-+} + \boldsymbol{X}^{+-} + \boldsymbol{X}^{--} , \tag{9.33}$$

where the first and the second superscript signs correspond to Hermiticity and time-reversal symmetry, respectively. The vectors $\boldsymbol{X}^{++}$, $\boldsymbol{X}^{-+}$, $\boldsymbol{X}^{+-}$ and $\boldsymbol{X}^{--}$ are complex. In a non-relativistic framework, the time-reversal symmetry cannot be exploited and is, in a sense, replaced by the introduction of spin-adapted excitation operators. The algorithm of Villaume *et al*. may be simplified to be applicable to the non-relativistic damped response equation in Eq. (7.3). Villaume *et al.* convert time-reversal anti-symmetric elements into symmetric ones by extracting an imaginary phase, which also reverses the Hermiticity

$$\boldsymbol{X} = \boldsymbol{X}^{++} + \boldsymbol{X}^{-+} + i(\bar{\boldsymbol{X}}^{-+} + \bar{\boldsymbol{X}}^{++}) . \tag{9.34}$$

Inserting Eq. (9.34) into Eq. (7.3) and assuming that $\boldsymbol{g}^b$ in Eq. (7.3) is a Hermitian property gradient, $\boldsymbol{G}^H$, gives four coupled sets of linear equations

$$\begin{aligned}
\boldsymbol{E}^{[2]}\boldsymbol{X}^+ - \omega\boldsymbol{S}^{[2]}\boldsymbol{X}^- + \gamma\boldsymbol{S}^{[2]}\bar{\boldsymbol{X}}^- &= \boldsymbol{G}^+ , \\
\boldsymbol{E}^{[2]}\boldsymbol{X}^- - \omega\boldsymbol{S}^{[2]}\boldsymbol{X}^+ + \gamma\boldsymbol{S}^{[2]}\bar{\boldsymbol{X}}^+ &= 0 , \\
\boldsymbol{E}^{[2]}\bar{\boldsymbol{X}}^- - \omega\boldsymbol{S}^{[2]}\bar{\boldsymbol{X}}^+ - \gamma\boldsymbol{S}^{[2]}\boldsymbol{X}^+ &= 0 , \\
\boldsymbol{E}^{[2]}\bar{\boldsymbol{X}}^+ - \omega\boldsymbol{S}^{[2]}\bar{\boldsymbol{X}}^- - \gamma\boldsymbol{S}^{[2]}\boldsymbol{X}^- &= 0 .
\end{aligned} \tag{9.35}$$

Eq. (9.35) is analogous to Eq. (9.27) with the difference that $\boldsymbol{X}^+$, $\boldsymbol{X}^-$, $\bar{\boldsymbol{X}}^-$ and $\bar{\boldsymbol{X}}^+$ in Eq. (9.35) are complex while $\boldsymbol{X}_g^R$, $\boldsymbol{X}_u^R$, $\boldsymbol{X}_u^I$ and $\boldsymbol{X}_g^I$ in Eq. (9.27) are real. Eq. (9.35) is solved in the reduced space and new trial vectors are obtained by using a very efficient preconditioner similar to Eq. (9.31).

Eq. (9.35) could be written in symmetric form analogous to Eq. (9.28), where the solution vector is expressed in terms of the complex components $\mathbf{X}^H$, $\mathbf{X}^A$, $\bar{\mathbf{X}}^A$ and $\bar{\mathbf{X}}^H$, while the solution to Eq. (9.28) is written in terms of real vectors. In the case where the gradient vector $\boldsymbol{G}^H$ is either purely real or purely imaginary, the algorithm presented by Villaume *et al.* gives trial vectors that are either purely real or imaginary, and the iterative sequence of the algorithm becomes identical to the one obtained when algorithm presented in Section 9.4 is used.

9.5 Comparison to the algorithm with paired trial vectors

In Chapter 8 advantages of the algorithm with paired trial vectors comparing to the general iterative subspace approach described in Chapter 7 have been discussed. In this chapter, the algorithm with symmetrized trial vectors was introduced. It may be shown that a set of a symmetric and an antisymmetric vector span the same space as the set of a trial vector and its paired counterpart. Therefore, the algorithm with symmetrized trial vectors has the same advantages over the general iterative subspace approach as the algorithm with paired trial vectors.

Symmetric (g) and antisymmetric (u) components of a vector may be obtained from the paired trial vectors in Eqs. (8.2) and (8.3) as

$$\boldsymbol{b}_g = \frac{1}{2}(\boldsymbol{b} + \boldsymbol{b}^P) = \frac{1}{2}\begin{pmatrix} b_{AI} + b_{JB} \\ b_{JB} + b_{AI} \end{pmatrix} , \tag{9.36a}$$

$$\boldsymbol{b}_u = \frac{1}{2}(\boldsymbol{b} - \boldsymbol{b}^P) = \frac{1}{2}\begin{pmatrix} b_{AI} - b_{JB} \\ b_{JB} - b_{AI} \end{pmatrix} . \tag{9.36b}$$

Table 9.1: Residual norm obtained when solving the standard response equation Eq. (7.2) for a single water molecule using the algorithm with paired trial vectors (**second column**) and the algorithm with symmetrized trial vectors (**third–fifth columns**) , HF/cc-pVDZ, threshold=10^{-4}

Iteration number	iterative approach with trial vectors of the type:			
	paired	symmetrized		
	$\lvert\boldsymbol{R}\rvert$	$\lvert\boldsymbol{R}_g\rvert$	$\lvert\boldsymbol{R}_u\rvert$	$\lvert\boldsymbol{R}_g + \boldsymbol{R}_u\rvert$
1	1.17004	0.14243	1.16134	1.17004
2	0.61652	0.09143	0.60971	0.61652
3	0.10515	0.01461	0.10413	0.10515
4	0.01494	0.00329	0.01457	0.01494
5	0.00181	0.00043	0.00176	0.00181
6	0.00019	0.00006	0.00018	0.00019
7	0.00002	0.00001	0.00001	0.00002

Adding one symmetric and one antisymmetric trial vector in a subspace algorithm is thus equivalent to adding a set of paired vectors and thus ensures an implicit paired structure of the reduced space equation.

In Table 9.1, iteration sequences for the algorithms with paired and symmetrized trial vectors are given, for solving the standard response equation in Eq. (7.2) for a single water molecule at frequency $\omega = 0.2$ a.u. The calculations have been performed at the HF/cc-pVDZ level of theory, and the response equation have been solved to a residual norm of 10^{-4}. Residuals $\boldsymbol{R}$, $\boldsymbol{R}_g$ and $\boldsymbol{R}_u$ are given in Eqs. (8.11), (9.26a) and (9.26b), respectively. From the second and the fifth column, it can easily be concluded that the algorithms with paired and symmetrized trial vectors span the same space, and therefore give identical iteration sequence. It is due to the fact that symmetrized trial vectors may be considered as a special set of paired trial vectors, as discussed above.

When the algorithm with symmetrized trial vectors is used, the response equations are split into their symmetric and antisymmetric components, and they may be viewed as a linear equation problem with a symmetric matrix. The standard and damped response equations can, in principle, be solved using the CG/CR algorithms. However, although in several numerical examples performance of the preconditioned CR algorithm for a non-positive definite matrix (and preconditioner) is correct (as will be reported in the next

section), these algorithms cannot be safely used for higher frequencies.

Although the convergence rate of both algorithm is identical, using symmetrized trial vectors is advantageous over the paired set for solving the damped response equation, due to the fact that new trial vectors are determined efficiently with a very effective preconditioner [in Eq. (9.31)] and the disk storage is reduced compared to the case when the two-level-subspace approach, presented in Section 8.4 was used.

10 Illustrative results

The results presented in this chapter demonstrate the performance of various algorithms used for solving response equations. The different algorithms were presented in details in Chapters 6–9. The convergence of the eigenvalue response equation, Eq. (7.4), using the Davidson and Olsen algorithms, is discussed in Section 10.1. The performance of different algorithms for solving the standard response equation, Eq. (7.2), is described in Section 10.2. In Section 10.3, the efficiency of different algorithms in the context of solving the damped response equation, Eq. (7.3), is compared. In addition, calculations of the real and imaginary components of the linear polarizability for different systems are also reported in Section 10.3.

All calculations have been carried out using a local version of DALTON [1] and LSDALTON [2] packages, where all discussed algorithms have been implemented. Preconditioned algorithms have been used in the calculations reported in this chapter unless otherwise stated.

10.1 The eigenvalue response equation

In Table 10.1, the convergence of response eigenvalue equation in Eq. (7.4) is reported for a dipeptide alanine-tryptophan (Ala-Trp), displayed in Fig 10.1a. The calculations have been performed at the CAM-B3LYP/6-31G [142,161] level of theory, using the geometry obtained in the MAESTRO program [162] without carrying out any additional optimization. The response eigenvalue equation has been solved for the first eigenvalue, to a residual norm of 10^{-4}. Three different iterative algorithms have been used: (i) the Davidson algorithm with paired trial vectors (described in Section 8.1), (ii) the Davidson algorithm with symmetrized trial vectors (described in Section 9.2.1) and (iii) the Olsen algorithm with symmetrized trial vectors (described in Section 9.2.2). The residual $\boldsymbol{R}$ in the Davidson algorithm with paired trial vectors is given in Eq. (8.9). The residuals $\boldsymbol{R}_g$ and $\boldsymbol{R}_u$ in the algorithms with the symmetrized trial vectors are given in Eqs. (9.26a) and (9.26b), respectively.

As can be seen from the second and the third column in Table 10.1, the Davidson algorithms with paired and with symmetrized trial vectors give identical iteration sequences. This is due to the fact that symmetrized vectors may be considered as a special set of paired vectors, as discussed in Section 9.5. Therefore, vectors in both algorithms span the same space in each iteration. Since the paired structures of the reduced Hessian and metric matrices ($\boldsymbol{E}^{[2]}_{red}$ and $\boldsymbol{S}^{[2]}_{red}$) are preserved during the iterative procedure, paired eigenvalues are obtained in the reduced subspace in both cases.

From the third and the fourth column in Table 10.1, it can be seen that the iteration

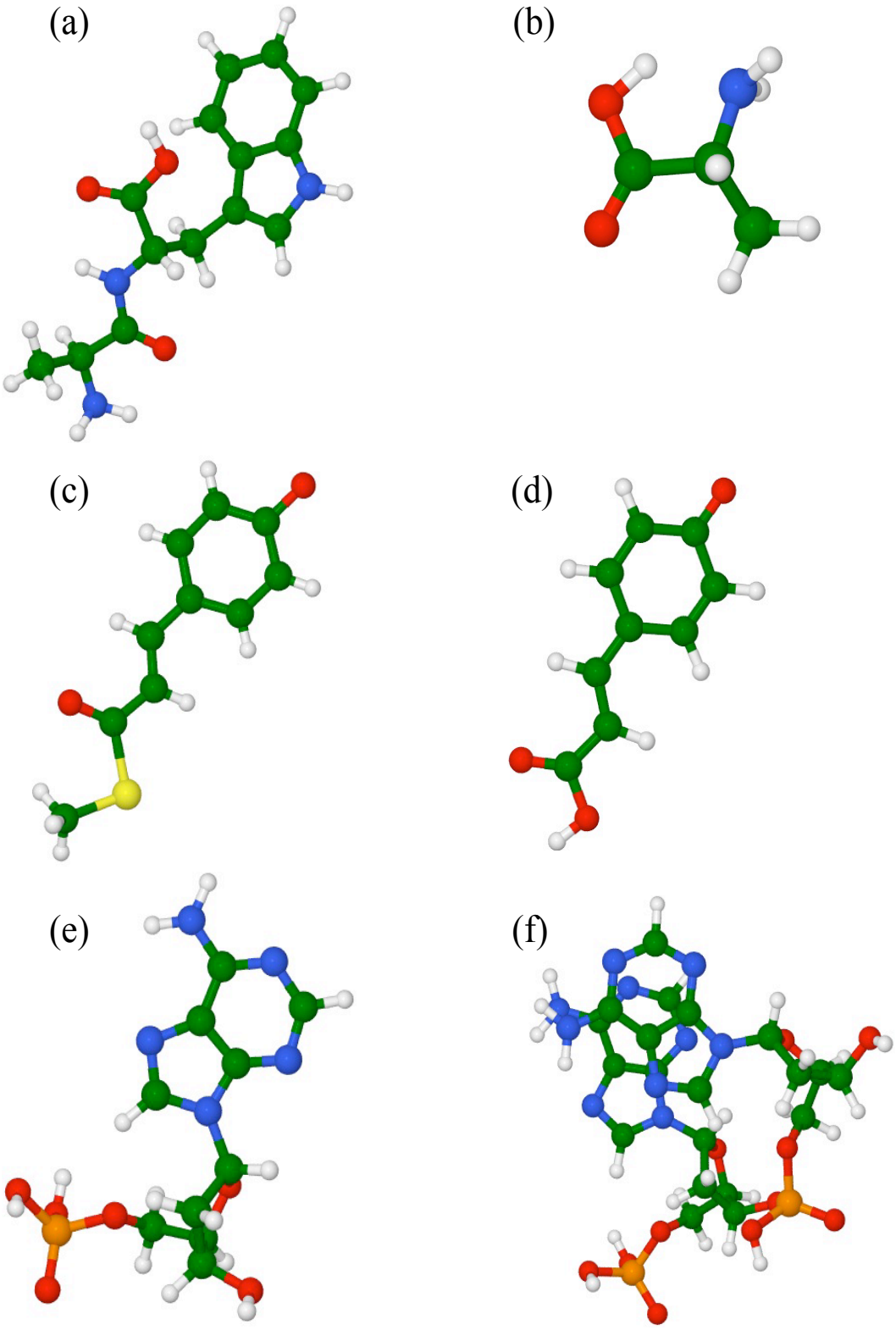

Figure 10.1: Molecular structures of **(a)** Ala-Trp, **(b)** alanine, **(c)** pCT^{-}, **(d)** pCA^{-}, **(e)** one nucleotide and **(f)** two nucleotides.

Table 10.1: Residual norm obtained when solving the eigenvalue equation for the first eigenvalue, for Ala-Trp, using (i) the Davidson algorithm with paired trial vectors (**second column**), (ii) the Davidson algorithm with symmetrized trial vectors (**third column**) and (iii) the Olsen algorithm with symmetrized trial vectors (**fourth column**). CAM-B3LYP/6-31G, threshold=10^{-4}.

Iteration number	Davidson alg.		Olsen alg.
	paired	symmetrized	symmetrized
	$\lvert\boldsymbol{R}\rvert$	$\lvert\boldsymbol{R}_g + \boldsymbol{R}_u\rvert$	$\lvert\boldsymbol{R}_g + \boldsymbol{R}_u\rvert$
1	0.11663	0.11663	0.11663
2	0.03819	0.03819	0.03819
3	0.02775	0.02775	0.02782
4	0.01723	0.01723	0.01725
5	0.02148	0.02148	0.02149
6	0.02492	0.02492	0.02488
7	0.03624	0.03624	0.03628
8	0.03034	0.03034	0.03036
9	0.02421	0.02421	0.02423
10	0.01862	0.01862	0.01860
11	0.01692	0.01692	0.01676
12	0.01282	0.01282	0.01276
13	0.01272	0.01272	0.01266
14	0.00688	0.00688	0.00687
15	0.00343	0.00343	0.00341
16	0.00228	0.00228	0.00226
17	0.00141	0.00141	0.00139
18	0.00146	0.00146	0.00144
19	0.00134	0.00134	0.00132
20	0.00068	0.00068	0.00068
21	0.00045	0.00045	0.00045
22	0.00030	0.00030	0.00030
23	0.00018	0.00018	0.00018
24	0.00008	0.00008	0.00008

sequences obtained using the Olsen and the Davidson algorithms are nearly identical. The Olsen algorithm does not give significant improvement unless $\boldsymbol{E}_0^{[2]}$ is approaching $\boldsymbol{E}^{[2]}$ in Eq. (9.11), and this is, in general, not the case when response eigenvalue equations are solved. Therefore, it may be concluded that response eigenvalue equations may safely be solved using the Davidson algorithm with paired or symmetrized trial vectors.

10.2 The standard response equation

In this section, the convergence of various algorithms for solving the standard response equation in Eq. (7.2), is compared for alanine (see Fig. 10.1b). Calculations are performed at the HF/6-31G level of theory using the geometry taken from the NIST on-line database [163]. The response equations have been solved to a residual norm of 10^{-4}. The calculations have been performed in two frequency regions: at $\omega = 0.1$ a.u. (relatively low frequency in the non-resonance region, $\omega_1 = 0.2129$ a.u.) presented in Section 10.2.1, and at $\omega = 0.4$ a.u. (relatively large frequency in the resonance region) reported in Section 10.2.2.

10.2.1 Performance of standard response algorithms in the off-resonance region

In Table 10.2, the convergence of the standard response equation is presented for alanine at the frequency $\omega = 0.1$ a.u.. Four different iterative algorithms have been used: (i) the general subspace approach (described in Section 7.3), (ii) the subspace algorithm with symmetrized trial vectors (described in Section 9.3), (iii) the conjugate gradient (CG) algorithm with symmetrized trial vectors (described in Sections 6.2 and 9.3) and (iv) the conjugate residual (CR) algorithm with symmetrized trial vectors (described in Sections 6.3 and 9.3). The CG and CR algorithms may be applied, since for $\omega = 0.1$ a.u., both the matrix in Eq. (9.23) and the preconditioner are positive definite. Results obtained using the subspace algorithm with paired trial vectors (described in Section 8.2) are not listed in Table 10.2, due to the fact that the iteration sequence is identical to the one obtained using the subspace algorithm with symmetrized trial vectors, as presented in Table 9.1. The residuals $\boldsymbol{R}$ (in the general subspace approach), $\boldsymbol{R}_g$ and $\boldsymbol{R}_u$ (in the algorithms with the symmetrized trial vectors) are given in Eqs. (7.12), (9.26a) and (9.26b), respectively.

When comparing the results obtained using the subspace algorithm with symmetrized trial vectors (third–fifth column) to the iterative sequence obtained with the general subspace approach (second column), a reduction in number of iterations is observed. This is due to the fact that a larger subspace is spanned when symmetrized trial vectors are introduced. The

Table 10.2: Residual norm obtained when solving the standard response equation for alanine at $\omega = 0.1$ a.u., using different algorithms: (i) the general subspace approach (**second column**), (ii) the subspace algorithm with symmetrized trial vectors (**third–fifth column**), (iii) the CG algorithm with symmetrized trial vectors (**sixth column**) and (iv) the CR algorithm with symmetrized trial vectors (**seventh column**); HF/6-31G, threshold=10^{-4}.

Iteration	iterative approach with trial vectors of the type:					
number	general	symmetrized				
		subspace			CG	CR
	$\|\boldsymbol{R}\|$	$\|\boldsymbol{R}_g\|$	$\|\boldsymbol{R}_u\|$	$\|\boldsymbol{R}_g + \boldsymbol{R}_u\|$	$\|\boldsymbol{R}_g + \boldsymbol{R}_u\|$	$\|\boldsymbol{R}_g + \boldsymbol{R}_u\|$
1	4.51473	0.12568	1.81342	1.81777	0.81189	0.71915
2	1.85994	0.04235	0.68710	0.68841	0.23247	0.22109
3	0.47364	0.02104	0.18558	0.18677	0.09411	0.08346
4	0.17550	0.01044	0.08186	0.08252	0.05206	0.04005
5	0.08012	0.00363	0.04100	0.04116	0.03190	0.02242
6	0.04412	0.00180	0.02361	0.02368	0.01961	0.01384
7	0.03078	0.00076	0.00930	0.00933	0.00698	0.00591
8	0.01389	0.00045	0.00396	0.00399	0.00364	0.00301
9	0.00523	0.00014	0.00177	0.00178	0.00151	0.00133
10	0.00198	0.00004	0.00050	0.00050	0.00047	0.00043
11	0.00084	0.00001	0.00018	0.00018	0.00018	0.00017
12	0.00054	0.00001	0.00004	0.00004	0.00005	0.00005
13	0.00019					
14	0.00005					

improvement is not dramatic, however, it is obtained without additional cost, as discussed in Chapter 9.

When comparing the fifth and the sixth columns in Table 10.2, it can be seen that the iteration sequence for the subspace algorithm with symmetrized trial vectors differs from its CG counterpart. This is related to the fact that in the CG algorithm, optimal coefficients are determined for vectors of the form $\boldsymbol{b} = \begin{pmatrix} \boldsymbol{b}_g \\ \boldsymbol{b}_u \end{pmatrix}$ [see Eq. (6.18)], while in the subspace approach, optimal coefficients are obtained for the individual components $\boldsymbol{b}_g$ and $\boldsymbol{b}_u$ as expressed in Eq. (9.24). However, as can be seen in Table 10.2, this does not change the convergence rate. Comparing the sixth and the seventh columns in Table 10.2 leads to the conclusion that the

convergence rates of the CG and CR algorithms are similar (as discussed in Ref. [148]).

10.2.2 Performance of standard response algorithms in the resonance region

In Fig. 10.2, the convergence of the standard response equation is reported for alanine in the resonance region ($\omega = 0.4$ a.u.). Three different iterative algorithms have been used: (a) the general subspace approach, (b) the subspace algorithm with symmetrized trial vectors and (c) the CR algorithm with symmetrized trial vectors. The CG algorithm has not been used, due to the fact that for $\omega = 0.4$ a.u., the matrix in Eq. (9.23) is not positive definite, which is a requirement for applying the CG algorithm. In fact, in this case also the preconditioner is non-positive definite and preconditioned CR algorithm cannot be safely applied. However, the results obtained using the CR algorithm are reported in Fig. 10.2 for analysis purposes.

When comparing the results presented in Fig. 10.2 and listed in Table 10.2, it is seen that the standard response equation in the higher frequency region converges in a significantly larger number of iterations. Solving the equation is also more problematic when calculations are performed at a frequency in a region with a high density of excited states. This is due to the fact that when the frequency ω is equal to an excitation energy, the standard response equation in Eq. (7.2) becomes singular and diverges, as discussed in Chapter 4.

An improved convergence is obtained when the standard response equation is solved using the algorithm with symmetrized trial vectors, compared to the general subspace approach (see Figs. 10.2a and 10.2b), as discussed in the previous section. The number of iterations is similar for the CR algorithm (Fig. 10.2c) and the subspace approach with symmetrized trial vectors (Fig. 10.2b). One extra iteration is reported for the CR (compared to the subspace) algorithm, however, the disk storage has been significantly truncated to only four vectors during the whole iterative procedure. Although, good performance of the CR algorithm may be seen in Fig. 10.2c, *i.e.*, the residual decreases in each iteration, the CR algorithm cannot be safely applied when a non-positive definite preconditioner is used.

10.3 The damped response equation

In this section, results obtained for solving the damped response equation in Eq. (7.3) are reported. The general performance of various algorithms for solving damped response equations (described in Chapters 7–9) is compared. The calculations of the real and imaginary components of the linear polarizability (associated with dispersion and absorption, respectively), for different systems, are reported.

In all calculation shown in this section, the damped response equations have been solved to a residual norm of 10^{-4}.

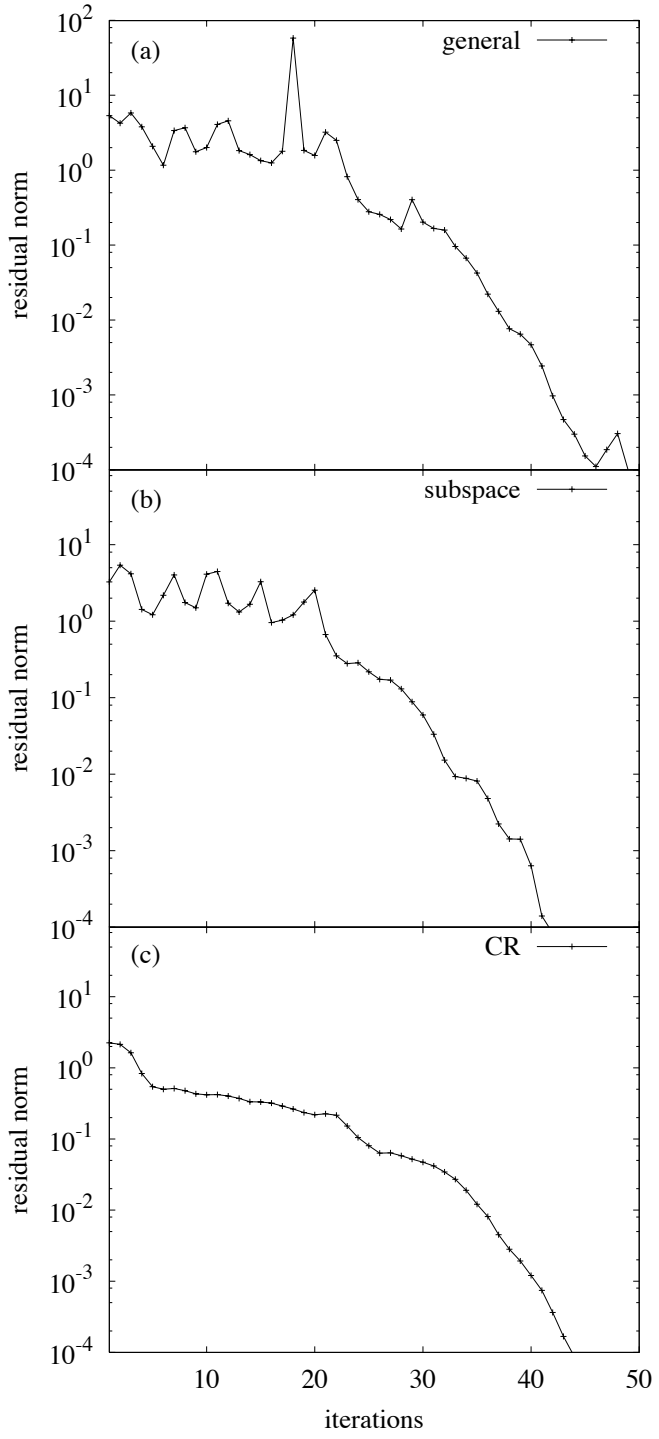

Figure 10.2: Convergence of the standard response equation for alanine in resonance region (ω = 0.4 a.u.), using different approaches: **(a)** the general subspace approach, **(b)** the subspace algorithm with symmetrized trial vectors, **(c)** the CR algorithm with symmetrized trial vectors; HF/6-31G, threshold=10^{-4}.

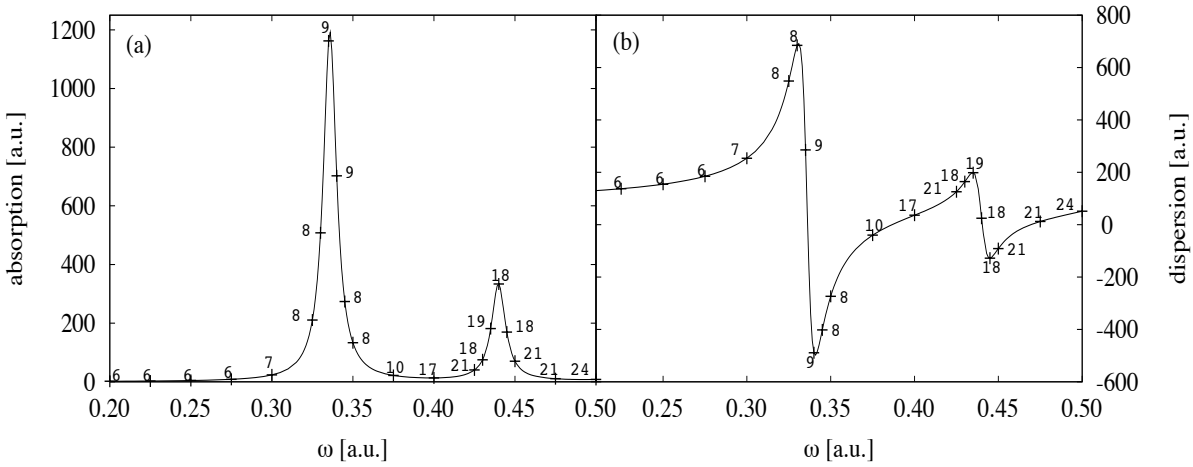

Figure 10.3: The xx component of **(a)** the imaginary part (absorption), **(b)** the real part (dispersion) of the linear polarizability for pCT$^-$, $\gamma = 0.005$ a.u. Above points: number of iterations needed to solve complex response equations for each frequency.

10.3.1 Deprotonated *trans*-thiomethyl-*p*-coumarate

In this section, calculations of the xx component of the linear polarizability, $\bar{\alpha}_{xx}$, for deprotonated *trans*-thiomethyl-*p*-coumarate (pCT$^-$), displayed in Fig. 10.1c, are reported. pCT$^-$ is a model of the protein chromophore of the photo-active yellow protein (PYP). Calculations have been carried out at the HF/6-31G level of theory, using the experimental geometry [164].

In Figs. 10.3a and 10.3b, the imaginary and real components, respectively, of $\bar{\alpha}_{xx}$ are presented, for the excited-state lifetime broadening parameter γ equal to 0.005 a.u.. For the selected frequencies, the number of iterations obtained with the subspace iterative algorithm with symmetrized trial vectors (described in Section 9.4) is reported.

As can be seen in Fig. 10.3, the computational cost of the calculation depends on how close the frequency of interest ω is to resonance, and on the density of excited states in this region. If the frequency of interest is in the far-off-resonance region (in Fig. 10.3, the region below $\omega = 0.3$ a.u.), a rapid convergence is obtained, due to a small coupling between the real and imaginary components of the solution vector. In the resonance region, a large coupling between the real and the imaginary component of the solution vector occurs in particular in a frequency region with a high density of excited states. This has a significant influence on the convergence and increases the computational cost of the calculations. It can be seen in Fig. 10.3 that the computational cost for the calculations in the region above $\omega = 0.4$ a.u. is much higher, compared to the calculations in the lower frequency region (even though, there is a strong excitation around $\omega = 0.33$ a.u.). This behavior is related to a high density of

excited states in higher frequency regions.

In Table 10.3, the total number of Fock matrices constructed when solving the damped response equation in the $\bar{\alpha}_{xx}$ calculation for pCT^- is reported for selected frequencies. Six different approaches have been used: (i) the approach by Norman *et al.* [29], (ii) the one-subspace approach, (described in Section 8.4.1), (iii)-(v) the two-level-subspace approaches (described in Section 8.4.2), where in each macro-iteration sets of trial vectors from micro-iterations are not stored, where they are stored, and the preconditioned two-level-subspace approach (described in Section 8.4.3), where the trial vectors from all micro-iterations are stored and (vi) the subspace algorithm with symmetrized trial vectors (described in Section 9.4). The total number of Fock matrices (linear transformations $\boldsymbol{E}^{[2]}\boldsymbol{b}$) is reported, since this is the computationally most demanding part of an iteration in the iterative algorithm, and therefore determines a cost of a calculation, as discussed in Section 7.3. The results presented in Table 10.3 differ from the ones reported in Paper A [33]. This is due to the fact that at the time the calculations presented of Table III in Ref. [33] had been performed, in each iteration of the one-subspace approach and in each macro-iteration in the two-level-subspace approach, two linear transformations (for the real and the imaginary component of the trial vector) were carried out sequentially. However, in an improved implementation, linear transformations are carried simultaneously, and the cost is independent of the number of trial vectors. Performance in the micro-subspace level has not changed and in each micro-iteration in the two-level-subspace approach, one linear transformation is carried out.

From Table 10.3 it can be seen that the computational cost of the calculations performed using the approaches presented in Section 8.4 (third–sixth column), is less than half of what has been obtained using the approach presented by Norman *et al.* [29](second column).[15] Application of the one-subspace approach (third column), if it converges, decreases the cost of calculations up to 4 times, compared to the cases where the two-level-subspace approach without preconditioning (fourth column) or the approach of Norman *et al.* have been used. This advantage is related to the fact that none of these algorithms exploits the small coupling in the far-off-resonance region. It can be also seen in Table 10.3 that using the two-level-subspace approach where sets of trial vectors from micro-iterations obtained in each macro-iteration are stored and used as start guesses in the next macro-iterations (fifth column),

[15]However, it should be mentioned that in the algorithm by Norman *et al.* [29], Eq. (7.3) can be solved for several frequencies simultaneously, which is not (yet!) available for the algorithms presented in this thesis. Since the calculations reported in Table 10.3 have been performed for only one frequency, this advantage of the algorithm by Norman *et al.* could not be exploited.

Table 10.3: Number of Fock matrices constructed (for selected frequencies) when determining the xx component of the linear polarizability of pCT^- molecule using: (i) the approach by Norman *et al.* (**second column**), (ii) the one-subspace approach, (**third column**), (iii-v) the two-level-subspace approaches, where in each macro-iteration sets of trial vectors from micro-iterations are not stored (**fourth column**), where they are stored (**fifth column**), the preconditioned two-level-subspace approach, where the trial vectors from all micro-iterations are stored (**sixth column**) and (vi) the subspace algorithm with symmetrized trial vectors (**seventh column**); $\gamma = 0.005$ a.u., threshold=10^{-4}.

ω [a.u.]	approach by Norman *et al.* [29]	One subspace approach	Two-level subspace approach			alg. with symmetrized trial vect.
			no storing	storing	precond.	
0.000	31	4	11	11	11	4
0.100	31	7	18	18	18	6
0.200	51	7	19	19	19	6
0.225	52	7	19	19	19	6
0.250	65	7	21	21	21	6
0.275	71	8	21	21	21	6
0.300	91	8	33	33	33	7
0.325	100	10	47	41	24	8
0.330	101	-	56	42	25	8
0.335	117	-	82	49	38	9
0.340	119	-	60	45	25	9
0.345	119	14	58	41	25	8
0.350	120	9	58	40	24	8
0.375	138	9	58	46	32	10
0.400	147	-	101	55	41	17
0.425	185	-	147	70	54	21
0.430	192	16	96	64	61	18
0.435	195	-	135	74	67	19
0.440	191	-	195	80	66	18
0.445	190	-	155	72	61	18
0.450	197	19	80	60	58	21
0.475	234	-	221	88	78	21
0.500	245	-	280	118	81	24

is computationally less expensive, compared to the approach where vectors are not stored (fourth column) [see also Fig. 8.2]. No difference is noted in the far-off-resonance region, due to the fact that convergence is obtained in one macro-iteration and the cost of the first macro-iteration is identical in both approaches (see the left panel in Fig. 8.2). In the region with a high density of excited states (above $\omega = 0.4$ a.u.), the results using the two-level-subspace approach without storing vectors have been obtained in twice as many iterations as for the approach where vectors are stored. By comparing the fifth and the sixth column in Table 10.3, it can be seen that introducing preconditioning in the macro-subspace level[16] has significantly improved convergence.

It should be noted that even though the one-subspace approach yields a significantly better convergence compared to the other approaches, it may only be applied in a far-off-resonance frequency region. For this reason, it cannot be used in practice for large molecular systems, which are characterized by high density of excited states in the entire frequency range. It should also be noted that even though a significant improvement is reported for calculations performed using the preconditioned two-level-subspace approach where all trial vectors have been stored, this algorithm may not be applied for very large molecular systems, due to the tremendous storage requirements of the current implementation.

Comparing the number of Fock matrices constructed during the calculations using the preconditioned two-level-subspace approach (sixth column) and the algorithm with symmetrized trial vectors (seventh column), an astonishing improvement is observed. When the algorithm with symmetrized trial vectors is used in the region of a single strong excitation (around $\omega = 0.33$ a.u.), only 2–3 iterations more are required to converge Eq. (7.3), compared to the off-resonance region. In the region with a high density of excited states (above $\omega = 0.4$ a.u.), the number of iterations increases, however not drastically, as when the preconditioned two-level-subspace approach was used. It can be seen that the computational cost of the calculations carried out using the algorithm with symmetrized trial vectors is, in the higher frequency region, about half of what has been reported for the preconditioned two-level-subspace approach. This is due to a very efficient way of obtaining new trial vectors in the algorithm with the symmetrized trial vectors, using the preconditioner in Eq. (9.31) that includes all the coupling between solution vector components. It should also be noted that in the preconditioned two-level-subspace approach, all the trial vectors are stored on disk, which makes it inefficient for treating large molecular systems, whereas for the approach with symmetrized trial vectors, storage is reduced.

[16] In the micro-subspace level, preconditioning is introduced in all approaches.

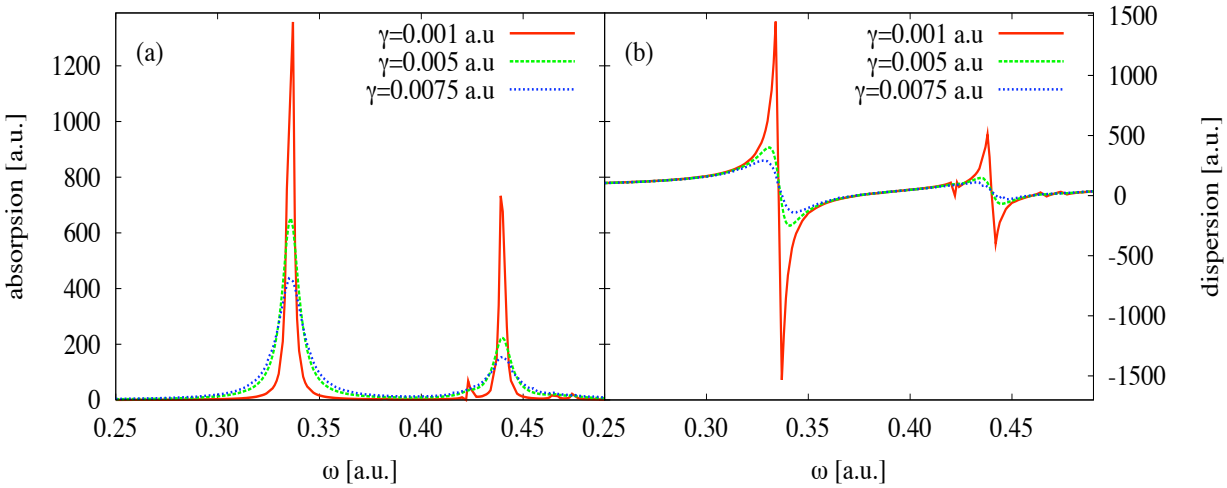

Figure 10.4: Comparison of the yy component of **(a)** absorption and **(b)** dispersion curves for pCT^- for different values of the excited-state lifetime broadening parameter γ.

In Figure 10.4, an investigation of absorption and dispersion spectra has been performed for different values of the excited-state lifetime broadening parameter γ. It can be seen that higher values of γ lead to broader peaks. For very small γ, the absorption spectra is similar to the stick spectrum obtained from the residues of the response functions in standard response theory.

10.3.2 Deprotonated *trans-p*-coumaric acid

In this section, calculations of the imaginary component of the linear polarizability for deprotonated *trans-p*-coumaric acid (pCA^-), displayed in Fig. 10.1c, are reported. Calculations have been carried out using the geometry in Ref. [165] at the CAM-B3LYP/cc-pVDZ [139] level of theory. The reported absorption spectrum contains isotropically averaged values.

In Fig. 10.5, the absorption spectrum calculated using damped response theory (b) is compared with the results determined using the standard response theory (a) and with the experimental findings measured by Nielsen *et al.* [166] (c). The Lorentzian line-shape function (Fig. 4.1a) has been fitted to the experimental data (dots) in Fig. 10.5c to obtain the excited-state lifetime broadening parameter γ. Using this parameter, the calculations of the absorption spectra have been performed using standard and damped response theory. Results presented in Fig. 10.5a are obtained by superimposing a Lorentzian line-shape function with $\gamma = 0.00263$ a.u. (determined from Fig. 10.5c) onto the stick spectrum, obtained from the residues of the linear response function in standard response theory. It is, as expected,

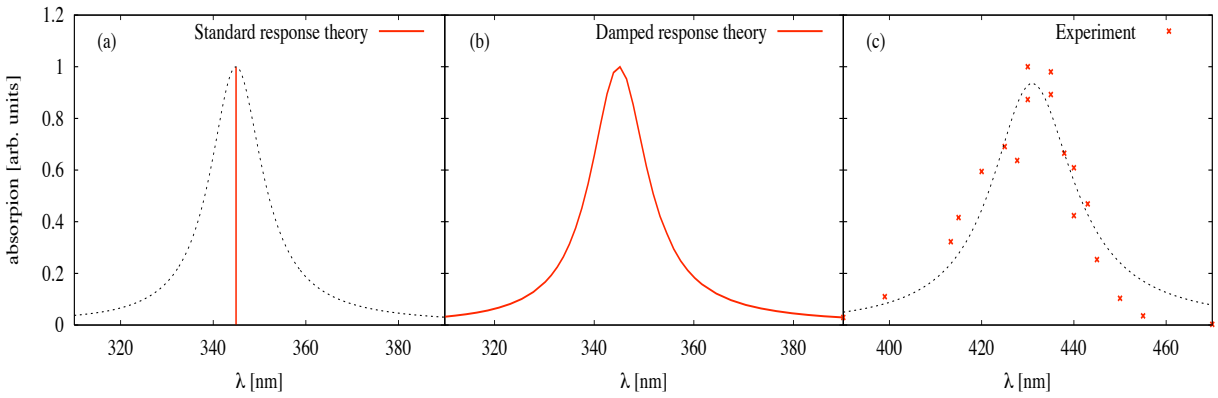

Figure 10.5: Absorption curves for pCA^-, **(a)** stick spectrum with superimposed Lorentzian line-shape function,$\gamma = 0.00263$ a.u., **(b)** results obtained using the approach described in Chapter 8.4, $\gamma = 0.00263$ a.u., **(c)** experimental data (dots) [166] with fitted Lorentzian line-shape function.

identical to the spectrum calculated using the damped response theory, shown in Fig. 10.5b. The absorption peak is shifted to higher frequencies compared to the experiment, but it is known that the excitation energies obtained using DFT methods may be shifted.

In Fig. 10.6, the convergence of the damped response equation for pCA^- is reported for $\gamma = 0.005$ a.u.. The residual norms are plotted for each iteration, determined with: (i) the CR algorithm with general trial vectors (discussed in Sections 6.3 and 7.4), (ii) the CR algorithm with symmetrized trial vectors (discussed in Sections 6.3 and 9.4) and (iii) the subspace algorithm with symmetrized trial vectors (discussed in Section 9.4). It should be noted that, in principle, the CR algorithm should not have been used, since the preconditioner is non-positive definite, as discussed in Section 6.3.2, and results obtained using the CR algorithms are reported only for analysis purposes. The convergence is presented in the off-resonance region ($\omega = 0.08$ a.u.) and close to an excitation energy $\omega_1 = 0.1321$ a.u. ($\omega = 0.13$ a.u.). From Fig. 10.6, it can be seen that an improvement in convergence is obtained when the algorithms with symmetrized trial vectors (middle and bottom panels) are used for solving the damped response equation, compared to the approach with general trial vectors (top panel). The performance in the off-resonance region (left panel) is similar to what is obtained for the standard response equation (see Table 10.2 and Fig. 10.2). In the resonance region (right panel), a significant improvement is observed. The CR algorithms cannot be applied safely and this is reflected in the rather erratic convergence displayed in the top and middle panel, while the residual should decrease in each iteration. The monotonic convergence would be observed if a positive definite preconditioner had been used.

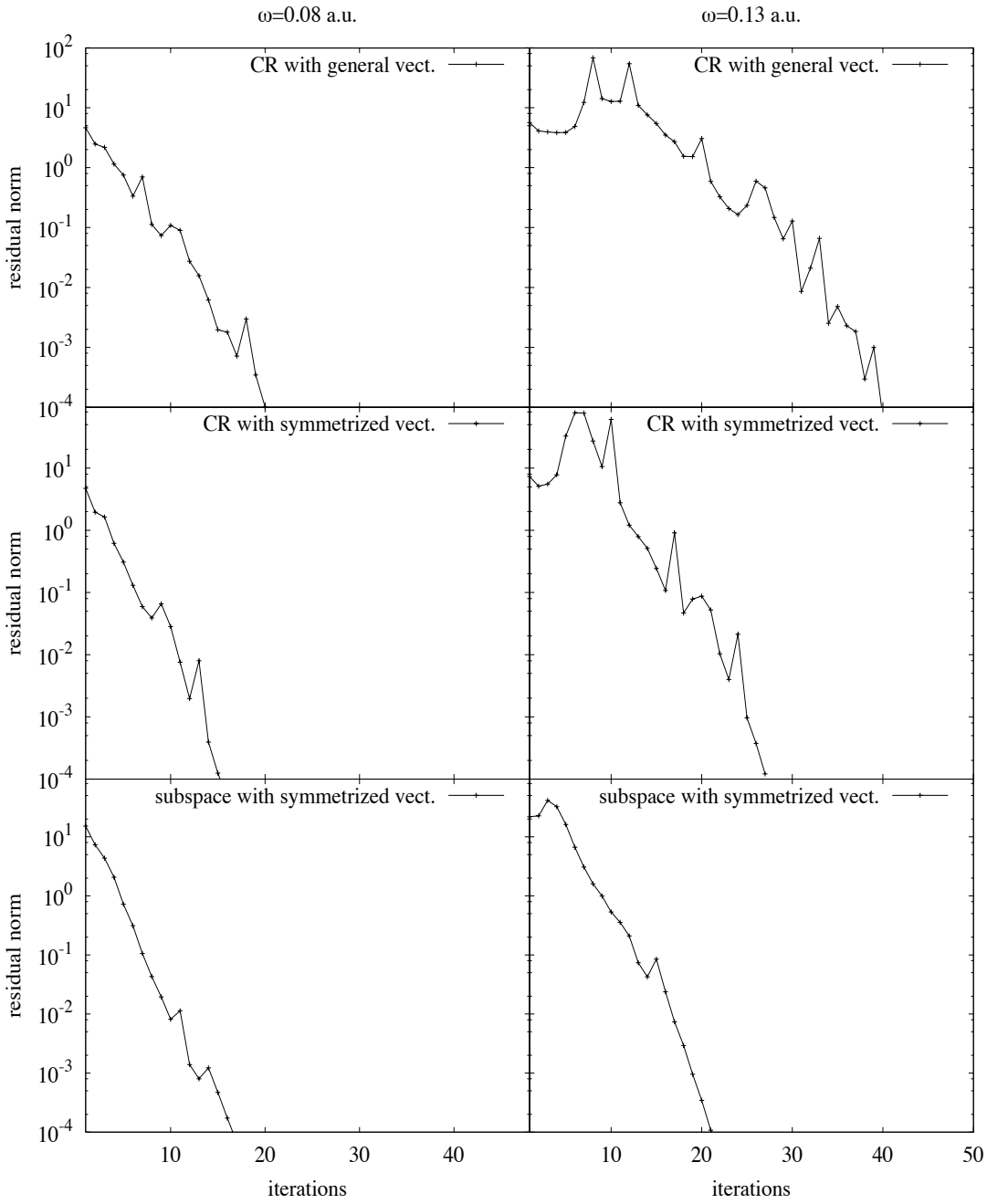

Figure 10.6: Convergence of the response equation for pCA^-, CAM-B3LYP/cc-pVDZ for different values of ω, γ=0.005 a.u., **Top panel:** the CR algorithm with general vectors, **Middle panel:** CR algorithm with symmetrized trial vectors, **Bottom panel:** the subspace algorithm with symmetrized trial vectors.

10.3.3 Convergence dependence on frequency and damping parameters

In this section, an analysis of frequency and damping parameter dependence is presented. The damped response equations have been solved for Ala-Trp, using the subspace iterative approach with symmetrized trial vectors, at the CAM-B3LYP/6-31G level of theory.

In Fig. 10.7, convergence of the damped response equation is reported at different frequencies, $\omega = 0.1$ a.u. and $\omega = 0.3$ a.u., and for different values of damping parameters γ, equal to 0.0, 0.005 and 0.01 a.u.. From Fig. 10.7, it can be concluded that the convergence is independent of the damping parameter γ, when the algorithm with symmetrized trial vectors is used. This is due to the fact that an efficient preconditioner in Eq. (9.31) has been used to obtain new trial vectors. By comparing the top and the bottom panel in Fig. 10.7, it can be seen that convergence of the damped response equation is obtained in significantly larger number of iterations for the higher frequency. This is related to the fact that in the higher frequency region with a high density of excited states, the contribution to the large eigenvalues is not removed by preconditioning.

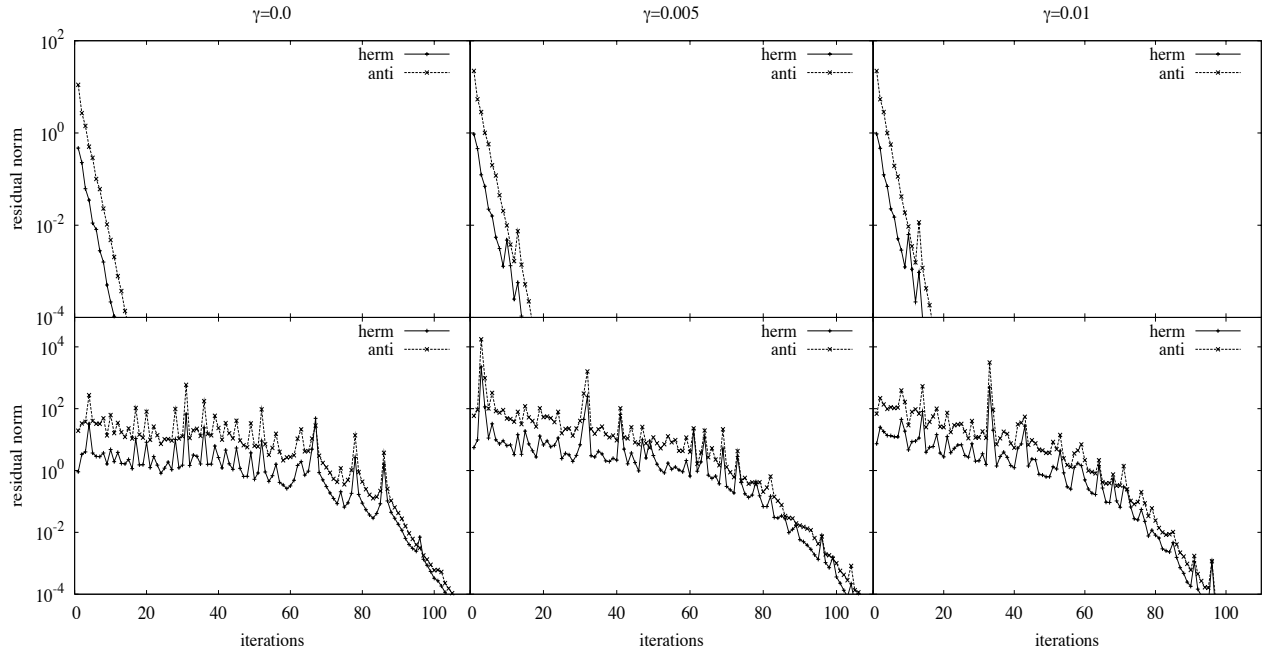

Figure 10.7: Convergence of the response equation for Ala-Trp, CAM-B3LYP/6-31G, for different values of γ and ω. **Upper panel:** $\omega = 0.1$ a.u., **Lower panel:** $\omega = 0.3$ a.u..

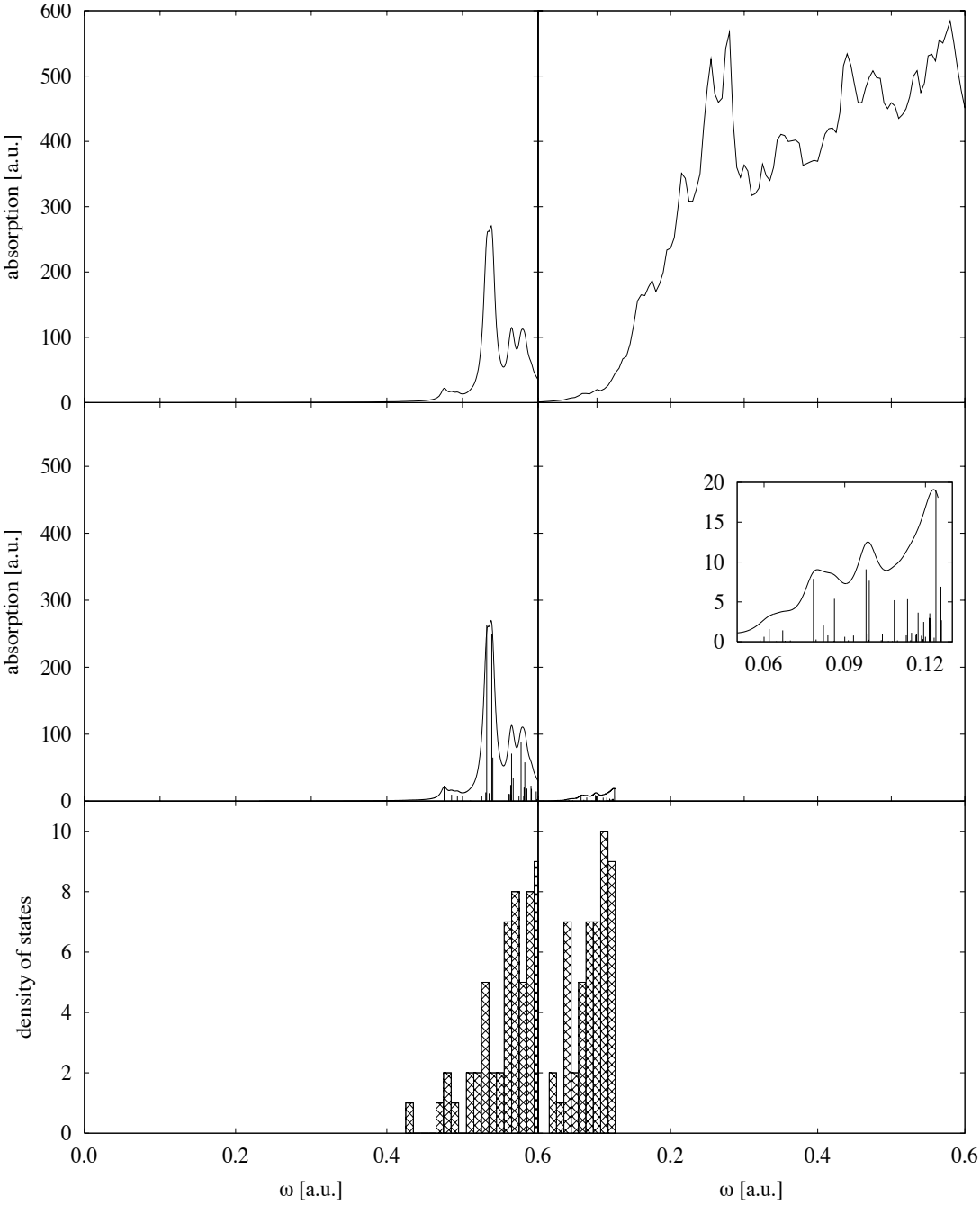

Figure 10.8: The xx component of the imaginary part of the linear polarizability for a DNA fragment consisting of one (left panel) and two (right panel) nucleotides, $\gamma = 0.005$ a.u.; **Top panel:** Absorption spectra obtained using damped response theory; **Middle panel:** first 50 excitation energies stick spectrum with superimposed Lorentzian line-shape function; **Bottom panel:** density of the first 50 excited states.

10.3.4 DNA fragments containing one and two nucleotides

In Fig. 10.8, calculations of the xx imaginary component of the linear polarizability for a DNA fragment consisting of one and two nucleotides are presented (see Figs. 10.1e and 10.1f, respectively). The calculations have been carried out using a geometry obtained with the Maestro program [162] at the HF/6-31G level of theory. The excited-state lifetime broadening parameter γ is equal 0.005 a.u.. In the top panels in Fig. 10.8, the xx component of the absorption spectra obtained from damped response theory are shown. In the middle panels, the stick spectra containing the first 50 excitations are presented (obtained from the residues of the linear response function in standard response theory) with an imposed Lorentzian line-shape function. In the bottom panels, the density of the first 50 excited states is reported. It can be seen that the density of the excited states increases drastically in higher frequencies regions and with the size of the system. As can be seen from the middle panels in Fig. 10.8, the first 50 excitation energies can give quite a good approximation for the absorption spectrum of one nucleotide, whereas for a DNA fragment consisting of two nucleotides, the first 50 excitations only include very low lying states and cannot be used for obtaining the absorption spectrum in the higher frequency region. It is expected that DNA fragments consisting of more nucleotides have even more low lying excited states and it may be impossible to obtain the spectrum in higher density regions using standard response theory. However, damped response theory can be successfully applied for obtaining absorption spectra for large systems in higher frequency regions. Furthermore, since any frequency interval of interest may be chosen, a high density of low lying states does not cause any problems when the damped response theory is applied.

11 Conclusion

Molecular properties are obtained by solving response equations. The response equations in Hartree–Fock, multi-configurational self-consistent field, and Kohn–Sham density functional theory have identical structures. Different algorithms for solving eigenvalue, standard and damped response equations have been presented and compared. New efficient algorithms have been introduced based on the splitting of trial vectors into symmetric and antisymmetric components.

A phenomenological formulation of damped response theory based on the quasi-energy formalism has been presented. Application of damped response theory, as has been shown, leads to physically correct dispersion and absorption spectra, which may be obtained from the real and the imaginary components of damped response functions, respectively. Damped response theory has also been successfully applied to higher-order properties, such as magnetic circular dichroism and two-photon absorption. Qualitatively correct spectra have been obtained for these properties.

In standard response theory, absorption processes are determined from residues of response functions. Absorption spectra are constructed by imposing a line-shape function onto a stick spectrum. However, for large molecular systems it may be impossible to obtain a stick spectrum for higher frequencies, when a vast amount of low lying excitations is present. In contrast, damped response theory may be applied for any frequency of interest and therefore spectra may be compassed in the entire frequency range.

Several algorithms for solving damped response equations have been introduced. They have been implemented as an extension to the linear-scaling response equation solver presented by Coriani *et al.* in Ref. [23]. Introducing symmetrized trial vectors in the response equations, effects in transformation to a form in which they may be solved conveniently due to the fact that very efficient preconditioners may be used. An attempt has been made to apply the conjugate gradient and conjugate residual algorithms to response equations.

It can be concluded that the most efficient algorithm for solving the standard and damped response equation is the iterative subspace algorithm with symmetrized trial vectors. For the standard response equation at low frequencies ω, the preconditioned CG/CR algorithms may be used, thereby avoiding the storing and handling of a large set of trial vectors to set up the reduced space equations. However, these algorithms may only be applied for the angular frequency lower than the first excitation energy (only then the matrix in the standard response equation is positive definite), and therefore, in practice, they cannot be used for large molecular systems, characterized by a high density of low lying excited states.

For solving the response eigenvalue equations, it is equally efficient to use algorithms with paired as with symmetrized trial vectors and no improvement is obtained by using the Olsen algorithm.

In conclusion, damped response theory together with a linear-scaling framework is an excellent tool for a qualitatively correct description of absorption processes and may be used for determining spectra for large molecular systems.

A The Conjugate gradient algorithm with pairing

The paired trial vectors will now be introduced in the CG algorithm presented in Section 6.2.

When Eq. (6.1) is solved using the CG algorithm with paired trial vectors after n iterations, $2n$ solution vectors $\mathbf{x}^{2n}$, $2n$ residuals $\mathbf{r}^n$ and $2n-2$ directions $\mathbf{p}^{2n-2}$ given as

$$\mathbf{x}^{2n} = \{\mathbf{x}_1, \mathbf{x}_1^P, \mathbf{x}_2, \mathbf{x}_2^P, ..., \mathbf{x}_n, \mathbf{x}_n^P\}\,, \tag{A.1}$$

$$\mathbf{r}^{2n} = \{\mathbf{r}_1, \mathbf{r}_1^P, \mathbf{r}_2, \mathbf{r}_2^P, ..., \mathbf{r}_n, \mathbf{r}_n^P\}\,, \tag{A.2}$$

$$\mathbf{p}^{2n-2} = \{\mathbf{p}_1, \mathbf{p}_1^P, \mathbf{p}_2, \mathbf{p}_2^P ..., \mathbf{p}_{n-1}, \mathbf{p}_{n-1}^P\}\,, \tag{A.3}$$

respectively, are known. The paired vectors are defined as in Eqs. (8.2) and (8.3). It may be shown that the previous direction and residuals fulfill the relations

$$\mathbf{r}_i^T\mathbf{p}_j = 0, \quad \mathbf{r}_i^{P,T}\mathbf{p}_j = 0, \qquad i,j = 1,2,\ldots,n, \quad i > j, \tag{A.4a}$$

$$\mathbf{r}_i^T\mathbf{r}_j = 0, \quad \mathbf{r}_i^{P,T}\mathbf{r}_j = 0, \qquad i,j = 1,2\ldots,n, \quad i > j, \tag{A.4b}$$

$$\mathbf{r}_i^T\mathbf{A}\mathbf{p}_j = 0, \qquad i,j = 1,2,\ldots,n, \quad i > j+1, \tag{A.4c}$$

$$\mathbf{p}_i^T\mathbf{A}\mathbf{p}_j = \mathbf{p}_i^T\mathbf{A}\mathbf{p}_j\delta_{ij}, \qquad i,j = 1,2,\ldots,n-1, \tag{A.4d}$$

$$\mathbf{p}_i^{P,T}\mathbf{A}\mathbf{p}_j = \mathbf{p}_i^{P,T}\mathbf{A}\mathbf{p}_j\delta_{ij}, \qquad i,j = 1,2,\ldots,n-1, \tag{A.4e}$$

$$\mathbf{p}_i^T\mathbf{A}\mathbf{r}_j^P = \mathbf{p}_i^T\mathbf{A}\mathbf{r}_j^P\delta_{ij}, \qquad i,j = 1,2,\ldots,n-1\,. \tag{A.4f}$$

The new trial vector can be written as a general vector in the space spanned by the previous search directions $\mathbf{p}^n$ and their paired counterparts $\mathbf{p}^{n,P}$, the current residual $\mathbf{r}_n$ and its paired vector $\mathbf{r}_n^P$

$$\mathbf{x}_{n+1} = \mathbf{x}_n + \sum_{i=1}^{n-1}(\alpha_i^{(n)}\mathbf{p}_i + \alpha_i^{(n),P}\mathbf{p}_i^P) + \alpha_n^{(n)}\mathbf{r}_n + \alpha_n^{(n),P}\mathbf{r}_n^P\,. \tag{A.5}$$

Minimizing $g(\mathbf{x}_{n+1})$ with respect to $2n$ free parameters leads to the subspace equation

$$\begin{pmatrix}
\mathbf{p}_1^T\mathbf{A}\mathbf{p}_1 & \mathbf{p}_1^T\mathbf{A}\mathbf{p}_1^P & \cdots & \mathbf{p}_1^T\mathbf{A}\mathbf{p}_{n-1} & \mathbf{p}_1^T\mathbf{A}\mathbf{p}_{n-1}^P & \mathbf{p}_1^T\mathbf{A}\mathbf{r}_n & \mathbf{p}_1^T\mathbf{A}\mathbf{r}_n^P \\
\mathbf{p}_1^{P,T}\mathbf{A}\mathbf{p}_1 & \mathbf{p}_1^{P,T}\mathbf{A}\mathbf{p}_1^P & \cdots & \mathbf{p}_1^{P,T}\mathbf{A}\mathbf{p}_{n-1} & \mathbf{p}_1^{P,T}\mathbf{A}\mathbf{p}_{n-1}^P & \mathbf{p}_1^{P,T}\mathbf{A}\mathbf{r}_n & \mathbf{p}_1^{P,T}\mathbf{A}\mathbf{r}_n^P \\
\cdots & \cdots & \cdots & \cdots & \cdots & \cdots & \cdots \\
\mathbf{p}_{n-1}^T\mathbf{A}\mathbf{p}_1 & \mathbf{p}_{n-1}^T\mathbf{A}\mathbf{p}_1^P & \cdots & \mathbf{p}_{n-1}^T\mathbf{A}\mathbf{p}_{n-1} & \mathbf{p}_{n-1}^T\mathbf{A}\mathbf{p}_{n-1}^P & \mathbf{p}_{n-1}^T\mathbf{A}\mathbf{r}_n & \mathbf{p}_{n-1}^T\mathbf{A}\mathbf{r}_n^P \\
\mathbf{p}_{n-1}^{P,T}\mathbf{A}\mathbf{p}_1 & \mathbf{p}_{n-1}^{P,T}\mathbf{A}\mathbf{p}_1^P & \cdots & \mathbf{p}_{n-1}^{P,T}\mathbf{A}\mathbf{p}_{n-1} & \mathbf{p}_{n-1}^{P,T}\mathbf{A}\mathbf{p}_{n-1}^P & \mathbf{p}_{n-1}^{P,T}\mathbf{A}\mathbf{r}_n & \mathbf{p}_{n-1}^{P,T}\mathbf{A}\mathbf{r}_n^P \\
\mathbf{r}_n^T\mathbf{A}\mathbf{p}_1 & \mathbf{r}_n^T\mathbf{A}\mathbf{p}_1^P & \cdots & \mathbf{r}_n^T\mathbf{A}\mathbf{p}_{n-1} & \mathbf{r}_n^T\mathbf{A}\mathbf{p}_{n-1}^P & \mathbf{r}_n^T\mathbf{A}\mathbf{r}_n & \mathbf{r}_n^T\mathbf{A}\mathbf{r}_n^P \\
\mathbf{r}_n^{P,T}\mathbf{A}\mathbf{p}_1 & \mathbf{r}_n^{P,T}\mathbf{A}\mathbf{p}_1^P & \cdots & \mathbf{r}_n^{P,T}\mathbf{A}\mathbf{p}_{n-1} & \mathbf{r}_n^{P,T}\mathbf{A}\mathbf{p}_{n-1}^P & \mathbf{r}_n^{P,T}\mathbf{A}\mathbf{r}_n & \mathbf{r}_n^{P,T}\mathbf{A}\mathbf{r}_n^P
\end{pmatrix}
\begin{pmatrix}
\alpha_1^{(n)} \\ \alpha_1^{(n),P} \\ \vdots \\ \alpha_{n-1}^{(n)} \\ \alpha_{n-1}^{(n),P} \\ \alpha_n^{(n)} \\ \alpha_n^{(n),P}
\end{pmatrix}
=
\begin{pmatrix}
\mathbf{p}_1^T\mathbf{r}_n \\ \mathbf{p}_1^{P,T}\mathbf{r}_n \\ \vdots \\ \mathbf{p}_{n-1}^T\mathbf{r}_n \\ \mathbf{p}_{n-1}^{P,T}\mathbf{r}_n \\ \mathbf{r}_n^T\mathbf{r}_n \\ \mathbf{r}_n^{P,T}\mathbf{r}_n
\end{pmatrix}, \tag{A.6}$$

that is equivalent to

$$\mathbf{A}_{red}\boldsymbol{\alpha}_{red} = \mathbf{b}_{red} \tag{A.7}$$

where

$$\mathbf{A}_{red} = \begin{pmatrix} \mathbf{p}_1^T\mathbf{A}\mathbf{p}_1 & \mathbf{p}_1^T\mathbf{A}\mathbf{p}_1^P & 0 & \mathbf{p}_1^T\mathbf{A}\mathbf{p}_2^P & \cdots & 0 & \mathbf{p}_1^T\mathbf{A}\mathbf{p}_{n-1}^P & 0 & 0 \\ \mathbf{p}_1^{P,T}\mathbf{A}\mathbf{p}_1 & \mathbf{p}_1^{P,T}\mathbf{A}\mathbf{p}_1^P & 0 & \mathbf{p}_1^{P,T}\mathbf{A}\mathbf{p}_2^P & \cdots & 0 & \mathbf{p}_1^{P,T}\mathbf{A}\mathbf{p}_{n-1}^P & \mathbf{p}_1^{P,T}\mathbf{A}\mathbf{r}_n & \mathbf{p}_1^{P,T}\mathbf{A}\mathbf{r}_n^P \\ 0 & 0 & \mathbf{p}_2^T\mathbf{A}\mathbf{p}_2 & \mathbf{p}_2^T\mathbf{A}\mathbf{p}_2^P & \cdots & 0 & \mathbf{p}_2^T\mathbf{A}\mathbf{p}_{n-1}^P & 0 & 0 \\ \mathbf{p}_2^{P,T}\mathbf{A}\mathbf{p}_1 & \mathbf{p}_2^{P,T}\mathbf{A}\mathbf{p}_1^P & \mathbf{p}_2^{P,T}\mathbf{A}\mathbf{p}_2 & \mathbf{p}_2^{P,T}\mathbf{A}\mathbf{p}_2^P & \cdots & 0 & \mathbf{p}_2^{P,T}\mathbf{A}\mathbf{p}_{n-1}^P & \mathbf{p}_2^{P,T}\mathbf{A}\mathbf{r}_n & \mathbf{p}_2^{P,T}\mathbf{A}\mathbf{r}_n^P \\ \cdots & \cdots & \cdots & \cdots & \cdots & \cdots & \cdots & \cdots & \cdots \\ 0 & 0 & 0 & 0 & \cdots & \mathbf{p}_{n-1}^T\mathbf{A}\mathbf{p}_{n-1} & \mathbf{p}_{n-1}^T\mathbf{A}\mathbf{p}_{n-1}^P & \mathbf{p}_{n-1}^T\mathbf{A}\mathbf{r}_n & \mathbf{p}_{n-1}^T\mathbf{A}\mathbf{r}_n^P \\ \mathbf{p}_{n-1}^{P,T}\mathbf{A}\mathbf{p}_1 & \mathbf{p}_{n-1}^{P,T}\mathbf{A}\mathbf{p}_1^P & \mathbf{p}_{n-1}^{P,T}\mathbf{A}\mathbf{p}_2 & \mathbf{p}_{n-1}^{P,T}\mathbf{A}\mathbf{p}_2^P & \cdots & \mathbf{p}_{n-1}^{P,T}\mathbf{A}\mathbf{p}_{n-1} & \mathbf{p}_{n-1}^{P,T}\mathbf{A}\mathbf{p}_{n-1}^P & \mathbf{p}_{n-1}^{P,T}\mathbf{A}\mathbf{r}_n & \mathbf{p}_{n-1}^{P,T}\mathbf{A}\mathbf{r}_n^P \\ 0 & \mathbf{r}_n^T\mathbf{A}\mathbf{p}_1^P & 0 & \mathbf{r}_n^T\mathbf{A}\mathbf{p}_2^P & \cdots & \mathbf{r}_n^T\mathbf{A}\mathbf{p}_{n-1} & \mathbf{r}_n^T\mathbf{A}\mathbf{p}_{n-1}^P & \mathbf{r}_n^T\mathbf{A}\mathbf{r}_n & \mathbf{r}_n^T\mathbf{A}\mathbf{r}_n^P \\ 0 & \mathbf{r}_n^{P,T}\mathbf{A}\mathbf{p}_1^P & 0 & \mathbf{r}_n^{P,T}\mathbf{A}\mathbf{p}_2^P & \cdots & \mathbf{r}_n^{P,T}\mathbf{A}\mathbf{p}_{n-1} & \mathbf{r}_n^{P,T}\mathbf{A}\mathbf{p}_{n-1}^P & \mathbf{r}_n^{P,T}\mathbf{A}\mathbf{r}_n & \mathbf{r}_n^{P,T}\mathbf{A}\mathbf{r}_n^P \end{pmatrix}, \tag{A.8}$$

and $\boldsymbol{\alpha}_{red}$ and $\mathbf{b}_{red}$ are given as

$$\boldsymbol{\alpha}_{red} = \begin{pmatrix} \alpha_1^{(n)} \\ \alpha_1^{(n),P} \\ \alpha_2^{(n)} \\ \alpha_2^{(n),P} \\ \vdots \\ \alpha_{n-1}^{(n)} \\ \alpha_{n-1}^{(n),P} \\ \alpha_n^{(n)} \\ \alpha_n^{(n),P} \end{pmatrix}, \quad \mathbf{b}_{red} = \begin{pmatrix} 0 \\ 0 \\ 0 \\ 0 \\ \vdots \\ 0 \\ 0 \\ \mathbf{r}_n^T\mathbf{r}_n \\ \mathbf{r}_n^{P,T}\mathbf{r}_n \end{pmatrix}. \tag{A.9}$$

It can be seen from Eq. (A.8) that not only the last three, but all trial vectors in the reduced space are necessary to obtain the optimal solution vector in iteration $n+1$ and the subspace equation in Eq. (A.7) needs to be solved. The CG algorithm does not benefit from using pairing property due to the fact that not all relations similar to Eqs. (6.12a)–(6.12c) can be obtained for the elements containing the paired counterparts. It is due to the fact that the linear transformation $\mathbf{A}\mathbf{x}^P$ is not equal to $(\mathbf{A}\mathbf{x})^P$, therefore only some elements in the matrix in Eq. (A.8) are equal to zero. In consequence, when trial vectors are added in pairs to the reduced subspace in the CG iterative algorithm, all the vectors need to be stored on disk.

Solving the standard response equations using the CR algorithm also does not benefit from using pairing property. It is due to the same reasons, as shown above for the CG algorithm.

B Solving response equations using the Casida approach

A different approach for solving the standard response equations has been presented by Casida [86]. In this approach the standard response equation in the two component form

$$\left[\begin{pmatrix} \boldsymbol{A} & \boldsymbol{B} \\ \boldsymbol{B} & \boldsymbol{A} \end{pmatrix} - \omega \begin{pmatrix} \boldsymbol{\Sigma} & \mathbf{0} \\ \mathbf{0} & -\boldsymbol{\Sigma} \end{pmatrix}\right] \begin{pmatrix} \boldsymbol{X} \\ \boldsymbol{Y} \end{pmatrix} = \begin{pmatrix} \boldsymbol{G}_1 \\ \boldsymbol{G}_2 \end{pmatrix}, \tag{B.1}$$

using the unitary transformation $\boldsymbol{U}$ in Eq. (3.60), is expressed as

$$\left[\begin{pmatrix} \boldsymbol{A}+\boldsymbol{B} & \mathbf{0} \\ \mathbf{0} & \boldsymbol{A}-\boldsymbol{B} \end{pmatrix} - \omega \begin{pmatrix} \mathbf{0} & -\boldsymbol{\Sigma} \\ -\boldsymbol{\Sigma} & \mathbf{0} \end{pmatrix}\right] \begin{pmatrix} \boldsymbol{X}' \\ -\boldsymbol{Y}' \end{pmatrix} = \begin{pmatrix} \boldsymbol{G}'_1 \\ -\boldsymbol{G}'_2 \end{pmatrix}, \tag{B.2}$$

where

$$\boldsymbol{X}' = \boldsymbol{X} + \boldsymbol{Y}; \quad \boldsymbol{Y}' = \boldsymbol{X} - \boldsymbol{Y}; \quad \boldsymbol{G}'_1 = \boldsymbol{G}_1 + \boldsymbol{G}_2; \quad \boldsymbol{G}'_2 = \boldsymbol{G}_1 - \boldsymbol{G}_2\,. \tag{B.3}$$

(for details, see Ref. [86]). From Eq. (B.2) two separate equations are obtained

$$[(\boldsymbol{A}+\boldsymbol{B}) - \omega^2\boldsymbol{\Sigma}(\boldsymbol{A}-\boldsymbol{B})^{-1}\boldsymbol{\Sigma}]\boldsymbol{X}' = \boldsymbol{G}'_1 + \omega\boldsymbol{\Sigma}(\boldsymbol{A}-\boldsymbol{B})^{-1}\boldsymbol{G}'_2\,, \tag{B.4}$$

and

$$[(\boldsymbol{A}-\boldsymbol{B}) - \omega^2\boldsymbol{\Sigma}(\boldsymbol{A}+\boldsymbol{B})^{-1}\boldsymbol{\Sigma}]\boldsymbol{Y}' = \boldsymbol{G}'_2 - \omega\boldsymbol{\Sigma}(\boldsymbol{A}+\boldsymbol{B})^{-1}\boldsymbol{G}'_1\,. \tag{B.5}$$

The solution to the standard response equation is thus in this approach replaced by solving two sets of linear equations of half the dimension of $\boldsymbol{E}^{[2]}$. When solving Eqs. (B.4) and (B.5) the inverse matrices $(\boldsymbol{A}-\boldsymbol{B})^{-1}$ and $(\boldsymbol{A}+\boldsymbol{B})^{-1}$ are required. When the matrices $(\boldsymbol{A}-\boldsymbol{B})$ and $(\boldsymbol{A}+\boldsymbol{B})$ are constructed explicitly these inverse matrices may be obtained straightforwardly. When the dimension of $(\boldsymbol{A}-\boldsymbol{B})$ and $(\boldsymbol{A}+\boldsymbol{B})$ is large and the iterative subspace algorithms need to be used the separation of Eq. (B.2) into a two component form in Eqs. (B.4) and (B.5) becomes inefficient as it require the determination of $(\boldsymbol{A}-\boldsymbol{B})^{-1}$. Eq. (B.2) is identical to Eq. (9.23) and should be used directly.

If we assume an orthonormal MO representation $\boldsymbol{\Sigma}$ is the unit matrix. To avoid inverting the matrices $\boldsymbol{A}+\boldsymbol{B}$ and $\boldsymbol{A}-\boldsymbol{B}$ Eqs. (B.4) and (B.5) may be expressed as

$$[(\boldsymbol{A}-\boldsymbol{B})(\boldsymbol{A}+\boldsymbol{B}) - \omega^2]\boldsymbol{X}' = (\boldsymbol{A}-\boldsymbol{B})\boldsymbol{G}'_1 + \omega\boldsymbol{G}'_2\,, \tag{B.6}$$

and

$$[(\boldsymbol{A}+\boldsymbol{B})(\boldsymbol{A}-\boldsymbol{B}) - \omega^2]\boldsymbol{Y}' = (\boldsymbol{A}+\boldsymbol{B})\boldsymbol{G}'_2 - \omega\boldsymbol{G}'_1\,, \tag{B.7}$$

that is analogous to what was presented in Ref. [85]. The condition number for the set sets of linear equations in Eqs. (B.6) and (B.7) is the condition number of $(\boldsymbol{A}-\boldsymbol{B})(\boldsymbol{A}+\boldsymbol{B})$ and

$(\boldsymbol{A}+\boldsymbol{B})(\boldsymbol{A}-\boldsymbol{B})$, respectively. Since the matrix $\boldsymbol{B}$ is small compared to $\boldsymbol{A}$ the condition number of Eqs. (B.6) and (B.7) is determined by the matrix $\boldsymbol{A}^2$. This means that both Eqs. (B.6) and (B.7) have a condition number that is the square of the condition number of the standard response equation in Eq. (B.1) (see Section 7.3).

References

[1] DALTON, *an ab initio electronic structure program*, *Release 2.0.*, (2005). See http://www.kjemi.uio.no/software/dalton/dalton.html.

[2] LSDALTON, to be published.

[3] E. SCHRÖDINGER, *Ann. Phys.* **79**, 361 (1926).

[4] D. R. HARTREE, *Math. Proc. Cambridge Philos. Soc.* **24**, 89 (1928).

[5] V. FOCK, *Z. Phys.* **61**, 126 (1930).

[6] V. FOCK, *Z. Phys.* **62**, 795 (1930).

[7] C. MØLLER and M. S. PLESSET, *Phys. Rev.* **46**, 618 (1934).

[8] F. COESTER, *Nucl. Phys.* **7**, 421 (1958).

[9] J. ČÍŽEK, *J. Chem. Phys.* **45**, 4256 (1966).

[10] P. JØRGENSEN, T. HELGAKER and J. OLSEN, *Molecular Electronic-Structure Theory*, Wiley (2000).

[11] W. KOCH and M. C. HOLTHAUSEN, *A Chemist's Guide to Density Functional Theory*, Wiley (2001)

[12] P. HOHENBERG and W. KOHN, *Phys. Rev.* **140**, B864 (1964).

[13] W. KOHN and L. J. SHAM, *Phys. Rev.* **140**, A1133 (1965).

[14] P. PULAY, *Mol. Phys.* **17**, 197 (1969).

[15] J. OLSEN and P. JØRGENSEN, *Modern electronic structure theory, Vol. 2*, edited by D. R. YARKONY, World Scientific (1995) pp. 857-990.

[16] J. OLSEN and P. JØRGENSEN, *J. Chem. Phys.* **82**, 3235 (1985).

[17] J. GAUSS, *Modern Methods and Algorithms of Quantum Chemistry* **1**, 509 (2000).

[18] G. D. PURVIS III and R. J. BARTLETT, *J. Chem. Phys.* **76**, 1910 (1982).

[19] K. RAGHAVACHARI, G. W. TRUCKS, J. A. POPLE and M. HEAD-GORDON, *Chem. Phys. Lett.* **157**, 479 (1989).

[20] S. GOEDECKER and G. E. SCUSERIA, *Comp. Sci. Eng.* **5**, 14 (2003).

[21] S. GOEDECKER, *Rev. Mod. Phys.* **71**, 1085 (1999).

[22] P. SAŁEK, S. HØST, L. THØGERSEN, P. JØRGENSEN, P. MANNINEN, J. OLSEN, B. JANSÍK, S. REINE, F. PAWŁOWSKI, E. TELLGREN, T. HELGAKER and S. CORIANI, *J. Chem. Phys.* **126**, 114110 (2007).

[23] S. CORIANI, S. HØST, B. JANSÍK, L. THØGERSEN, J. OLSEN, P. JØRGENSEN, S. REINE, F. PAWŁOWSKI, T. HELGAKER and P. SAŁEK, *J. Chem. Phys.*, **126**, 154108 (2007).

[24] T. KJÆRGAARD, P. JØRGENSEN, J. OLSEN, S. CORIANI and T. HELGAKER, *J.*

Chem. Phys. **129**, 054106 (2008).

[25] J. R. Bunch and J. E. Hopcroft, *Math. of Comp.* **28**, 231 (1974)

[26] K. A. Atkinson, *An Introduction to Numerical Analysis, Second Edition*, Wiley (1989).

[27] D. Bau III and L. N. Trefethen, *Numerical linear algebra*, SIAM (1997).

[28] P. Norman, D. M. Bishop, H. J. Aa. Jensen and J. Oddershede, *J. Chem. Phys.* **123**, 194103 (2005).

[29] P. Norman, D. M. Bishop, H. J. Aa. Jensen and J. Oddershede, *J. Chem. Phys.* **115**, 10323 (2001).

[30] B. J. Orr and J. F. Ward, *Mol. Phys.* **20**, 513 (1971).

[31] A. S. Davydov, *Quantum Mechanics*, Pergamon Press Ltd. (1965).

[32] L. Barron, *Molecular Light Scattering and Optical Activity, Second Edition*, Cambridge University Press (2004).

[33] K. Kristensen, J. Kauczor, T. Kjærgaard and P. Jørgensen, *J. Chem. Phys.* **131**, 044112 (2009).

[34] R. W. Boyd, *Nonlinear Optics*, Academic (1992).

[35] J. J. Sakurai, *Modern quantum mechanics*, Addison-Wesley (1994).

[36] C. N. Banwell and E. M. McCash, *Fundamentals of Molecular Spectroscopy, Fourth Edition*, McGraw-Hill International (1994).

[37] J. A. Pople, R. Krishnan, H. B. Schlegel and J. S. Binkley, *Int. J. Quantum Chem* **14**, 545 (1979).

[38] P. E. S. Wormer, F. Visser and J. Paldus, *J. Comp. Phys.* **48**, 23 (1982).

[39] M. R. Hestenes and E. Stiefel, *J. Res. Natl. Bur. Stand.* **49**, 409 (1952).

[40] E. Stiefel, *Comment. Math. Helv.* **29**, 157 (1955).

[41] J. Olsen, H. J. Aa. Jensen and P. Jørgensen, *J. Comp. Phys.* **74**, 265 (1988).

[42] E. R. Davidson, *Comp. Phys.* **17**, 87 (1975).

[43] O. Christiansen, P. Jørgensen and C. Hättig, *Int. J. Quantum Chem.* **68**, 1 (1998).

[44] K. Sasagane, F. Aiga and R. Itoh, *J. Chem. Phys.* **99**, 3738 (1993).

[45] K. Kristensen, P. Jørgensen, A. J. Thorvaldsen and T. Helgaker, *J. Chem. Phys.* **129**, 214103 (2008).

[46] M. Born and J. R. Oppenheimer, *Ann. der Phys.* **84**, 457 (1927).

[47] T. Helgaker, M. Jaszuński and K. Ruud, *Chem. Rev.* **99**, 293 (1999).

[48] C. C. J. Roothaan, *Rev. Mod. Phys.* **23**, 69 (1951).

[49] G. G. Hall, *Proc. Roy. Soc.* **A205**, 541 (1951).

[50] P. Pulay, *Chem. Phys. Lett.* **73**, 393 (1980).

[51] P. Pulay, *J. Comp. Chem.* **3**, 556 (1982).

[52] L. Thøgersen, J. Olsen, A. Köhn, P. Jørgensen, P. Sałek and T. Helgaker, *J. Chem. Phys.* **123**, 074103 (2005).

[53] L. Thøgersen, J. Olsen, D. Yeager, P. Jørgensen, P. Sałek and T. Helgaker, *J. Chem. Phys.* **121**, 16 (2004).

[54] S. Høst, J. Olsen, B. Jansík, L. Thøgersen, P. Jørgensen and T. Helgaker, *J. Chem. Phys.* **129**, 124106 (2008).

[55] T. Helgaker, P. Jørgensen and J. Olsen, *Density Functional Theory*, to be published.

[56] D. C. Langreth and M. J. Mehl, *Phys. Rev. B* **28**, 1809 (1983).

[57] A. D. Becke, *J. Phys. Chem.* **84**, 4524 (1986).

[58] J. P. Perdew and Y. Wang, *Phys. Rev. B* **33**, 8800 (1986).

[59] J. M. Millam and G. E. Scuseria, *J. Chem. Phys.* **106**, 5569 (1997).

[60] L. Greengard and V. Rokhlin, *J. Comp. Phys.* **73**, 325 (1987).

[61] C. A. White, B. G. Johnson, P. M. W. Gill and M. Head-Gordon, *Chem. Phys. Lett.* **230**, 8 (1994).

[62] M. C. Strain, G. E. Scuseria and M. J. Frisch, *Science* **271**, 51 (1996).

[63] M. Challacombe and E. Schwegler, *J. Chem. Phys.* **106**, 5526 (1997).

[64] Y. Shao and M. Head-Gordon, *Chem. Phys. Lett.* **323**, 425 (2000).

[65] J. L. Whitten, *J. Chem. Phys.* **58**, 4496 (1973).

[66] B. I. Dunlap, J. W. D. Connolly and J. R. Sabin, *J. Chem. Phys.* **71**, 3396 (1979).

[67] E. J. Baerends, D. E. Ellis and P. Ros, *Chem. Phys.* **2**, 41 (1973).

[68] Y. Jung, A. Sodt, P. Gill and M. Head-Gordon, *P. Natl. Acad. Sci. Usa.* **102**, 6692 (2005).

[69] O. Vahtras, J. Almöf and M. Feyereisen, *Chem. Phys. Lett.* **213**, 514 (1993).

[70] A. Sodt, J. E. Subotnik and M. Head-Gordon, *J. Chem. Phys.* **125**, 194109 (2006).

[71] R. T. Gallat and A. St-Amant, *Chem. Phys. Lett.* **256**, 569 (1996).

[72] E. Schwegler and M. Challacombe, *J. Chem. Phys.* **105**, 2726, (1996).

[73] G. E. Scuseria, J. C.Burant and M. J. Frisch, *J. Chem. Phys.* **105**, 8969 (1996).

[74] M. Challacombe, E. Schwegler and M. Head-Gordon, *J. Chem. Phys.* **106**, 9708, (1997).

[75] C. Ochsenfeld, C. A. White and M. Head-Gordon, *J. Chem. Phys.* **109**, 1663 (1998).

[76] J. M. Pérez-Jordá and W. Yang, *Chem. Phys. Lett.* **241**, 469 (1995).

[77] R. E. Stratmann, G. E. Scuseria and M. J. Frisch, *Chem. Phys. Lett.* **257**, 213 (1996).

[78] M. Challacombe, *J. Chem. Phys.* **113**, 10037 (2000).

[79] J. Kong, S. T. Brown and L. Fusti-Molnar, *J. Chem. Phys.* **124**, 094109 (2006).

[80] D. N. Zubarev, *Nonequilibrium Statistical Thermodynamics*, Consultants Bureau (1974).

[81] H. Hellmann, *Einführing in die Quanten Theori* (Franz Deuticke, Leipzig), 285 (1937).

[82] R. Feynman, *Phys. Rev.* **56**, 340 (1939).

[83] R. M. Stevens, R. M. Pitzer and W. N. Lipscomb, *J. Chem. Phys.* **38**, 550 (1963).

[84] L. Brillouin, *Actual. Sci. Ind.* **71** (1933), **159** (1934).

[85] P. Jørgensen and J. Linderberg, *Int. J. Quantum Chem.* **4**, 587 (1970).

[86] M. E. Casida, *Recent Advances in Density Functional Methods, Vol. 1*, edited by D. P. Chong, World Scientific (1995), pp. 155-192

[87] J. Čížek and J. Paldus, *J. Chem. Phys.* **47**, 3976 (1967).

[88] H. Larsen, P. Jørgensen, J. Olsen and T. Helgaker, *J. Chem. Phys.* **113**, 8908 (2000).

[89] P. Norman, A. Jiemchooroj and B. E. Sernelius, *J. Chem. Phys.* **118**, 9167 (2003).

[90] A. Jiemchooroj, P. Norman and B. E. Sernelius, *J. Chem. Phys.* **123**, 124312 (2005).

[91] A. Jiemchooroj, P. Norman and B. E. Sernelius, *J. Chem. Phys.* **125**, 124306 (2006).

[92] X. Blase and P. Ordej'on, *Phys. Rev. B* **69**, 085111 (2004).

[93] L. Jensen, J. Autschbach and G. C. Schatz, *J. Chem. Phys.* **122**, 224115 (2005).

[94] R. A. Mata, B. J. C. Cabral, C. Millot, K. Coutinho and S. Canuto, *J. Chem. Phys.* **130**, 014505 (2009).

[95] P. Norman, K. Ruud and T. Helgaker, *J. Chem. Phys.* **120**, 5027 (2004).

[96] A. Jiemchooroj and P. Norman, *J. Chem. Phys.* **126**, 134102 (2007).

[97] J. Autschbach, L. Jensen, G. C. Schatz, Y. C. E. Tse and M. Krykunov, *J. Phys. Chem. A* **110**, 2461 (2006).

[98] M. Krykunov and J. Autschbach, *J. Chem. Phys.* **125**, 034102 (2006).

[99] M. Krykunov, M. D. Kundrat and J. Autschbach, *J. Chem. Phys.* **125**, 194110 (2006).

[100] U. Ekström, P. Norman, V. Carravetta and H. Ågren, *Phys. Rev. Lett.* **97**, 143001 (2006).

[101] U. Ekström and P. Norman, *Phys. Rev. A* **74**, 042722 (2006).

[102] G. Tu, Z. Rinkevicius, O. Vahtras, H. Ågren, U. Ekström and P. Norman, *Phys. Rev. A* **76**, 022506 (2007).

[103] A. Jiemchooroj, U. Ekström and P. Norman, *J. Chem. Phys.* **127**, 165104 (2007).

[104] A. Jiemchooroj and P. Norman, *J. Chem. Phys.* **128**, 234304 (2008).

[105] M. Linares, S. Stafström and P. Norman, *J. Chem. Phys.* **130**, 104305 (2009).

[106] M. Krykunov and J. Autschbach, *J. Chem. Phys.* **126**, 024101 (2007).

[107] A. Devarajan, A. Gaenko and J. Autschbach, *J. Chem. Phys.* **130**, 194102 (2009).

[108] L. Jensen, L. L. Zhao, J. Autschbach and G. C. Schatz, *J. Chem. Phys.* **123**, 174110 (2005).

[109] L. L. Zhao, L. Jensen and G. C. Schatz, *Nano Lett.* **6**, 1229 (2006).

[110] L. L. Zhao, L. Jensen and G. C. Schatz, *J. Am. Chem. Soc* **128**, 2911 (2006).

[111] L. Jensen and G. C. Schatz, *J. Phys. Chem. A* **110**, 5973 (2006).

[112] C. M. Aikens and G. C. Schatz, *J. Phys. Chem. A* **110**, 13317 (2006).

[113] L. Jensen, J. Autschbach, M. Krykunov and G. C. Schatz, *J. Chem. Phys.* **127**, 134101 (2007).

[114] L. Jensen, L. L. Zhao and G. C. Schatz, *J. Phys. Chem. C* **111**, 4756 (2007).

[115] L. Jensen, C. M. Aikens and G. C. Schatz, *Chem. Soc. Rev.* **37**, 1061 (2008).

[116] Y. B. Zheng, Y.-W. Yang, L. Jensen, L. Fang, B. K, Juluri, A. H. Flood, P. S. Weiss, J. F. Stoddart and T. J. Huang, *Nano Lett.* **9**, 819 (2009).

[117] A. Mohammed, H. Ågren and P. Norman, *Chem. Phys. Lett.* **468**, 119 (2009).

[118] A. Mohammed, H. Ågren and P. Norman, *Phys. Chem. Chem. Phys.* **468**, 119 (2009).

[119] M. Krykunov, M. Seth, T. Ziegler and J. Autschbach, *J. Chem. Phys.* **127**, 244102 (2007).

[120] H. Solheim, K. Ruud, S. Coriani and P. Norman, *J. Chem. Phys.* **128**, 094103 (2008).

[121] H. Solheim, K. Ruud, S. Coriani and P. Norman, *J. Phys. Chem. A* **112**, 9615

(2008).

[122] A. J. Thorvaldsen, K. Ruud, K. Kristensen, P. Jørgensen and S. Coriani, *J. Chem. Phys.* **129**, 214108 (2008).

[123] B. H. Bransden and C. J. Joachain, *Physics of Atoms and Molecules, Second edition*, Pearson Education Limited (2003).

[124] P. W. Milonni and J. H. Eberly, *Lasers*, Wiley (1988).

[125] E. Wigner, *Math. Naturw. Anz. Ung. Akad. Wiss.* **53**, 477 (1935).

[126] E. M. Verdet, *Ann. Chim. (3rd Ser.)* **41**, 370 (1854).

[127] D. J. Caldwell and H. Eyring, *The Theory of Optical Activity*, Wiley Interscience (1971).

[128] A. D. Buckingham and P. J. Stephens, *Adv. Res. Chem. Phys.* **17**, 399 (1966).

[129] M. Faraday, *Philos. Mag.* **28**, 294 (1846).

[130] M. Faraday, *Philos. Trans. R. Soc. London.* **136**, 1 (1846).

[131] P. N. Schatz and A. McCaffery, *Q. Rev. Chem. Soc.* **23**, 552 (1969).

[132] R. Serber, *Phys. Rev.* 41 (1932).

[133] P. J. Stephens, *Chem. Phys. Lett.* **2**, 241 (1968).

[134] P. J. Stephens, *J. Chem. Phys.* **52**, 3489 (1970).

[135] P. J. Stephens, *Annu. Rev. Phys. Chem.* **25**, 201 (1974).

[136] P. J. Stephens, *Adv. Chem. Phys.* **35**, 197 (1976).

[137] C. H. Henry, S. E. Schnatterly and C. P. Slichter, *Phys. Rev.* **137**, A583 (1965).

[138] A. D. Becke, *J. Chem. Phys.* **98**, 5648 (1993).

[139] T. H. Dunning, *J. Chem. Phys.* **90**, 1007 (1989).

[140] M. Göeppert-Mayer, *Ann. Phys. Leipzig* **9**, 273 (1931).

[141] P. R. Monson and W. M. McClain, *J. Chem. Phys.* **53**, 29 (1970).

[142] T. Yanai, D. P. Tew and N. C. Handy, *Chem. Phys. Lett.* **393**, 51 (2004).

[143] G. D. Purvis III and R. J. Bartlett, *J. Chem. Phys.* **75**, 1284 (1981).

[144] W. H. Press, B. P. Flannery, S. A. Teukolsky, and W. T. Vetterling, *Numerical Recipes in C++: The Art of Science Computing, Second edition*, Cambridge University Press (2002).

[145] J. R. Shewchuk, *An introduction to the Conjugate Gradient method Without the Agonizing Pain*, Carnegie Mellon University (1994).

[146] Y. Saad, *Iterative Methods for Sparse Linear Systems, Second edition*, SIAM (2003).

[147] O. Axelsson, *Iterative Solution Methods*, Cambridge University Press (1996).

[148] M. Ziółkowski, V. Weijo, P. Jørgensen and J. Olsen, *J. Chem. Phys.* **128**, 204105 (2008).

[149] *Advances in Quantum Chemistry 50 - Response Theory and Molecular Properties (A Tribute to Jan Linderberg and Poul Jørgensen)*, edited by H. J. Aa. Jensen, Elsevier (2005).

[150] J. Olsen, P. Jørgensen and J. Simons, *Chem. Phys. Lett.* **169**, 463 (1990).

[151] B. N. Parlett, *The Symmetric Eigenvalue Problem*, Prentice Hall (1980).

[152] J. K. L. MacDonald, *Phys. Rev.* **43**, 830 (1933).

[153] T. D. Bouman, Aa. E. Hansen, B. Voigt and S. Rettrup, *Int. J. Quant. Chem.* **23**, 595 (1983).

[154] J. P. Flament and H. G. Gervais, *Int. J. Quant. Chem.* **16**, 1347 (1979).

[155] H. Larsen, J. Olsen, P. Jørgensen and T. Helgaker, *J. Chem. Phys.* **115**, 9685 (2001).

[156] B. C. Carlson and J. M. Keller, *Phys. Rev.* **105**, 102 (1957).

[157] T. Saue, *Relativistic Electronic Structure Theory - Part 1 : Fundamentals*, chapter 7, edited by P. Schwerdtfeger, Elsevier (2002).

[158] T. Saue and H. J. Aa. Jensen, *J. Chem. Phys.* **118**, 522 (2003).

[159] R. Bast, H. J. Aa. Jensen and T. Saue, *Int. J. Quant. Chem.* **109**, 2091 (2009).

[160] S. Villaume, T. Saue and P. Norman, *J. Chem. Phys.* **133**, 064105 (2010).

[161] W. J. Hehre, R. Ditchfield and J. A. Pople, *J. Chem. Phys.* **56**, 2257 (1972).

[162] Maestro v. 8.5, See http://www.schrodinger.com.

[163] http://webbook.nist.gov/chemistry

[164] U. K. Genick, S. M. Soltis, P. Kuhn, I. L. Canestrelli and E. D. Getzoff, *Nature* **392**, 206 (1998).

[165] T. Rocha-Rinza, O. Christiansen, J. Rajput, G. Aravind D. Rahbek,L. H. Andersen, A. V. Bochenkova, A. A. Granovsky, K. B. Bravaya, A. V. Nemukhin, K. L. Christiansen and M. B. Nielsen, *J. Phys. Chem. A* **113**, 9442 (2009).

[166] I. B. Nielsen, S. Boyé-Péronne, M. O. A. El Ghazaly, M. B. Kristensen, S. Brøndsted Nielsen and L. H. Andersen, *Biophys J.* **89**, 2597 (2005).

Articles included in this thesis

A. *Quasienergy formulation of damped response theory*
Kasper Kristensen, Joanna Kauczor, Thomas Kjærgaard and Poul Jørgensen
J. Chem. Phys. **131**, 044112 (2009).

B. *On the efficiency of algorithms for solving Hartree–Fock and Kohn–Sham response equations*
Joanna Kauczor, Poul Jørgensen and Patrick Norman
J. Chem. Theory Comput. **7**, 1610 (2011).

C. *Comparison of standard and damped response formulations of Magnetic Circular Dichroism*
Thomas Kjærgaard, Kasper Kristensen, Joanna Kauczor, Poul Jørgensen, Sonia Coriani and Andreas J. Thorvaldsen
J. Chem. Phys. **135**, 024112 (2011).

D. *Damped response theory of two photon absorption*
Kasper Kristensen, Joanna Kauczor, Thomas Kjærgaard, Poul Jørgensen, Andreas J. Thorvaldsen and Antonio Rizzo
J. Chem. Phys. **134**, 214104 (2011).